On the Dynamics and Predictability of the Atlantic Niño

Dissertation

zur Erlangung des Doktorgrades
der Mathematisch-Naturwissenschaftlichen Fakultät
der Christian-Albrechts-Universität zu Kiel

vorgelegt von

Tina Dippe

Kiel, 2018

Erster Gutachter: Prof. Dr. Richard J. Greatbatch
Zweite Gutachterin: Prof. Dr. Joke F. Lübbecke

Tag der mündlichen Prüfung: 19. 12. 2018
Zum Druck genehmigt: 19. 12. 2018

gez. Prof. Dr. Frank Kempken, Dekan

Abstract

This thesis seeks to broaden our understanding of the Atlantic Niño. The Atlantic Niño is the dominant mode of coupled interannual climate variability in the equatorial Atlantic. Its sea surface temperature (SST) signature is reminiscent of the Pacific El Niño-Southern Oscillation (ENSO). SST anomalies stretch from the Angolan and Namibian coast into the central equatorial Atlantic in a tongue-shaped pattern, with a preference for the southern hemisphere. Because the atmosphere and ocean are tightly coupled at the equator, SST co-varies with both zonal surface wind in the western equatorial ocean basin, and thermocline depth and upper ocean heat content in the central and eastern ocean basin. The Atlantic Niño peaks in boreal summer, when SST anomalies reach values of up to $\pm 1^{\circ}C$ relative to the climatological seasonal cycle. A secondary, weaker Niño-like phenomenon occurs in boreal winter. Both the summer and winter Niños are the source of teleconnections that affect seasonal climate variability locally and in remote regions. Socio-economic impacts, especially in northwestern Brazil and Africa, can be devastating.

An important question about the Atlantic Niño is to what extent it is driven by dynamical, potentially predictable processes. Using multiple linear regression and the dynamical framework of the Bjerknes feedback, SST variability in the central equatorial Atlantic is decomposed into a dynamically driven part, and a residual part that is mainly associated with stochastic processes. During boreal summer and winter, when the Atlantic Niño is active, the dynamical contribution to SST variability clearly dominates stochastic SST variability, indicating that the Bjerknes feedback is involved in establishing the Atlantic Niño.

Previous research has shown that the Atlantic Niño is much more symmetric than the Pacific ENSO. In contrast to the Pacific, where warm events tend to grow to larger amplitudes than cold events, Atlantic warm and cold events have SST signatures that are effectively mirror images of each other. Does the symmetry (or asymmetry) of the Atlantic and Pacific Niños correspond the symmetry (or asymmetry) of the respective Bjerknes feedbacks? Decomposing the Bjerknes feedback into three interacting feedback elements, robust regression is used to diagnose the strength of the feedback elements when they act on either positive or negative anomalies ("composites"). In the Pacific, clear asymmetries emerge for all feedback elements, with the positive composites dominating the negative composites. In the Atlantic, differences between positive and negative composites

are less consistent across feedback elements. Additionally, assessing the stationarity of the Bjerknes feedback shows that both the feedback elements and their symmetries vary substantially on decadal time scales.

A strong, coupled warm bias in the equatorial Atlantic inhibits realistic simulations of the Atlantic Niño in virtually all coupled global climate models (CGCMs) of the current generation. A review of the issue synthesises our current understanding of the processes that create and maintain the equatorial Atlantic warm bias, concluding that intrinsic biases exist in both the atmospheric and oceanic modules of a CGCM. When the modules are coupled to each other, feedbacks enhance the intrinsic biases, forming a complex coupled bias signature. It is shown that the coupled bias creates a background which is not compatible with the observed physical processes in the equatorial Atlantic. Biased models are unable to capture the dynamics of the real ocean, and hence fail to simulate the Atlantic Niño.

Another important question is how the bias affects the ability of a model to predict the Atlantic Niño. Analysing two suites of hindcasting experiments – one using a standard model that develops the equatorial Atlantic warm bias, the other employing surface heat flux correction to effectively alleviate the bias –, shows that bias alleviation enhances the predictability of SST variability in boreal summer, promising improved forecasts of the Atlantic Niño in the future.

Zusammenfassung

Diese Dissertation versucht unser Verständnis des Atlantischen Niño auszubauen. Der Atlantische Niño ist die dominante Form zwischenjährlicher, gekoppelter Klimavariabilität im äquatorialen Atlantik. Seine Signatur der Meeresoberflächentemperatur (SST) erinnert an die pazifische El Niño-Southern Oscillation (ENSO). SST-Anomalien erstrecken sich von der angolanischen und namibischen Küste bis in den zentralen äquatorialen Atlantik, vorzugsweise auf der Südhalbkugel. Da die Atmosphäre und der Ozean in Äquatornähe stark miteinander gekoppelt sind, treten SST-Anomalien zusammen mit Schwankungen des zonalen, oberflächennahen Windfeldes im westlichen Ozeanbecken sowie mit der Tiefe der Thermokline und des Wärmeinhalts des oberen Ozeans im zentralen und östlichen Ozeanbecken auf. Der Atlantische Niño ist während des Sommers der Nordhalbkugel am stärksten ausgeprägt. In dieser Zeit können SST-Anomalien Werte von bis zu $\pm 1°C$ relativ zum klimatologischen Jahresgang erreichen. Ein zweites, deutlich schwächeres Niño-ähnliches Phänomen tritt im borealen Winter auf. Sowohl Sommer- als auch Winter-Niños erzeugen Telekonnektionen, die globale und regionale Klimaschwankungen auslösen und teils verheerende sozioökonomische Folgen haben können, insbesondere im nordwestlichen Brasilien und Teilen Afrikas.

Ein wichtiger Streitpunkt der gegenwärtigen Forschung ist, in welchem Maß der Atlantische Niño von dynamischen, möglicherweise vorhersagbaren Prozessen angetrieben wird. Um diese Frage zu beantworten, wird die SST-Variabilität im zentralen äquatorialen Atlantik mit Hilfe multipler linearer Regression in zwei Komponenten zerlegt: Einen dynamischen Anteil, der dem Konzept des Bjerknes-Feedbacks entspricht, und einen komplementären, hauptsächlich von stochastischen Prozessen erzeugten Anteil. Im borealen Sommer und Winter, wenn der Atlantische Niño aktiv ist, dominiert die dynamische Komponente die SST-Variabilität. Dies legt nahe, dass der Atlantische Niño mit dem Bjerknes-Feedback zusammen hängt und teilweise dynamisch angetrieben wird.

Studien haben gezeigt, dass der Atlantische Niño symmetrischer ist als die pazifische ENSO. Während pazifische Warm-Events in der Regel stärker ausgeprägt sind als kalte Events, entwickeln sich warme und kalte Events im Atlantik für gewöhnlich spiegelbildlich zueinander. Entspricht die Symmetrie (bzw. Asymmetrie) der atlantischen und pazifischen Niños der Symmetrie (bzw. Asymmetrie) des jeweiligen Bjerknes Feedbacks? Um diese Frage zu beantworten, wird das Bjerknes Feedback in drei miteinander interagierende Elemente zerlegt. Diese Elemente werden anschließend in Komposite aufgeteilt, die jeweils

auf positiven oder negativen Anomalien basieren. Mit Hilfe robuster Regression wird die Stärke der Komposite abgeschätzt, so dass Asymmetrien zwischen positiven und negativen Kompositen bewertet werden können. Im Pazifik treten für alle Feedback-Elemente Asymmetrien auf, wobei positive Komposite negative Komposite deutlich dominieren. Im Atlantik sind die Unterschiede zwischen positiven und negativen Kompositen weniger konsistent. Zusätzlich wird die Stationarität des Bjerknes-Feedbacks untersucht. Sowohl im Atlantik als auch im Pazifik variieren die Elemente des Bjerknes-Feedbacks sowie ihre Symmetrien erheblich auf dekadischen Zeitskalen.

Ein ausgeprägter, gekoppelter Warm-Bias im äquatorialen Atlantik verhindert realistische Simulationen des Atlantischen Niño in praktisch allen gegenwärtigen gekoppelten globalen Klimamodellen (CGCMs). Ein Review fasst den aktuellen Kenntnisstand zum Thema zusammen und zeigt auf, welche Prozesse den atlantischen Warm-Bias erzeugen. Sowohl in den atmosphärischen als auch den ozeanischen Komponenten moderner CGCMs treten intrinsische, systematische Verzerrungen auf, die durch Feedback-Prozesse verstärkt werden, sobald man beide Komponenten miteinander koppelt. Im Ergebnis entwickelt sich ein stark verzerrter klimatologischer Grund-Zustand, der mit den beobachteten physikalischen Prozessen im äquatorialen Atlantik nicht kompatibel ist. Modelle, die vom atlantischen Warm-Bias betroffen sind, können die Dynamik des realen Ozeans nicht nachbilden und den Atlantischen Niño daher nicht simulieren.

Ein weiterer wichtiger Forschungsgegenstand ist, wie sich der Warm-Bias auf die Vorhersage-Fähigkeiten eines Models in Bezug auf den Atlantischen Niño auswirkt. Um diese Frage zu beantworten, werden zwei Hindcast-Experimente analysiert (retrospektive Vorhersagen von historischen Ereignissen). Das erste Experiment wird mit einem Standard-Modell durchgeführt, das den typischen atlantischen Warm-Bias erzeugt; für das zweite Experiment wird der Bias reduziert, indem die Klimatologie der Wärmeflüsse an der Meeresoberfläche korrigiert wird. Die Experimente zeigen, dass der Warm-Bias die Vorhersagbarkeit des Atlantischen Niño verringert. Im Umkehrschluss versprechen die Ergebnisse verbesserte Vorhersagen des Atlantischen Niño, sobald effektive Wege gefunden worden sind, um den atlantischen Warm-Bias zu beheben.

Contents

Abstract **3**

Zusammenfassung **5**

1 Introduction **9**

1.1 What is the Atlantic Niño? 10

1.2 Dynamics of the Atlantic Niño 13

1.2.1 Background state 13

1.2.2 The Bjerknes feedback as the main driver of Atlantic Niño variability 14

1.2.3 Alternative mechanisms 15

1.3 The Atlantic and Pacific Niños: A comparison 17

1.4 Modelling and predicting the Atlantic Niño: Facing the challenge of the equatorial Atlantic warm bias 19

1.5 Research questions of this thesis 22

2 On the Dynamics of the Atlantic Niño **23**

3 A comparison of the Atlantic and Pacific Bjerknes feedbacks: Seasonality, Symmetry, and Stationarity **41**

4 Can Climate Models simulate the observed strong Summer Surface Cooling in the equatorial Atlantic? **83**

5 Seasonal Predictions of equatorial Atlantic SST in a low-resolution CGCM with Surface Heat Flux Correction **101**

6 Summary, Discussion, Outlook **129**

6.1 Summary 129

6.2 Discussion 134

6.3 Outlook 136

List of Figures **139**

Bibliography **143**

Own Publications **155**

Acknowledgements **157**

Selbstständigkeitserklärung **159**

Chapter 1

Introduction

The Atlantic Niño is the dominant mode of coupled interannual climate variability in the equatorial Atlantic. During boreal summer, sea surface temperatures (SSTs) can deviate by up to $1°C$ from the climatological values if their seasonal cycle, affecting local and remote areas and creating profound socio-economic impacts.

Previous research has suggested a number of mechanisms that generate the Atlantic Niño. First, the Bjerknes feedback – the dominant positive feedback of the equatorial ocean basins that ties atmospheric and oceanic variability into a coupled process – is involved with establishing both the seasonal cycle in the equatorial Atlantic, and the interannual variability of the Atlantic Niño. Second, additional dynamical ocean processes contribute to the Atlantic Niño. Last, atmospheric stochastic forcing has been suggested as an alternative driver of the variability. This abundance of theories about its nature demonstrates how intricate a phenomenon the Atlantic Niño is.

Simulating realistic Atlantic Niño variability and predicting it on seasonal time scales poses substantial challenges to the scientific community. A crucial factor exacerbating this struggle is a strong coupled warm bias in the equatorial Atlantic ocean that alters the background state of the basin relative to observations. Several key properties that are instrumental in generating the Atlantic Niño cannot be reproduced by the current generation of climate models, deeming useful seasonal predictions of the Atlantic Niño a futile enterprise.

The goal of this thesis is (i) to improve our understanding of the mechanisms that form the Atlantic Niño, and (ii) to assess how the equatorial Atlantic warm bias affects our ability to simulate and predict observed Atlantic Niño variability, using coupled global climate models (CGCMs).

1.1 What is the Atlantic Niño?

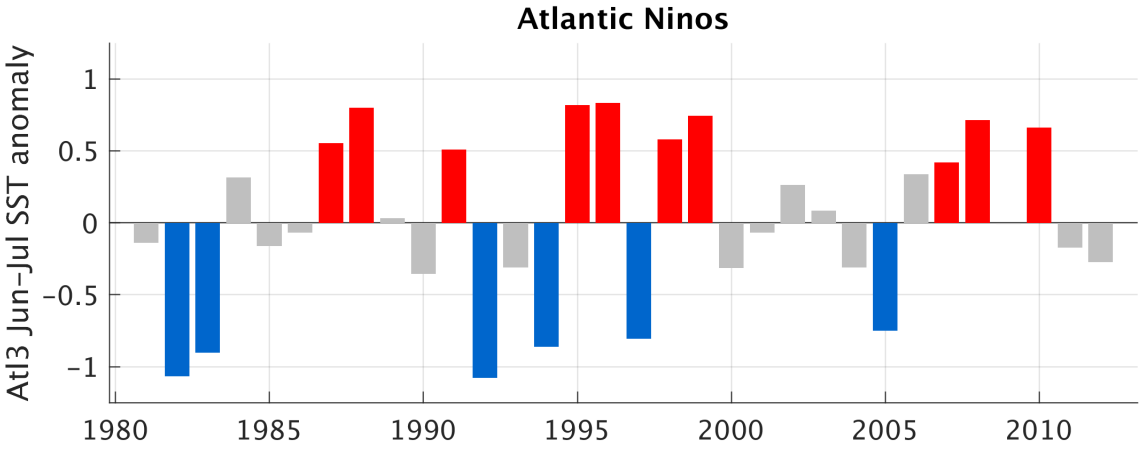

Figure 1.1: *Time series of an Atlantic Niño index, based on the HadISST dataset (Rayner et al., 2003) for the period 1981-2012. The Atlantic Niño index averages monthly mean SST for June and July – when Atlantic Niño events tend to peak – over the Atl3 region ($3°S$ to $3°N$, $20°W$ to $0°E$). Event years were chosen as follows. Calculate anomalies and the standard deviation of the Atlantic Niño time series and select all years in which the time series exceeds $\pm 0.7 \times \sigma_{AN}$, with σ_{AN} being the standard deviation of the time series. Red, blue, and grey bars indicate warm (1987, 1988, 1991, 1995, 1996, 1998, 1999, 2007, 2008, and 2010), cold (1982, 1983, 1992, 1994, 1997, and 2005), and neutral events.*

Every few years in early boreal summer, sea surface temperatures (SSTs) in the central equatorial Atlantic deviate from their expected seasonal cycle by up to 1°C (Fig. 1.1). Figure 1.2 illustrates the general evolution of such an event. In early boreal spring, the first anomalies appear off the southern coast of Angola. The anomalies intensify and spread northwestward. Around June, anomalies reach their maximum amplitude and form a clear tongue-shaped pattern that stretches from the Angolan coast into the central equatorial Atlantic. In August and September, the event dissipates quickly, and anomalies throughout the equatorial and subtropical Atlantic of the southern hemisphere vanish[1].

In concert with the SST anomalies, additional elements of the equatorial Atlantic climate system vary and produce a distinct coupled signature of the event. Prior to the growth of the SST anomalies, zonal surface winds in the western equatorial Atlantic deviate from their seasonal cycle. Weakening trade winds usually – but not always, see

[1] An interesting feature of Fig. 1.2 is that, for the period 1981-2012, warm and cold Atlantic Niño events in the HadISST dataset are clearly asymmetric, with cold events having a mean amplitude of $-0.91°C$ in June and July, in contrast to $0.66°C$ for warm events. This asymmetry, however, depends on the details of the analysis, including which dataset and analysis period were used (not shown). Repeating the analysis with the ERSSTv2 dataset (Huang et al., 2017; Smith and Reynolds, 2003), for example, produces a much more symmetric Atlantic Niño. Likewise, extending the analysis period back into the mid-1950s considerably weakens the HadISST asymmetry between warm and cold Atlantic Niño events. This indicates that the symmetry of the Atlantic Niño is not too robust a property of tropical Atlantic variability.Losada and Rodríguez-Fonseca (2016) and Martín-Rey et al. (2017) draw similar conclusions.

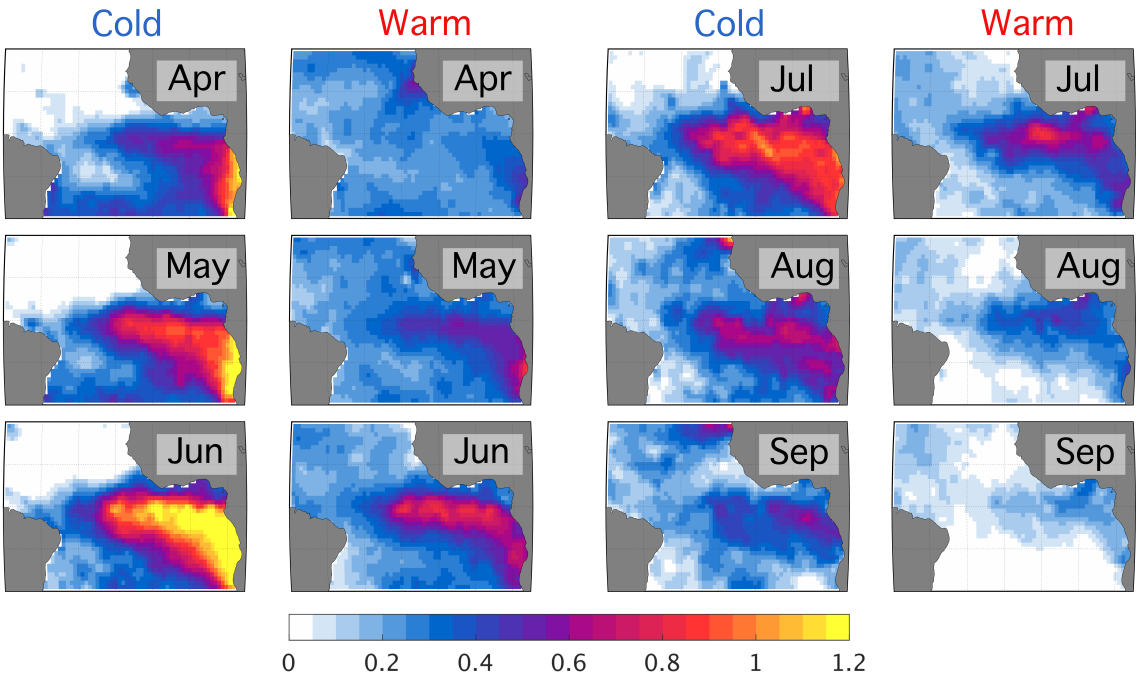

Figure 1.2: *Composite evolution of Atlantic Niño events, based on the HadISST dataset for the period 1981-2012. Years contributing to the cold (first and third column, monthly composites running from April to September) and warm (second and fourth column) composites are shown in Fig. 1.1 as blue and red bars, respectively. For cold events, SST anomalies in the central equatorial Atlantic are negative, but are shown here with the same sign as the warm events to facilitate a direct comparison.*

Section 1.2.3 – precede warm equatorial events, while intensifying trade winds pave the way for cold events. The rain band of the intertropical convergence zone (ITCZ) deviates from its climatological meridional position, affecting rainfall patterns over the surrounding continents. The intricate system of equatorial surface currents adjusts to the changing atmospheric circulation, and the subsurface structure of the ocean changes, with ocean heat content being distributed more evenly across the zonal extent of the equatorial Atlantic for warm events. All of these processes are related to each other and form a coupled event whose signature feature, from an oceanic point of view, is the formation of a distinct SST anomaly pattern.

This mode of coupled interannual variability is called the "Atlantic Niño". Alternatively, research addresses the "Atlantic zonal mode" or the "Atlantic cold tongue mode". While these names emphasise subtly different aspects of the Atlantic Niño[2], Lübbecke

[2]The "Niño" highlights similarities to the much stronger El Niño-Southern Oscillation in the Pacific (ENSO; see Section 1.3). The "zonal mode" stresses that, in contrast to the Pacific, the equatorial Atlantic hosts a number of SST modes that interact on different time scales; the zonal mode in this case is the second-most important mode in addition to the Atlantic meridional mode, which is active mainly in boreal spring and acts on decadal time scales (Sutton, Jewson, and Rowell, 2000). Last, the "cold tongue mode" emphasises the close relationship between the Atlantic Niño and the formation of the Atlantic cold tongue in boreal summer, the dominant feature of the seasonal cycle in the equatorial Atlantic.

et al. (2018) argue that they refer to the same phenomenon. Throughout this thesis, the conventional term "Atlantic Niño" is used.

In addition to the summer Niño, a secondary Niño-like phenomenon occurs during early boreal winter. Okumura and Xie (2006) show that a weak seasonal intensification of the equatorial trade wind regime in late boreal fall briefly organizes atmosphere-ocean variability into the Bjerknes feedback, setting the stage for the emergence of the Atlantic winter Niño. While the winter Niño resembles the summer Niño dynamically, it is much weaker in amplitude and restricted to a short period of just a few weeks.

Because the atmosphere-ocean system is tightly coupled in an equatorial ocean basin, the Atlantic Niño is the source of a number of teleconnections that impact local and remote areas of the globe (e.g. Carton et al., 1996; Carton and Huang, 1994; Ding, Keenlyside, and Latif, 2012; Folland et al., 2001; Fontaine and Janicot, 1996; Keenlyside and Latif, 2007; Kucharski et al., 2008; Losada and Rodríguez-Fonseca, 2016; Lübbecke et al., 2018; C. Wang, 2006). Nobre and Shukla (1996) show that equatorial Atlantic SST variability in general can have devastating effects on rainfall variability in Brazil's Nordeste region. The 1958 drought, for example, forced an approximate 10 million people to temporarily emigrate (Namias, 1972). The impact of (oceanic) SST on (atmospheric) precipitation over the surrounding continents is mediated by the close relationship between tropical SST variability and the meridional position of the ITCZ (e.g. Harzallah, Rocha de Aragão, and Sadourny, 1996).

1.2 Dynamics of the Atlantic Niño

The Atlantic Niño is intimately related to the seasonal cycle of the equatorial Atlantic. Below, the background state on which the Atlantic Niño acts is briefly introduced, and the main mechanisms that have been proposed to explain the characteristics of the Atlantic Niño are discussed.

1.2.1 Background state

The basic characteristics of the equatorial Atlantic are related to its unique location on earth. The tropics receive the most insolation on the planet, setting up the easterly trade wind regimes in both hemispheres. The trade wind regimes converge in the intertropical convergence zone (ITCZ), creating a band of intense precipitation. Due to air-sea interaction and the shape of the West-African shoreline, the Atlantic marine ITCZ resides north of the equator on average (Xie and Carton, 2004). Direct wind forcing and interhemispheric thermohaline forcing create an intricate current system that consists of (i) a system of alternating zonal surface currents (e.g. Brandt et al., 2006; Schott et al., 2003; Stramma and Schott, 1999), (ii) the superimposed circulation of the shallow subtropical cells (McCreary and Lu, 1994), and (iii) the subsurface Equatorial Undercurrent (EUC) (Cromwell, 1953; Cromwell, Montgomery, and Stroup, 1954), one of the most intense currents on the planet. Additionally, the vanishing Coriolis force allows the easterly wind stress forcing to push warm surface water towards the western basin, piling up the Atlantic warm pool. The equatorial Atlantic thermocline slopes upward, from being relatively deep in the western warm pool region to being relatively shallow in the central and eastern equatorial Atlantic. At the surface, the uneven distribution of heat content creates a pronounced zonal SST gradient. Warm pool waters in the west reach surface temperatures of up to $28°C$, while the eastern and central equatorial basin – depleted of warm surface waters and additionally cooled by upwelling – provide annual mean SSTs of approximately $26°C$.

This basic set-up varies considerably over the course of the year. Air-sea interaction and a number of seasonal processes act in concert to establish the seasonal cycles of the meridional location of the ITCZ, the strength of the trade wind regimes and hence easterly wind forcing, the configuration of the equatorial current system, and the distribution of heat content and SST along the equator. The dominant feature of the coupled seasonal cycle is the formation of the Atlantic cold tongue in boreal summer. Within a few months, SSTs in the central equatorial Atlantic drop, on average, from $28.5°C$ in April to $24.5°C$ in August, forming a distinct tongue of cold water that resembles the shape of the Atlantic Niño pattern.

Dippe et al. (2018) review the physics of the equatorial Atlantic seasonal cycle in detail. In boreal spring, the cross-equatorial meridional SST gradient is smallest, and the ITCZ resides in its southernmost position almost directly on the equator. Until boreal summer, the ITCZ migrates north and pulls the trade wind regime of the southern hemisphere

across the equator into the northern hemisphere. Easterly wind stress forcing in the western ocean basin intensifies, creating upwelling Kelvin waves that propagate along the thermocline to the east, thinning out the mixed layer in the central Atlantic (e.g. Merle, 1980). Under these conditions, climatological upwelling at the base of the mixed layer cools the mixed layer more efficiently, and the first cooling signals appear along the central and eastern equator in late boreal spring. Simultaneously, the West African Monsoon sets in (e.g. Caniaux et al., 2011; Okumura and Xie, 2004). Northward meridional wind stress forcing in the Gulf of Guinea strengthens, intensifying upwelling in the eastern equatorial Atlantic just to the south of the equator and providing additional cooling to the incipient cold tongue. Last, the relative strengths of the westward surface current and the eastward EUC vary over the course of the year as well, producing the strongest shear in boreal spring (e.g. Hazeleger and Haarsma, 2005; Hummels, Dengler, and Bourlès, 2013; Hummels et al., 2014; Jouanno et al., 2011). As a result, more cold subsurface water is mixed into the mixed layer in the central and eastern equatorial Atlantic, contributing to SST cooling.

Once the initial seasonal cooling is established in the equatorial Atlantic, the Bjerknes feedback sets in and quickly grows the incipient cold tongue (e.g. Burls et al., 2011; Keenlyside and Latif, 2007, see Section 1.2.2 for details). In August, the feedback breaks down, and the cold tongue dissipates.

The Atlantic Niño is a modulation of the seasonal cycle outlined above. The next subsections discuss the two main mechanisms that have been proposed to explain these interannual variations.

1.2.2 The Bjerknes feedback as the main driver of Atlantic Niño variability

In the canonical approach, the Atlantic Niño is driven by dynamical processes that weave atmospheric and oceanic variability into one coupled phenomenon (e.g. Burls et al., 2012; Keenlyside and Latif, 2007; Lübbecke and McPhaden, 2013; Zebiak, 1993). The basic framework of this approach is the Bjerknes feedback.

The Bjerknes feedback is the dominant, positive feedback in the equatorial oceans (Bjerknes, 1966; Bjerknes, 1969). It couples atmospheric and oceanic variability in an equatorial ocean basin by relating three key parameters to each other: SST in the eastern ocean basin, zonal surface wind in the western basin, and thermocline depth along the equator. Because the Bjerknes feedback requires the Coriolis force to vanish, it operates exclusively in the equatorial ocean basins.

Numerous studies have documented that the Bjerknes feedback is active in the Atlantic, both in observations (Carton and Huang, 1994; Keenlyside and Latif, 2007) and modelling studies (Burls et al., 2011; Deppenmeier, Haarsma, and Hazeleger, 2016; Jansen, Dommenget, and Keenlyside, 2009; Lübbecke and McPhaden, 2013). In contrast to the Pacific, the Atlantic Bjerknes feedback is involved with the seasonal cycle by supporting the growth of the Atlantic cold tongue. Keenlyside and Latif (2007) and Burls et al. (2011)

show that the feedback is active during boreal summer and again, weakly, during early boreal winter. Based on this, Burls et al. (2012) argue that the Atlantic summer Niño arises from a modulation of the seasonally active Atlantic Bjerknes feedback. An enhanced Bjerknes feedback produces more intense cold tongues and hence cold Atlantic Niño events ("Niñas"), while a weak Bjerknes feedback grows a weak cold tongue associated with a warm Atlantic Niño event.

Placing the equatorial Bjerknes feedback into a wider context, Lübbecke et al. (2010), Lübbecke et al. (2014) and Nnamchi et al. (2016) argue that the Atlantic Niño is the equatorial manifestation of a basin-wide mode of variability that spans the Atlantic ocean of the southern hemisphere. Lübbecke et al. (2010) show that SST events in the Angola Benguela frontal zone off the Angolan coast are dynamically linked to equatorial Niño events by wind-induced Kelvin waves that propagate first along the equatorial thermocline, then continue southwards along the African coast. Additionally, their study demonstrates that wind variability in the western equatorial Atlantic – a crucial element of the Bjerknes feedback – is related to the variability of the South Atlantic (Saint Helena) Anticyclone in boreal spring. Lübbecke et al. (2014) expand this work and expose the relationship between the South Atlantic Anticyclone and the wind variability associated with the Atlantic Niño. However, they point out that this physical link is not present in all years, providing an extra-tropical connection for only about half of the investigated Atlantic Niño events. In agreement with this, Richter et al. (2014a) suggest that (a substantial) part of western equatorial wind variability during boreal spring is associated with internal atmospheric variability. Finally, Nnamchi et al. (2016) argue that the Atlantic Niño is the intrinsic equatorial arm of the South Atlantic Ocean Dipole, a mode of variability that includes a second center of SST variability in the southwestern Atlantic and is maintained by a feedback between wind, evaporation, and SST (WES feedback, Xie and Philander, 1994).

1.2.3 Alternative mechanisms

Richter et al. (2013) show that some warm Atlantic Niño events do not conform with the Bjerknes feedback. Indeed, instead of being associated with weak trade winds in the western basin during boreal spring, they are preceded by anomalously strong trade winds. The authors demonstrate that meridional advection from the northern hemisphere contributes to these non-canonical warm events, establishing a direct link between equatorial and subtropical Atlantic variability. In a related study about the non-canonical cold event of 2009, Burmeister, Brandt, and Lübbecke (2016) show that the reflection of Rossby waves at the western boundary can contribute to non-canonical events as well. These results agree with Foltz and McPhaden (2010a,b), who argue that meridional mode events in boreal spring can precondition the equatorial Atlantic for Niño events that do not rely on the Bjerknes feedback as their main driver.

Brandt et al. (2011) propose that Atlantic equatorial variability is additionally influenced by the deep equatorial ocean. (A direct link to the Atlantic Niño in boreal summer,

however, has yet to be demonstrated). They show that surface variability in the eastern equatorial Atlantic shares the 4.5-yr period of the Atlantic equatorial deep jets. The deep jets are vertically stacked zonal jets of small vertical wavelength that propagate their energy upwards and can reach velocities of more than $10cms^{-1}$ (e.g. Claus, Greatbatch, and Brandt, 2014).

Last, Nnamchi et al. (2015) raise the controversial hypothesis that the Atlantic Niño does not rely on ocean dynamics but is rather driven by stochastically excited thermodynamic feedbacks. Using slab ocean simulations contributing to the third phase of the Coupled Model Intercomparison Project (CMIP3, Meehl et al., 2007), they argue that wind and subsequent heat flux perturbations agree with a first-order auto-regressive model, challenging the paradigm of the dynamically driven Atlantic Niño. The Bjerknes feedback, they hypothesise, enhances the Niño-like spatial characteristics of the Atlantic Niño but is not instrumental in generating the variability in the first place.

The wealth of hypotheses about the nature of the Atlantic Niño demonstrates how complex a phenomenon it is. With respect to this, Zebiak (1993) argues in his early modelling work that equatorial dynamics seem to play "an important but not exclusive role" in establishing the Atlantic Niño. He writes: "It appears that the coupling is sufficiently strong to leave its imprint on the total variability, but too weak to dictate it entirely, even at the equator."

1.3 The Atlantic and Pacific Niños: A comparison

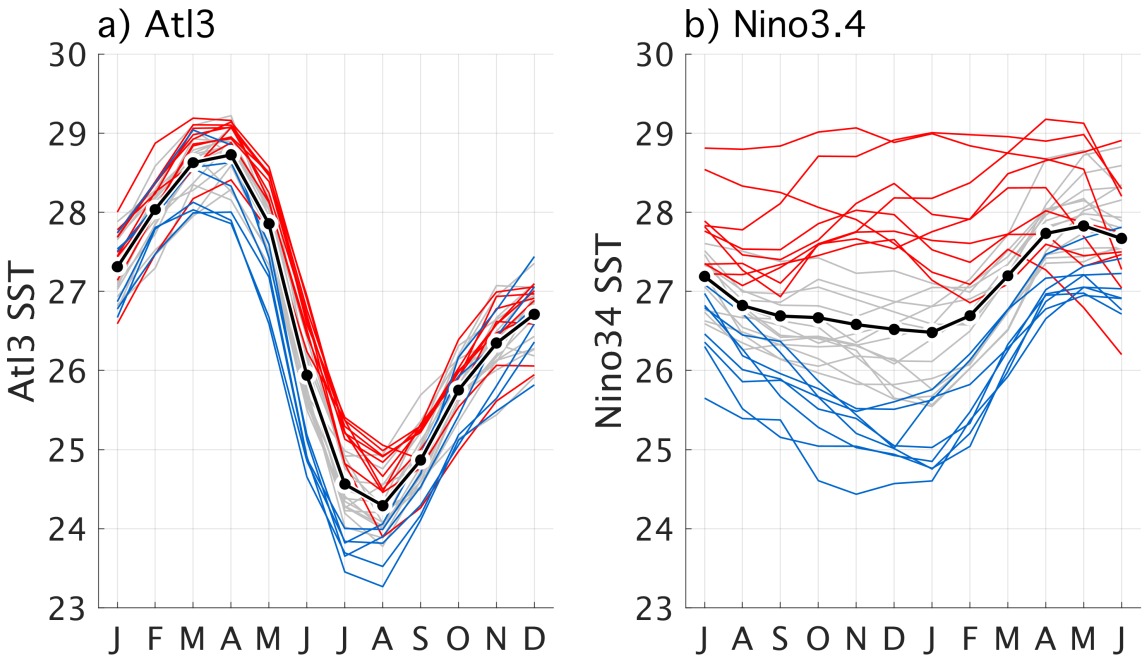

Figure 1.3: *Seasonal cycle and evolution of individual warm and cold Niño events in a) the Atlantic Atl3 region (3°S to 3°N, 20°W to 0°E) and b) the Pacific Nino3.4 region (5°S to 5°N, 170 to 120°W). Event years were diagnosed as in Fig. 1.1. For the Pacific, the Niño time series includes monthly mean SST from November, December, and the subsequent January. During the analysis period nine warm events (El Niños, 1982/83, 1986/87, 1987/88, 1991/92, 1994/95, 1997/98, 2002/03, 2006/07, and 2009/10) and eight cold events (La Niñas, 1983/84, 1984/85, 1988/89, 1998/99, 1999/2000, 2007/08, 2010/11, and 2011/12) were detected. The black line indicates the climatological seasonal cycle. Thin red, blue, and grey lines trace the evolution of individual warm, cold, and neutral events over the course of the year during which the event occurred. Note that an "event year" lasts from January to December in the Atlantic, but from July to the subsequent June in the Pacific, due to the seasonal phase-locking of ENSO to boreal winter (see different x-axes).*

The Atlantic and the Pacific share many attributes. Both basins have similar physical set-ups consisting of easterly trade wind regimes in both hemispheres, quasi-uninterrupted easterly wind forcing on the equator, and a pronounced zonal equatorial SST gradient arising from the contrast of a western warm pool and a seasonally strengthening cold tongue in the central-to-eastern ocean basin. Additionally, both basins are dominated by a "Niño" on interannual time scales, a coupled mode of variability that is strongest in the eastern ocean basin and stretches south and eastward along the continental coast.

However, important differences between the two basins exist. Their zonal extent differs – the equatorial Pacific spans roughly 140° longitude, more than a third of Earth's circumference, while the Atlantic extents across 60° longitude –, as are the characteristics

of their cold tongues. The Pacific cold tongue is most pronounced in boreal winter (e.g. Fu and B. Wang, 2001; Horel, 1982; Mitchell and Wallace, 1992; Wyrtki, 1965), offset against the Atlantic cold tongue by approximately five months (cf. seasonal cycles in Fig. 1.3). Zebiak (1993) argues that these distinctions are due to both differences in the basin geometries and their climatological mean fields.

The Niños of the two basins are distinct from each other as well (e.g. Keenlyside and Latif, 2007; Lübbecke and McPhaden, 2012; Richter et al., 2013). Figure 1.3 summarises the main differences between them. Pacific Niños are phase-locked to boreal winter and last several months, while the Atlantic Niño occurs in boreal summer and rarely outlasts a season. This is shown by the clear separation of warm and cold events that lasts from May to July in the Atlantic, but persists from at least July to the following May in the Pacific. The Pacific Niño overrides the seasonal cycle, particularly for warm events (thin red lines in Fig. 1.3b). The Atlantic seasonal cycle on the other hand always dominates the evolution of SST over the course of a year, regardless of whether a Niño occurs (Fig. 1.3a). Amplitudes of the SST signal in the Atlantic are about $30 - 50\%$ of their Pacific counterparts (a maximum of $1°C$ in the Atlantic versus $3°C$ in the Pacific). Last, (linear) stability analysis suggests that the equatorial climate system in the Atlantic is more stable than in the Pacific (Keenlyside and Latif, 2007; Lübbecke and McPhaden, 2013; Xie et al., 1999; Zhu, Huang, and Wu, 2012).

1.4 Modelling and predicting the Atlantic Niño: Facing the challenge of the equatorial Atlantic warm bias

Simulating the Atlantic Niño continues to pose substantial challenges to the scientific community. A major reason for this is that virtually all state-of-the-art coupled global climate models (CGCMs) suffer from a severe warm bias in the equatorial Atlantic.

A bias is a systematic difference between the modelled and the observed climate. Biases can affect any statistical property of any model variable. SST in a given location, for example, could be biased with respect to the (annual) mean, or its (monthly) variance or skewness, among other things. In these cases, SST would be too warm or too cold in general, produce anomalies that are generally too strong or too weak, or favour one type of anomalies over the other in a way that is inconsistent with observations.

Biases can have various causes. Mulholland et al. (2017), for example, assess the impact of globally applied model parameterisations on the development of regional biases. By training a neural network on a set of crowd-funded, perturbed physics simulations that span a large space of parameterisation settings, they were able to trace the manifestation of a given bias to a set of parameterisations, and hence a specific set of physical short-comings of the model. In general, the development of a bias is associated with mis-representations of physical processes within the model world.

Climatological SST is a notoriously biased variable in CGCMs. Figure 1.4a shows the annual mean SST bias of a suite of CGCMs that participated in the fifth phase of the Coupled Model Intercomparison Project (CMIP5, Taylor, Stouffer, and Meehl, 2012). Evidently, SST biases are abundant in the modelled ocean. Key features that are present in virtually every current-generation CGCM are the severe warm biases in the western subtropical ocean basins that reach annual mean amplitudes of up to $5°C$ (Richter and Xie, 2008; Richter et al., 2014b). In the Atlantic, the spatial characteristics of the mean bias are comparable to the structure of the Atlantic Niño. The bias is strongest off the Namibian coast in the area of the Angola-Benguela front, with CMIP5-mean values exceeding $5°C$. It stretches northwestward into the central equatorial Atlantic, producing an equatorial warm bias with mean amplitudes of $1 - 2°C$.

As in the real world, the mean state of a CGCM varies over the course of the year. Consequently, a bias, too, can have a seasonal cycle. Figure 1.4b illustrates the seasonal cycle of the Atlantic warm bias in a standard run of the Kiel Climate Model (KCM, Dippe, Greatbatch, and Ding, 2018; Park et al., 2009) that consists of three ensemble members. The bias is measured in the crucial, central equatorial region Atl3[3]. It is relatively small at the beginning of the year in the KCM, producing amplitudes that are hardly larger than $1°C$. Interestingly, as in observations, the biased KCM starts cooling the equatorial Atlantic in April, but is not able to sustain the intense cooling associated with the cold

[3]Atl3 is the Atlantic equivalent of the Pacific Nino3.4 region, the area in which ocean-atmosphere coupling is most vigorous. Atl3 spans the area $3°S$ to $3°N$, and $20°W$ to $0°E$.

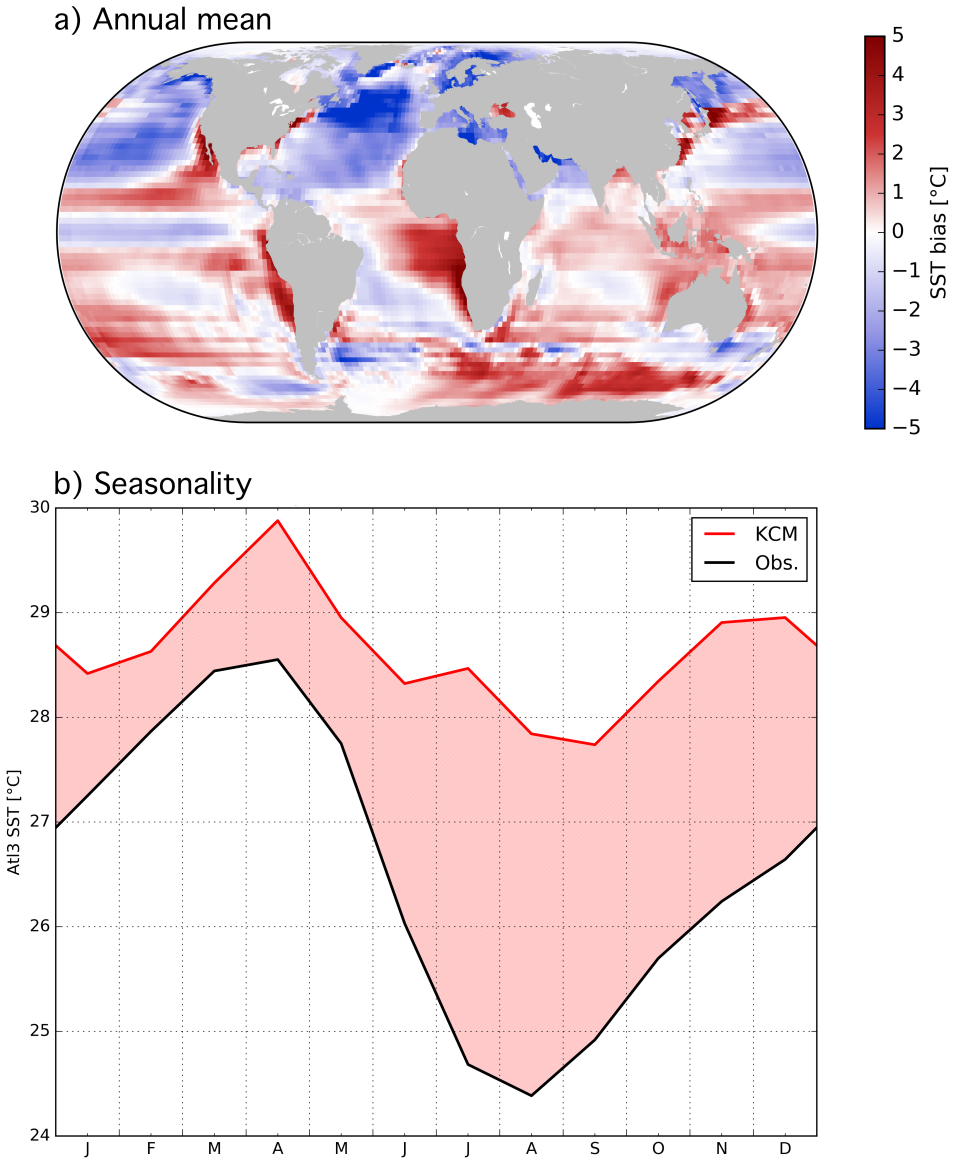

Figure 1.4: *The equatorial Atlantic warm bias, diagnosed with respect to NOAA's observational OISST dataset (Banzon et al., 2016; Reynolds et al., 2007) for the period 1982-2009. a) Annual mean SST bias of the ensemble mean of 33 CGCMs contributing to CMIP5. b) Seasonal cycle of the SST bias in the Atlantic Atl3-region in a standard integration of the Kiel Climate Model (KCM, red), relative to OISST (black). Both Figures from Dippe et al. (2018).*

tongue formation after May. In July and August, when the observed cold tongue is fully developed, the KCM's warm bias exceeds $3°C$. The KCM has failed to establish the Atlantic cold tongue.

A host of research has addressed the dynamics of the equatorial Atlantic warm bias. Because the atmosphere and the ocean are tightly coupled in the equatorial Atlantic, too-warm SSTs are only one symptom of a coupled bias that links systematic errors in the ocean and atmosphere and enhances them via a feedback mechanism akin to the Bjerknes feedback.

Many studies emphasise the importance of a pronounced westerly wind bias in the western equatorial Atlantic for the development of the equatorial warm bias (Richter et al., 2012). The westerly wind bias weakens the trade wind regime by substantially reducing the strength of the easterly surface winds. When the bias is most pronounced in boreal spring, it can reverse the direction of the zonal wind, turning easterly into weakly westerly wind stress forcing. The reduced surface wind is in agreement with a systematic southward displacement of the ITCZ (e.g. Doi et al., 2012; Richter et al., 2012; Siongco, Hohenegger, and Stevens, 2015) and has been linked to a seesaw pattern of precipitation biases over South America and Africa (C. Y. Chang et al., 2007; Patricola et al., 2012; Richter et al., 2014b, 2012). Biased precipitation is related to systematic errors in tropical deep convection, which in turn affects the gradient of surface pressure along the equator. The equatorial wind field adapts to the anomalous surface pressure and as a result produces the westerly wind bias.

The westerly wind bias is present in forced atmospheric simulations. It is an intrinsic feature of most state-of-the-art atmosphere general circulation models (e.g. Harlaß, Latif, and Park, 2017; Richter et al., 2014b).

In the strongly coupled equatorial Atlantic, the ocean adapts to the weak equatorial winds and develops consistent oceanic biases. In agreement with reduced zonal wind stress forcing, oceanic heat content is distributed more evenly along the equator, and the western Atlantic warm pool is displaced towards the central ocean basin (C. Y. Chang et al., 2007; Liu et al., 2013; Richter and Xie, 2008). The modelled thermocline is deeper than in observations. Strengthening equatorial westerlies in late boreal spring are not sufficient to shoal the thermocline in the central basin, and the initial cooling that sets off the formation of Atlantic cold tongue cannot be established. The westerly wind bias keeps the seasonal variations of surface wind stress in the western ocean basin from preconditioning the central equatorial Atlantic for the formation of the cold tongue.

While the westerly wind bias is a key ingredient of the equatorial Atlantic warm bias, the ocean models used in CGCMs are not free of error, either. For example, Grodsky et al. (2012) show that forced ocean simulations in the tropical Atlantic are intrinsically biased as well. Feedback processes between the atmosphere and the ocean amplify the intrinsic biases of the stand-alone models and produce a severely biased system that is inconsistent with the physical processes observed in the real world.

Based on a biased background that is unable to establish the Atlantic cold tongue, past attempts to seasonally predict the variability of the Atlantic Niño have not been successful (Hu and Huang, 2007; Kushnir et al., 2006; Stockdale, Balmaseda, and Vidard, 2006). While many studies have proposed methods to alleviate the equatorial Atlantic warm bias in a physically consistent way (e.g. DeWitt, 2005; Harlaß, Latif, and Park, 2015; Richter et al., 2014a,b; Tozuka et al., 2011; Voldoire et al., 2014; Zermeño-Diaz and Zhang, 2013), whether reducing the equatorial Atlantic warm bias will unlock additional predictive potential is under debate.

1.5 Research questions of this thesis

A NUMBER OF MECHANISMS HAVE BEEN PROPOSED to explain the Atlantic Niño. The majority of existing research supports a dynamical Niño that is mainly driven by the Bjerknes feedback (Burls et al., 2012; Carton et al., 1996; Keenlyside and Latif, 2007; Zebiak, 1993). Nnamchi et al. (2015), on the other hand, argue that the Atlantic Niño is a product of stochastic processes, discounting the role of dynamical ocean processes. Chapter 2 seeks to reconcile these two approaches and raises the question

- **How dynamical is the Atlantic Niño?**

The dynamical interpretation of the Atlantic Niño relies on the framework of the Bjerknes feedback, which also supports the growth of the Pacific Niño. Chapter 3 takes a closer look at the Bjerknes feedbacks in the two basins and asks

- **How symmetric are the Atlantic and Pacific Bjerknes feedbacks? Are they stationary on decadal time scales?**

Chapter 4 reviews the equatorial Atlantic warm bias and attempts to synthesise from current research an answer to the question

- **What drives the development of the equatorial Atlantic warm bias?**

Last, Chapter 5 assesses the impact of the equatorial warm bias on the predictability of the Atlantic Niño, asking

- **Does the equatorial Atlantic warm bias affect the ability of a model to predict the Atlantic Niño?**

Chapter 2

On the Dynamics of the Atlantic Niño

Previous studies on the mechanisms generating and sustaining an Atlantic Niño event have identified numerous processes, both dynamical and stochastic in nature. Here, the relative contributions of ocean dynamics and residual stochastic processes to SST variability in the equatorial Atlantic are assessed.

Citation: **Dippe, T., R. J. Greatbatch, and H. Ding (2018). "On the relationship between Atlantic Niño variability and ocean dynamics". In: *Climate Dynamics* 51.1, pp. 597-612. DOI:** `10.1007/s00382-017-3943-z`

The candidate's contributions to this manuscript are as follows. She

- Conceived the basic question that is discussed in the manuscript;
- Developed the statistical method to answer the research question;
- Performed all the analyses;
- Produced all the figures;
- Authored the manuscript from first to final draft.

Clim Dyn
DOI 10.1007/s00382-017-3943-z

On the relationship between Atlantic Niño variability and ocean dynamics

Tina Dippe[1] · **Richard J. Greatbatch**[1,2] · **Hui Ding**[3]

Received: 21 December 2016 / Accepted: 30 September 2017

Abstract The Atlantic Niño is the dominant mode of interannual sea surface temperature (SST) variability in the eastern equatorial Atlantic. Current coupled global climate models struggle to reproduce its variability. This is thought to be partly related to an equatorial SST bias that inhibits summer cold tongue growth. Here, we address the question whether the equatorial SST bias affects the ability of a coupled global climate model to produce realistic dynamical SST variability. We assess this by decomposing SST variability into dynamical and stochastic components. To compare our model results with observations, we employ empirical linear models of dynamical SST that, based on the Bjerknes feedback, use the two predictors sea surface height and zonal surface wind. We find that observed dynamical SST variance shows a pronounced seasonal cycle. It peaks during the active phase of the Atlantic Niño and is then roughly 4–7 times larger than stochastic SST variance. This indicates that the Atlantic Niño is a dynamical phenomenon that is related to the Bjerknes feedback. In the coupled model, the SST bias suppresses the summer peak in dynamical SST variance. Bias reduction, however, improves the representation of the seasonal cold tongue and enhances dynamical SST variability by supplying a background state that allows key feedbacks of the tropical ocean–atmosphere system to operate in the model. Due to the small zonal extent of the equatorial Atlantic, the observed Bjerknes feedback acts quasi-instantaneously during the dynamically active periods of boreal summer and early boreal winter. Then, all elements of the observed Bjerknes feedback operate simultaneously. The model cannot reproduce this, although it hints at a better performance when using bias reduction.

1 Introduction

The Atlantic Niño is the dominant mode of interannual variability in equatorial Atlantic sea surface temperature (SST). It modulates the seasonal development of the equatorial Atlantic cold tongue and peaks during May–August (Xie and Carton 2004). Similar to other modes of equatorial SST variability, it is the source of a number of teleconnections (e.g. Janicot et al. 1998; Mohino and Losada 2015), both regionally and globally. Through its close relationship with the Inter-Tropical Convergence Zone, it especially affects rainfall variability over the surrounding continents, exerting an important socio-economic impact (Hirst and Hastenrath 1983).

Efforts to simulate and predict equatorial Atlantic seasonal-to-interannual SST variability with state-of-the-art coupled global climate models (CGCMs) have not been very successful (Stockdale et al. 2006; Kushnir et al. 2006; Hu and Huang 2007). One reason for this is that most CGCMs suffer from a strong coupled bias in the tropical eastern Atlantic (e.g. Richter and Xie 2008; Grodsky et al. 2012; Wang et al. 2014). The SST signature of this bias stretches from the coast of Namibia and Angola into the equatorial Atlantic and is well established in the cold tongue region in the annual mean. Chang et al. (2007) and Richter et al. (2012) show that the equatorial SST bias is associated with

✉ Tina Dippe
tdippe@geomar.de

[1] GEOMAR Helmholtz Centre for Ocean Research Kiel, Kiel, Germany

[2] Faculty of Mathematics and Natural Sciences, Christian Albrechts University, Kiel, Germany

[3] Cooperate Institute for Research in Environmental Sciences, University of Colorado and NOAA Earth Systems Research Laboratory, Boulder, USA

Published online: 28 October 2017

a fundamentally biased mean state in this region. The pool of warm surface waters that is observed in the western ocean basin shifts into the central ocean basin in biased simulations. The thermocline in the cold tongue region deepens, and upwelling is strongly reduced. The Atlantic cold tongue—the dominant feature of the SST seasonal cycle in the tropical Atlantic—cannot be established. Without a realistic cold tongue, however, CGCMs struggle to capture the observed Atlantic Niño, even in the presence of realistic forcing. Another factor that likely contributes to the models' problems is that the dynamical nature of the Atlantic Niño is not yet fully understood.

While the name Atlantic "Niño" suggests a phenomenon that is essentially an Atlantic version of the Pacific El Niño-Southern Oscillation (ENSO), a number of differences exist between the two phenomena (e.g. Keenlyside and Latif 2007; Burls et al. 2011; Lübbecke and McPhaden 2012; Richter et al. 2013). Obvious are the differences in timing characteristics: Both positive and negative ENSO events generally peak in boreal winter and last for several months and in some cases even longer than a year. Atlantic Niño events on the other hand are phase-locked to boreal summer and rarely outlast a season. They have a smaller amplitude than their Pacific counterparts and appear to be the result of weaker atmosphere–ocean coupling. Additionally, while the canonical ENSO agrees with a self-sustained mode in the tropical Pacific, the Atlantic Niño requires external excitation (Zhu et al. 2012).

The dominant process that couples equatorial atmospheric and oceanic variability is the Bjerknes feedback (Bjerknes 1969). In a positive feedback, it relates SST and thermocline variability in the eastern ocean basin to zonal surface wind variability in the western ocean basin (u10) and lends growth to the Pacific (Bjerknes 1969) and Atlantic Niños (e.g. Keenlyside and Latif 2007; Burls et al. 2012; Lübbecke and McPhaden 2013; Deppenmeier et al. 2016). Traditionally, three elements of the Bjerknes feedback are considered when assessing the overall strength of the feedback: (1) Eastern ocean basin SST anomalies force u10 anomalies in the western ocean basin, (2) u10 anomalies trigger a thermocline response across the basin that can be measured via thermocline variability in the eastern ocean basin, and (3) eastern basin thermocline anomalies amplify the initial SST anomaly. A closed Bjerknes feedback loop is present when all three elements of the Bjerknes feedback are active simultaneously.

Note, however, that the simplified Bjerknes feedback outlined above is not the only process that acts in the equatorial oceans. Specifically, the "forcing direction" in the feedback elements (1)–(3) is not strict. In the closely coupled system of the equatorial oceans, wind variability in the western ocean basin for example can feed back directly to SST variability via the zonal advection feedback (e.g. Dijkstra 2006). Nevertheless, for the purpose of this study we will rely mainly on the dynamical framework of the simplified Bjerknes feedback.

An important aspect of the Bjerknes feedback is that it must not necessarily act instantaneously. This means that the individual elements of the Bjerknes feedback may be delayed (note that this delay within the positive Bjerknes feedback is not identical with the range of delayed negative feedbacks discussed in Neelin et al. (1998) that ultimately stop anomaly growth in the eastern ocean basin during an El Niño or La Niña event). Physically, the delay within the elements of the positive Bjerknes feedback is due to the fact that information about anomalies on one side of the ocean basin need to be transmitted across the basin to be able to affect the other side. In the atmosphere, this is done via relatively quick atmospheric adjustment to eastern ocean basin SST anomalies, which in turn produce anomalous zonal pressure gradients and result in western ocean basin zonal wind anomalies. In the ocean, zonal wind stress anomalies are translated into equatorial Kelvin waves (e.g. Dijkstra 2006). These Kelvin waves than travel westward across the ocean basin and feed the information about the wind variability in the west to the eastern ocean basin. Depending on the width of the ocean basin, the Kelvin wave transmission can happen on a time scale on the order of months. In the tropical Atlantic, Keenlyside and Latif (2007) and Richter et al. (2013), among others, have shown that wind variability in the western ocean basin precedes SST variability in the eastern ocean basin by about 1 month in boreal spring. In the tropical Pacific, this delay is longer due to the larger basin size.

Returning to the dynamical nature of the Atlantic Niño in comparison to ENSO events, Burls et al. (2011) show that the Atlantic and Pacific Niños rely on the Bjerknes feedback in subtly different ways. The Pacific Niño generally is the result of a free mode of interannual variability that is driven by the Bjerknes feedback; interactions with the seasonal cycle occur, but do not dominate ENSO SST variability. In the tropical Atlantic, on the other hand, the Bjerknes feedback is seasonally active (Richter 2016). It helps to develop the cold tongue and is involved in establishing the seasonal cycle. Burls et al. (2012) argue that the Atlantic Niño hence reflects a modulation of the seasonally active Bjerknes feedback instead of an independent mode of interannual variability.

Lastly, and in contrast to numerous studies that have provided evidence for a relationship between Atlantic Niño variability and the Atlantic Bjerknes feedback, Nnamchi et al. (2015, 2016) have proposed that the Atlantic Niño is essentially driven by stochastic processes in the atmosphere rather than by dynamical ocean processes that are potentially predictable. Likewise, Richter et al. (2014b) present

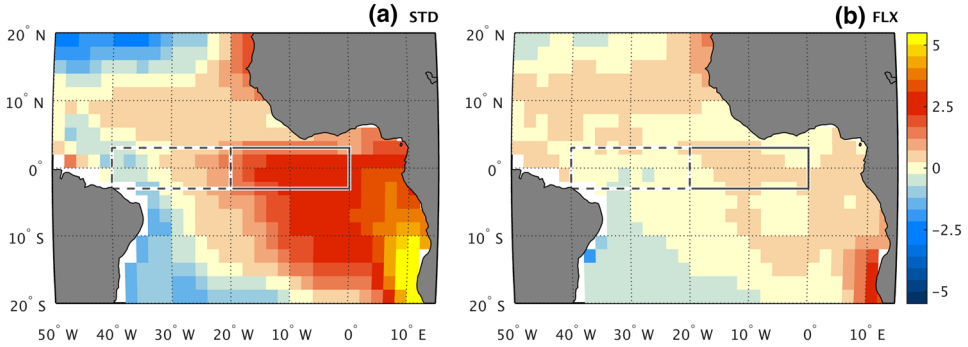

Fig. 1 Annual mean SST bias relative to ERA-Interim SST in the **a** STD and **b** FLX assimilation runs in the tropical Atlantic. Positive values indicate that the model climatology is too warm. Solid (dashed) boxes show the Atl3 (WAtl) region

evidence for a significant stochastic component of Niño-like variability in the tropical Atlantic.

Here, we address two questions. First, do dynamical processes contribute to SST variability in the tropical Atlantic? Is there a seasonality to the ratio of dynamical and stochastic contributions? And second, does the presence of the SST bias—and hence the flawed mean state and missing summer cold tongue—affect the models' ability to accurately reproduce the observed dynamical SST variance? To answer these questions, we use two assimilation runs of the Kiel Climate Model (KCM) as well as reanalysis data and decompose SST variance into a part that is due to dynamical processes in the ocean and a stochastic part that is driven by noise.

The rest of the paper is structured as follows: Sect. 2 sketches the Kiel Climate Model and the method that we used to produce our assimilation runs, Sect. 3 reviews the assimilation runs with respect to the impact of the equatorial Atlantic SST bias. Section 4 presents our SST variance decomposition method; results for our assimilation runs and observations are compared in Sect. 5. Section 6 discusses the impact of lagged feedbacks on our results. A summary and discussion of the results is provided in Sect. 7.

2 Model and methods

To compare our results with the evolution of the observed climate system, we use the ERA-Interim (Dee 2011) and the Archiving, Validation, and Interpretation of Satellite Oceanographic (AVISO) datasets. We find that differences between ERA-Interim SST and other SST datasets are negligibly small. (Analysis results for alternative validation datasets such as the HadISST dataset (Rayner et al. 2003) are not shown. They differ from the analysis with respect to ERA-Interim only in details.) Furthermore, our variance decomposition approach requires additional surface zonal wind (u10) and sea surface height (SSH) data. We use u10 provided by ERA-Interim for the period 1981–2012, and the AVISO monthly mean SSH anomaly dataset for the period 1993–2012. Throughout this study, we refer to ERA-Interim (AVISO) when we discuss an "observed" feature of SST and u10 (SSH).

Figure 1 shows important regions for our study as boxes. Atl3 spans the region 3°S–3°N, 20°W–0°E and is the Atlantic counterpart to the Pacific Nino3.4-region. It is the part of the equatorial Atlantic in which ocean–atmosphere coupling is most vigorous and that is hence used to assess SST variability associated with the Atlantic Niño. It is also the region in which the cold tongue is most pronounced in boreal summer. To the west of Atl3 is the western Atlantic region WAtl (3°S–3°N, 40– 20°W). In terms of the Bjerknes feedback, WAtl is crucial for the wind stress contributions to the feedback.

Model runs were performed with the Kiel Climate Model (KCM, Park et al. 2009), a coupled global climate model (CGCM). We used a low-resolution version of the KCM. The atmospheric component ECHAM5 (Roeckner et al. 2003) is run with 19 vertical levels in T31 horizontal resolution. The ocean component of the NEMO model (Océan Parallelisé Version 9, OPA9 Madec et al. 1998; Madec 2008) is run in the ORCA2-setup. ORCA2 has 31 vertical levels and an average horizontal resolution of 1.3°. Towards the equator, the horizontal resolution is refined to 0.5°. The model uses seasonally varying radiative forcing that corresponds to mid-twentieth century conditions. In particular, changes in greenhouse gas concentrations and aerosol loading are not considered.

We conducted two sets of experiments. The first set uses a standard version of the KCM ("STD"). The STD-SST climatology contains the SST bias in the southern subtropical Atlantic (Fig. 1), which is qualitatively comparable to the bias in other CGCMs (shown for example by Davey 2002; Richter and Xie 2008). The second experiment employs additional surface heat flux correction ("FLX", see below for details) to reduce the SST bias. We run three and eight ensemble members for the STD and FLX experiments runs, respectively. All ensemble members use the same wind stress forcing (see below), but differ in their initial conditions, which are taken from a control run at a time when the model is close to equilibrium.

The STD and FLX experiments were run in partially coupled mode. Partial coupling is an assimilation technique that seeks to minimize the equatorial initialization shock in fully coupled hindcasts when they are started from partially coupled initial conditions (e.g. Ding et al. 2013; Thoma et al. 2015). In a partially coupled model the ocean and sea ice components are forced with observed wind stress anomalies that are added to the model's monthly mean wind stress climatology. All other aspects of the model are identical to the fully coupled model. In particular, thermal coupling between the ocean and the atmosphere is preserved, and SST and the atmospheric wind field remain fully prognostic variables.

Surface heat flux correction is employed in the FLX experiment to reduce the SST bias of the KCM. To diagnose the heat flux correction, we use the same methodology as Ding et al. (2015): During a control integration, we nudge the first ocean level of the model towards the monthly climatology of observed SST with a restoring time scale of 10 days. After 470 years, when the model has reached an equilibrium state, we continue our integration for another 70 years to diagnose the monthly climatological heat flux term that is associated with the SST restoring. This climatology of the "heat flux correction" is then added as a non-flow-interactive correction to the SST tendency while integrating the heat-flux corrected version of the KCM. For an overview of the performance of the two experiments in the equatorial Atlantic and the impact of the bias on the coupled system, refer to Sect. 3. Here, we note that Ding et al. (2015) showed a substantial improvement in the ability of the partially coupled model runs to reproduce observed SST variability in boreal summer in FLX compared to STD.

Monthly anomalies for the model integrations and validation datasets are calculated by detrending the data via least-squares fitting, applied to each month separately. Note that we did not subtract the seasonal cycle from the monthly data prior to the detrending, since it did not yield qualitatively different results. We chose this method to not only calculate our anomalies relative to a static seasonal cycle but allow the possibility that the seasonal cycle itself may vary (linearly) on long time scales. The analysis period is 1981–2012 (1993–2012) for ERA-Interim and the KCM experiments (AVISO). For the KCM experiments, we detrend each ensemble member separately. The ensemble mean monthly anomaly is the average of the monthly anomalies of all ensemble members.

3 Impact of the coupled bias on the equatorial Atlantic

In this section, we assess SST and zonal wind biases in the tropical Atlantic for our KCM experiments. Because all ensemble members for both the STD and FLX assimilation

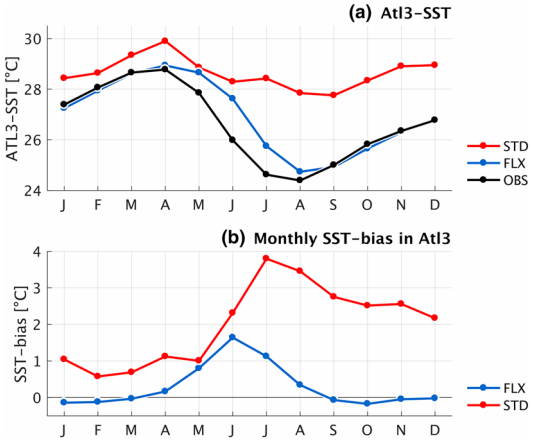

Fig. 2 **a** Seasonal cycle of SST in Atl3 for (black) ERA-Interim, (red) STD, and (blue) FLX for 1981–2012. **b** Monthly mean bias of Atl3 SST for (red) STD and (blue) FLX

experiments share their forcing of observed wind stress anomalies, the only difference between the ensemble means must be due to the bias correction in FLX. Hence, our analyses illustrate the impact that the bias has on the coupled equatorial system.

First, we assess the SST bias in STD and FLX. In the annual mean, the STD experiment shows the familiar pattern of the equatorial SST bias (Fig. 1a, 2.00 °C in Atl3). FLX clearly reduces this bias (Fig. 1b, 0.29 °C in Atl3). Additionally and in contrast to STD, FLX is able to produce a cold tongue similar to observations (Fig. 2). An interesting detail of Fig. 2 is that the STD experiment, too, simulates Atl3 cooling between April and May, but fails to intensify this cooling to establish the cold tongue from May onwards. In contrast, Atl3 cooling in FLX really only starts in May-June. Effectively, cold tongue development in FLX lags behind observations by roughly 1 month (Fig. 2a). Nevertheless, heat flux correction clearly reduces the SST bias in the tropical Atlantic (Fig. 2b).

Richter and Xie (2008) and Richter et al. (2012) have shown in different CGCMs that the equatorial Atlantic SST bias is related to a bias in zonal surface wind in the western equatorial Atlantic, which in turn can be traced back to precipitation deficiencies of the models. Based on observations, Marin et al. (2009) argue that weak variability in WAtl zonal surface wind fails to precondition the basin-wide thermocline slope for the subsequent summer—the initial cooling of the cold tongue is hence weakened or delayed. In agreement with Richter et al. (2014a), a similar process could be at work in CGCMs: Spring zonal winds that are systematically too weak in the western equatorial Atlantic could inhibit seasonal thermocline shoaling in the eastern ocean basin and hence intense surface cooling during early boreal summer.

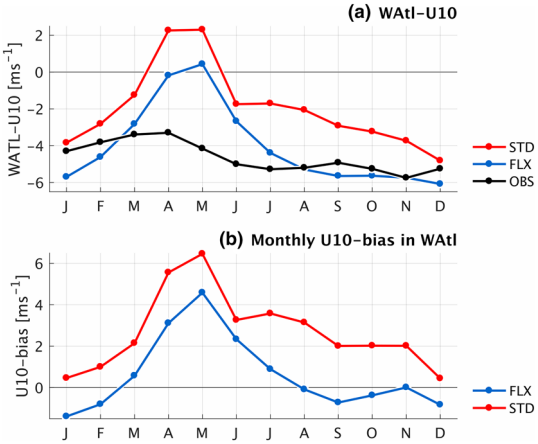

Fig. 3 Same as Fig. 2 but for zonal surface wind u10 in WAtl

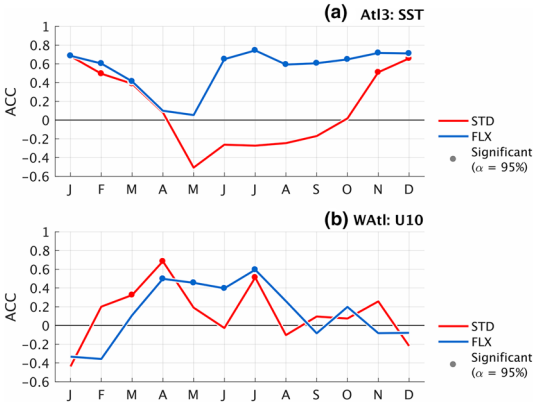

Fig. 4 Monthly anomaly correlation coefficients (ACCs) between ERA-Interim and the ensemble mean from the (red) STD and (blue) FLX experiments for **a** Atl3 SST and **b** WAtl u10 and the period 1981–2012

Here, we demonstrate that the KCM, too, develops a zonal wind bias in boreal spring that is, however, largely independent of the SST bias in the eastern ocean basin. Figure 3 shows that zonal surface wind in WAtl is greatly reduced in boreal spring relative to ERA-Interim. Surprisingly, this behaviour is hardly altered qualitatively in the FLX experiment, indicating that the zonal wind bias depends only weakly on eastern basin SST in the model. In agreement with the recent findings of Richter et al. (2014b) and Harlaß et al. (2015) we suspect that the zonal wind bias is at least partly due to the insufficient vertical resolution of the atmosphere model and related deficiencies in vertical momentum transport.

Additionally, we assess how the bias affects the KCM's ability to simulate observed SST and u10 variability. Figure 4 shows, for each calendar month, the anomaly correlation coefficient (ACC) between the ensemble means of the

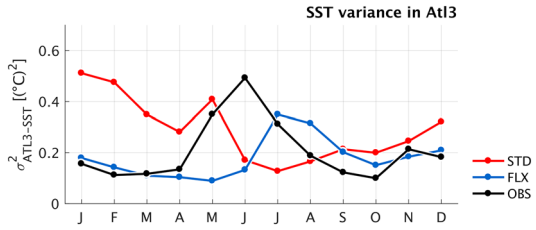

Fig. 5 Monthly SST variance in Atl3 for (black) ERA-Interim, (red) STD, and (blue) FLX

partially coupled KCM assimilation runs and ERA-Interim. Again, because the FLX and STD experiments only differ in whether they reduce the SST bias or not, differences in the "skill" of the assimilation runs to simulate the observed variability are due to the equatorial SST bias.

In agreement with Ding et al. (2015), bias reduction substantially increases the "skill" of the assimilation runs for boreal summer SST variability. This again supports the notion that the cold tongue is a crucial requirement for Atlantic Niño variability. Zonal wind variability, on the other hand, is only marginally improved by SST bias reduction in late boreal spring and early boreal summer.

An interesting aside with respect to the STD experiment is the strongly negative correlation coefficient for modelled and ERA-Interim SST during May. The value is almost −0.5, indicating a relationship that could be interesting to explore further. However, analysing in depth the physical processes that give rise to such an outstanding relationship in the biased experiment is not the scope of this paper and should be addressed in future research.

4 SST variance decomposition method

Figure 5 shows the SST variance in the tropical Atlantic and its seasonality. In ERA-Interim, Atl3 SST variance is subject to a well-defined seasonal cycle that peaks in May–July, consistent with the peak phase of the Atlantic Niño. In agreement with Okumura and Xie (2006) a secondary peak occurs early in boreal winter.

The KCM struggles to reproduce the observed SST variance. While bias alleviation improves model performance, SST variance in FLX is too low and peaks 1 month late (Fig. 5). On the other hand, the STD experiment shows a seasonal cycle of SST variance that is almost the opposite of observations: Variance is high in boreal winter and decreases in boreal summer, reaching its minimum in July. Because the STD experiment is strongly biased in the tropical Atlantic (Figs. 1, 2), the cold tongue cannot develop in boreal summer and cold tongue variability is not captured.

Next, we decompose total SST variance into a dynamically-driven and a stochastically-forced component. We term the variance of the dynamical (stochastic) portion of the signal the dynamical (stochastic) variance.

The canonical approach for such a decomposition is as follows: For an ensemble simulation, average the individual ensembles into the ensemble mean to constrain the uncertainty of the simulation (for example due to imperfect initial conditions or model physics). For a given signal, equate the ensemble mean with the dynamical—i.e. predictable—contribution to the signal. The difference between the ensemble mean and the individual ensemble integrations represents the noise of the climate system—the stochastic, i.e. unpredictable, contribution to the signal. Note that in our specific case, the ensemble mean of a simulation is the dynamical response of the partially coupled model to the imposed wind stress anomalies.

The observed climate record, however, corresponds to a single realization of a climate simulation. Decomposing variance via ensemble averaging is not possible. To nevertheless diagnose observed dynamical SST variance, we use an alternative, empirical approach. Below, we first outline the basic concept of our approach and then present the technical details of the SST decompositions discussed in Sects. 5 and 6.

Conceptually, we model dynamical SST variability with the help of linear empirical models that employ multiple predictors. The idea is very simple: We identify feedbacks that are involved in growing SST anomalies in the tropical Atlantic and attempt to capture the effect of these feedbacks in empirical models. Lübbecke and McPhaden (2017) have used a similar approach to diagnose and compare feedback strengths in the equatorial Atlantic and Pacific oceans. The difference here is that we use more than one predictor and hence attempt to combine a number of feedbacks into a single model of SST. Because we consider feedbacks that are related to dynamical processes in the equatorial system, we equate the portion of the full SST anomaly that is captured by our empirical models with the dynamical SST anomaly. The residual SST anomaly is our stochastic SST anomaly.

For example, consider a set-up in which we use the thermocline feedback as the dynamical core of SST variability (for simplicity's sake, only consider a single feedback for now). To diagnose the observed dynamical SST variance, we use observed thermocline depth in the eastern equatorial Atlantic to model ERA-Interim SST variability in the same region. Note that our empirical models are of the simplest possible nature: We use linear regression. Once we have built the empirical model of (thermocline-driven) dynamical SST, we use this model to "hindcast" SST based on the time series of thermocline depth. The result of this empirical hindcast is our dynamical SST. When we subtract the (thermocline-driven) dynamical SST from the full SST of our original ERA-Interim dataset, the residual is the stochastic SST anomaly *that can not be explained by thermocline depth variability*. We then have three time series of SST: The original ERA-Interim SST, dynamical SST based on the thermocline feedback, and the residual stochastic SST. The SST variances that we are interested in are obtained by calculating the variances of these three SST time series. Note that our decomposition approach heavily relies on empirical linear models, but that the resulting decomposition of the SST variance is not linear, i.e., the full SST variance is not the sum of the stochastic and dynamical SST variance. (The basic decomposition of the SST anomaly, however, is.)

Here, we use the Bjerknes feedback as the dynamical framework for our empirical models of dynamical SST. With respect to the first and third elements of the Bjerknes feedback, i.e. the SST–zonal wind relationship and the surface–subsurface coupling between thermocline depth and SST, we choose zonal wind variability (u10) in WAtl and thermocline depth variability in Atl3 as predictors for SST.[1] Because the ERA-Interim reanalysis does not provide thermocline depth, we use AVISO sea surface height (SSH) in Atl3 as a stand-in. SSH is a reasonable proxy for thermocline depth in Atl3, since Cane (1984) showed that SSH, thermocline depth, and upper ocean heat content are tightly related in the equatorial oceans. This in agreement with the notion that the tropical oceans can be considered as a 1.5-layer system (e.g. Keenlyside and Latif 2007).

To resolve the seasonality of dynamical and stochastic SST variability in the equatorial Atlantic, we build empirical models of dynamical SST for each calendar month. We do this separately for ERA-Interim/AVISO (our "observations") and all ensemble members of the STD and FLX experiments. The resulting SST variance is (1) for ERA-Interim: the variance of the time series of dynamical and stochastic SST, and (2) for the KCM experiments: the variance of the SST time series that *concatenates* the time series of all ensemble members for the respective KCM experiment.

In this study, we build empirical models via least-squares fitting. During the building process, however, we use two different approaches.

[1] Note that an alternative approach is to identify feedbacks that lend positive growth to SST anomalies in Atl3 and choosing as SST predictors the variables that are associated with these feedbacks. Dijkstra (2006) discusses the Ekman and zonal advection feedbacks as suitable feedbacks for our purpose. However, we prefer to motivate our decomposition with the Bjerknes feedback, since it represents a more integrated view of coupled variability in the equatorial oceans. For completeness' sake, the Ekman feedback can be associated with the third element of the Bjerknes feedback, i.e. surface–subsurface coupling in the eastern ocean basin, while the zonal advection feedback is related to the two-way relationship between SST and u10 and not strictly a part of the Bjerknes feedback concept.

1. In the first approach, we *prescribe the predictors* that the empirical model should use. This is the most straightforward approach, and it ensures that all models always use SSH and u10 as predictors, regardless of whether they are "necessary" for the prediction or not. Our predictors are a linear combination of the SSH and u10, and our simple empirical models have the form $sst \sim ssh + u10$.
2. In the second approach, we do not prescribe the exact form of the empirical model but a pool of predictors from which an *algorithmic model adjustment* chooses the "ideal" combination of predictors for the given dataset and calendar month. From this pool of possible predictors, algorithmic model adjustment sequentially builds a whole range of empirical models for the same response variable—dynamical SST, in our case—and seeks to identify the model that performs best in terms of model accuracy and overfitting (e.g. Draper and Smith 1998). Based on a selection criterion, the adjustment algorithm ranks the models. The final adjusted model is the model that beats the competing models in the adjustment sequence. An interesting feature of algorithmic model adjustment is that it allows non-linear combinations of predictors, such as quadratic terms or predictor products.

For example, the adjustment process might start with the simple model $sst \sim ssh + u10$. It then removes the predictor u10 and ranks the model $sst \sim ssh$ relative to the original model. It might then proceed to test the non-linear predictor combinations $sst \sim ssh^2$ and $sst \sim \frac{ssh}{u10}$ to arrive at the conclusion that $sst \sim ssh$ is the "best" model in terms of the chosen selection criterion.

We implemented the algorithmic model adjustment with the function *step()* of Matlab version 2016b. For more technical details about the adjustment process, please refer to the extensive Matlab documentation.[2]

In this study, we apply model adjustment to identify the simplest form of our empirical models. Three outcomes are possible: (1) model adjustment reduces model complexity and removes one of our two predictors. This indicates either that the co-variability between our predictors is strong during the respective month and that using either of them provides sufficient information to produce reasonable dynamical SST; or that the removed predictor does not have a strong impact on SST variability during this month. (2) Model adjustment keeps both predictors in a linear combination. (3) Model adjustment increases the complexity of the model by adding a non-linear predictor term, i.e. a quadratic term or a product of SSH and u10. This could indicate that SST variability during the respective month is more complex and requires further constraints in the form of additional predictors. Because non-linear predictor terms are the only possible addition to the model in the context of our model adjustment, the algorithm evaluates them. Another possibility is that the non-linear terms capture actual non-linear interaction in the climate system.

Our model selection criterion is the sum of squared errors (SSE). Because the number of our data points (20)[3] is large compared to the size of the initial predictor pool (2), it is unnecessary to penalise the number of predictors to avoid overfitting. This could be achieved by basing selection on the Akaike or Bayesian information criteria instead of on SSE. Since we do not intend to use our SST models for true forecasting purposes, we do not conduct extensive cross-validation.

In this study, we discuss three different empirical models of dynamical SST: (1) The *fixed* model of dynamical SST corresponds to the straight-forward model discussed above. It uses the empirical model of the form $sst \sim ssh + u10$. Model adjustment is not allowed. (2) *Single* models use either SSH or u10 as a single predictor for dynamical SST, i.e. they are of the form $sst \sim ssh$ or $sst \sim u10$. They help to identify periods during which the respective feedback is active in isolation. They offer a focused interpretation of the impact of either SSH or u10, but ignore their interaction in the complex tropical climate system. (3) The *adjusted* model employs algorithmic model adjustment, based on the initial predictors SSH and u10. Note that model adjustment is done for observations only, and the adjusted models obtained from observations are then used to estimate dynamical SST from the KCM experiments. An alternative approach would be to apply model adjustment to the individual experiments as well. However, using these "native" adjusted models yields results that are only marginally different (not shown). For the purpose of this study, we thus only use adjusted models that were derived from observations. For all models, the analysis period to fit the models is short: 1993–2012, the overlap between AVISO SSH-data and the rest of our data.

To test the validity of our approach, we conduct SST variance decompositions with both the ensemble averaging approach outlined above and the empirical model approach for the STD and FLX experiments. Figure 6 illustrates the two approaches. Thin and thick coloured lines show the SST

[2] https://de.mathworks.com/help/matlab/. The exact documentation of the `step()`-function for the `linear model`-class can currently be found here: https://de.mathworks.com/help/stats/linearmodel.step.html.

[3] For each month, regardless of whether the empirical models are built for observations or the KCM experiments, use the overlapping period of ERA-Interim (SST, u10) and AVISO (SSH), i.e. 1993–2012—this gives time series that all have a length of 20 data points.

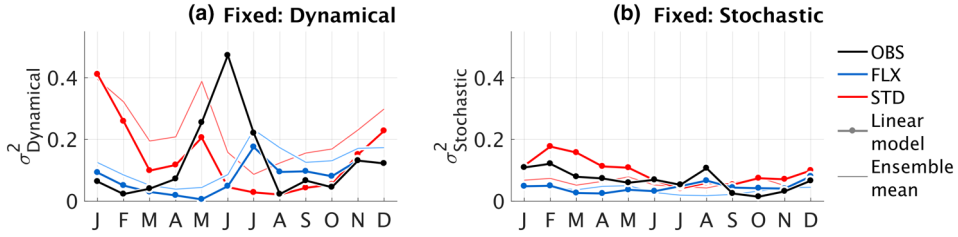

Fig. 6 Atl3 SST variance decomposition into **a** dynamical and **b** stochastic SST variance for (black) ERA-Interim/AVISO, (red) STD, and (blue) FLX. Stochastic SST variance is the variance of the residual of total SST after dynamical SST has been subtracted. Dynamical SST is subtracted from each ensemble member individually, and the time series of residual (stochastic) SST are concatenated before the variance is calculated. Thick lines denote SST variance decomposition based on the empirical models for dynamical SST (see text for details). Thin lines for FLX and STD denote SST variance decomposition based on ensemble averaging. The empirical model is the fixed model

variances based on ensemble averaging and our fixed empirical models, respectively. Overall, results are comparable for the STD and FLX experiments. Empirical modelling underestimates dynamical SST variance (Fig. 6a) while simultaneously overestimating stochastic SST variance (Fig. 6b). This suggests that our simple empirical approach fails to capture all processes that are relevant to dynamical SST variability. On the other hand, qualitative differences between the two seasonal distributions of dynamical SST variability are small, regardless of the presence of the bias.

We conclude that empirical modelling is a reasonable alternative to the ensemble mean approach.

Lastly, we point out a limitation of our models that is in line with the discussion of the Bjerknes feedback presented in the introduction. Our SST variance decomposition approach allows us to identify periods of the seasonal cycle when the dynamical Bjerknes feedback contributes substantially to SST variability in Atl3. It would be easy to conclude from our analysis that dynamical processes contribute to SST variability and that these dynamical processes must hence be associated with enhanced SST predictability. However, such a conclusion might be overly optimistic. The reason is that our SST decomposition approach relies on the *empirical* method of linear regression. When our empirical models pick up a statistical relationship between SST and our two predictors SSH and u10, they do not automatically provide a clear causality or "forcing direction". Consider again, for example, the relationship between SST and u10, and imagine a scenario in which SST is driven by ocean processes that are possibly off-equatorial in nature, such as variability associated with the subtropical cells. In the coupled equatorial system, the atmosphere would react to the ocean-induced SST variability and our empirical models would pick up a statistical co-variability between SST and u10 that would be partly reflected in our SST decomposition—*even though u10 in this idealized example was not fundamental in causing the SST variability in the first place*. From this example, it is clear that the interpretation of our results *with respect to SST predictability* might not be straightforward. However, keep in mind that the scope of this study is not to measure SST predictability, but to assess when dynamical processes are active in the equatorial Atlantic.

5 Seasonality of dynamical SST Variance in the tropical Atlantic

Figure 6 shows the dynamical and stochastic SST variances from our fixed model for the equatorial Atlantic; Fig. 7 shows the ratio of the two variances. Results are displayed for observations and the two KCM experiments.

Observations (black): dynamical SST clearly dominates observed SST variance during early boreal summer (May–July, Fig. 6a). Dynamical SST variance then is roughly 4–7 times larger than the stochastic contribution to total SST variability (Fig. 7). A secondary peak occurs during October and November. These two periods of enhanced dynamical SST variability are separated by phases during which stochastic SST variance is larger than dynamical SST variance. This is the case in January-March and again in August, when dynamical SST variance vanishes and observed stochastic SST variance reaches its peak. Note that observed stochastic SST variance is much less variable over the course of the year (Fig. 6b). This

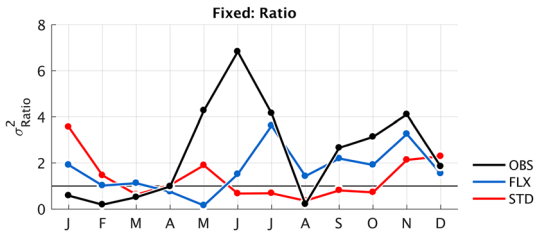

Fig. 7 Ratio of dynamical and stochastic SST variance in the fixed model for Atl3. Ratios are shown for (black) ERA-Interim/AVISO, (red) STD, and (blue) FLX

suggests that stochastic SST variance is indeed driven by processes that are independent of seasonal processes—it represents noise.

Comparing dynamical SST variance from the fixed model (Fig. 6a) with total SST variance (Fig. 5) shows a generally good agreement. In August, however, when dynamical SST variance vanishes according to our empirical models, total SST variance continues to decrease evenly. Here, stochastic SST variance contributes to total SST variability (Fig. 6b).

The overall similarity between the total and dynamical SST variance suggests that the seasonal cycle of total SST variability in the tropical Atlantic is largely shaped by the variable dynamical contribution.

The dynamical and stochastic SST variances for the model experiment FLX are comparable to observations (blue). Dynamical SST variance peaks in boreal summer and again, more weakly, in early boreal winter (Fig. 6a). However, the timing of the dynamical SST variance peaks does not match observations. The summer peak lags behind observations by 1 month and is strongly reduced in amplitude. The absolute minimum of dynamical SST variance occurs in May—when observed dynamical SST variance is already high and contributes substantially to the overall boreal summer peak. Additionally, dynamical SST variance does not decrease as strongly in August, and the secondary peak is hardly a peak at all.

One reason for these shortcomings in the FLX dynamical SST variance is most likely related to systematic differences between the observed and heat-flux corrected seasonal cycles (Fig. 2). While the bias correction strongly reduces the annual mean bias (Fig. 1), it is not able to fully constrain the model to the observed seasonal cycle. Instead, cold tongue development in the FLX experiments sets in systematically too late and lags behind the observed cold tongue development by about 1 month. The observed and simulated seasonal cycles only converge in August, when the cold tongue is fully developed and starts to dissolve. In the framework of our empirical models, this delay in cold tongue development explains the absence of dynamical processes during May, because these processes depend on the presence of the cold tongue. However, once the cold tongue is established, the feedbacks set in and contribute to dynamical SST variability. Stochastic SST variance is similar to observations in both magnitude and seasonality (Fig. 6b). The ratio of the variances in the bias-corrected model run bears similarities to observations but lacks the clear double peak structure (Fig. 7), because dynamical SST variance does not vanish in FLX. One reason could be that, similar to the delayed cooling during the onset of the cold tongue, initial warming in August–September is weaker in FLX than in observations (0.61 and 0.20 °C month^{-1} in ERA-Interim and FLX, not shown). In contrast to observations—where the surface–subsurface coupling in Atl3 is disrupted in August—, the thermocline feedback stays active in FLX (see Sect. 6).

The STD experiment does not capture the observed dynamical SST variance distribution (red). On the contrary: With the exception of May, when the eastern equatorial Atlantic starts to cool in STD but then aborts the cooling to develop the strong boreal summer bias (Fig. 2), dynamical SST variance is at its lowest in boreal summer and increases in boreal winter. This is most likely because the equatorial cold tongue dissolves in late boreal summer and the background states of observations, FLX, and STD become more similar. The STD SST bias decreases and our empirical models operate on comparable conditions, resulting in dynamical SST variances in the STD experiment that are similar to observations in boreal fall and early boreal winter. Note that while dynamical SST variance appears to be rather high in STD during late boreal winter and even comparable in magnitude to observations, stochastic SST variance in STD is systematically higher than in observations throughout most of the year (Fig. 6). The resulting SST variance ratio (Fig. 7) shows that dynamical processes in STD almost never have the same impact on SST variability as in FLX or observations. An exception is January–February, when STD simulates dynamical contributions to SST variability that dominate stochastic contributions.

These findings suggest that the background state—i.e. the seasonal cycle of the system—is crucial for a realistic simulation of dynamical SST variance. While the FLX experiment is not perfect, it is clearly an improvement on the STD experiment that lacks the Atlantic cold tongue in its background state.

Additionally, our findings show that observed SST is dominated by dynamical SST variance in May–July. This coincides with the peak phase of the Atlantic Niño and suggests that a major part of the Atlantic Niño-variability could indeed be caused by dynamical—but not necessarily predictable—processes. This appears to be at odds with the results of Nnamchi et al. (2015), who find in CMIP3-based slab model simulations (i.e. simulations that omit ocean dynamics) that Niño-like variability in the equatorial Atlantic can be produced by stochastic atmospheric forcing alone. To explain this, Nnamchi et al. (2016) argue that the Atlantic Niño is the equatorial manifestation of the more general South Atlantic Ocean SST Dipole (SAOD). They demonstrate that SOAD-variability is related to the variability of the South Atlantic (St Helena) Anticyclone and is sustained by the wind-evaporation-SST feedback. While this is in agreement with Lübbecke et al. (2014)'s work on the relationship between the Atlanic Niño and the St Helena Anticyclone, it still does not fully explain how our results tie in with Nnamchi et al. (2015).

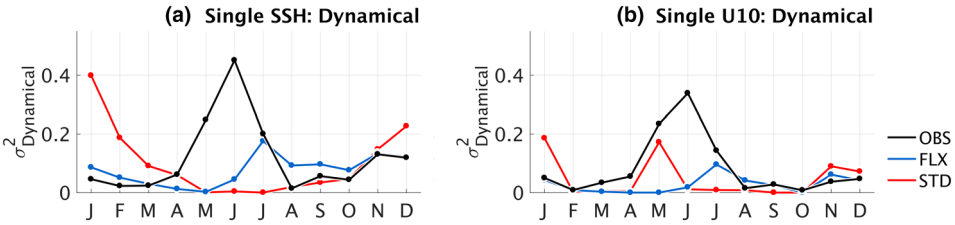

Fig. 8 Dynamical Atl3 SST variance based on **a** the single SSH model, and **b** the single u10 model. SST variances are shown for (black) ERA-Interim/AVISO, (red) STD, and (blue) FLX

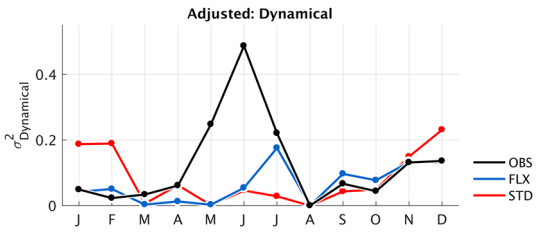

Fig. 9 Dynamical Atl3 SST variance based on the adjusted model for (black) ERA-Interim/AVISO, (red) STD, and (blue) FLX

We propose that reality is a mixture of both a dynamically and stochastically driven Atlantic Niño. Specifically, we find that ocean dynamics are important to *grow* Atlantic Niño events in early boreal summer. This does not contradict the notion that initial anomalies in the equatorial Atlantic need to be "excited" by stochastic forcing that in turn could be related to the St Helena Anticyclone. Once these initial anomalies develop in late boreal spring, the presence of the cold tongue allows the Bjerknes feedback to amplify them.

However, we point out that we are still not able to fully reconcile our results with Nnamchi et al. (2015)'s findings with respect to the question how a slab ocean can not only respond to initial atmospheric perturbations but also help to grow them. An interesting future analysis could address this apparent discrepancy by assessing the relative impact of both the dynamical Bjerknes feedback and the thermodynamic wind-evaporation-SST feedback on tropical Atlantic SST anomaly growth during boreal summer.

To complement the analysis above, we repeat our analysis using different sets of predictors in our empirical models. Figure 8 shows the dynamical SST variance based on the single SSH and u10 models; Fig. 9 shows the same for the adjusted model.

Comparing Figs. 6a and 8a, b, shows that observed dynamical SST variances (black) of the single SSH and u10 models share the prominent boreal summer peak with the fixed model. This suggests that, even in isolation, both zonal surface wind and thermocline processes are involved in establishing the boreal summer variability of SST. In boreal winter, the single u10 model does not contribute to dynamical SST variance.

The adjusted model produces SST variances that are very similar to the fixed model (Figs. 6a, 9). Table 1 shows the predictors that the algorithmic model adjustment chose to model observed SST for each month. Late boreal winter SST variability is generally well modelled by either SSH or u10, indicating prevalent co-variability between SSH and u10 or that the excluded predictor does not contribute substantially to constraining dynamical SST. June and July require more than one predictor and even non-linear interaction of SSH and u10 in June. This suggests that variability during the early stage of cold tongue development can be mainly explained by thermocline variability, while the cause of variability during the growth phase of the cold tongue is more complex. Then, it does not suffice to isolate a single feedback. Rather, to explain Atlantic Niño variability during climatological cold tongue growth, a number of factors have to be considered.

In August, model adjustment chooses to use no predictor. This means that in our statistical framework, observed August SST variability is unconstrained by SSH and u10. SSH and u10 start to contribute to SST variability again in September. In December dynamical SST again depends on non-linear interactions.

Overall, our analysis suggests that the relative importance of either thermocline processes or zonal surface wind varies over the course of the year in the observed climate system. Especially during the early stages of cold tongue

Table 1 Predictors of dynamical SST for each calendar month in Atl3 based on observations

J	F	M	A	M	J	J	A	S	O	N	D
	SSH		SSH	SSH	SSH	SSH		SSH	SSH	SSH	SSH
u10		u10			u10	u10		u10			u10
					prd						prd

The basic predictors are SSH in Atl3 and 10 m zonal wind anomalies (u10) in WAtl. "prd" refers to a product of the two individual predictors and indicates non-linear interaction in the climate system

development, our empirical models chose not a single predictor but a combination of them, while August is basically unpredictable by statistical means.

Single and adjusted models that are based on FLX and STD produce different dynamical SST variances (Figs. 8, 9). For FLX, the same 1 month lag in boreal summer is present that has already been identified in the fixed model.

6 Feedback strengths in the tropical Atlantic

Our SST decomposition approach is based on the dynamical framework of the Bjerknes feedback. For this reason, we now take a closer look at the Bjerknes feedback—both observed and modelled—and its three elements in the tropical Atlantic. Recall that the three relationships that make up the closed Bjerknes feedback in our framework are (1) Atl3 SST produces WAtl u10 variability, (2) WAtl u10 variability is translated into Atl3 thermocline—here: SSH— variability via equatorial wave dynamics, and (3) Atl3 SSH positively feeds back to Atl3 SST and lends growth to the initial SST anomaly.

Here, we first consider the *instantaneous* Bjerknes feedback, and then analyse how the feedback strengths change when we allow lagged relationships for the individual feedback elements. In particular, we incorporate lagged relationships into the building process of our empirical models and assess their impact on the seasonal distribution of dynamical SST variance. This measures the robustness of our results.

We begin with the instantaneous Bjerknes feedback, which is made up of instantaneous relationships of the form (1) to (3). With this constraint, May SST is only able to affect May u10, May u10 is only able to affect May SSH, and so on. Figure 10 assesses the strength of the instantaneous Atlantic Bjerknes feedback in terms of correlation strengths between the relevant variables. Note that for the partially coupled KCM experiments, we use the model u10 for relationship (1), but observed u10 when we assess the relationship strength between u10 and SSH in relationship (2).

It is clear that the strength of the Bjerknes feedback elements varies considerably over the course of the year. In agreement with Keenlyside and Latif (2007) and Deppenmeier et al. (2016), all observed feedback elements are generally strongest in early boreal summer, establishing a closed Bjerknes feedback loop in May–July (Fig. 10a). This coincides with both the peak of total SST variance (Fig. 5) and the active phase of the Atlantic Niño, supporting the hypothesis that Atlantic Niño variability is related to the Bjerknes feedback. Note that the coupling between the ocean subsurface and surface that is captured in the SST–SSH relationship is strong in boreal fall as well but dips in August. This implies that the communication between surface processes

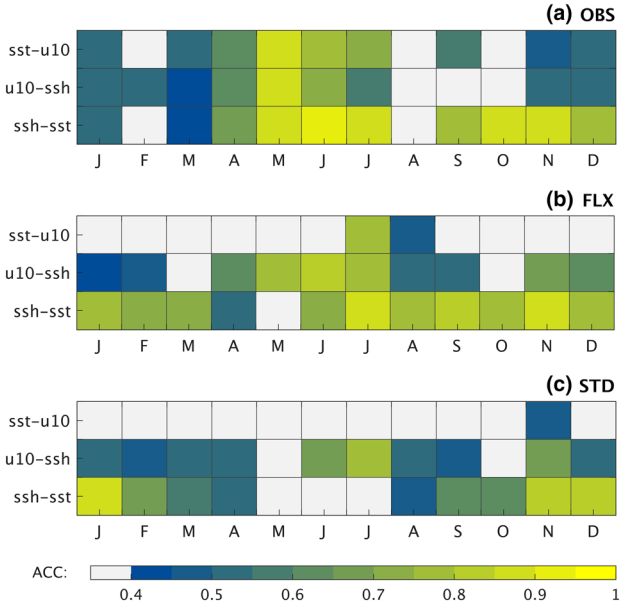

Fig. 10 Anomaly correlation coefficients between SST, u10, and SSH for each calendar month in **a** ERA-Interim/AVISO, **b** FLX, and **c** STD. Because our model experiments are partially coupled, we use observed u10 to assess the u10–SSH-relationship (second rows). For the SST–u10-relationship (first row), on the other hand, we use the model winds. SST and SSH anomalies are averaged in Atl3, u10 anomalies in WAtl. ACC values that are not significantly different from 0 at the 95% level according to a Student t test are shown in grey

and the ocean interior temporarily fades in late boreal summer, disrupting the Bjerknes feedback loop.

The KCM experiments struggle to capture the observed relationships that form the instantaneous Bjerknes feedback in the tropical Atlantic (Fig. 10b, c). The SST–u10 relationship is hardly captured at all in either experiment. A single exception is July in the FLX experiment: Here, the KCM captures a relationship that is comparable to observations and is able to simulate a closed Bjerknes feedback loop. As in observations, this coincides with the occurrence of the peak in total SST variance (Fig. 5). Note that FLX simulates a reasonable SSH–SST relationship in boreal winter, but fails to produce this crucial relationship in May. Again, we suspect that the bias in the onset of the cold tongue is responsible for this behaviour. Because cold tongue development only really sets in in June in FLX (Fig. 2), the thermocline cannot communicate with SST in May. FLX fails to establish the observed relationship. For the same reason, STD is not able to produce the SST–SSH relationship of the instantaneous Bjerknes feedback in boreal summer.

Our results agree with the observations-based part of Deppenmeier et al. (2016)'s analysis of the Bjerknes feedback in the tropical Atlantic. However, while Deppenmeier et al. (2016) point out that it is mainly the relationship between upper ocean heat content (approximated by our

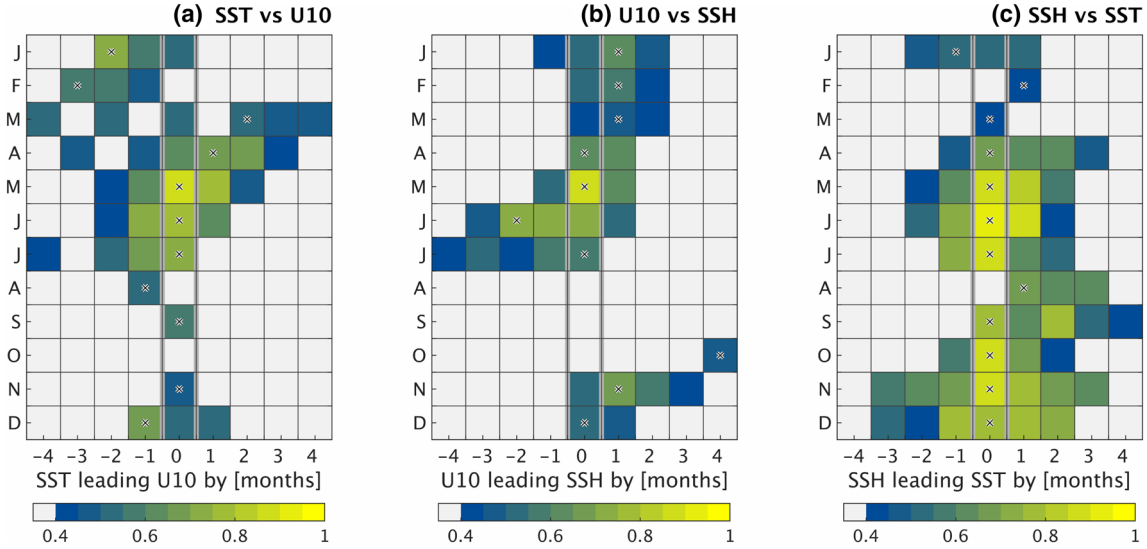

Fig. 11 ERA-Interim/AVISO-based monthly stratified anomaly cross correlation for **a** Atl3-SST vs WAtl-u10 [corresponds to Bjerknes feedback element (1)], **b** element (2): WAtl-u10 vs Atl3-SSH, and **c** element (3): Atl3-SSH vs Atl3-SST. Only ACC values that are significantly different from 0 at the 95% level are shown as coloured shading. To calculate the cross correlation values for each month, we fix the "response agent" of the respective element (the second element in the figure titles) in time and correlate it sequentially with the monthly time series that corresponds to each lag. For the January-analysis of element (3), for example, the correlation of January SST with the following May is given in the January rows at a lag of −4 months, and so on. Negative lags indicate that SST variability precedes SSH variability ("SST leads SSH"), positive lags indicate that SSH leads SST. Calendar months are indicated on the y-axis. Black crosses indicate the lag—shown on the x-axis—at which the ACC value of the respective element is maximum. For example, in element (3), August-SST is strongest related to SSH when SSH leads by 1 month, i.e. August-SST is strongest correlated to July-SSH

SSH) and SST that is too weak in CMIP5-simulations, the KCM's problems are mainly related to the SST–u10 relationship, possibly due to the low atmospheric vertical resolution. In the current version of the KCM, FLX produces a closed Bjerknes feedback loop only in July (May–July in observations)—the model's ability to produce a Bjerknes feedback akin to observations is severely impaired by the delayed onset of the cold tongue.

In summary, our analysis shows that a relationship exists between the equatorial Atlantic bias and the degree to which the instantaneous Atlantic Bjerknes feedback is active in summer. The instantaneous feedback clearly relies on the presence of the cold tongue to make use of it's potential.

However, previous studies have shown that both the Atlantic and Pacific Bjerknes feedbacks do not necessarily operate instantaneously (see Introduction). For this reason, we now consider a lagged Bjerknes feedback. We first assess the observed lagged relationships in the tropical Atlantic, and then repeat our SST variance decomposition, this time allowing for lagged relationships between SST and the two predictors SSH and u10. We assess the degree of lag for each of the three Bjerknes relationships via a cross-correlation analysis for each month.

For this to work, we assume that each Bjerknes feedback element describes a relationship of clear causality: one quantity "forces" the other. In element (1), for example, SST "forces" u10. As discussed previously, this concept is highly idealized and does not realistically describe the entire spectrum of atmosphere–ocean interaction in the equatorial Atlantic. However, in the framework of our lagged Bjerknes feedback, we will make use of the idealized relationships and refer to the involved quantities of a Bjerknes feedback element either as the "forcing" or "response" agents.

In our cross-correlation analysis for each calendar month and Bjerknes feedback element, we fix the response agent to the calendar month and correlate it sequentially with the forcing agent of all relevant lags. Our maximum lag is ± 4 months. As an example, consider Bjerknes feedback element (1). SST is the forcing, u10 the response agent. For the cross correlation analysis of January, we select the time series of monthly mean WAtl u10 in January. Then, for all lags, we select the corresponding SST time series and correlate it with January u10. This means that for a lag of −4 months, January u10 is correlated with May SST, for −3 months with April SST, and so on. Note that a negative lag indicates that, in this example, the chosen u10 variability precedes the SST variability, i.e. u10 "leads" SST. For positive lags, SST leads u10.

Figure 11 shows the results for the observed tropical Atlantic. Color shading indicates anomaly correlation coefficients that are significantly different from 0 at the 95% level. A lag of 0 months (from here-on "lag 0") is framed

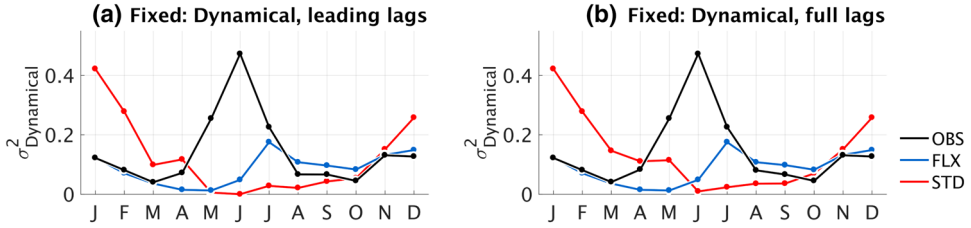

Fig. 12 Same as Fig. 6a, but including lagged relationships when building the empirical models of dynamical SST. The chosen lags correspond to the maximum correlation values. For observations, these "peak months" are indicated by black crosses in Fig. 11. **a** Positive lags only, i.e. the predictors are allowed to lead SST only. When SST leads the predictor, the instantaneous relationship—i.e. lag 0—is used. **b** Full lags, i.e. Predictors can lead and lag SST

by grey vertical bars for better visibility. Note that lag 0 in Fig. 11 is identical with the corresponding instantaneous relationship shown in Fig. 10. Black crosses indicate the lag for which the relationship in terms of the ACC is strongest for the considered calendar month and Bjerknes feedback element. For the remainder of the study, we refer to these lags as "peak lags".

Figure 11 shows that the Bjerknes feedback in the tropical Atlantic is essentially instantaneous during the peak time of the Atlantic Niño from May to July. (This is not necessarily the case during other seasons, including during boreal spring, when enhanced western tropical Atlantic wind stress has been shown to precondition the development of the cold tongue in boreal summer, e.g. Marin et al. 2009). This agrees with Lübbecke et al. (2014), who demonstrate that the relationship between SST and wind power anomalies in the tropical Atlantic is basically symmetrical around lag 0. An interesting interpretation of this finding is offered by Frankignoul et al. (1977). They argue that a positive feedback produces a clear signature in a cross-correlation analysis, with peak ACC values at lag 0 that decrease symmetrically for increasing lags of both signs. In such a positive feedback, the involved agents reinforce each other and lend growth to small perturbations. This interpretation of a positive feedback supports the notion that the Bjerknes feedback in the tropical Atlantic consists of three partial feedbacks that each, in terms of monthly means, act more or less simultaneously as positive feedbacks during boreal summer.

Note that our cross-correlation analysis appears to be at odds with earlier studies that find that wind variability consistently leads SST variability in the tropical Atlantic (e.g. Keenlyside and Latif 2007; Richter et al. 2013). Two important details that could contribute to this apparent discrepancy are (1) that these studies used different datasets and periods for their analysis, and (2) that their evidence is based on yearly or seasonal data. Here, on the other hand, we stratify our data into monthly means and present cross-correlation analysis for individual calendar months. We chose this approach in agreement with recent findings (e.g. Lübbecke and McPhaden 2017) that stress how relevant short time scales of 1 month and possibly even less are for establishing the tropical Atlantic seasonal cycle. Temporally averaging (monthly) data over as little as 2 months already runs the risk of blurring important signals in the tropical Atlantic.

Returning to our results, we find that both in the instantaneous and the lagged analysis (Figs.10, 11), the strongest relationship throughout the year is related to surface–subsurface coupling. Wind-related feedback elements are active less consistently.

Next, we incorporate the lagged relationships into our linear models of dynamical SST. We diagnose each month's peak lags separately for all datasets and all ensemble members.[4] Once we identified all peak lags, we rebuild our empirical models of dynamical SST and replace the monthly time series of the predictor with the time series that corresponds to the appropriate peak lag. For example, for observations and the SST–SSH relationship in February, we do not use February but January SSH to build our empirical model of dynamical SST, because the peak lag of February is +1 (Fig. 11c), indicating that SSH leads SST variability by 1 month for February SST.

When including the peak lags into our dynamical models, we distinguish two cases: (1) empirical models that incorporate lagged relationships only when the predictor variables lead SST. The assumption here is that we are interested in the response of SST to a prescribed forcing and that this response cannot, physically, precede the forcing. (2) All peak lags are used when building the empirical models, including those when, statistically, SST leads its own predictors. The resulting dynamical SST variances are shown in Fig. 12.

[4] An important detail is that for feedback element (1), the relationship between SST and u10, we swap the forcing and response roles of the two agents while performing the cross correlation analysis. The reason is that we use u10 as a *predictor* of dynamical SST and hence implicitly assume that u10 is, to some degree, directly forcing SST variability. While this is not strictly in line with the conceptual model of the Bjerknes feedback, it is physically consistent with our empirical modelling framework.

A comparison with the distribution of the dynamical SST variance of the unlagged case (Fig. 6a) immediately shows that the impact of lagged relationships is negligible at best (this is true for both observations and the model experiments, indicating that lagged relationships in FLX and STD do not substantially influence dynamical SST variance in the two experiments, even though the lag relationships are most likely not identical with their observed counterparts). The simple reason for this is that the three Bjerknes feedback elements are essentially instantaneous when they are strong and only stray from lag 0 peak lags when they decrease (Fig. 11). This means that Bjerknes feedback elements in the tropical Atlantic are mostly instantaneous when the tropical Atlantic is dynamically "active", i.e. during late boreal spring and early summer and again in early boreal winter.

7 Summary and discussion

We assess the impact of the equatorial Atlantic bias in coupled climate models on their ability to realistically simulate the variability and dynamics of the Atlantic Niño. To that end, we decompose SST variability into a dynamically driven and a stochastically forced component. Our study is based on experiments that were produced with the Kiel Climate Model, a CGCM: the STD experiment is heavily biased in the equatorial Atlantic, the FLX experiment reduces the bias by applying surface heat flux correction. To decompose total SST variance, we model dynamical SST with empirical linear models that use two predictors, SSH and u10. The choice of our predictors is motivated by the Bjerknes feedback that provides a robust dynamical framework for our purpose. However, the simple concept of the Bjerknes feedback is not always appropriate, and we were careful to note that especially the relationship between SST and u10 works in both directions.

In agreement with numerous previous studies on the dynamics of the Atlantic Niño (e.g. Zebiak 1993; Carton et al. 1996; Ding et al. 2010), we find that dynamical SST variance contributes substantially to equatorial Atlantic SST variability in boreal summer (May–July), the peak phase of the Atlantic Niño. This is in contrast to a recent study by Nnamchi et al. (2015), who found that the Atlantic Niño is driven primarily by stochastic forcing.

Here, we highlight again that a biased background state affects the physics of the tropical Atlantic and can inhibit realistic dynamical behaviour. Our biased experiment fails to simulate a dynamical component of SST variability in boreal summer. The reason is that the biased experiment cannot produce the seasonal cold tongue in the tropical Atlantic. The Atlantic Niño, however, can be understood as a modulation of the cold tongue (Burls et al. 2012). In the absence of the cold tongue, the Atlantic Bjerknes feedback cannot work properly. *The biased mean state is not compatible with the dynamic Atlantic Niño that we find in observations*.

Taking into account a number of previous studies that found non-negligible lagged relationships in the tropical Atlantic that are related to the Bjerknes feedback, we assess the degree of lag in the Bjerknes feedback elements both in observations and our KCM experiments. In the observations, the Bjerknes feedback is active in the tropical Atlantic in April–May until July and again in November and December. The equatorial bias severely impacts the KCM's ability to simulate a realistic Bjerknes feedback. Additionally, we find that the Atlantic Bjerknes feedback is near-instantaneous during the dynamically active phases of the year. As a consequence, incorporating realistic lagged relationships into our empirical models of dynamical SST hardly impacts the resulting dynamical SST variances. Especially during the important peak phase of the Atlantic Niño both the instantaneous and the lagged empirical models produce identical results.

One consequence of this finding is that we expect potential predictability[5] of seasonal SST variability to be rather low in the tropical Atlantic. Reasons for this are: (1) when we measure the strength of the Bjerknes feedback elements in terms of anomaly correlation coefficients, Atlantic feedbacks are substantially weaker than their Pacific counterparts, implying that dynamical processes in the equatorial Atlantic are less deterministic than in the tropical Pacific. This is true for both the instantaneous and lagged relationships (not shown). (2) The lack of substantial lags in the Atlantic Bjerknes feedback elements suggests that dynamical processes in the equatorial Atlantic happen on much shorter time scales than in the tropical Pacific. These observations-based conclusions are in line with modelling studies that found the equatorial Atlantic on seasonal time scales to be much less predictable than the equatorial Pacific (e.g. Stockdale et al. 2006).

In addition to the strong dynamical contributions to the Atlantic Niño, we identify a secondary peak in observed dynamical SST variance in November–December in observations. This peak could be associated with Okumura and Xie (2006)'s Atlantic Niño II, a secondary Niño-like phenomenon in the tropical Atlantic that is able to organize SST anomaly growth into a Bjerknes feedback. Note that our adjusted models choose SSH, u10, and an interaction term between the two predictors to capture dynamical SST in December. While this could hint at the empirical models having difficulties to predict dynamical SST during December, it could also be due to a feedback linking

[5] By potential predictability we mean the predictability that is inherent to the physical climate system and hence independent of whether or not a specific CGCM is able to realise it or not.

the three variables to each other, in this case the Bjerknes feedback. Okumura and Xie (2006)'s findings support the second possibility. Note that, in contrast to May and June, the December peak of enhanced dynamical SST variance is captured by both the FLX and STD experiments, indicating that the KCM appears to be able to reproduce the variability associated with Okumura and Xie (2006)'s Atlantic Niño II.

Our study presented a simple method to decompose eastern equatorial SST variability into dynamic and stochastic contributions while taking into account prominent feedbacks in the region. We are aware that our approach requires assumptions about the processes that could be relevant to SST variability and that we introduce a subjective element into our analysis by selecting a pool of possible predictors that our model adjustment algorithm works on. A thing to keep in mind is that we limit the dynamical processes that can possibly contribute to dynamical SST variability in our empirical models. Figure 6b shows that our decomposition approach produces stochastic SST variances that are consistently higher than the stochastic contributions to SST variability that a standard ensemble averaging approach yields. The reason is most likely that the full CGCM incorporates additional dynamical processes that affect SST evolution. In this sense, ensemble averaging is the more straightforward and complete method to estimate dynamical SST variability. The advantage of our method is that it allows for direct comparisons between observations and model simulations.

While we have provided further evidence for a dynamically driven Atlantic Niño, research is not yet clear on what exactly these dynamics are: If the Bjerknes feedback is involved in establishing the seasonal cold tongue, which processes govern the feedback modulation that produces the interannual variability of the Atlantic Niño? Future study will help to further our understanding of the Atlantic Niño and its predictability.

Acknowledgements We are grateful for extensive reviews by two anonymous reviewers that greatly helped to improve the manuscript. We also thank Ingo Richter and Joke Lübbecke for additional helpful discussions. This study has been supported by the German Ministry for Education and Research (BMBF) through MiKlip2, subproject 01LP1517D (ATMOS-MODINI) and SACUS (03G0837A), and by the European Union 7th Framework Programme (FP7 2007–2013) under Grant agreement 603521 PREFACE project. RJG is also grateful for continuing support from GEOMAR. The data used in this study can be obtained from Tina Dippe (tdippe@geomar.de) on request.

References

Bjerknes J (1969) Atmospheric teleconnections from the equatorial pacic. Mon Weather Rev 97(3):163–172. doi:10.1175/1520-0493(1969)097<0163:ATFTEP>2.3.CO;2

Burls NJ, Reason CJC, Penven P, Philander SG (2011) Similarities between the tropical Atlantic seasonal cycle and ENSO: an energetics perspective. J Geophys Res Oceans 116(C11):C11010. doi:10.1029/2011JC007164

Burls NJ, Reason CJC, Penven P, Philander SG (2012) Energetics of the Tropical Atlantic zonal mode. J Clim 25(21):7442–7466. doi:10.1175/JCLI-D-11-00602.1

Cane MA (1984) Modeling sea level during El Niño. J Phys Oceanogr 14(12):1864–1874. doi:10.1175/1520-0485(1984)014<1864:MSLDEN>2.0.CO;2

Carton JA, Cao X, Giese BS, Da Silva AM (1996) Decadal and interannual SST variability in the tropical. Atlantic Ocean. doi:10.1175/1520-0485(1996)838026<1165:DAISVI>2.0.CO;2

Chang CY, Carton JA, Grodsky SA, Nigam S (2007) Seasonal climate of the tropical Atlantic sector in the NCAR community climate system model 3: Error structure and probable causes of errors. J Clim 20(6):1053–1070. doi:10.1175/JCLI4047.1

Davey M et al (2002) STOIC: A study of coupled model climatology and variability 844 in tropical ocean regions. Clim Dyn 18(5):403–420. doi:10.1007/845 s00382-001-0188-6

Dee DP et al (2011) The ERA-Interim reanalysis: configuration and performance of the data assimilation system. Q J R Meteorol Soc 137(656):553–597. doi:10.1002/qj.828

Deppenmeier AL, Haarsma RJ, Hazeleger W (2016) The Bjerknes feedback in the tropical Atlantic in CMIP5 models. Clim Dyn 1–17. doi:10.1007/s00382-016-2992-z

Dijkstra H (2006) The ENSO phenomenon: theory and mechanisms. Adv Geosci 6:3

Ding H, Keenlyside NS, Latif M (2010) Equatorial Atlantic interannual variability: role of heat content. J Geophys Res Oceans 115(C9):C09020. doi:10.1029/2010JC006304

Ding H, Greatbatch RJ, Latif M, Park W, Gerdes R (2013) Hindcast of the 1976/77 and 1998/99 climate shifts in the Paciffic. J Clim 26(19):7650–7661. doi:10.1175/JCLI-D-12-00626.1

Ding H, Greatbatch RJ, Latif M, Park W (2015) The impact of sea surface temperature bias on equatorial Atlantic interannual variability in partially coupled model experiments. Geophys Res Lett 42(13):5540–5546. doi:10.1002/2015GL064799

Draper NR, Smith H (1998) Applied regression analysis. 3rd edn. Wiley, Hoboken. doi:10.1002/9781118625590

Frankignoul C, Hasselman K, Hasselmann K (1977) Stochastic climate models, Part II Application to sea-surface temperature anomalies and thermocline variability. Tellus 29(4):289–305. doi:10.1111/j.2153-3490.1977.tb00740.x

Grodsky SA, Carton JA, Nigam S, Okumura YM (2012) Tropical Atlantic biases in CCSM4. J Clim 25(11):3684–3701. doi:10.1175/JCLI-D-11-00315.1

Harlaß J, Latif M, Park W (2015) Improving climate model simulation of tropical Atlantic sea surface temperature: the importance of enhanced vertical atmosphere model resolution. Geophys Res Lett 42(7):2401–2408. doi:10.1002/2015GL063310

Hirst AC, Hastenrath S (1983) Atmosphere–ocean mechanisms of climate anomalies in the Angola-tropical Atlantic sector. J Phys Oceanogr 13(7):1146–1157. doi:10.1175/1520-0485(1983)013<1146:AOMOCA>2.0.CO;2

Hu Z-Z, Huang B (2007) The predictive skill and the most predictable pattern in the tropical Atlantic: the effect of ENSO. Mon Weather Rev 135(5):1786–1806. doi:10.1175/MWR3393.1

Janicot S, Harzallah A, Fontaine B, Moron V (1998) West African monsoon dynamics and eastern equatorial Atlantic and

Pacific SST anomalies (1970–88). J Clim 11(8):1874–1882. doi:10.1175/1520-0442(1998)011<1874:WAMDAE>2.0.CO;2
Keenlyside NS, Latif M (2007) Understanding equatorial Atlantic Interannual variability. J Clim 20(1):131–142. doi:10.1175/JCLI3992.1
Kushnir Y, Robinson WA, Chang P, Robertson AW (2006) The physical basis for predicting Atlantic sector seasonal-to-interannual climate variability. J Clim 19(23):5949–5970. doi:10.1175/JCLI3943.1
Lübbecke JF, McPhaden MJ (2012) On the inconsistent relationship between Pacific and Atlantic Nifngos. J Clim 25(12):4294–4303. doi:10.1175/JCLI-D-11-00553.1
Lübbecke JF, McPhaden MJ (2013) A comparative stability analysis of Atlantic and Paciffic Niño modes. J Clim 26(16):5965–5980. doi: 10.1175/JCLI-D-12-00758.1
Lübbecke JF, McPhaden MJ (2017) Symmetry of the Atlantic Niño mode. Geophys Res Lett 44(2):965–973. doi:10.1002/2016GL071829
Lübbecke JF Burls NJ, Reason CJC, McPhaden MJ (2014) Variability in the South Atlantic Anticyclone and the Atlantic Nifñgo Mode. J Clim 27(21):8135–8150. doi:10.1175/JCLI-D-14-00202.1
Madec G, Delecluse P, Imbard M, Levy C (1998) OPA 8.1 general circulation model reference manual. Tech. rep. Paris: Institut Pierre-Simon Laplace
Madec G (2008) NEMO ocean general circulation model reference mannuel. Tech. rep. Paris: Institut Pierre-Simon Laplace
Marin F, Caniaux G, Giordani H, Bourlès B, Gouriou Y, Erica K (2009) Why were sea surface temperatures so different in the eastern equatorial Atlantic in June 2005 and 2006? J Phys Oceanogr 39(6):1416–1431. doi:10.1175/2008JPO4030.1
Mohino E, Losada T (2015) Impacts of the Atlantic equatorial mode in a warmer climate. Clim Dyn 45(7–8):2255–2271. doi:10.1007/s00382-015-2471-y (**English**)
Neelin JD, Battisti DS, Hirst AC, Jin F-F, Wakata Y, Yamagata T, Zebiak SE (1998) ENSO theory. J Geophys Res 103(C7):14261. doi:10.1029/97JC03424
Nnamchi HC, Li J, Kucharski F, Kang IS, Keenlyside NS, Chang P, Farneti R (2015) Thermodynamic controls of the Atlantic Niño. Nat Commun 6:8895. doi:10.1038/ncomms9895
Nnamchi HC, Li J, Kucharski F, Kang I-S, Keenlyside NS, Chang P, Farneti R (2016) An equatorial–extratropical dipole structure of the Atlantic Niño. J Clim 29(20):7295–7311. doi:10.1175/JCLI-D-15-0894.1
Okumura Y, Xie SP (2006) Some overlooked features of tropical Atlantic climate leading to a new Nino-like phenomenon. J Clim 19(22):5859–5874
Park W, Keenlyside N, Latif M, Ströh A, Redler R, Roeckner E, Madec G (2009) Tropical Paciffic climate and its response to globalwarming in the Kiel climate model. J Clim 22(1):71–92. doi:10.1175/2008JCLI2261.1
Rayner NA, Parker D, Horton E, Folland C, Alexander L, Rowell D, Kent E, Kaplan A (2003) Global analyses of sea surface temperature, sea ice, and night marine air temperature since the late nineteenth century. J Geophys Res 108(D14):4407. doi:10.1029/2002JD002670
Richter I, Xie S-P (2008) On the origin of equatorial Atlantic biases in coupled general circulation models. Clim Dyn 31(5):587–598. doi:10.1007/s00382-008-0364-z (**English**)
Richter I, Xie SP, Wittenberg AT, Masumoto Y (2012) Tropical Atlantic biases and their relation to surface wind stress and terrestrial precipitation. Clim Dyn 38(5–6):985–1001. doi:10.1007/s00382-011-1038-9
Richter I, Behera SK, Masumoto Y, Taguchi B, Sasaki H, Yamagata T (2013) Multiple causes of interannual sea surface temperature variability in the equatorial Atlantic Ocean. Nat Geosci 6(1):43–47. doi:10.1038/ngeo1660
Richter I, Xie SP, Behera SK, Doi T, Masumoto Y (2014a) Equatorial Atlantic variability and its relation to mean state biases in CMIP5. Clim Dyn 42(1–2):171–188. doi:10.1007/s00382-012-1624-5
Richter I, Behera SK, Doi T, Taguchi B, Masumoto Y, Xie SP (2014b) What controls equatorial Atlantic winds in boreal spring? Clim Dyn 43(11):3091–3104. doi:10.1007/s00382-014-2170-0
Richter I, Xie SP, Morioka Y, Doi T, Taguchi B, Behera S (2016) Phase locking of equatorial Atlantic variability through the seasonal migration of the ITCZ. Clim Dyn 1–15. doi:10.1007/s00382-016-3289-y
Roeckner E, Bäuml G, Bonaventura L, Brokopf R, Esch M, Giorgetta M, Hagemann S, Kirchner I, Kornblueh L, Rhodin A, Schlese U, Schulzweida U, Tompkins A (2003) The atmospheric general circulation model ECHAM5: Part 1: Model description. MPI Rep 349:1–140. doi:10.1029/2010JD014036
Stockdale TN, Balmaseda MA, Vidard A (2006) Tropical Atlantic SST prediction with coupled Ocean–Atmosphere GCMs. J Clim 19(23):6047–6061. doi:10.1175/JCLI3947.1
Thoma M, Greatbatch RJ, Kadow C, Gerdes R (2015) Decadal hindcasts initialized using observed surface wind stress: evaluation and prediction out to 2024. Geophys Res Lett. doi:10.1002/2015GL064833
Wang C, Zhang L, Lee S, Wu L, Mechoso CR (2014) A global perspective on CMIP5 climate model biases. Nat Clim Change 4:201–205. doi:10.1038/NCLIMATE2118
Xie SP, Carton JA (2004) Tropical Atlantic variability: patterns, mechanisms, and impacts. Earth's Clim. American Geophysical Union 121–142. doi:10.1029/147GM07
Zebiak SE (1993) Air–sea interaction in the equatorial Atlantic region. J Clim 6(8):1567–1586. doi:10.1175/1520-0442(1993)006<1567:AIITEA>2.0.CO;2
Zhu J, Huang B, Wu Z (2012) The role of ocean dynamics in the interaction between the Atlantic meridional and equatorial modes. J Clim 25(10):3583–3598. doi:10.1175/JCLI-D-11-00364.1

Chapter 3

A comparison of the Atlantic and Pacific Bjerknes feedbacks: Seasonality, Symmetry, and Stationarity

The Bjerknes feedback is a main driver of the Atlantic and Pacific Niños. The following chapter takes a closer look at the symmetries of the Atlantic and Pacific Bjerknes feedbacks and assesses their stationarity on decadal time scales.

Citation: **Dippe, T., J. F. Lübbecke, and R. J. Greatbatch (2018). "A comparison of the Atlantic and Pacific Bjerknes feedbacks: Seasonality, Symmetry, and Stationarity". Submitted to *Journal of Geophysical Research: Oceans***

The candidate's contributions to this manuscript are as follows. She

- Conceived the basic question that is discussed in the manuscript;
- Performed all the analyses;
- Produced all the figures;
- Authored the manuscript from first to final draft.

A comparison of the Atlantic and Pacific Bjerknes feedbacks: Seasonality, Symmetry, and Stationarity

T. Dippe[1*], J. F. Lübbecke[1,2], R. J. Greatbatch[1,2]

[1]GEOMAR Helmholtz Centre for Ocean Research Kiel, Germany
[2]Faculty of Mathematics and Natural Sciences, Christian Albrechts University, Kiel, Germany

Key Points:

- The elements of the Atlantic Bjerknes feedback display asymmetries.
- These asymmetries are less consistent in the Atlantic, compared to their Pacific counterparts.
- The Atlantic Bjerknes feedback varies substantially on decadal time scales.

*GEOMAR Helmholtz Center for Ocean Research Kiel

Corresponding author: T. Dippe, tdippe@geomar.de

Abstract

The Bjerknes feedback is the dominant positive feedback in the equatorial ocean basins. Here, we examine the seasonality, symmetry, and stationarity of the Pacific and Atlantic Bjerknes feedbacks, decomposing them into three feedback elements that link thermocline depth, sea surface temperature (SST), and western basin wind stress variability. We further partition each feedback element into composites associated with either positive or negative anomalies. Using robust regression, we diagnose the strength of each composite.

For the recent period 1993-2012, composites of the Pacific Bjerknes feedback elements agree well with previous work. Positive composites are generally stronger than negative composites, and all feedback elements are weakest in late boreal spring. In the Atlantic, the difference between positive and negative composites is less consistent across feedback elements. However, a clear seasonality emerges: Feedback elements are generally strong in boreal summer and, for the negative composites, again in boreal winter. The Atlantic Bjerknes feedback is dominated by subsurface-surface coupling.

Applying our analysis to overlapping 25-year periods for 1958-2012 shows that the strengths of feedback elements in both ocean basins vary on decadal time scales. While the overall asymmetry of the Pacific Bjerknes feedback is robust, the strength and symmetry of Atlantic feedback elements vary considerably between decades. Our results indicate that the Atlantic Bjerknes feedback is non-stationary on decadal time scales.

1 Introduction

The Bjerknes feedback is the dominant coupled, positive feedback in the equatorial oceans (Bjerknes, 1966, 1969) and plays a crucial role in shaping Atlantic and Pacific equatorial variability. It ties three key properties of an equatorial ocean basin into a closed feedback loop. These properties are (i) the thermocline depth along the equator, which can be approximated by sea surface height (SSH) in the central and eastern ocean basin (Cane, 1984; Rebert et al., 1985); (ii) eastern basin sea surface temperature (SST); and (iii) western basin zonal wind stress (USTR).

The closed feedback loop can be decomposed into three feedback elements that act in concert:

(i) SSH→SST: "*Subsurface-surface coupling*". The thermocline depth in the eastern ocean basin is related to both net upwelling of cold water into the surface mixed layer, and mixing at the base of the mixed laxer (Hummels et al., 2013). A deepening thermocline in the eastern ocean basin effectively increases the warm water volume in this region, which weakens the cooling effect of upwelling at the base of the mixed layer and produces a net warming. In contrast, a shoaling thermocline decreases the warm water volume and allows the upwelling to cool the surface layer more effectively, producing cold SST anomalies when upwelling is constant. When discussing this feedback element, recall that SSH is a valid stand-in for thermocline depth only in the eastern and central equatorial ocean basin (Cane, 1984), and results must be treated cautiously in the western ocean basins.

(ii) SST→USTR: "*SST-wind coupling*". Eastern basin SST anomalies produce a local, Gill-type atmospheric response (Gill, 1980), altering the sea level pressure gradient along the equator. Positive SST anomalies create a local anomalous low that weakens the zonal surface pressure gradient. The trade winds in the western ocean basin weaken and the zonal wind stress at the ocean surface decreases.

(iii) USTR →SSH: "*Wind-thermocline coupling*". Zonal wind anomalies in the western ocean basin change the local balance between zonal wind stress and the subsurface pressure gradient in the ocean. The thermocline, in turn, adapts to the

varying subsurface pressure gradient, and changes in thermocline depth are transmitted eastward along the equator via an equatorial Kelvin wave. In the case of weakening trade winds, the subsurface pressure gradient decreases and a downwelling g Kelvin wave propagates eastward. Once the Kelvin wave reaches the relatively shallow thermocline of the eastern basin, it deepens the thermocline there, engaging it in subsurface-surface coupling and closing the Bjerknes feedback loop.

The Bjerknes feedback operates as a positive feedback for both positive and negative anomalies in either SSH, SST, or USTR. It is active exclusively at the equator, since the transmission of information via Kelvin waves along the zonal extent of the ocean basin requires the Coriolis force to vanish.

Since Bjerknes (1966) first described the closed feedback loop outlined above, different studies have referred to different mechanisms as "the Bjerknes feedback", sometimes focusing on the atmospheric or ocean parts of the coupled feedback only. Here, when we discuss "the" Bjerknes feedback, we refer to the coupled feedback that relates variability in both the ocean and the atmosphere.

In the equatorial Atlantic and Pacific Oceans, the Bjerknes feedback supports the growth of coupled air-sea anomalies associated with the Atlantic and Pacific Niños (Bjerknes, 1969; Keenlyside & Latif, 2007; Burls et al., 2012; Lübbecke & McPhaden, 2013; Deppenmeier et al., 2016; Dippe et al., 2018). While the phrase "Pacific Niño" in a strict sense refers to the SST manifestation of a positive El Niño-Southern Oscillation (ENSO) event, in this paper we use the name to refer to the entire coupled process. Likewise, when we talk about the "Atlantic Niño ", we mean the complete coupled atmosphere-ocean process, including negative events that are generally known as Pacific and Atlantic Niñas. Alternative names for the Atlantic Niño are "Atlantic zonal mode" and "Atlantic cold tongue mode", which highlight slightly different aspects of the same phenomenon (Lübbecke et al., 2018).

In their respective basins, the Niños are the dominant mode of interannual SST variability. They are associated with tongue-shaped patterns of SST anomalies that stretch from the coastal upwelling regions in the eastern subtropics into the central equatorial ocean basins. While their corresponding names and similar patterns suggest that they are essentially manifestations of the same process, significant differences exist (Xie et al., 1999; Burls et al., 2011; Lübbecke & McPhaden, 2013; Richter et al., 2013). The canonical Pacific Niño generally peaks in boreal winter and lasts for several months, while the Atlantic Niño is tightly phase-locked to boreal summer and rarely outlasts a season, achieving roughly half of the Pacific SST anomaly amplitude. The phase-locking of the Niños is accompanied by a strong seasonality of their supporting Bjerknes feedbacks. The Pacific Bjerknes feedback operates for most of the year, while the Atlantic Bjerknes feedback is active for a few months only twice a year, in boreal summer and again, briefly, at the beginning of boreal winter (Burls et al., 2011; Dippe et al., 2018).

Another interesting feature of the Atlantic is that it hosts a secondary, Niño-like phenomenon in boreal winter. Okumura and Xie (2006) found that the "winter Niño" – their "Niño II" – is the product of a secondary, seasonal weakening of the trade winds in the Gulf of Guinea, which is able to briefly organize coupled atmosphere-ocean variability into the Bjerknes feedback.

Both in the Atlantic and the Pacific, variability associated with the coupled Niños strongly affects the surrounding continents and establishes atmospheric teleconnections to remote areas. Teleconnections associated with the Pacific Niño can encompass the globe and have devastating consequences (Rasmusson & Wallace, 1983; Trenberth et al., 1998). Similarly, tropical Atlantic SST variability affects the rainfall patterns of the surrounding continents (Nobre & Shukla, 1996; Harzallah et al., 1996; Lübbecke et al., 2018).

Characteristics of the Atlantic and Pacific Niños vary on decadal and longer time scales. Losada and Rodríguez-Fonseca (2016) and Martín-Rey, Polo, Rodríguez-Fonseca, Losada, and Lazar (2017) report that the Atlantic Multidecadal Oscillation (AMO) – a low-frequency phenomenon that is mainly characterized by variations of basin-wide SST in the North Atlantic (Schlesinger & Ramankutty, 1994; Delworth & Mann, 2000; Knight et al., 2006) – modulates both the spatial configuration of the Atlantic Niño SST pattern and the atmospheric response to these patterns. Martín-Rey et al. (2017) argue that eastern equatorial Atlantic SST variability is enhanced by more than 150% in boreal summer during negative AMO phases. Similarly, Cobb et al. (2013) and Li et al. (2013) demonstrate for centennial and millennial time scales that the spatiotemporal characteristics of the Pacific Niño are subject to low-frequency variations. For the recent decades, studies such as Lübbecke, Burls, Reason, and McPhaden (2014) show that low-frequency variations in the Pacific background state modulate the strength of the Pacific Bjerknes feedback and hence the characteristics of the Pacific Niño.

Additionally, the spatiotemporal characteristics of warm and cold Pacific Niño events are subject to a number of asymmetries (Takahashi et al., 2011; Dommenget et al., 2013; Capotondi et al., 2015; Chen et al., 2015; Takahashi & Dewitte, 2016). For example, warm events are generally stronger in terms of their SST amplitude than cold events, while cold events last longer and evolve in a different spatial manner. Another aspect of the complex nature of the Pacific Niño is highlighted by the existence of different manifestations of Pacific Niño events that have seemingly distinct spatiotemporal signatures (Yeh et al., 2009; Takahashi et al., 2011; Capotondi et al., 2015; Takahashi & Dewitte, 2016). For example, Yeh et al. (2009) document that the last decades saw an increase in the frequency of the central Pacific Niño (or, equivalently El Niño Modoki). In contrast to the canonical eastern Pacific Niño with its clear signature in the eastern Pacific and seesaw-response in the anomalous Walker circulation, the pattern of the central Pacific Niño is constrained to the region between $160°E$ and $120°W$ and splits the Walker circulation into two cells (Ashok & Yamagata, 2009). Additionally, teleconnections manifest in distinct ways, depending on whether they originate from central or eastern Pacific Niño events. A generalizations of these ENSO "flavours" has recently been proposed by Timmermann et al. (2018), who provide an overview on what they call ENSO complexity.

Some of the above asymmetries in the Pacific have been linked to asymmetries in the strength of the Pacific Bjerknes feedback elements. Dommenget et al. (2013) and DiNezio and Deser (2014) show that the different durations of warm and cold events are related to non-linearities in the SSH-SST and SST-USTR feedback elements. In a different approach, Hu et al. (2017) shows that the "recharge/discharge" processes associated with wind-thermocline coupling operate differently for warm and cold events, favoring long cold events and rather short, intense warm events. Furthermore, Levine and McPhaden (2016) find that state-dependent noise forcing contributes to the SST amplitude asymmetry of the Pacific Niño. State-dependent noise provides an additional positive feedback between warm Pacific Niño events and zonal wind variability. The evolving warm event amplifies its own wind forcing by creating a state that promotes the occurrence of subsequent strong westerly wind bursts in the western and central ocean basin. This mechanism enhances wind-thermocline coupling.

In contrast to the prominent Pacific SST amplitude asymmetry, the Atlantic Niño is rather symmetric. Lübbecke and McPhaden (2017) show that warm and cold Atlantic Niño events are effectively mirror images of each other. Additionally, they diagnose the strength of the Bjerknes feedback elements for both positive and negative summer events and conclude that, unlike the Pacific Bjerknes feedback, the Atlantic summer Bjerknes feedback is largely symmetric.

Here, we revisit the work of Lübbecke and McPhaden (2017) by taking into account zonal, seasonal, and decadal variations of the Bjerknes feedback strengths associated with positive and negative events in the equatorial Atlantic. Specifically, we seek to answer

the following question: For the summer and winter Niños in the equatorial Atlantic, does the Bjerknes feedback operate symmetrically for cold and warm events? Are these findings stationary, or do they depend on the analysis period?

The remainder of the paper is structured as follows. Section 2 explains how we estimate the Bjerknes feedback and on which datasets we base our analysis. Section 3 discusses the results of our analysis. In Section 4, we discuss our findings in comparison to Lübbecke and McPhaden (2017) and attempt to assess the stationarity of our results. A discussion is provided in the last section.

2 Data and Methods

2.1 Data

Our analysis is based on two groups of datasets that each contain monthly mean SSH, SST, and USTR in the equatorial Atlantic and Pacific ocean basins.

1. "*OBS*", 1993-2012: This group blends direct satellite observations with reconstructions and reanalysis. We use SSH provided by AVISO (`https://www.aviso.altimetry.fr/en/home.html`); SST from NOAA's Extended Reconstructed Sea Surface Temperature (Smith & Reynolds, 2003, ERSST), version 5 (Huang et al., 2017); and USTR from the ERA-Interim Reanalysis (Dee et al., 2011). While ERA-Interim is not an observational dataset, we decided to use the name "OBS" for this group for the sake of readability.
2. "*ORAS4*", 1958-2009: The data in this group are taken from ECMWF's Ocean Reanalysis System Version 4 (Balmaseda et al., 2012), which provides dynamically consistent SSH, SST, and USTR. SSH and three-dimensional ocean potential temperature data were downloaded from the University of Hamburg's Integrated Climate Data Center (`http://icdc.cen.uni-hamburg.de/projekte/easy-init/-easy-init-ocean.html`). We use SSH as provided by the reanalysis; the first level of the ocean potential temperature as SST; and the same wind stress dataset as in Lübbecke and McPhaden (2017), which corresponds to the wind stress forcing of ORAS4, using ERA-40 (Uppala et al., 2006) data from January 1958 to December 1988, and ERA-Interim data afterwards. Note that reanalysis products potentially suffer from model-induced biases. Additionally, the accuracy of results is highly sensitive to the quality of the assimilated data. Uncertainties are generally larger prior to the advent of satellite observations in the late 1970s. Because of this, our discussion of ORAS4-based results in Section 4 will focus on general issues rather than on exact numerical values.

As pointed out in the Introduction, SSH is a reliable proxy for thermocline depth in the central and eastern equatorial ocean basins only (Cane, 1984). Hence, results involving SSH should be treated cautiously in the western warm pool regions.

Anomalies in this study are calculated as follows: We first remove the linear trend from the entire time series, then subtract the seasonal cycle to obtain monthly anomalies. For each analysis, we calculate the anomalies with respect to the chosen analysis periods.

For the overlap period 1993-2009, we compare the time series of anomalies and the seasonal distribution of the standard deviation between the two dataset groups for each variable (Fig. 1). To facilitate comparison, we averaged our data into indices of the Atl3 and Nino3.4 regions ($3°S$ to $3°N$, $20°W$ to $0°E$, and $5°S$ to $5°N$, $170°$ to $120°W$, respectively) in the Atlantic and Pacific for both SSH and SST; and into the WAtl and Nino4 regions ($3°S$ to $3°N$, $40°$ to $20°W$, and $5°S$ to $5°N$, $160°E$ to $150°W$) for USTR. The datasets agree well with each other, and anomaly correlation values between pairs of the

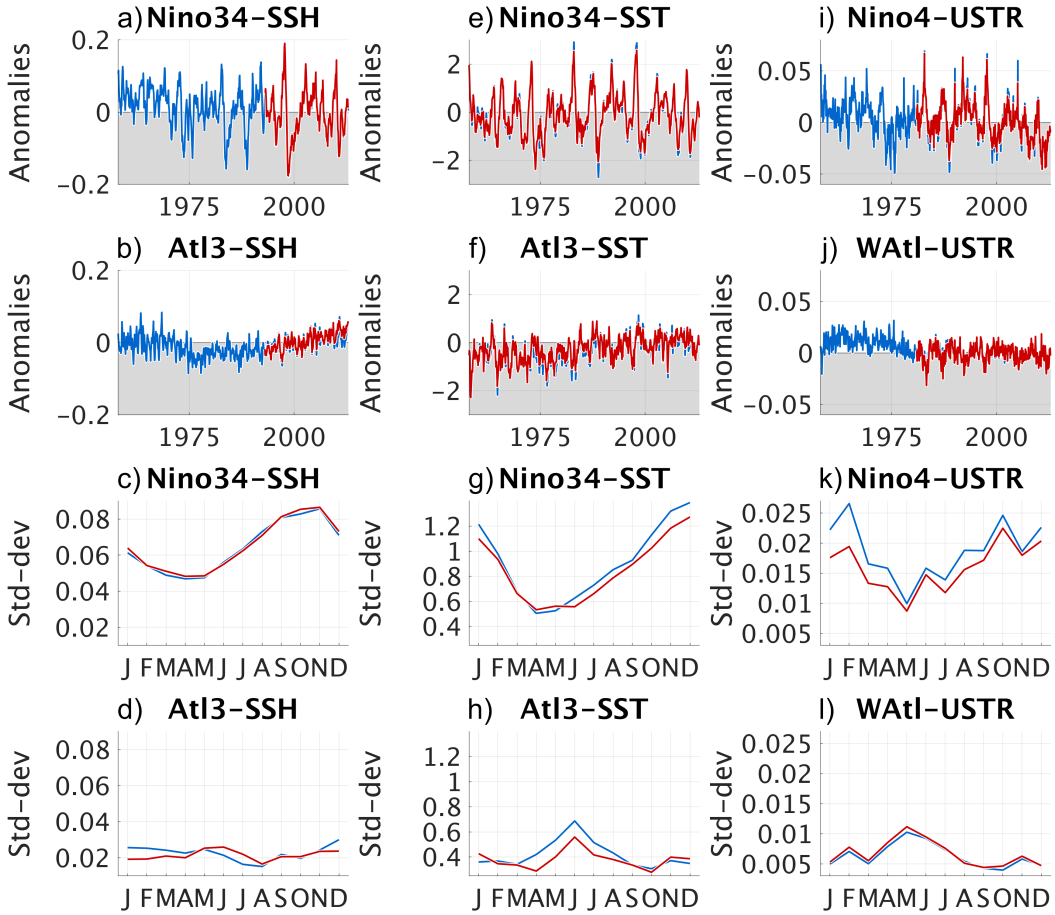

Figure 1: *Key features of employed datasets. Time series of anomalies with respect to the linear trend and the seasonal cycle (upper two rows, panels a-b, e-f, i-j), and monthly stratified standard deviations (lower two rows, c-d, g-h, k-l, months from January to December indicated by their first letter on the x-axis). Both quantities have been diagnosed with respect to the overlap period of the two dataset groups, 1993-2009. Each panel shows the same quantity for the OBS and ORAS4 dataset groups as red and blue lines, respectively, and all quantities are shown for SSH, SST, and USTR in the left-hand (a-d), middle (e-h), and right-hand row (i-l). The OBS group contains AVISO-SSH, ERSST-SST, and ERA-Interim zonal wind stress (USTR). Data has been averaged into the Atl3 and Nino3.4 regions in the Atlantic and Pacific for both SSH and SST; and into the WAtl and Nino4 regions for USTR.*

same variable all exceed values of 0.9. Additionally, Fig. 1 highlights some of the differences between the Atlantic and Pacific Niños that have been discussed in the Introduction. It is obvious that Pacific Niño events have a distinct signature in the anomaly time series of SSH, SST, and USTR, with intermittent, strong events that are clearly phase-locked to boreal winter (Fig. 1a,e,i). In contrast, variances in the Atlantic are much smaller (note identical y-axes) and events occur more regularly, producing anomaly time series that resemble white noise more closely than their intermittent Pacific counterparts (Fig. 1b,f,j). Another interesting feature is that the seasonal variances of Atlantic SSH do not fully agree with each other in the OBS and ORAS4 dataset groups. Particularly, AVISO-SSH variance peaks in June, simultaneously with ERSST-SST variance, while ORAS4-SSH peaks one month early in May and reaches its global maximum in December; the

variances of ORAS4-SSH and ORAS4-SST do not peak simultaneously (Fig. 1d,h). Last, panels 1k,l indicate that the ERA-Interim and ORAS4 USTR data are not exactly equal, although they are both ERA-products. This could be due to the blending in ORAS4, and to a lesser degree to the different horizontal resolutions of the two datasets, with the ORAS4 USTR being higher resolved than the ERA-Interim data used in this study.

2.2 Estimating the strength of the Bjerknes feedback elements

To diagnose the strength of the individual Bjerknes feedback elements, we use robust linear regression (Holland & Welsch, 1977; Street et al., 1988; Huber & Ronchetti, 2009). In statistical analysis, developing a model of a given dataset requires assumptions about the process(es) that generated the data. Ordinary least squares-based linear regression (OLS) can become unreliable when these assumptions are violated, especially in the presence of outliers. The reason for this is that OLS minimizes the squared distance of the residuals to the guess of the predicted values. Robust regression techniques – a collection of methods that seek to lessen the sensitivity of the regression coefficients to outliers – generally change the weight that is attributed to each residual when considering its impact on the final regression coefficients. A common approach is to assign a relatively strong weight to small residuals, and decrease the weight of large residuals that are likely associated with outliers. While robust regression has been designed with outliers in mind, Zheng, Fang, Yu, and Zhu (2014) demonstrated that it is a valid way to perform regression analysis based on small datasets in climate science. We adopt this approach here, using Matlab's implementation of robust regression (`robustift`, current documentation provided by `https://de.mathworks.com/help/stats/robustfit.html`). For our analysis, we use the default `robustfit` of the 2018-distribution, which iteratively re-weights least squares with a bisquare weighting function.

To diagnose the strength of the Bjerknes feedback elements in our zonal analysis, we average equatorial SSH and SST into 4° longitude $\times$4° latitude boxes that slide along the equator. Zonal wind stress (USTR), in contrast, is fixed to WAtl in the Atlantic, and Nino4 in the Pacific, no matter which longitude is analyzed. The reason for this choice is that it is the western basin wind stress that dominantly contributes to the closed Bjerknes feedback, and not the local wind stress.

2.3 Including lagged feedback elements into the analysis

Unless stated otherwise, we take into account that any of the Bjerknes feedback elements could be lagged in nature when we calculate composite strengths in this study (see Section 2.4 below for details on the feedback element composites). This means that the feedback must not necessarily be strongest when both variables are measured in the same calendar month, but rather when one variable leads the other. To identify possible lags in the Bjerknes feedback elements, we conduct a cross-regression analysis before we diagnose the composite strengths, and we do this separately for each analysis period. For example, wind-thermocline coupling is strongest when wind variability precedes thermocline variability by a few months – it leads SSH variability. The cross-regression analysis identifies such lags. To perform it, we use robust regression. During the cross-regression analysis, we fix the forcing variable of the feedback element – the variable that "drives" the feedback element, i.e. SSH, SST, and USTR for the SSH-SST, SST-USTR, and USTR-SSH feedback elements – to our analysis month and shift the month at which the response variable is measured, for values of up to $\pm$8 months.

Negative lags indicate that the relationship is strongest when the response variable leads the forcing variable (for the example above, when SSH-variability precedes wind variability). In this case, the causality of the three relationships forming the Bjerknes feedback is severed; our framework breaks down. To establish the Bjerknes feedback, all three feedback elements must have positive strengths in addition to neutral or positive

lags, since a negative relationship would inhibit anomaly growth. Neutral or positive lags are hence a sufficient, but not the exclusive condition for the Bjerknes feedback to be active.

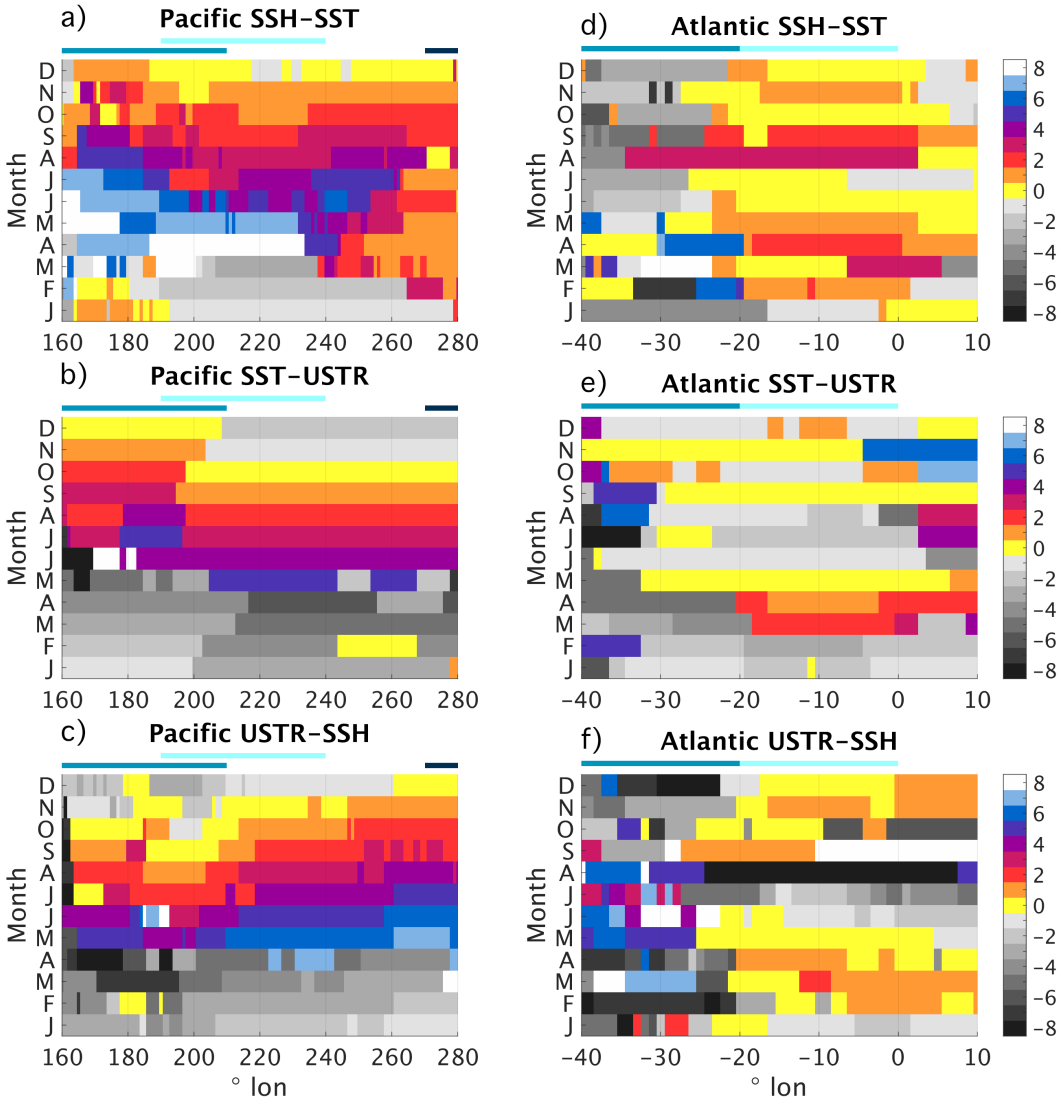

Figure 2: *Lag in months at which the relationship for each of the three Bjerknes feedback elements is strongest. Data is shown along the equator (x-axis) and stratified into calendar months (y-axis) for both the Pacific (left column, panels a-c), and the Atlantic (right column, d-f). The sign of the lag is with respect to the forcing variable of the feedback element, i.e. SSH, SST, and USTR for the SSH-SST, SST-USTR, and UTRS-SSH feedback elements, respectively. A positive lag indicates that the forcing variable leads the response variable. Positive lags are shown in colour, with a lag of zero months indicated by yellow. Negative lags are shown in grey shading. The top, middle, and bottom rows show results for subsurface-surface coupling (a,d), SST-wind coupling (b,e), and wind-thermocline coupling (c,f). For each longitude, data has been averaged into 4° longitude ×4° latitude bins prior to calculation. This binning has been done for each analysis, unless stated otherwise.*

Figure 2 shows the lags that our cross-regression analysis identified, for the OBS dataset group and the period 1993-2012. To produce the results shown in Section 3, we assume that the lags are independent of the subset of data that was used to diagnose them, i.e. of whether positive or negative composites were considered (see Section 2.4). In Section A.1 of the Appendix, we briefly discuss the validity of this assumption and find that it generally holds. However, using lags that do not consider the two types of composites discussed in Section 2.4 *locally* degrades the strength of the feedback element in comparison to using no lags at all. This means that using composite-independent lags can weaken the resulting Bjerknes feedback element, demonstrating again how diverse the mechanisms are that produce the variability of the Atlantic and Pacific Niños, and that it may not be justified to make equivalent assumptions for warm and cold events.

Figure 2 shows that in the Pacific, all feedback elements are generally characterized by positive lags that start to occur in May and decrease until boreal winter, indicating that the closed feedback loop becomes more instantaneous in the latter half of the year (Fig. 2a-c). Zonal variations are rather small, and lags tend to occur uniformly across large parts of the Pacific.

In the Atlantic, lags for the subsurface-surface coupling are generally positive (Fig. 2d), indicating that SSH leads SST variability by three months at most. During June and July, and again in boreal winter, lags vanish and subsurface-surface coupling acts instantaneously. The SST-USTR and USTR-SSH feedback elements, on the other hand, are characterized by lags ≥ 0 only during spring and early summer, and again during boreal winter. In agreement with previous studies on the seasonality of the Atlantic Bjerknes feedback (Keenlyside & Latif, 2007; Burls et al., 2011), this indicates that the Bjerknes feedback can only establish a closed feedback loop during early summer and winter. Another feature of Fig. 2d-f is that the lags of the feedback elements are not distributed evenly across the zonal extent of the basin. Rather, positive lags occur predominantly in or close to the Atl3 region (overlaid light-blue rectangle), showing that not only is the Atlantic Bjerknes feedback constrained to two short periods, but also to a narrow spatial domain.

When we include lags into our robust regression analysis, we do this by shifting the time series of the response variable according to the identified lag. For example, when our cross-regression analysis identified a lag of +2 months for a given calendar months, we use the the forcing variable for the calendar month, and the response variable for the calendar months +2 months when diagnosing our composite strengths.

2.4 Assessing the symmetry of the Bjerknes feedback: Compositing feedback elements

To assess the symmetry of a Bjerknes feedback element, we partition it into positive and negative composites. An important distinction: We do *not* separate our feedback elements into consistent warm/cold composites according to the SST conditions in the equatorial Atlantic, but rather assign individual composites to each feedback element, based on the forcing variable of the feedback element. For each feedback element, the composites are diagnosed and can be interpreted as follows.

- SSH-SST: Composites are based on the sign of the SSH anomaly. The positive and negative composites are associated with deep and shallow thermoclines, respectively.
- SST-USTR: Composites are based on the sign of the SST anomaly. Positive and negative composites are associated with warm and cold SSTs, respectively.
- USTR-SSH: Composites are based on the sign of the USTR anomaly (in Nino4 and WAtl in the Pacific and Atlantic, respectively). Positive and negative com-

posites are associated with easterly and westerly wind stress anomalies, respectively.

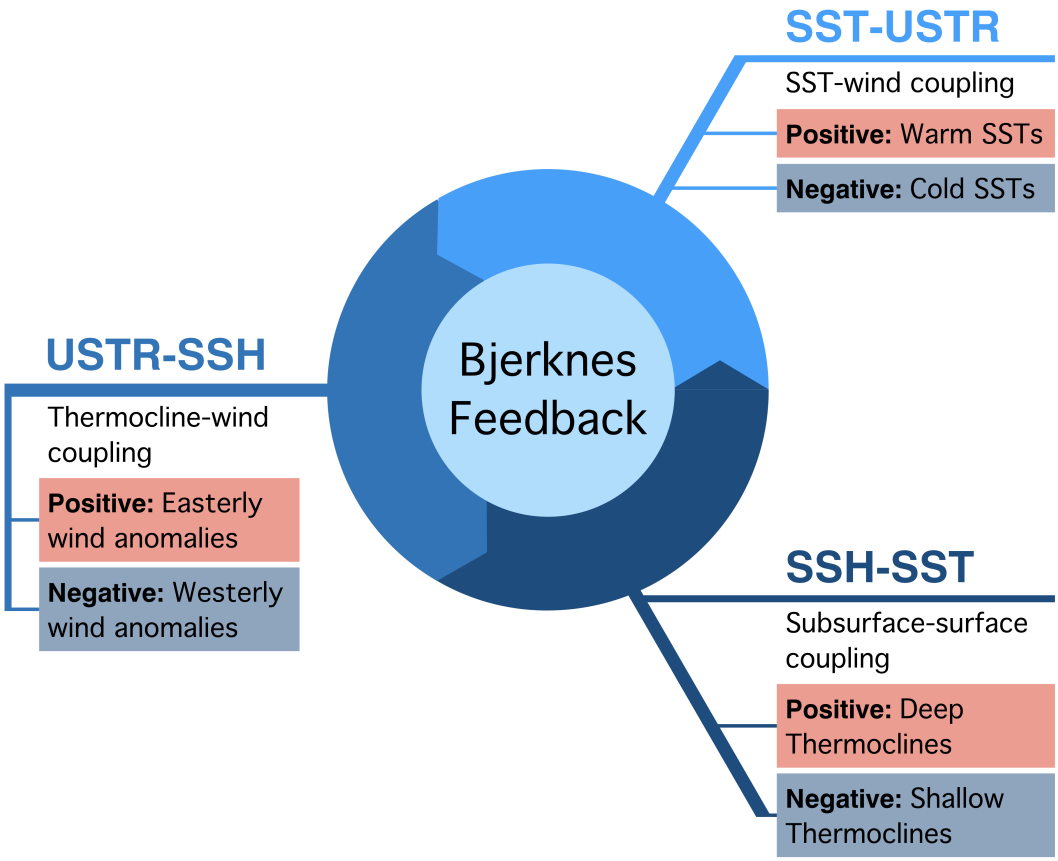

Figure 3: *Schematic of the feedback decomposition approach. The closed Bjerknes feedback loop is decomposed into three interacting* feedback elements *(partitioned ring around the central circle). These feedback elements are the subsurface-surface coupling (SSH-SST, dark blue, bottom right), SST-wind coupling (SST-USTR, light blue, top right), and wind-thermocline coupling (USTR-SSH, blue, left). Each feedback element is additionally partitioned into two* composites *(red and blue boxes below each feedback element). Composites are based on the sign of the anomalies of the forcing variable, i.e. SSH, SST, and USTR for the SSH-SST, SST-USTR, and USTR-SSH feedback elements, respectively. The text in the composite boxes explains how each composite can be interpreted with respect to its "parent" feedback element (see Section 2.4).*

This two-step decomposition of the Bjerknes feedback loop – into feedback *elements* first, then into *composites* of the feedback elements – is schematically illustrated in Fig. 3. Because of the partitioning of our base data pool into positive and negative composites prior to our regression analysis, the effective sample sizes for our robust regression are on the order of 10 for the period 1993-2012 (Section 3), and 12 for the 25-year periods considered in Section 4. This is a very small sample size. Even though we employ robust regression, we will refrain from attributing too much value to individual numbers, and will rather focus on general patterns.

2.5 Bootstrapping significances

Significance in our study indicates that a given composite of a feedback element (or their difference) is significantly different from the expected strength (difference) of that feedback element when it is diagnosed from a random sub-sample of the data. We estimate this significance using the simple bootstrapping approach outlined below.

For a (strength) composite of a Bjerknes feedback element, we generate a distribution of the expected feedback element strength by re-diagnosing the robust regression coefficients for random sub-samples of the full data pool. Sub-samples ignore composites, but obey the same lags as the composite strengths they test (see Fig. 2), and have the same sample size. By iterating through a large number of sub-samples, we bootstrap a distribution of pseudo-composite strengths, whose expected value corresponds to the relationship strength of the feedback element when the data is not partitioned into composites. Next, we use the bootstrapped distribution to perform a simple significance test. If the composite strength is outside the 90%-area of the bootstrapped distribution for a significance level of $\alpha = 0.1$ and the case of a one-sided test, we reject the null hypothesis that the composite strength is equal to the relationship strength based on the full dataset. The composite strength is significant.

For the difference between the positive and negative composites, we repeat the above method, but use the difference between the calculated composite strengths as the target of the test, instead of the absolute composite strength. For this, we again determine the size of our sub-sample, randomly draw a new sample of the same size, and use the remaining data in the pool as the pseudo-counter composite.

In this study, we perform 1,000 bootstraps and use a significance level of 0.1 for each of our significance tests.

3 Symmetry of the Atlantic and Pacific Bjerknes feedbacks 1993-2012

3.1 Bjerknes feedback element strengths

To validate our method of partitioning the strength of the Bjerknes feedback elements into positive and negative composites, we first discuss our results based on the OBS dataset group for the tropical Pacific during the period 1993-2012 (Fig. 4, differences shown in Fig. 5a-c). We include the lags shown in Fig. 2 into our analysis.

In agreement with the equatorial Pacific "spring barrier", both composites of the SST-USTR and USTR-SSH feedback elements decline during late boreal winter and spring in the Pacific (Fig. 4b-c,e-f). The spring barrier is a concept that originates from seasonal predictability studies and refers to the drop in predictability of the Pacific Niño during boreal spring (Torrence & Webster, 1998; Duan & Wei, 2013). Wengel, Latif, Park, Harlaß, and Bayr (2018) showed that the spring barrier is associated with a weakening of the atmosphere-ocean coupling in the tropical Pacific that temporarily decreases the strength of the Bjerknes feedback estimated by Jin, Kim, and Bejarano (2006)'s Bjerknes stability index (see Section 5). Our results agree with this. The closed Bjerknes feedback loop breaks down at the end of boreal winter, indicated, too, by the negative lags presented in Fig. 2.

In the Nino3.4 region and the eastern ocean basin, negative composites are significantly different from the expected relationship strength more frequently than positive composites. This is shown by the distribution of significances, indicated by overlaid black crosses in Fig. 4. Recall from Section 2.5 that "significance" indicates a significant difference relative to the expected strength of the feedback element when it is diagnosed for the full dataset. The dominance of positive events over negative events is in agreement with previous studies on Pacific Niño asymmetries. In particular, while cold events

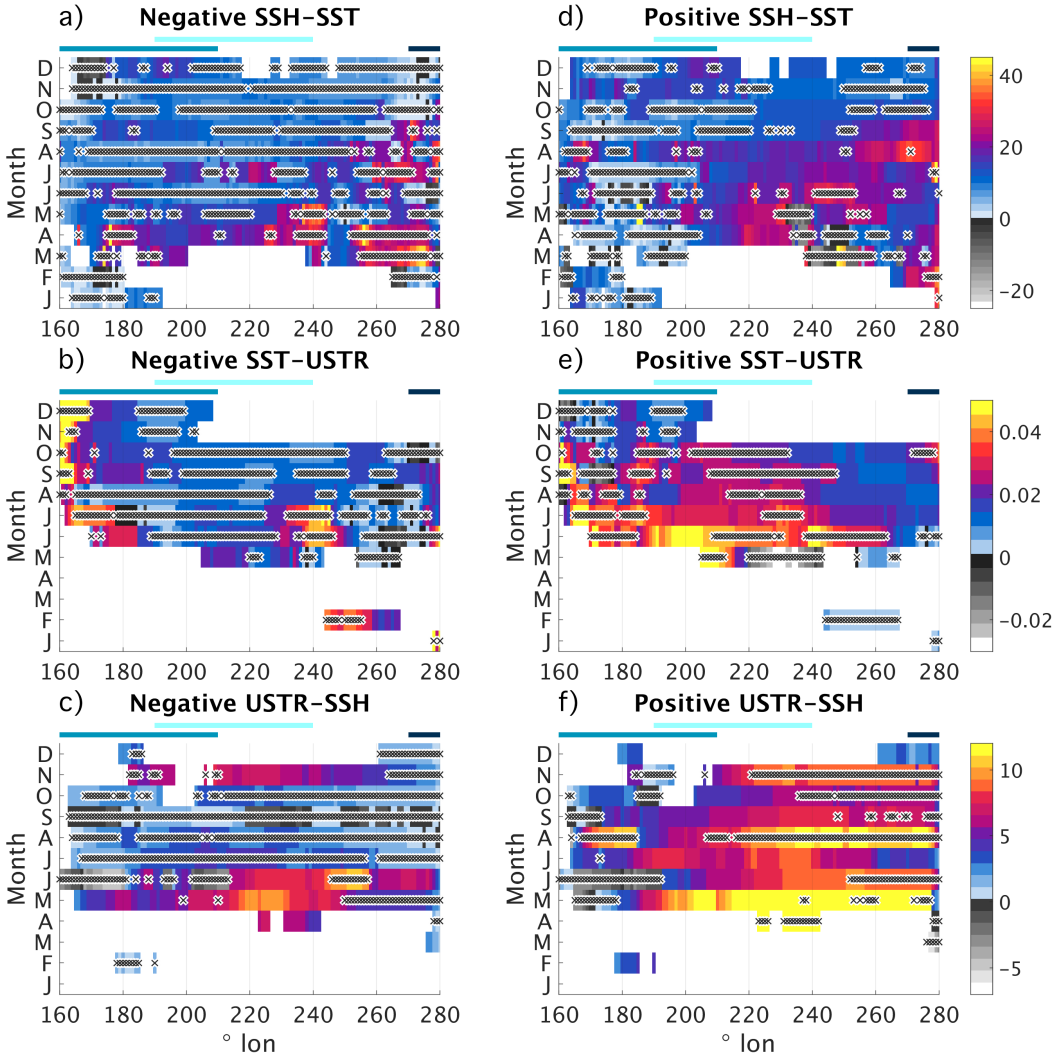

Figure 4: *Composites of the OBS-based feedback elements in the Pacific, for the recent period 1993-2012 along the equator (x-axis) and stratified into calendar month (y-axis) with respect to the forcing variable. The top, middle, and bottom row show results for the SSH-SST (panels a,d), SST-USTR (b,e), and USTR-SSH feedback elements (c,f), with forcing variables SSH, SST, and USTR, respectively. To estimate the sensitivity of the two involved variables for the case of either positive or negative anomalies of the forcing variable, cf. Section 2.4, we use the slope parameter provided by robust regression. Colour shading indicates positive values, with small values shown in blue, and the highest values shown in reds and yellows. Negative values, indicating that a feedback element disrupts the closed Bjerknes feedback, are shown in grey shading, with the lightest greys indicating the largest negative values. White indicates that, at the given longitude and month, the lag diagnosed in Fig. 2 is negative and hence is not in agreement with the framework of the Bjerknes feedback. Sensitivities are given in units of K/m, $N/(m^2K)$, and m^3/N for the three feedback elements, respectively. The left and right columns show the sensitivities for the negative (a-c) and positive composites (d-f). Significance is indicated by black crosses with a white outline (see text for details). Coloured bars below the title indicate the zonal extent of the Nino4, Nino3.4, and Nino1.2 regions in blue, light blue, and dark blue, respectively.*

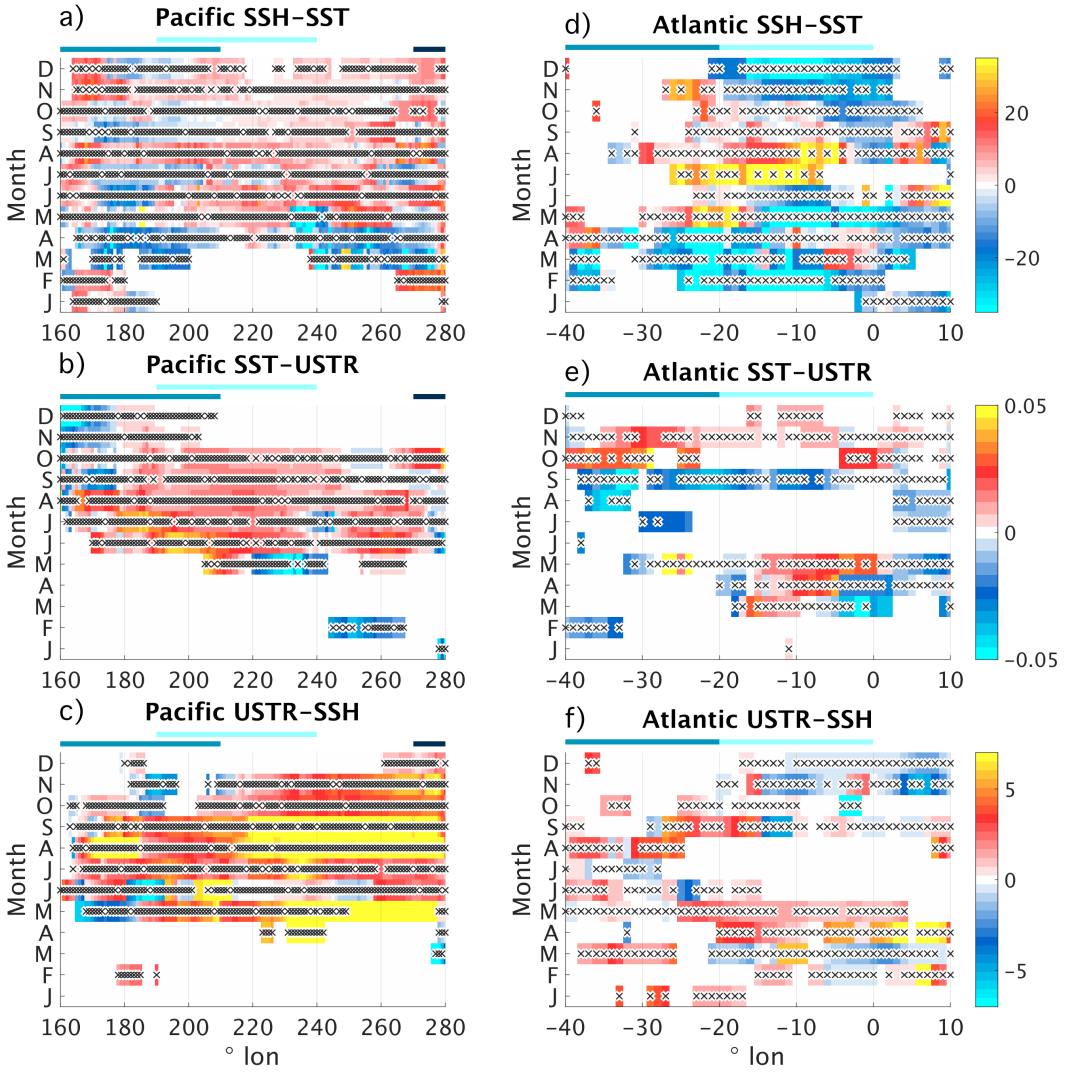

Figure 5: *Similar to Fig. 4, but showing the difference between positive and negative composites of the feedback elements in the Pacific (left column, panels a-c) and the Atlantic (right column, d-f), for the SSH-SST (a,d), SST-USTR (b,e), and USTR-SSH (c,f) feedback elements. Blue (red-yellow) shading indicates that the negative composite is larger (smaller) than the positive composite. Coloured bars below the titles indicate the zonal extent of the Nino4, Nino3.4, and Nino1.2 (WAtl and Atl3) regions in the Atlantic (Pacific) in blue, light blue, and dark blue (blue and light blue).*

are rather modest in magnitude, virtually all extreme events are warm and hence strongly shape the overall characteristics of the Pacific Niño (note, however, that really only one "extreme event" occurred in the short period 1993-2012). Consequently, the positive composites of the feedback element strengths are in better agreement with the expected overall relationship strengths than the negative composites.

Pacific subsurface-surface coupling (Figs. 4a,d) is positive for almost the entire year and across most of the Pacific basin. East of $150°W$ ($210°E$), the positive composite is generally stronger than the negative composite (Fig. 5a), in particular in the far eastern basin during late boreal summer, coinciding with the main onset phase of warm Pacific Niño events.

Pacific SST-wind coupling, too, is generally stronger for the positive composite (Figs. 4b,e, and 5b). Physically, this could be due to a threshold dependence of equatorial deep convection. While warm SST anomalies promote overlying convection effectively, cold SSTs do not necessarily suppress convection to the same degree (Levine & Jin, 2017). Consequently, wind variability is more sensitive to warm SST anomalies than to cold SST anomalies.

An interesting feature of the positive composite of the Pacific SST-USTR feedback element is that it is strongest in the central Pacific (Fig. 4e) – it seems to operate more locally in our analysis framework than expected. (This, however, could be a consequence of USTR being fixed to the western ocean basin.) The strength of the positive feedback element peaks just after the collapse of the spring barrier in early boreal summer, when a clear asymmetry between the negative and positive composites emerges. This asymmetry persists into boreal winter and is strongest in the Nino3.4 region (Fig. 5b). SST-wind coupling stops contributing to a closed Bjerknes feedback in November for both composites (Fig. 4b,e, and lags shown in Fig. 2b).

Last, Figs. 4c,f, and 5c indicate that Pacific wind-thermocline coupling is highly asymmetric for the second half of the year, especially in the eastern portion of the basin. Again, the feedback element is strongest after the collapse of the spring barrier. The zonal distribution of the feedback strength composites indicates that the Nino4 wind stress indeed is strongly related to thermocline variability in the central and eastern ocean basin, in good agreement with the Bjerknes feedback framework.

Overall, the elements of the Pacific Bjerknes feedback display a clear asymmetry: Positive composites are generally stronger than negative composites, especially so in the eastern ocean basin when SSH is involved. Simultaneously, negative composites are more frequently significantly different from the overall expected relationship strength, indicating that the characteristics of the Pacific Bjerknes feedback elements are largely shaped by the positive composites. These findings are in excellent agreement with previous studies on Pacific Niño asymmetries – warm events tend to be stronger than cold events and occur farther to the east – and demonstrate that our lagged, robust regression-based feedback analysis is well suited to investigate feedback asymmetries in an equatorial ocean basin.

A peculiar finding is that our lagged feedback strengths appear to be phase-locked to early boreal summer rather than winter. While the feedback elements do persist into boreal winter, they are strongest in summer, just after the collapse of the spring barrier. This suggests that the weak spring coupling very rapidly turns into effective coupling that organizes incipient anomalies in the atmosphere and the ocean into the Bjerknes feedback. During the peak phase of the Pacific Niño these feedbacks elements are still active, but they are weaker than during the initial growth phase in boreal summer. On the one hand, these findings seem to be at odds with a number of previous studies, including Zhu, Kumar, and Huang (2015)'s discussion of the seasonality of Pacific subsurface-surface coupling (their "thermocline feedback"). They report that instantaneous subsurface-surface coupling is weakest in March, and then gradually increases until it peaks in October and November. However, their study does neither explicitly consider lags, nor does it distinguish between "deep" and "shallow" thermocline depths as we do here. On the other hand, recent work by Wengel et al. (2018), supported by early work by Zebiak and Cane (1987), suggests that atmosphere-ocean coupling in the tropical Pacific indeed is strongest in late boreal spring and early summer, in agreement with our findings. The discrepancies between these studies and our findings will have to be resolved by future research.

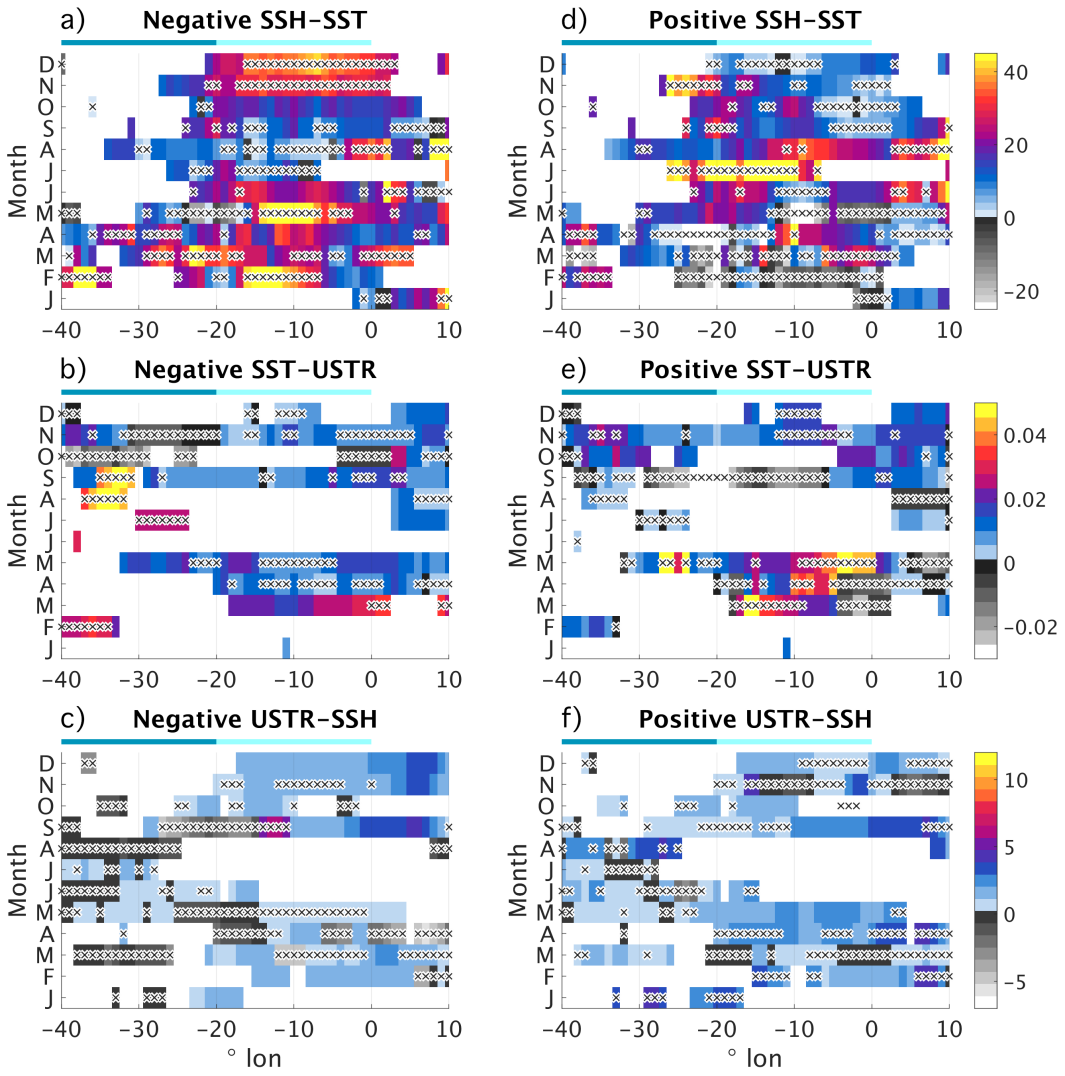

Figure 6: *Same as Fig. 4, but for the Atlantic. Coloured bars below the title indicate the zonal extent of the WAtl and Atl3 regions in dark and light blue, respectively.*

Next, we present our results for the Atlantic Bjerknes feedback (Figs. 5d-f, 6). In agreement with Lübbecke and McPhaden (2017), the range of the feedback element strengths is generally comparable to the Pacific, except for the weak Atlantic wind-thermocline coupling (Figs. 6c,g). In addition to the weak sensitivity between USTR and subsurface variability, additional factors are commonly discussed to explain the muted amplitude of the Atlantic Niño. These factors are (i) the zonal extent of the Atlantic is much smaller than that of the Pacific and that the development of the fully coupled feedback is hence constrained, and that (ii) the Bjerknes feedback operates on shorter time scales in the Atlantic, effectively coupling the atmosphere and the ocean for only two-to-three months in a row at best, diminishing the amplitude that anomalies can grow to, driven by the Bjerknes feedback. This is consistent with our analysis.

Atlantic subsurface-surface coupling appears to be the dominant element of the Atlantic Bjerknes feedback (Fig. 6). Clear asymmetries emerge throughout boreal summer and early winter (Fig. 5d). In boreal summer, during the peak season of the summer Niño,

the negative composite is stronger until July; for the remainder of boreal summer and early fall, the positive composite contributes more effectively to the overall feedback element. This suggests that subsurface-surface coupling sets in earlier for cold Atlantic Niño events. In general, it does make sense that the SSH-SST feedback element is stronger when the thermocline is shallow, since SST in this case is more sensitive to small changes in thermocline depth. (On the other hand, this reasoning clearly breaks down in the equatorial Pacific, where subsurface-surface coupling is strongest for deeper-than-normal thermoclines, cf. Fig. 5d. A possible explanation for this is that shallow thermoclines have to outcrop at some point, capping the maximum strength of the negative SSH-SST feedback element, while the thermocline can deepen more or less without constraints for the positive SSH-SST composite.) In boreal winter, the negative composite re-emerges, while the positive composite is practically absent. The overall seasonality of Atlantic subsurface-surface coupling is in good agreement with our understanding of the Atlantic Niño. An interesting side note is that the Atlantic SSH-SST feedback element appears to be stronger than its Pacific counterpart when it peaks (cf. Figs. 4a,d and 6a,d).

Atlantic SST-wind coupling, on the other hand, appears to be weaker than its Pacific counterpart (cf. Figs. 4b,e and 6b,e). Nevertheless, consistent asymmetries arise between positive and negative composites. In agreement with the enhanced sensitivity of wind variability to warm SST anomalies discussed for the Pacific SST-USTR feedback element, the positive composite is generally stronger than the negative composite. However, keep in mind that the lags that we used to diagnose the Atlantic SST-USTR feedback element are negative from June to September (Fig. 2f) and that SST-wind coupling hence only really contributes to a closed Bjerknes feedback loop in May. This limited contribution of the SST-USTR feedback element indicates that equatorial wind variability is less sensitive to ocean variability in the Atlantic than in the Pacific.

Last, Atlantic wind-thermocline coupling is clearly weaker than its Pacific counterpart (Figs. 6c,f). In the case of the negative composite, it changes from being weakly positive to negative in August, indicating that it blocks anomaly growth and hence effectively contributes to the break-down of the Atlantic Bjerknes feedback. This agrees with Dippe et al. (2018), who show that the closed Atlantic Bjerknes feedback collapses in August. Differences between the negative and positive composites are generally small, with the positive composite prevailing slightly. (The substantial difference in August is of no practical concern, since even the apparently overwhelming positive composite is only weakly positive in absolute terms, cf. Fig. 6f.) Similar to the SST-wind coupling discussed above, wind-thermocline coupling, too, can only contribute to a closed Bjerknes feedback in early boreal spring and winter, when the lag relationships are positive.

Overall, we identified asymmetries for all Atlantic Bjerknes feedback elements. These asymmetries occur mainly in boreal summer and are most pronounced for the SSH-SST feedback element associated with subsurface-surface coupling. The two feedback elements that involve wind variability produce a less straight-forward picture. They are weaker than their Pacific counterparts and constrain the Atlantic Bjerknes feedback to boreal summer and winter. This rather disruptive wind variability and decreased wind sensitivity to SST is in agreement with previous studies on the Atlantic Niño. A physical explanation of this difference between the Pacific and Atlantic Niños could be linked to the small zonal extent of the Atlantic, which substantially decreases the "fetch" of the wind stress variability in comparison to the Pacific. Additionally, enhanced interference, for example from mid-latitudes or the tropical Pacific, could explain why wind plays a somewhat different role for the Atlantic when compared with the Pacific Bjerknes feedback.

3.2 The total Bjerknes feedback

In Section 3.1, we have demonstrated that both the Atlantic and Pacific Bjerknes feedback elements can be asymmetrical. Here, we attempt to combine our findings for

the individual feedback elements, and assess how symmetric the overall effect of the closed Bjerknes feedback loop is for warm and cold conditions in the central equatorial ocean basin. We call this integrative measure the total Bjerknes feedback.

We diagnose the total Bjerknes feedback by adding the strengths of the instantaneous feedback elements of the positive and negative composites. Instantaneous feedback elements are calculated in the same manner as lagged feedback elements, but use a constant lag of zero months, i.e. the two time series contributing to each strength estimate have been sampled at the same calendar month. We use instantaneous feedback elements to avoid running into timing discrepancies.

Our approach of adding up the strength composites of the individual Bjerknes feedback elements is much simpler than the existing framework of Jin et al. (2006)'s Bjerknes stability (BJ) index. The BJ index assesses the overall stability of the coupled equatorial system, and hence the ability of the system to support self-sustained growth of SST anomalies. The BJ index implicitly considers both processes that damp and promote anomaly growth. Damping processes are associated with mean upwelling and thermal damping; amplifying processes are the positive thermocline, zonal advection, and Ekman feedbacks. Our analysis, on the other hand, is confined to the framework of the positive, anomaly-growth-promoting Bjerknes feedback. Jin et al. (2006)'s thermocline feedback considers the relationship of thermocline variations to wind and SST variability, matching our definition of the Bjerknes feedback fairly closely. (Note that Jin et al. (2006)'s thermocline feedback is a different process from Zhu et al. (2015)'s thermocline feedback.) The Ekman feedback of the BJ index is involved with our subsurface-surface coupling, and the BJ index's zonal advection feedback deals with wind-surface current-SST interaction at the eastern edge of the warm pool, which is not explicitly considered in our framework of the Bjerknes feedback. Overall, our framework is related to the BJ index in several ways, while neglecting processes that could counteract feedback-induced anomaly-growth.

In contrast to the Bjerknes feedback elements shown in Figs. 4 and 6, the total Bjerknes feedback corresponds to warm and cold SSTs in the equatorial ocean basin. Recall that in the case of the lagged feedback elements, positive and negative composites differed from each other between the three feedback elements. Here, for the total feedback, we use the same composites for all three feedback elements and have decided to partition our data with respect to SST. The total feedback strengths that we show below hence measures the strength of the Bjerknes feedback when SST is warmer or colder than on average. (See Section A.2 of the Appendix for the total Bjerknes feedback associated with westerly/easterly wind anomalies or with deep/shallow thermoclines, or in the case using the "native" composites of each feedback element.)

For the previous analysis, our estimate of the composite strengths was the regression parameter that we obtained from robust regression. This method produced strength estimates that preserved a meaningful physical unit. Now, we normalize our feedback strengths to constrain them to values between -1 and $+1$, without units. For the normalization in both the Atlantic and the Pacific basins, we use the values $60K/m$, $0.075N/(m^2K)$, and $11m^3/N$ for the SSH-SST, SST-USTR, and USTR-SSH feedback elements, respectively. Strength estimates whose magnitude exceeds these "cut-off values" are set to ± 1, depending on their sign. The cut-off values were chosen such that, based on all diagnosed strengths of the same composite in both basins, the magnitude of 95% of all values are smaller or equal to the cut-off value. Last, we add up all normalized feedback strengths contributing to the same composite, and obtain composites of the total Bjerknes feedback with respect to cold and warm SSTs.

Figure 7 shows the total feedback according to our simple measure. Instances where there feedback loop is "broken" by a single feedback element contributing negative values and hence inhibiting anomaly growth are shown in white.

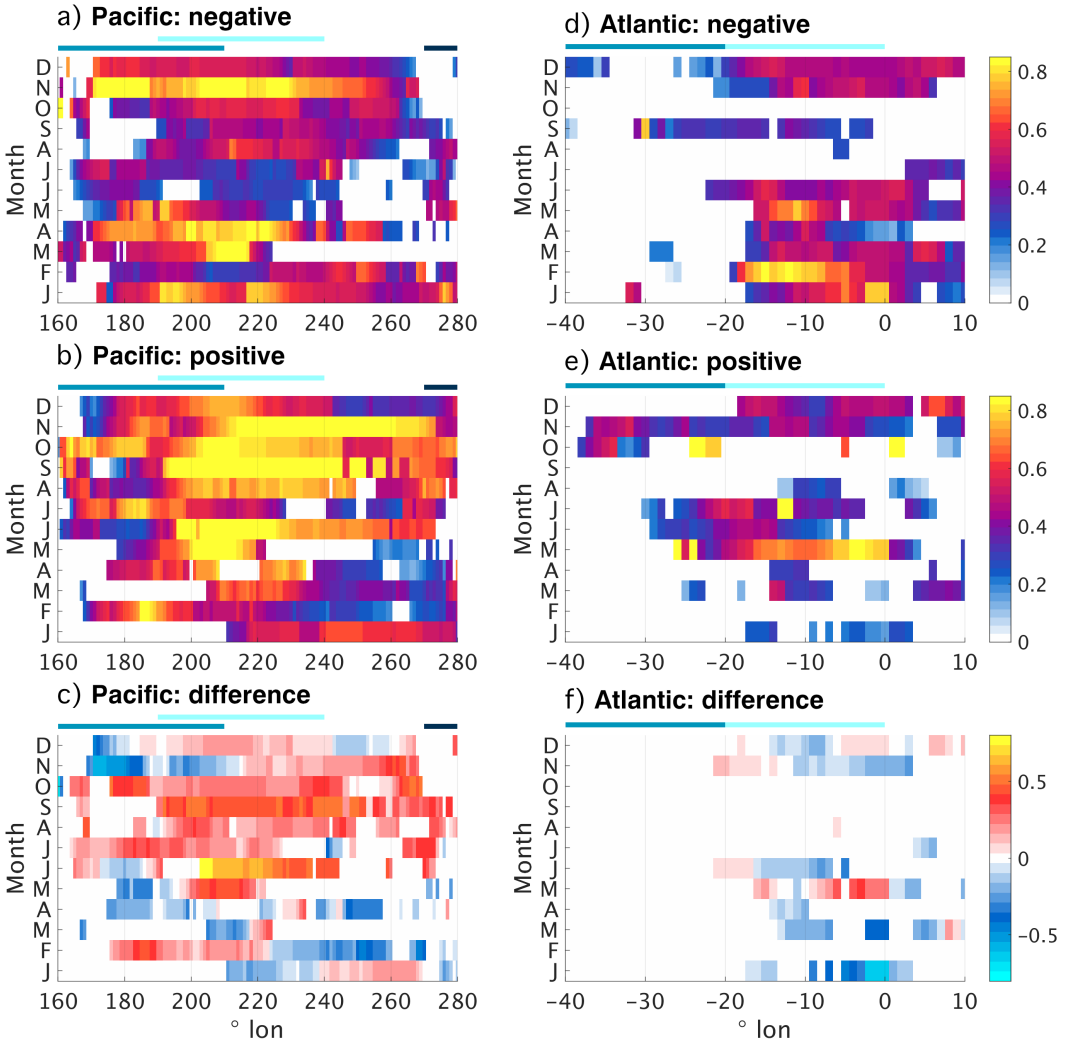

Figure 7: *SST-based estimate of the total Bjerknes feedback during 1993-2012 in the Pacific (panels a-c) and Atlantic (d-f), along the equator (x-axis) and stratified into calendar months (y-axis), diagnosed for the OBS dataset group. The top, middle, and bottom rows show the total of all negative composites (a,d), the total of all positive composites (b,e), and the difference between the positive and negative composites of the total Bjerknes feedback (c,f). Feedback strengths of the individual Bjerknes feedback elements have been normalized with* $60K/m$, $0.075N/(m^2K)$, *and* $11m^3/N$ *for the SSH-SST, SST-USTR, and USTR-SSH feedback elements, respectively. All feedback elements have been diagnosed without considering lag, and for each composite, they all use the same subsample of the data. These composites were diagnosed from the sign of the SST anomaly. Hence, the positive and negative composites of the total feedback assess the strength of the Bjerknes feedback when SSTs are warm or cold, respectively. The composites of the total feedback are the sum of all normalized composites. See text for additional details on how the total Bjerknes feedback was computed. White indicates that at least one of the feedback elements was negative, i.e. that the Bjerknes feedback loop was not closed. For the difference plots (c,f), white indicates that at least one feedback element was negative in* either *of the positive or negative composites.*

In agreement with previous studies, the total (instantaneous, SST-based) Pacific Bjerknes feedback is dominated by contributions from its positive composite, i.e. it is stronger for warm SSTs (Figs. 7a-c). The feedback forms a closed loop for practically the entire year, indicating that feedback-driven anomaly growth can be active for much of the year. A clear, common seasonality for both the cold and warm composites does not exist. The cold composite is weakest in boreal summer, while the warm composite is diminished at the beginning of the calendar year, indicating that the spring barrier affects positive and negative composites in a slightly different fashion. An interesting detail in the distribution of the composite totals is that the Bjerknes feedback is not closed in the negative composite in the far-eastern basin, not even during the peak time of the Pacific Niño in boreal winter. This is in agreement with studies on different regimes of the Pacific Niño arguing that negative Pacific Niño events ("La Niñas") tend to develop in the central basin and hardly ever manifest in the far eastern basin in their extreme form (Takahashi et al., 2011; Dommenget et al., 2013; Capotondi et al., 2015; Takahashi & Dewitte, 2016).

In contrast to the Pacific, the total Atlantic Bjerknes feedback displays a pronounced seasonality (Figs. 7d-f). Both the warm and cold composites are generally strong in summer and early boreal winter, but almost vanishing in-between. However, Fig. 7d,e shows that the timing and magnitude of these seasonal peaks is different for the warm and cold composites – asymmetries emerge in the total Atlantic Bjerknes feedback.

During boreal summer, the cold composite is strongest in May and June, while the warm composite lasts a month longer. This agrees with Burls et al. (2012), who argued that cold summer Niño events are associated with an early onset of the cold tongue, while cold tongue development is delayed during warm events. In boreal winter, cold SST anomalies feed coupled anomaly growth in late winter, with warm SST anomalies lending little support to anomaly growth. These results suggest that the Bjerknes feedback supporting the Atlantic summer Niño relies on contributions from both cold and warm conditions. The winter Niño and possible coupled variability during the first months of the year, on the other hand, is mainly associated with negative SST anomalies, at least within the framework of the dynamical Bjerknes feedback.

Another defining feature of the overall Atlantic Niño emerges from our measure of the total Bjerknes feedback as well: While the Bjerknes feedback is active for almost the entire year in the Pacific, it only operates in a closed loop in the Atlantic for short stretches of time – during early summer, and again in winter. This is in excellent agreement with previous studies on the topic (Keenlyside & Latif, 2007; Burls et al., 2011).

4 Stationarity of the Atlantic Bjerknes feedback

The results of the previous section for the Atlantic appear to be at odds with the results of Lübbecke and McPhaden (2017), as discussed below. We begin this section by comparing our OBS-based results with Lübbecke and McPhaden (2017)'s ORAS4-based analyses. We then assess the stationarity of our results and conclude that the Atlantic Bjerknes feedback and its symmetry, indeed, appear to vary on decadal time scales.

One core result of (Lübbecke & McPhaden, 2017) is that the SST anomalies associated with warm and cold Atlantic Niño events are effectively mirror images of each other, and that the associated, seasonal Bjerknes feedbacks appear to be symmetric as well. While Lübbecke and McPhaden (2017) find a weak disparity for the positive and negative composites of the SSH-SST feedback element, this asymmetry is not comparable to the pronounced asymmetries associated with the Pacific Niño. Lübbecke and McPhaden (2017) base their analysis on the approximately 50-year period 1958-2009, and diagnose feedback strengths using data of at least two months, allowing for lags of one month between the involved time series.

Our data situation is different: The OBS dataset group spans the 20-year period 1993-2012, and we have chosen to resolve our results as highly as possible, taking into account month-to-month variations and a possible dependence on longitude as well.

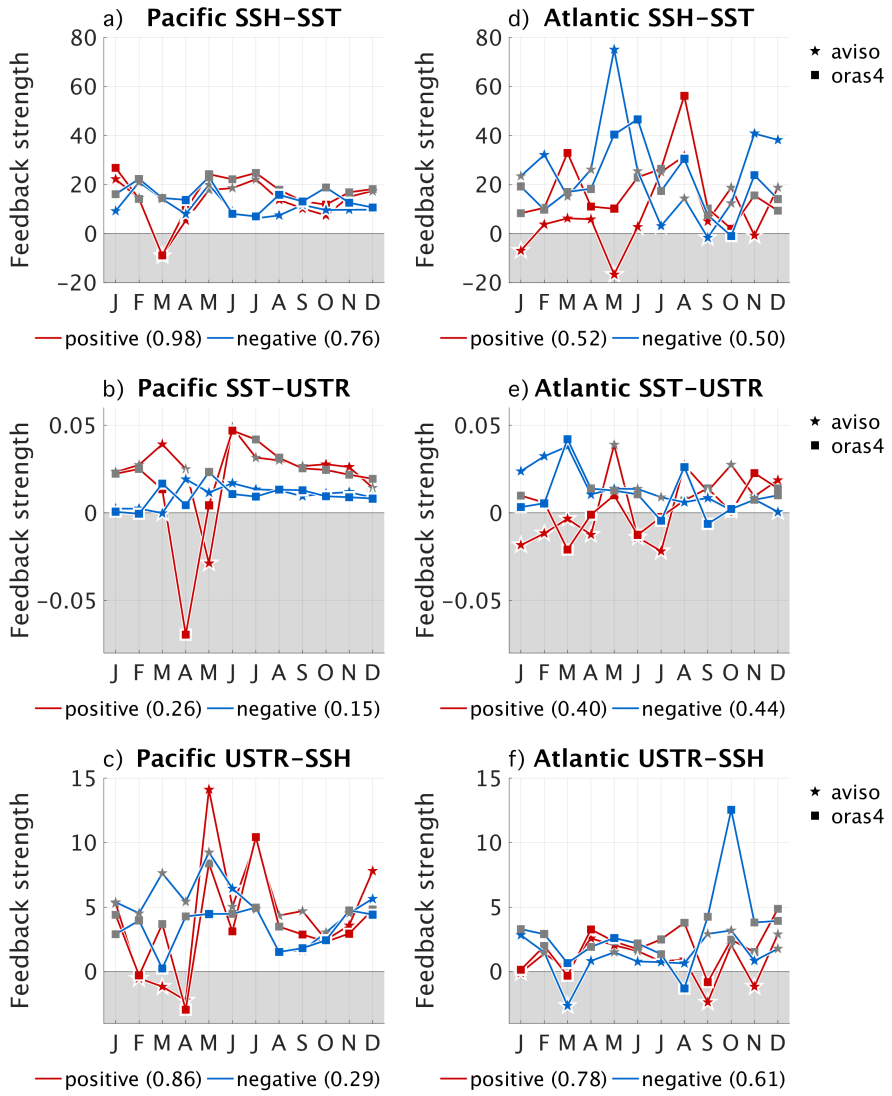

Figure 8: *Comparison of feedback element composites in the OBS and ORAS4 dataset groups in the Pacific (left column, panels a-c) and Atlantic (right column, d-f) for the overlap period 1993-2009. The top, middle, and bottom row shows results for the SSH-SST, SST-USTR, and USTR-SSH feedback elements, respectively. Composites of the feedback elements have been diagnosed with respect to Atl3/WAtl in the Atlantic, and Nino3.4/Nino4 in the Pacific, for SSH and SST/USTR, respectively. Line colour indicates the positive and negative composites in red and blue, resoectively. Star-shaped and square line markers indicate the OBS and ORAS4 dataset groups. Coloured (grey) line markers show that the respective composite is (not) significant (see text for details). For the two sets of twelve values each associated with the two dataset groups shown here, the resulting anomaly correlation coefficients are given in parentheses below each panel. Note, however, that correlations for small sample sizes can be unreliable. As in Fig. 4, white shading indicates that the associated lags (not shown) were negative.*

To facilitate a direct comparison and assess the robustness of our results, we calculate the index-based monthly composite strengths of all feedback elements for the overlap period of the OBS and ORAS4 dataset groups 1993-2009 (Fig. 8). The feedbacks have been calculated in the same manner as above, but using indices that have been averaged over the Atl3/WAtl and Nino3.4/Nino4 regions in the Atlantic and Pacific for SSH and SST/USTR, respectively. Lags have been re-diagnosed for the period 1993-2009, and incorporated in the same manner as in Section 3.

Agreement between the two dataset groups is excellent in the Pacific (Fig. 8d-f). Timing is mostly congruent, apart from the very sharp drop in the positive composite of the SST-USTR feedback element that occurs in May in the OBS, and in April in the ORAS4 dataset group, consistent with the spring barrier. Additional smaller discrepancies are apparent for wind-thermocline coupling, while preserving the overall seasonal structure of the two composites.

In the Atlantic, discrepancies are apparent mainly for the SSH-SST and SST-USTR feedback elements. Timing in these cases can be very different. For example, the negative composite of the SSH-SST feedback element peaks in June in ORAS4, but in May in OBS. ORAS4 also produces a stronger positive SSH-SST feedback element composite, however largely preserving significances. On the other hand, the dominant features identified in Section 3.1 are evident in both datasets: strong negative composites in early summer, strong positive composites in late summer, weak positive composites during winter.

In a similar fashion, small discrepancies are apparent for SST-wind coupling, while the general distribution of feedback strengths and asymmetries is present in both dataset groups. In particular, the negative composite is weakest in summer and strongest in late winter, while the positive composite peaks in May.

Last, subsurface-surface coupling is rather weak, but agrees well between the OBS and ORAS4 dataset groups. The negative composite strengthens slightly in boreal fall, while the positive component dominates during the first half of the year.

Overall, the OBS and ORAS4 dataset groups agree well in the Pacific, and support the main features identified in our analysis for the Atlantic, while differing in the details there. It follows that the apparent discrepancies between our work and Lübbecke and McPhaden (2017)'s study must be partially attributed to the different analysis periods (1993-2012 in our case, versus 1958-2009 in Lübbecke and McPhaden (2017)).

This suggests that the strengths of the Atlantic Bjerknes feedback elements depend on the analysis period. In agreement with Martín-Rey et al. (2017)'s proposed non-stationarity of the Atlantic Niño itself, the Atlantic Bjerknes feedback appears to vary on decadal time scales.

To illustrate this further, we apply a "running" analysis that highlights low-frequency variations in the composite strengths of the Bjerknes feedback elements and their symmetry. For this analysis, we again use ORAS4 index data confined to the Atl3/WAtl and Nino3.4/Nino4 regions employed above. For consecutive, overlapping periods of 25 years, we re-diagnose our lags and repeat our robust regression analysis, producing composites of running index-based feedback elements. Anomalies are calculated separately with respect to each period of the running analysis.

Figures 9 to 11 show the results of our running analysis. The Pacific Bjerknes feedback elements exhibit low-frequency variations (Fig. 9). All feedback elements, and generally both the positive and negative composites, show a basic change that occurs around the early 1970s and is characterized by (i) a weakening subsurface-surface coupling; (ii) SST-wind coupling that appears to decrease for the negative composite, but shows no clear change for the positive composite; and (iii) strengthening wind-thermocline cou-

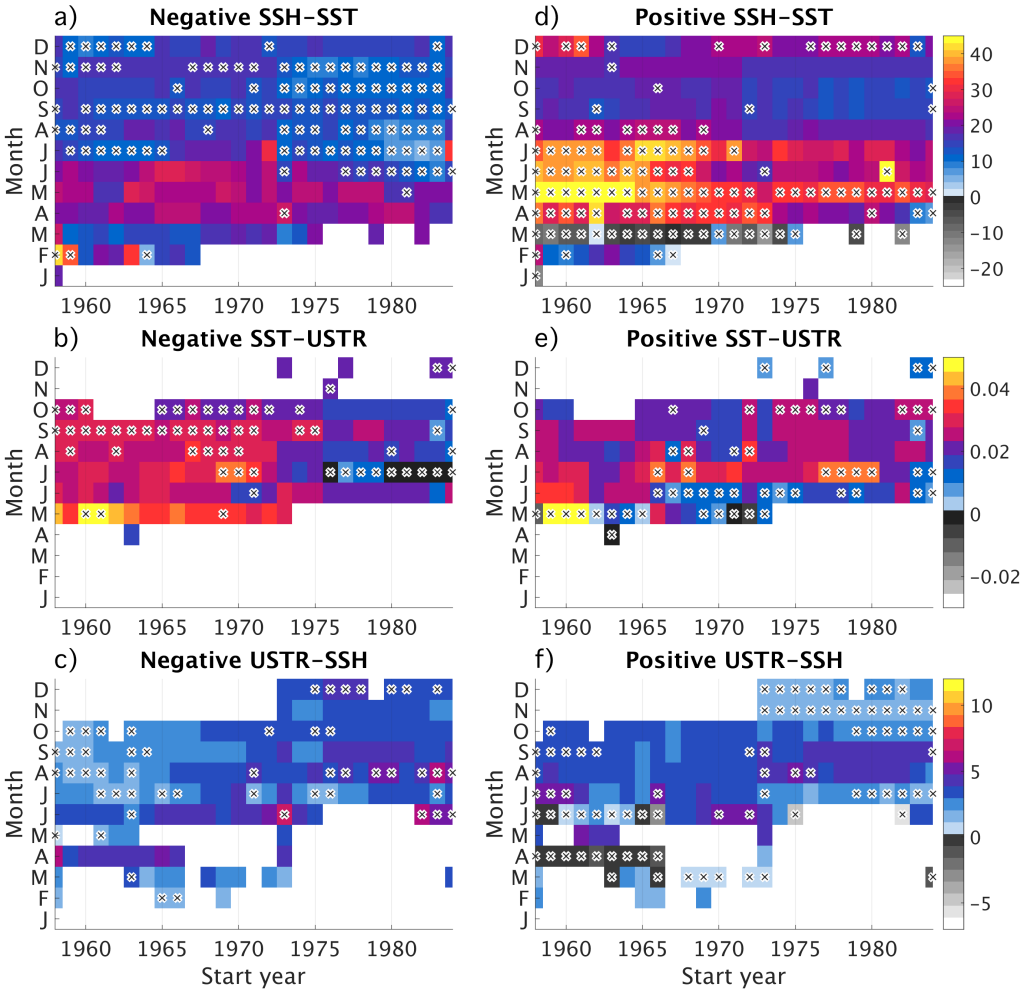

Figure 9: *Decadal variations of the composites of the Pacific Bjerknes feedback elements, based on the ORAS4 dataset group for running sub-periods (x-axis, shown dates label the* start *of each analysis period) and each calendar month (y-axis). The left and right columns show variations of the negative (panels a-c), and positive composites (d-f). Rows show variations of the individual feedback elements, for the SSH-SST (a,d), SST-USTR (b,e), and USTR-SSH feedback elements (c,f). Composites have been diagnosed with respect to Nino3.4 for SSH and SST, and with respect to Nino4 for USTR. Crosses indicate that the diagnosed feedback strength is significant (see text for details). Anomalies have been diagnosed with respect to the running analysis period. The width of the running window is 25 years.*

pling that is more apparent in the negative composite than in the positive composite. These changes are in rough agreement with the "Pacific climate shift" that took place in 1976/77 (Graham, 1994; Trenberth & Hurrell, 1994; Ding et al., 2013). A secondary climate shift in the Pacific occurred in 1998/99, exchanging intense, eastern warm events for a more moderate regime characterized by warm events that occur closer to the center of the basin and are reduced in amplitude (Lübbecke et al., 2014; Hu et al., 2012). Both climate shifts have been related to the low-frequency variability of the Pacific Decadal Oscillation (Minobe, 1997, 2000; Mantua & Hare, 2002, PDO). The 1998/99 shift, however, is not resolved in our analysis, since our datasets only span twelve years of the post-shift era, which constitutes half a period of our running analysis.

As for the OBS-based subsurface-surface coupling discussed in Section 3.1, our results for the SSH-SST feedback element are not in exact agreement with Zhu et al. (2015). Seasonalities of the two results disagree (with our SSH-SST feedback elements being strongest in April-June, while Zhu et al. (2015)'s thermocline feedback consistently peaks in September-December). Periods of enhanced subsurface-surface coupling, too, do not agree. In particular, our results indicate that the SSH-SST feedback element was strongest in the period spanning the 1960s to 1990s (the dates label the first year of each 25-year analysis period), for both the positive and the negative composites. Zhu et al. (2015) find fairly consistent thermocline feedbacks in winter, while relationships in boreal spring were very weak in 1960s-1980s, amd again in the mid-1990s to early 2000s. We suspect that methodological differences will most likely explain the apparent discrepancies in seasonality and timing of exceptionally weak or strong relationships: Zhu et al. (2015) used correlations as a measure for the sensitivity between thermocline depth – theirs diagnosed from the depth of the $20°C$-isotherm, ours gleaned from SSH –, their running analysis periods had lengths of eleven years in contrast to our 25, and they did not separate positive and negative composites from each other.

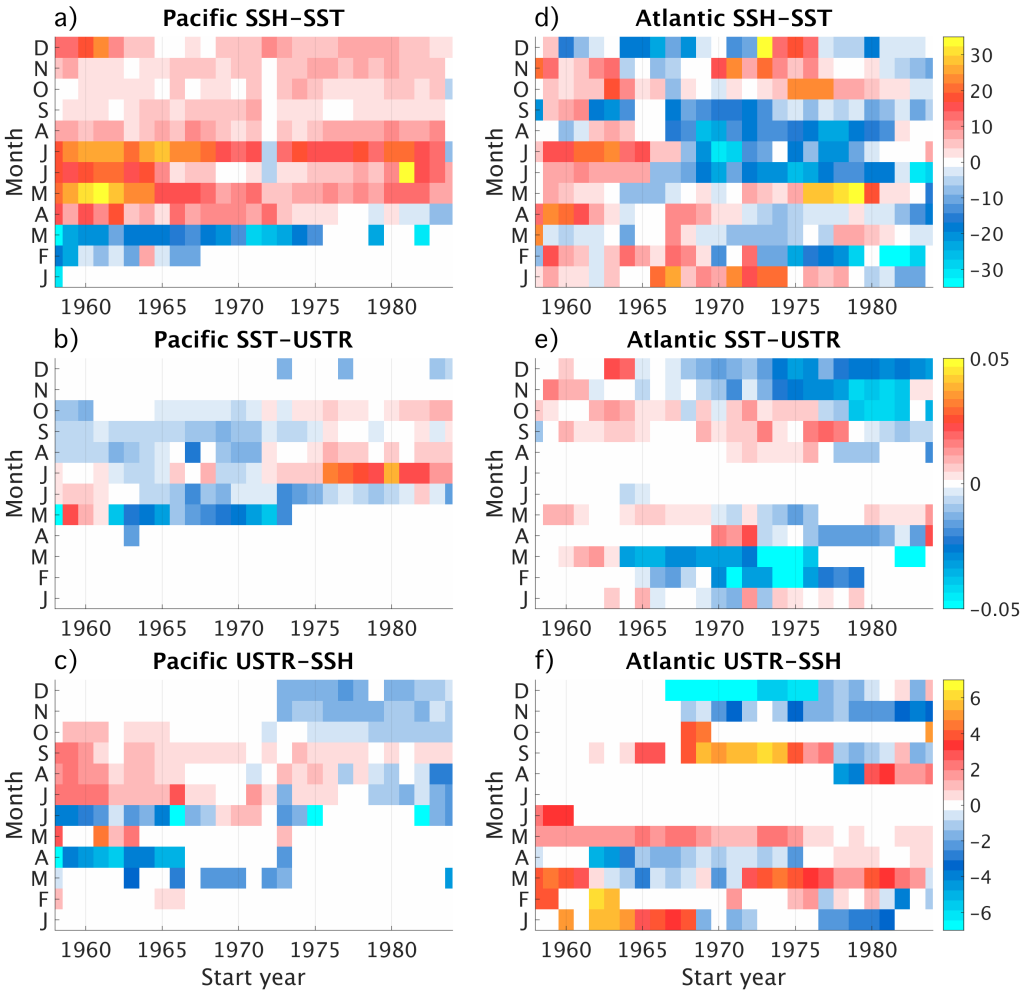

Figure 10: *Similar to Fig. 9, but showing the difference between positive and negative composites in the Pacific (left column, panels a-c) and the Atlantic (right column, d-f), for the SSH-SST (a,d), SST-USTR (b,e), and USTR-SSH (c,f) feedback elements.*

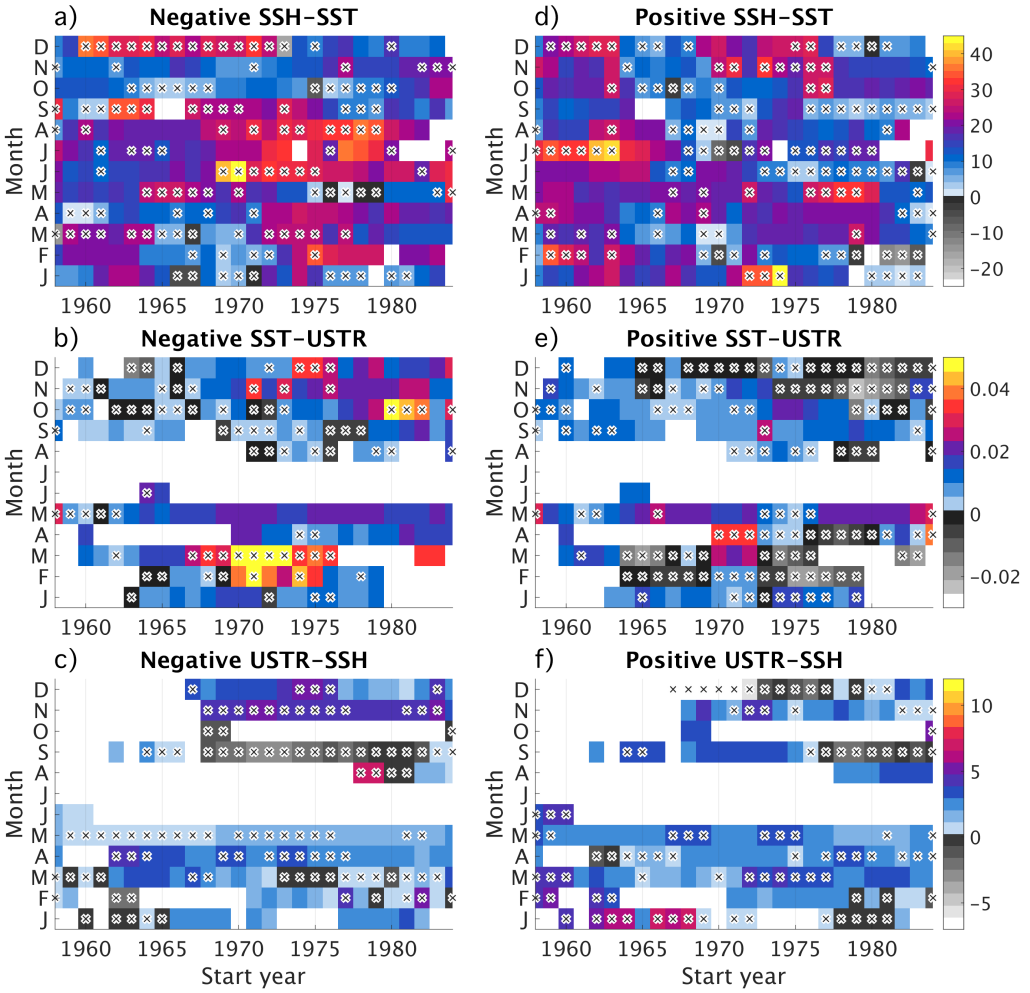

Figure 11: *Same as Fig. 9, but for the Atlantic. Feedback strengths have been diagnosed with respect to Atl3 for SSH and SST, and with respect to WAtl for USTR.*

While the overall strength composites of the Pacific feedback elements change, the asymmetry between them is largely preserved (Fig. 10). An exception is the SST-USTR feedback element (Fig. 10b), which displays varying ratios of the positive and negative strength composites.

In the Atlantic, all feedback elements vary substantially on decadal time scales (Fig. 11). Even when focusing on the important summer and winter seasons, the symmetries of the Bjerknes feedback elements change from decade to decade. Subsurface-surface coupling, for example, was the dominant feedback element during the period 1993-2012 (Figs. 11a,d, and 10d). On decadal time scales, this is not necessarily the case. The SSH-SST feedback element during early boreal summer was dominated by the positive composite in the 70s and 80s, and only recently started to draw more strongly from the negative composite. Similarly, the July feedback used to be strongly influenced by the negative composite, and only started to be dominated by the positive composite in the mid-80s. Subsurface-surface coupling in winter, too, has not always been exclusively supported by the negative composite. These shifting symmetries suggest that the relative contributions of positive and negative composites to the SSH-SST feedback element are highly variably on decadal time scales.

In a similar fashion, the overall strengths and symmetries of the two wind-related feedback elements changed over the course of the past 50 years.

We conclude that the Atlantic Bjerknes feedback and its symmetry are non-stationary. Keep in mind, however, that the absolute numerical values shown here might be subject to large uncertainties, due to rather short analysis periods and inhomogeneities in the data available to the ORAS4 reanalysis. Hence, while our analysis clearly demonstrates that the Atlantic Bjerknes feedback does vary on decadal time scales, the magnitudes of these variations may not be well constrained by our data basis.

An important consequence of our findings is that diagnosing the strength of the Atlantic Bjerknes feedback on the basis of a rather long dataset might obscure crucial, albeit non-stationary details, in the same manner that averaging over long time scales will effectively lose information on short-time scale processes.

5 Summary and Discussion

5.1 Summary

We have studied the symmetry of the Atlantic and Pacific Bjerknes feedbacks, using robust regression to diagnose the strength of the three feedback elements that form the closed Bjerknes feedback loop – the SSH-SST, SST-USTR, and USTR-SSH feedbacks that relate to coupling between the subsurface and surface, SST and wind, and wind and thermocline depth, respectively. Our analysis of the Pacific agrees will with previous research and lends credibility to our results for the Atlantic.

During the recent period 1993-2012 in the Atlantic, asymmetries emerge for all feedback elements during boreal winter and summer, when the Atlantic Bjerknes feedback forms a closed positive feedback loop. During these months, the sensitivities of all feedback elements is positive, for both types of composites. While both positive and negative composites are strong during boreal summer, the positive composites are much weaker during boreal winter. The two wind-related feedback elements are weaker than their Pacific counterparts, and produce summer and winter asymmetries to a varying degree. The total Atlantic Bjerknes feedback is dominated by the negative strength composites in boreal winter, and shows mixed influences from positive and negative composites in summer.

Comparing our work with Lübbecke and McPhaden (2017)'s study suggested that the results of a feedback analysis in the equatorial Atlantic are highly sensitive to the chosen analysis period. Indeed, our ORAS4-based running analysis of the Atlantic Bjerknes feedback elements provides further evidence for the non-stationarity of the Atlantic Bjerknes feedback. One important result of our study is that conclusions drawn for feedback-related issues in the tropical Atlantic will always have to explicitly consider the analysis period that they are based on.

5.2 Discussion

Taking into account the proposed non-stationarity of the Atlantic Bjerknes feedback, our study serves as a reminder that processes in the coupled equatorial Atlantic climate system can unfold on substantially smaller spatiotemporal scales than their Pacific counterparts. We concede that using even monthly mean data for our analysis might be insufficient to resolve the rapid processes that establish the intricate variability in the tropical Atlantic.

Another problem that we ran into are the very small sample sizes as soon as analysis periods are shorter than 30 years. For our analysis, we used period lengths between 20 and 25 years. Separating the data into positive and negative composites left us with

data pools that rarely exceeded the size of ten to twelve entries per analysis step. To reduce the arbitrariness of our results, we chose robust regression as our analysis method. As our results have demonstrated, decreasing the temporal and spatial extent of our analysis domain reveals important details of the mechanisms that govern the tropical Atlantic.

A related issue is that our results concerning the stationarity of the Bjerknes feedback elements rely on a single dataset, i.e. ORAS4, which in addition is a reanalysis. It would be interesting to assemble additional datasets, preferentially based on direct observations, and repeat our analysis.

To conclude our study, we seek to consolidate the asymmetries that we detected in the recent, OBS-based Pacific and Atlantic Bjerknes feedback with the symmetry of SST variability in the central equatorial ocean basins. Our analysis to this effect is based on SST "events". To identify an SST event, we first calculate the anomalies of the time series with respect to the local linear trend and the seasonal cycle. For both positive and negative anomalies separately, we calculate the local standard deviation. In either case, we select all instances for which anomalies exceed 0.5 times the local standard deviation. These are potential contributions to events. Then we identify periods during which potential contributions have the same sign for at least three consecutive months. These "persisting" anomalies form an SST event. For each event, the anomaly of the largest magnitude provides the strength of the event. We diagnose events in the same 4° longitude $\times 4°$ latitude boxes of SST data that we used for our previous analysis.

Figure 12 shows the average strength of positive and negative SST events along the equatorial Pacific and Atlantic, in the same period that we used to diagnose our lagged composite strengths in Section 3 (1993-2012). During boreal winter in the Pacific, the well-known amplitude asymmetry emerges (Fig. 12a). East of $170°W$ ($190°E$), Pacific warm events are substantially stronger than cold events, especially so in the Nino3.4 region. The difference between average warm and cold events can be as high as $1°C$.

In contrast, SST events are much more symmetric in the Atlantic. This agrees with Lübbecke and McPhaden (2017)'s findings. Summer Niños during the recent period seem to have been slightly dominated by cold events (Fig. 12b, with a maximum difference between negative and positive SST events of about $0.5°C$). This corresponds to the asymmetry of subsurface-surface coupling that we identified in Fig. 5a, were the SSH-SST feedback element is clearly stronger for shallow thermoclines (associated with reduced SSTs) than for deep thermoclines (warm SSTs). Considering the total Bjerknes feedback with respect to cold and warm SST conditions softens the relationship (cf. Fig. 7d-f). While the total Bjerknes feedback was indeed stronger when diagnosed with respect to cold SSTs in June, the response to warm SSTs dominated in May and July. (The absolute magnitude of this asymmetry depends on which method is chosen to diagnose the total feedback, cf. Section A.2 in the Appendix. All methods, however, agree on the negative composite dominating June, and the positive composite dominating July. This issue raises the question whether it is appropriate to weight all feedback elements equally when calculating the total Bjerknes feedback.) Both measures – the strength of subsurface-surface coupling by itself, including lags, and the estimate of the instantaneous total Bjerknes feedback – indicates a weak correspondence between the symmetry of the (total) Bjerknes feedback and the observed, weak amplitude asymmetry.

In contrast, the Atlantic winter Niño is mostly symmetric (Fig. 12c), even though the total Bjerknes feedback as well as the SSH-SST and the USTR-SSH feedback elements are clearly dominated by their negative composites during boreal winter (Figs. 7f, 5d,f). While the (total) Bjerknes feedback is asymmetrical in winter, it does not project onto the observed SST variability – indicating that the Bjerknes feedback plays a minor role in establishing the Atlantic winter Niño. This in agreement with Dippe et al. (2018) who have found that dynamical, Bjerknes feedback-related contributions to Atl3 SST variability do increase in winter, but are much smaller in magnitude than in sum-

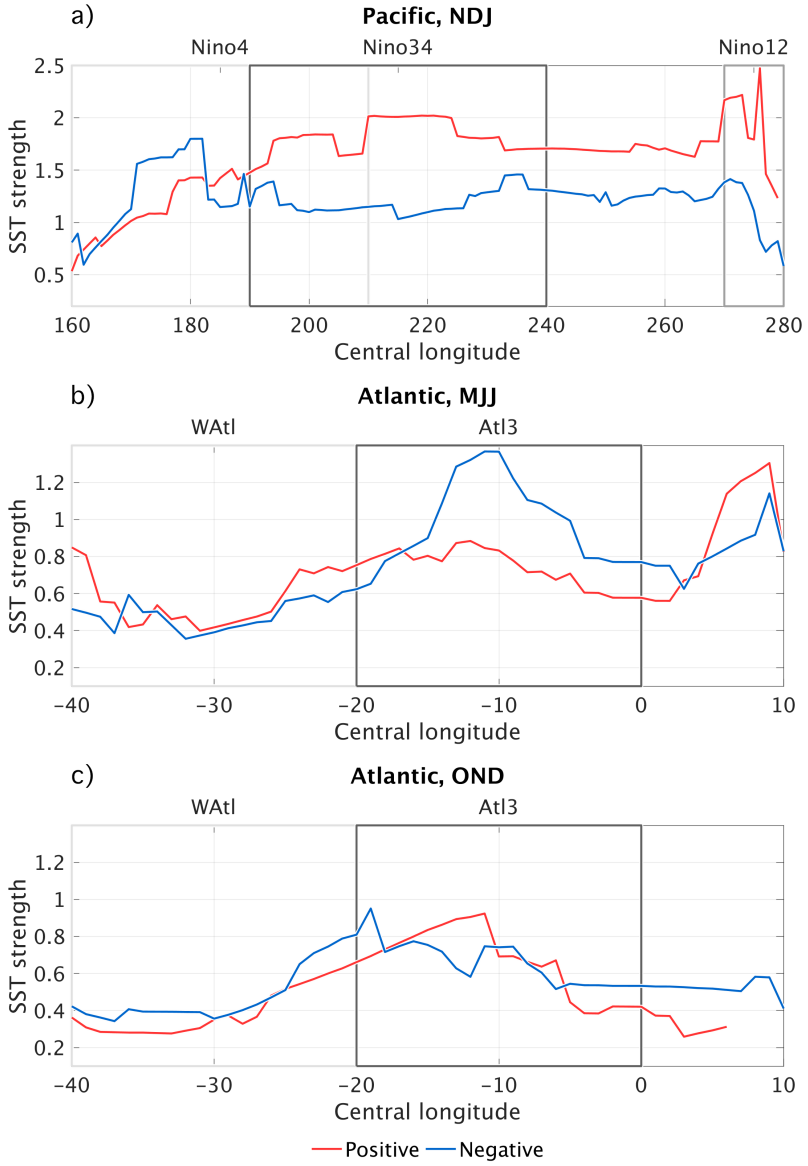

Figure 12: *Zonal distribution of the ERSST-based average strength of positive (red) and negative (blue) SST events for the period 1993-2012 (see text for details on how SST events have been diagnosed). SST events have been considered along the equatorial Pacific when they occurred between November and January (NDJ, panel a), and along the equatorial Atlantic when they occurred between May and July (MJJ, b), or between October and December (OND, c). Note that because our analysis period is very short (to match the period for which we diagnosed the lagged, OBS-based feedback element strengths), the number of events diagnosed for each longitude box is smaller than ten. Note also that the y-axes span different strengths for the Pacific and Atlantic analysis. Overlaid rectangles indicate the Nino4, Nino3.4, and Nino1.2 (WAtl and Atl3) regions in the Pacific (Atlantic).*

mer. Rather than being a dynamically driven phenomenon as in the Pacific, the Atlantic winter Niño appears to be much more susceptible to atmospheric noise forcing.

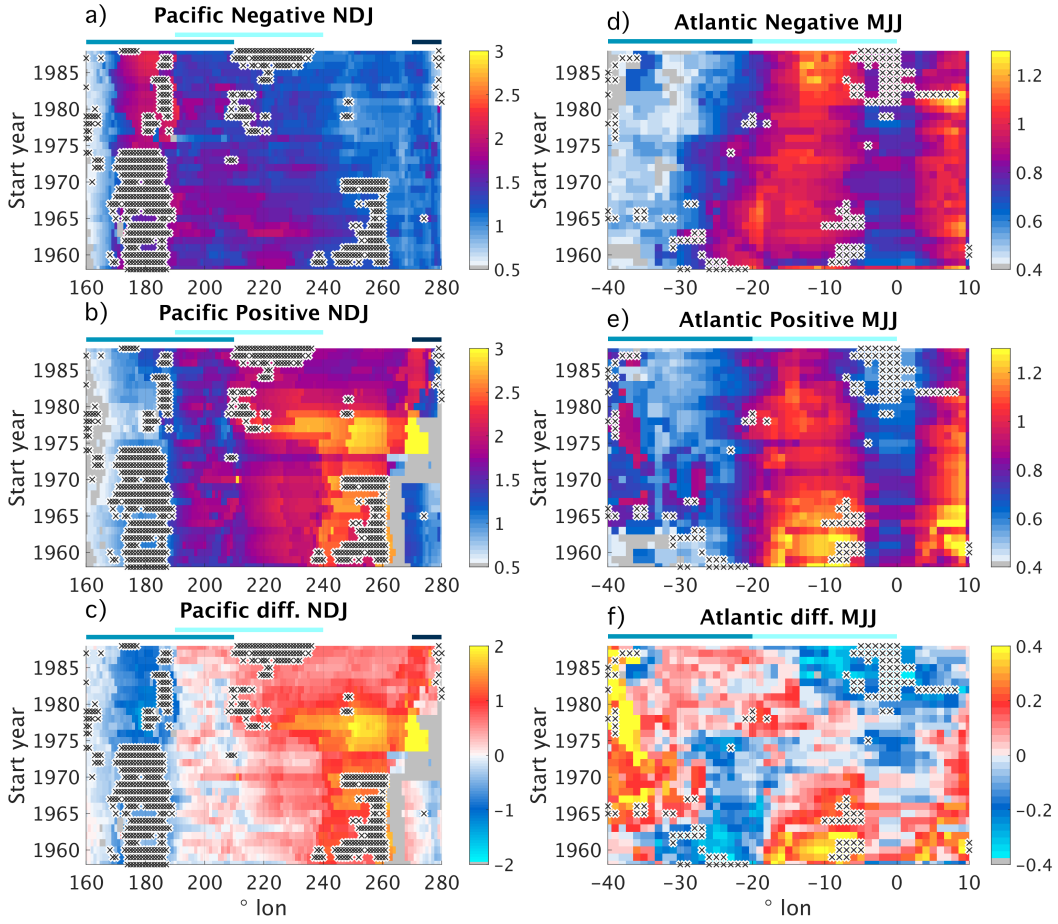

Figure 13: *Decadal variations of ERSST-SST event strengths along the equator (x-axis) for running sub-periods (y-axis, shown dates label the start of each analysis period) in the Pacific (left column, panels a-c) and the Atlantic (right column, d-f). SST events have only been considered when they peaked in November-January (NDJ) and May-July (MJJ) in the Pacific and Atlantic, respectively. The left, middle, and right columns show the strength of negative and positive SST events, as well as their difference, respectively (see text for details on how SST events have been diagnosed). Black crosses indicate that average negative and positive event strengths are significantly different from each other, according to a Student* t *test and the significance level 0.1. The length of each sub-period is 25 years, and events have been diagnosed with respect to each sub-period.*

Last, we briefly assess how stationary the symmetry of the Pacific and Atlantic Niños are. Figure 13 shows how the strength of positive and negative SST events varied over the past five decades, using again sliding analysis windows of a length of 25 years each, considering both Pacific events in boreal winter, and Atlantic events in boreal summer.

In the Pacific, the basic asymmetry between warm and cold events did not change over the past 50 years (Fig. 13a-c). However, how much warmer the warm events east of $120°W$ ($240°E$) are than the corresponding cold events is indeed varying from decade to decade. The strongest asymmetry so far occurred in the 1970s and 1980s, during a warm phase of the Pacific Decadal Oscillation, with average warm events exceeding average cold events by more than $1.5°C$.

In the Atlantic, general characteristics of equatorial SST events have not changed dramatically over the past 50 years, while minor variations do occur (Fig. 13d-f). The location of the strongest cold SST events, for example, appears to have slightly shifted from the western into the central Atl3 region (Fig. 13d). Additionally, cold SST events have become stronger within the last 30 years. Warm SST events, on the other hand, clearly weakened over the past 50 years (Fig. 13e), in agreement with Tokinaga and Xie (2011). The resulting effect is that cold events in the eastern equatorial Atlantic dominated the summer Niño during recent decades, while the 1960s and 1970s seem to have seen stronger warm events (Fig. 13f). An interesting detail of this analysis is that asymmetries identified in the Atl3 region do not extend homogeneously towards the eastern edge of the basin. Rather, positive SST events become more pronounced close to the African coast.

Overall, we have shown that the Atlantic Bjerknes feedback appears be configured in subtly different ways for positive and negative Atlantic Niño events, both during summer and winter. While these asymmetries project weakly onto the symmetry of summer SST events, the winter Niño is much more susceptible to other influences. Both the Atlantic Bjerknes feedback and the symmetry of the Atlantic Niño appear to vary on decadal time scales.

A Appendix

A.1 Using the same lags for positive and negative composites

In the main text, we presented composites of the Bjerknes feedback elements and, as discussed in the "Methods" section, included feedback lags that we previously diagnosed for our full anomaly time series, disregarding the sign of the forcing variable. Here, we take a detour to assess whether using these lags enhances our feedback strengths as expected and whether it affects positive and negative composites equally. We do this by repeating our regression analysis, but this time using a constant lag of 0 months for each feedback element ("instantaneous feedback elements"), at all locations and during all months. We then subtract the lagged feedback elements from the instantaneous feedback elements to assess when including lags into our analysis enhanced the composite of the feedback element (negative difference). Note that the positive and negative composites that we use are identical in both cases, because they are based on the forcing variable of each feedback element. It is the offset in time of the response variable that differs between the two cases.

Figures A.1 and A.2 show the difference between the instantaneous and the lagged feedbacks. Including feedback lags into our analysis does enhance the composites of the Bjerknes feedback elements in general. Calculating the mean across all pixels contributing to Figs. A.1 and A.2 yields, both in the Atlantic and the Pacific, negative values for all feedback elements and both composites, except for the positive composite of the Atlantic USTR-SSH feedback element. However, while the overall effect is in agreement with our goals, including the lags can have unexpected local effects.

In the Pacific, including lags into our analysis generally enhances the strength of the feedback composites (Fig. A.1), with three notable exceptions: First, the negative SSH-SST composite appears to be degraded by lags to the east of the Nino3.4 region for the entire year (Fig. A.1a). This indicates that subsurface-surface coupling operates in a slightly different manner for negative Pacific Niño events, which in turn is perhaps related to the different average thermocline depths associated with warm and cold Pacific Niños. Second, the negative SST-USTR feedback element composite is degraded by lags during the spring barrier. This, however, is of no practical concern, since the overall coupling during boreal spring in any case is decreased. Third, in a similar fashion, the pos-

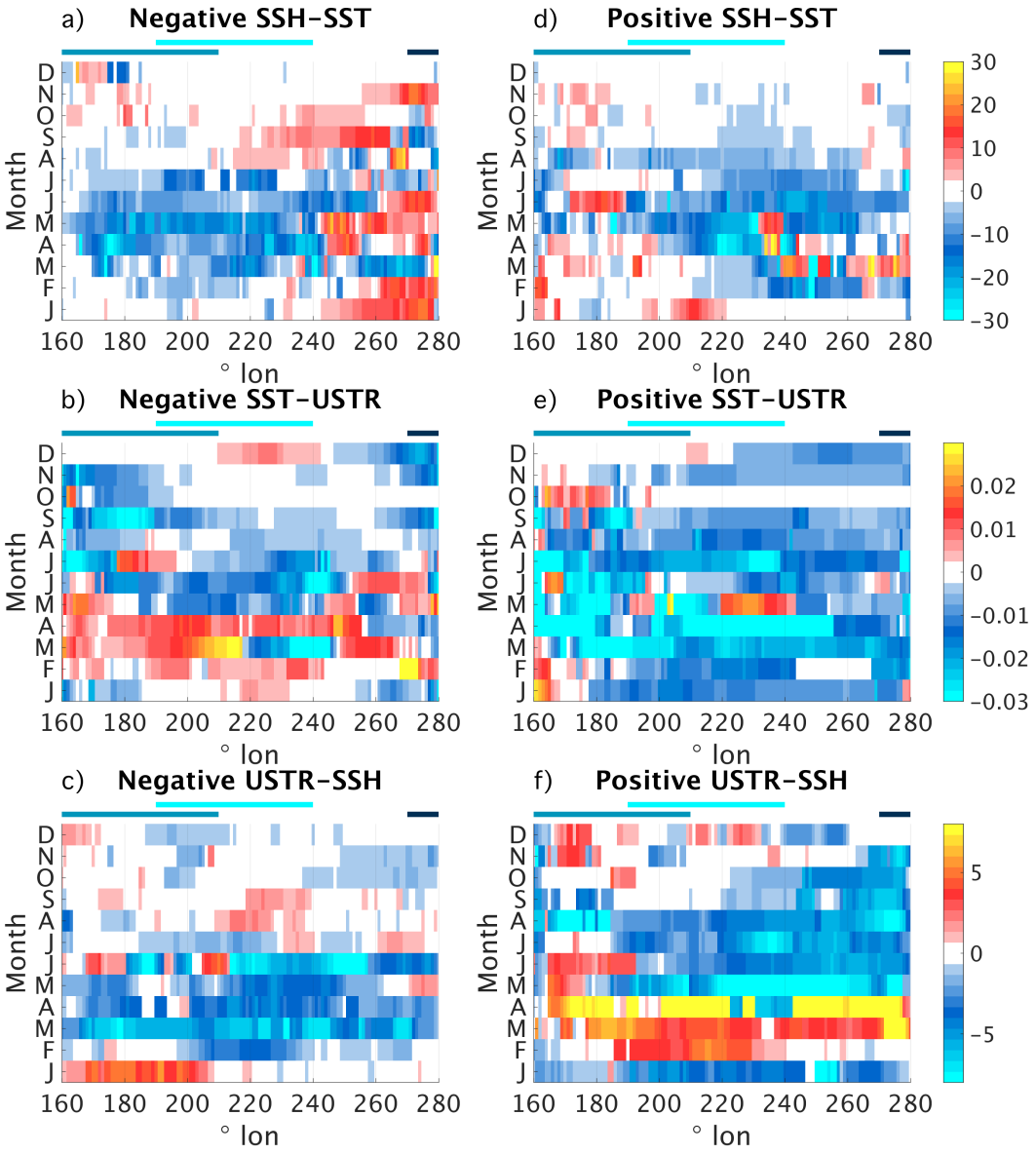

Figure A.1: *OBS-based comparison between lagged and instantaneous feedback element composites in the Pacific, along the equator (x-axis) and stratified into calendar months (y-axis). The instantaneous feedback elements have been diagnosed in the same manner as the lagged feedback elements shown in the main text, but using a constant lag of* 0 *months when performing robust regression. Positive values indicate that the instantaneous composites are stronger than the lagged composites. Coloured bars below the title indicate the zonal extent of the Nino4, Nino3.4, and Nino1.2 regions blue, light blue, and dark blue, respectively.*

itive USTR-SSH feedback element during the spring barrier clearly suffers when incorporating lags.

Figure A.2 shows that the impact of lags on Atlantic feedback strengths is less straight forward than in the Pacific. While lags generally enhance the feedback strengths, they can have severely detrimental effects in certain regions and seasons. Three notable cases

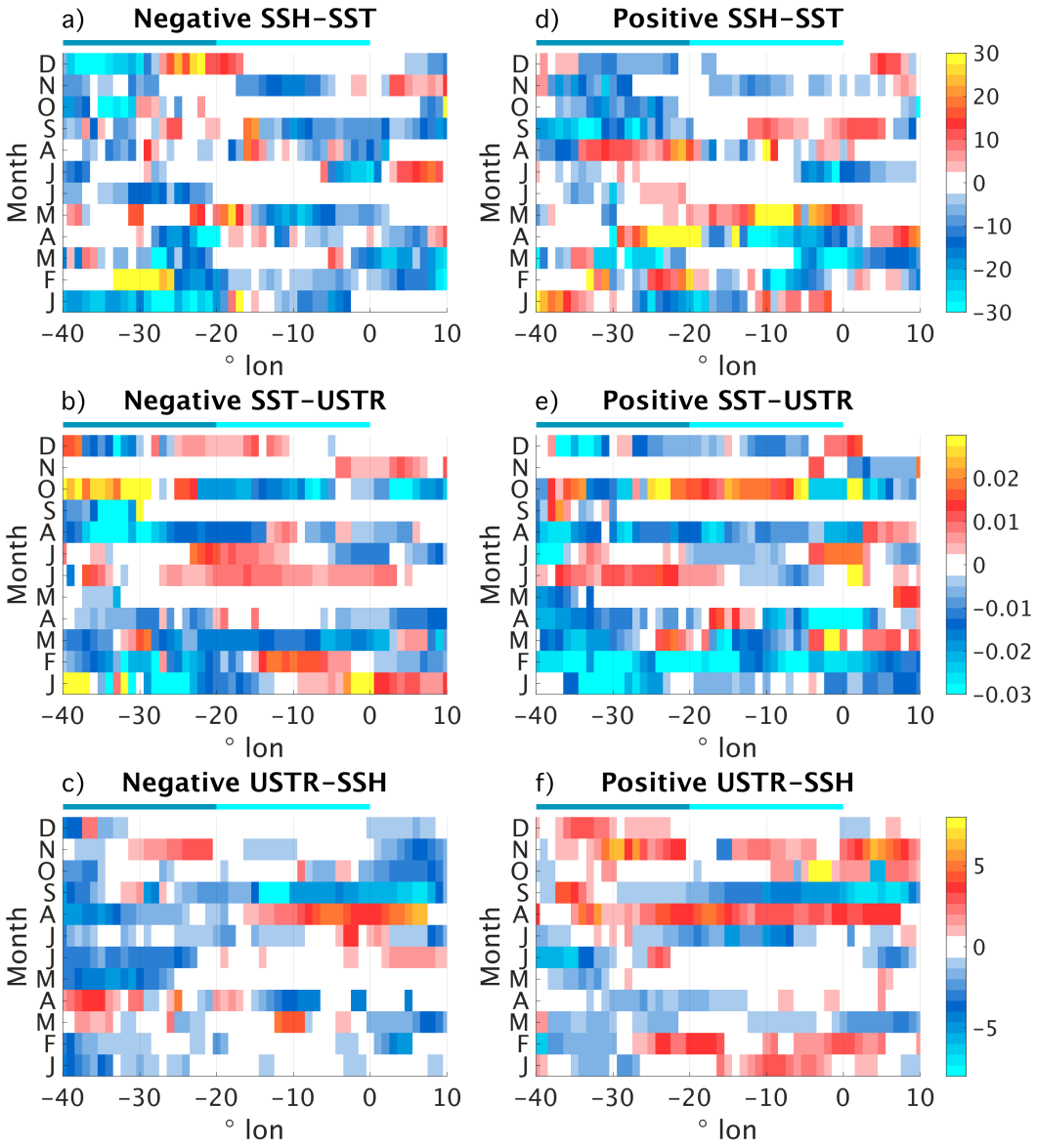

Figure A.2: *Same as Fig. A.1, but for the Atlantic. Overlaid coloured rectangles indicate the zonal extent of the WAtl and Atl3 regions.*

are: First, similar to the Pacific, the lags of the SSH-SST feedback element differ from each other; unlike in the Pacific, they do so during the crucial month of May (Fig. 2a,d of the main text). Here, lags strongly decrease the positive composite of the SSH-SST feedback element. The overall effect of this degradation, however, is small, since the corresponding lagged negative composite is clearly enhanced by the incorporation of lags. The overall May asymmetry between the positive and negative composites of the SSH-SST feedback element remains intact. Second, the negative SST-USTR feedback element composite suffers when using lags in June and July (Fig. A.2b). These months, however, are characterized by weakly negative lags (Fig. 2e of the main text) and we expect that they do not contribute substantially to the closed Atlantic Bjerknes feedback. Third, in a similar fashion, the August degradations of both the positive and the negative USTR-SSH feedback element composites are of no practical concern.

Overall, we conclude that using a constant lag for positive and negative feedback element strength composites does, in general, enhance the strength of the feedbacks as expected. When exceptions occur, they are usually related to negative lags that are of little importance for the closed Bjerknes feedback.

Nevertheless, this simple comparison serves to demonstrate again how diverse the mechanisms are that produce the variability of the Atlantic and Pacific Niños, and that it may not be justified to make equivalent assumptions for warm and cold events.

A.2 On the sensitivity of the total feedback to different diagnosis methods

In addition to the SST-based total feedback shown in the main text, we present three additional manifestations of the total Bjerknes feedback in Figs. A.3-A.5.

We diagnose the total Bjerknes feedback in two ways, depending on which subset of our data we select to calculate the strength of the three feedback elements contributing to the total feedback composites.

1. "*Constant-composite*" total feedbacks (panels a-b, d-e in Figs. A.3 to A.5): Composites of the individual Bjerknes feedback are identical. This is the method that was used to diagnose the SST-based total feedback shown in the main text. Total feedbacks of this class are directly linked to a single variable. The SST-based total feedbacks, for example, are a measure of the strength of the total feedback *when SST anomalies are either positive or negative*. Likewise, negative/positive USTR-based and SSH-based total feedback composites are associated with westerly/easterly wind stress anomalies and shallower/deeper thermocline depths, respectively.
2. "*Variable-composite*" total feedbacks (panels c,f in Figs. A.3 to A.5): For each feedback element, we use individual, "native" composites that depend on the specific feedback element. This method is congruent with the way we diagnosed our lagged feedback elements in Section 3.1 of the main text. Composites for the SSH-SST, SST-USTR, and USTR-SSH feedback are based on the sign of SSH, SST, and USTR anomalies, respectively. Again, this means that positive composites of any two feedback elements do not necessarily share the same base data.

In the Pacific, results are consistent between different manifestations of the total Bjerknes feedback (panels a-c of Figs. A.3 to A.5). Seasonalities of positive and negative total feedback composites are well comparable for all manifestations, as are the relative strengths. This highlights the large-scale character of the Pacific Niño, showing that SSH, SST, and USTR vary largely synchronously when measured at the same calendar months during periods when the total Bjerknes feedback is strong. On the other hand, constant-composite feedbacks can be twice as strong as the corresponding variable-composite feedbacks, according to our simple measure. This perhaps indicates that using constant composites prevents compensation effects between the three individual feedback elements. Providing consistent composites for all feedback elements in the constant-composite case emphasizes interactions between all three variables, while the variable-composite case focuses on interactions of only two variables, ignoring the third link in the Bjerknes feedback loop.

In the Atlantic, results are largely consistent for different manifestations of the total Bjerknes feedback as well (panels d-f of Figs. A.3-A.5d-f). Irrespective of the compositing type, total feedbacks are stronger when they are associated with negative anomalies in boreal winter, and weaker in summer. As in the Pacific, details differ between the three constant-composite manifestations, and the variable-composite manifestation produces weaker total feedbacks. A prominent example are the positive composites of the

constant-composite manifestations in July. For this calendar month, the total feedback is pronounced for deep thermoclines, moderately strong for warm SSTs, and effectively absent for easterly wind stress anomalies. However, as our base data pool only spans 20 years in total and we subdivide these further into positive and negative composites, we expect that the details of our analysis are subject to large uncertainties.

Overall, qualitative results are consistent when comparing different manifestations of the total Bjerknes feedback, lending some credibility to our method. While details differ for the three constant-composite feedbacks, results are much more sensitive to the choice of either constant or variable composites when diagnosing the individual feedback elements contributing to the total feedback.

Acknowledgments

This study has been supported by the German Ministry for Education and Research (BMBF) through MiKlip2, subproject 01LP1517D (ATMOS-MODINI) and SACUS (03G0837A), and by the European Union 7th Framework Programme (FP7 2007–2013) under Grant agreement 603521 PREFACE project. RJG is also grateful for continuing support from GEOMAR. The data used in this study can be obtained GEOMAR's OPeNDAP Service at `https://data.geomar.de`. Help is provided at the bottom of the page.

References

Ashok, K., & Yamagata, T. (2009). The El Ni{{ñ}}o with a difference. *Nature*, *461*(May), 481–484. doi: 10.1038/461481a

Balmaseda, M. A., Mogensen, K., & Weaver, A. T. (2012, dec). Evaluation of the ECMWF ocean reanalysis system ORAS4. *Quarterly Journal of the Royal Meteorological Society*, *139*(674), 1132–1161. Retrieved from `https://doi.org/10.1002/qj.2063` doi: 10.1002/qj.2063

Bjerknes, J. (1966). A possible response of the atmospheric Hadley circulation to equatorial anomalies of ocean temperature. *Tellus*, *18*(4), 820–829. Retrieved from `https://www.tandfonline.com/doi/full/10.3402/tellusa.v18i4.9712` doi: 10.3402/tellusa.v18i4.9712

Bjerknes, J. (1969). Atmospheric Teleconnections From The Equatorial Pacific. *Monthly Weather Review*, *97*(3), 163–172. Retrieved from `http://journals.ametsoc.org/doi/abs/10.1175/1520-0493(1969)097{\%}3C0163:ATFTEP{\%}3E2.3.CO;2` doi: 10.1175/1520-0493(1969)097⟨0163:ATFTEP⟩2.3.CO;2

Burls, N. J., Reason, C. J. C., Penven, P., & Philander, S. G. (2011, nov). Similarities between the tropical Atlantic seasonal cycle and ENSO: An energetics perspective. *Journal of Geophysical Research: Oceans*, *116*(C11), C11010. Retrieved from `http://dx.doi.org/10.1029/2011JC007164` doi: 10.1029/2011JC007164

Burls, N. J., Reason, C. J. C., Penven, P., & Philander, S. G. (2012, may). Energetics of the Tropical Atlantic Zonal Mode. *Journal of Climate*, *25*(21), 7442–7466. Retrieved from `http://dx.doi.org/10.1175/JCLI-D-11-00602.1` doi: 10.1175/JCLI-D-11-00602.1

Cane, M. A. (1984, jan). Modeling Sea Level During El Ni{ñ}o. *Journal of Physical Oceanography*, *14*(12), 1864–1874. Retrieved from `http://dx.doi.org/10.1175/1520-0485(1984)014{\%}7B{\%}3C{\%}7D1864:MSLDEN{\%}7B{\%}3E{\%}7D2.0.CO2http://dx.doi.org/10.1175/1520-0485(1984)014{\%}3C1864:MSLDEN{\%}3E2.0.CO` doi: 10.1175/1520-0485(1984)014⟨1864:MSLDEN⟩2.0.CO;2

Capotondi, A., Wittenberg, A. T., Newman, M., Di Lorenzo, E., Yu, J.-Y., Braconnot, P., ... Yeh, S.-W. (2015, sep). Understanding ENSO Diversity. *Bulletin of the American Meteorological Society*, *96*(6), 921–938.

Retrieved from https://doi.org/10.1175/BAMS-D-13-00117.1 doi: 10.1175/BAMS-D-13-00117.1

Chen, D., Lian, T., Fu, C., Cane, M. A., Tang, Y., Murtugudde, R., ... Zhou, L. (2015, may). Strong influence of westerly wind bursts on El Nino diversity. *Nature Geoscience*, *8*(5), 339–345. Retrieved from http://dx.doi.org/10.1038/ngeo2399http://10.0.4.14/ngeo2399

Cobb, K. M., Westphal, N., Sayani, H. R., Watson, J. T., Di Lorenzo, E., Cheng, H., ... Charles, C. D. (2013, jan). Highly Variable El Niño–Southern Oscillation Throughout the Holocene. *Science*, *339*(6115), 67 LP – 70. Retrieved from http://science.sciencemag.org/content/339/6115/67.abstract

Dee, D. P., Uppala, S. M., Simmons, A. J., Berrisford, P., Poli, P., Kobayashi, S., ... Vitart, F. (2011). The ERA-Interim reanalysis: Configuration and performance of the data assimilation system. *Quarterly Journal of the Royal Meteorological Society*, *137*(656), 553–597. doi: 10.1002/qj.828

Delworth, T. L., & Mann, M. E. (2000). Observed and simulated multidecadal variability in the Northern Hemisphere. *Climate Dynamics*, *16*(9), 661–676. Retrieved from https://doi.org/10.1007/s003820000075 doi: 10.1007/s003820000075

Deppenmeier, A.-L., Haarsma, R. J., & Hazeleger, W. (2016). The Bjerknes feedback in the tropical Atlantic in CMIP5 models. *Climate Dynamics*, 1–17. Retrieved from http://dx.doi.org/10.1007/s00382-016-2992-z doi: 10.1007/s00382-016-2992-z

DiNezio, P. N., & Deser, C. (2014, jul). Nonlinear Controls on the Persistence of La Niña. *Journal of Climate*, *27*(19), 7335–7355. Retrieved from https://doi.org/10.1175/JCLI-D-14-00033.1 doi: 10.1175/JCLI-D-14-00033.1

Ding, H., Greatbatch, R. J., Latif, M., Park, W., & Gerdes, R. (2013, oct). Hindcast of the 1976/77 and 1998/99 Climate Shifts in the Pacific. *Journal of Climate*, *26*(19), 7650–7661. Retrieved from http://journals.ametsoc.org/doi/abs/10.1175/JCLI-D-12-00626.1 doi: 10.1175/JCLI-D-12-00626.1

Dippe, T., Greatbatch, R. J., & Ding, H. (2018). On the relationship between Atlantic Niño variability and ocean dynamics. *Climate Dynamics*, *51*(1), 597–612. Retrieved from https://doi.org/10.1007/s00382-017-3943-z doi: 10.1007/s00382-017-3943-z

Dommenget, D., Bayr, T., & Frauen, C. (2013). Analysis of the non-linearity in the pattern and time evolution of El Niño southern oscillation. *Climate Dynamics*, *40*(11), 2825–2847. Retrieved from https://doi.org/10.1007/s00382-012-1475-0 doi: 10.1007/s00382-012-1475-0

Duan, W., & Wei, C. (2013, apr). The 'spring predictability barrier' for ENSO predictions and its possible mechanism: results from a fully coupled model. *International Journal of Climatology*, *33*(5), 1280–1292. Retrieved from http://dx.doi.org/10.1002/joc.3513 doi: 10.1002/joc.3513

Gill, A. E. (1980). Some simple solutions for heat-induced tropical circulation. *Quarterly Journal of the Royal Meteorological Society*, *106*(449), 447–462. Retrieved from http://doi.wiley.com/10.1002/qj.49710644905 doi: 10.1002/qj.49710644905

Graham, N. E. (1994). Decadal-scale climate variability in the tropical and North Pacific during the 1970s and 1980s: observations and model results. *Climate Dynamics*, *10*(3), 135–162. Retrieved from https://doi.org/10.1007/BF00210626 doi: 10.1007/BF00210626

Harzallah, A., Rocha de Aragão, J. O., & Sadourny, R. (1996, sep). Interannual rainfall variability in north-east Brazil: Observation and model simulation. *International Journal of Climatology*, *16*(8), 861–878. Retrieved from https://doi.org/10.1002/(SICI)1097-0088(199608)16:8{\%}3C861::AID-JOC59{\%}3E3.0.COhttp://2-d doi: 10.1002/(SICI)1097-0088(199608)16:8⟨861::AID-JOC59⟩3.0.CO;2-D

Holland, P. W., & Welsch, R. E. (1977, jan). Robust regression using iteratively reweighted least-squares. *Communications in Statistics - Theory and Methods*, *6*(9), 813–827. Retrieved from http://dx.doi.org/10.1080/03610927708827533 doi: 10.1080/03610927708827533

Hu, Z.-Z., Kumar, A., Huang, B., Zhu, J., Zhang, R.-H., & Jin, F.-F. (2017). Asymmetric evolution of El Niño and La Niña: the recharge/discharge processes and role of the off-equatorial sea surface height anomaly. *Climate Dynamics*, *49*(7), 2737–2748. Retrieved from https://doi.org/10.1007/s00382-016-3498-4 doi: 10.1007/s00382-016-3498-4

Hu, Z.-Z., Kumar, A., Ren, H.-L., Wang, H., L'Heureux, M., & Jin, F.-F. (2012, oct). Weakened Interannual Variability in the Tropical Pacific Ocean since 2000. *Journal of Climate*, *26*(8), 2601–2613. Retrieved from https://doi.org/10.1175/JCLI-D-12-00265.1 doi: 10.1175/JCLI-D-12-00265.1

Huang, B., Thorne, P. W., Banzon, V. F., Boyer, T., Chepurin, G., Lawrimore, J. H., ... Zhang, H.-M. (2017, jul). Extended Reconstructed Sea Surface Temperature, Version 5 (ERSSTv5): Upgrades, Validations, and Intercomparisons. *Journal of Climate*, *30*(20), 8179–8205. Retrieved from https://doi.org/10.1175/JCLI-D-16-0836.1 doi: 10.1175/JCLI-D-16-0836.1

Huber, P. J., & Ronchetti, E. M. (2009). *Robust Statistics* (Second Edi ed.). Wiley.

Hummels, R., Dengler, M., & Bourlès, B. (2013). Seasonal and regional variability of upper ocean diapycnal heat flux in the Atlantic cold tongue. *Progress in Oceanography*, *111*, 52–74. doi: 10.1016/j.pocean.2012.11.001

Jin, F. F., Kim, S. T., & Bejarano, L. (2006). A coupled-stability index for ENSO. *Geophysical Research Letters*, *33*(23). doi: 10.1029/2006GL027221

Keenlyside, N. S., & Latif, M. (2007). Understanding Equatorial Atlantic Interannual Variability. *Journal of Climate*, *20*(1), 131–142. Retrieved from http://dx.doi.org/10.1175/JCLI3992.1 doi: 10.1175/JCLI3992.1

Knight, J. R., Folland, C. K., & Scaife, A. A. (2006, sep). Climate impacts of the Atlantic Multidecadal Oscillation. *Geophysical Research Letters*, *33*(17). Retrieved from https://doi.org/10.1029/2006GL026242 doi: 10.1029/2006GL026242

Levine, A. F. Z., & Jin, F. F. (2017). A simple approach to quantifying the noise-ENSO interaction. Part I: Deducing the state-dependency of the wind-stress forcing using monthly mean data. *Climate Dynamics*, *48*(1), 1–18. Retrieved from http://dx.doi.org/10.1007/s00382-015-2748-1 doi: 10.1007/s00382-015-2748-1

Levine, A. F. Z., & McPhaden, M. J. (2016, jun). How the July 2014 easterly wind burst gave the 2015–2016 El Ni{ñ}o a head start. *Geophysical Research Letters*, *43*(12), 6503–6510. Retrieved from http://dx.doi.org/10.1002/2016GL069204 doi: 10.1002/2016GL069204

Li, J., Xie, S.-P., Cook, E. R., Morales, M. S., Christie, D. A., Johnson, N. C., ... Fang, K. (2013, jul). El Niño modulations over the past seven centuries. *Nature Climate Change*, *3*, 822. Retrieved from http://dx.doi.org/10.1038/nclimate1936http://10.0.4.14/nclimate1936https://www.nature.com/articles/nclimate1936{\#}supplementary-information

Losada, T., & Rodríguez-Fonseca, B. (2016). Tropical atmospheric response to decadal changes in the Atlantic Equatorial Mode. *Climate Dynamics*, *47*(3-4), 1211–1224. doi: 10.1007/s00382-015-2897-2

Lübbecke, J. F., Burls, N. J., Reason, C. J. C., & McPhaden, M. J. (2014, aug). Variability in the South Atlantic Anticyclone and the Atlantic Niño Mode. *Journal of Climate*, *27*(21), 8135–8150. Retrieved from http://dx.doi.org/10.1175/JCLI-D-14-00202.1 doi: 10.1175/JCLI-D-14-00202.1

Lübbecke, J. F., & McPhaden, M. J. (2013). A comparative stability analysis of Atlantic and Pacific Niño modes. *Journal of Climate*, *26*(16), 5965–5980. doi: 10.1175/JCLI-D-12-00758.1

Lübbecke, J. F., & McPhaden, M. J. (2017, jan). Symmetry of the Atlantic Niño mode. *Geophysical Research Letters*, *44*(2), 965–973. Retrieved from http://doi.wiley.com/10.1002/2016GL071829 doi: 10.1002/2016GL071829

Lübbecke, J. F., Rodríguez-Fonseca, B., Richter, I., Martín-Rey, M., Losada, T., Polo, I., & Keenlyside, N. S. (2018, may). Equatorial Atlantic variability—Modes, mechanisms, and global teleconnections. *Wiley Interdisciplinary Reviews: Climate Change*, *9*(4), e527. Retrieved from https://doi.org/10.1002/wcc.527 doi: 10.1002/wcc.527

Mantua, N. J., & Hare, S. R. (2002). The Pacific Decadal Oscillation. *Journal of Oceanography*, *58*(1), 35–44. Retrieved from https://doi.org/10.1023/A:1015820616384 doi: 10.1023/A:1015820616384

Martín-Rey, M., Polo, I., Rodríguez-Fonseca, B., Losada, T., & Lazar, A. (2017, jun). Is There Evidence of Changes in Tropical Atlantic Variability Modes under AMO Phases in the Observational Record? *Journal of Climate*, *31*(2), 515–536. Retrieved from https://doi.org/10.1175/JCLI-D-16-0459.1 doi: 10.1175/JCLI-D-16-0459.1

Minobe, S. (1997, mar). A 50–70 year climatic oscillation over the North Pacific and North America. *Geophysical Research Letters*, *24*(6), 683–686. Retrieved from https://doi.org/10.1029/97GL00504 doi: 10.1029/97GL00504

Minobe, S. (2000). Spatio-temporal structure of the pentadecadal variability over the North Pacific. *Progress in Oceanography*, *47*(2), 381–408. Retrieved from http://www.sciencedirect.com/science/article/pii/S0079661100000422 doi: https://doi.org/10.1016/S0079-6611(00)00042-2

Nobre, P., & Shukla, J. (1996, oct). Variations of Sea Surface Temperature, Wind Stress, and Rainfall over the Tropical Atlantic and South America. *Journal of Climate*, *9*(10), 2464–2479. Retrieved from https://doi.org/10.1175/1520-0442(1996)009{\%}3C2464:VOSSTW{\%}3E2.0.COhttp://0.0.0.2 doi: 10.1175/1520-0442(1996)009⟨2464:VOSSTW⟩2.0.CO;2

Okumura, Y., & Xie, S. P. (2006, nov). Some overlooked features of tropical Atlantic climate leading to a new Nino-like phenomenon. *Journal of Climate*, *19*(22), 5859–5874.

Rasmusson, E. M., & Wallace, J. M. (1983, dec). Meteorological Aspects of the El Niño/Southern Oscillation. *Science*, *222*(4629), 1195 LP – 1202. Retrieved from http://science.sciencemag.org/content/222/4629/1195.abstract

Rebert, J. P., Donguy, J. R., Eldin, G., & Wyrtki, K. (1985, sep). Relations between sea level, thermocline depth, heat content, and dynamic height in the tropical Pacific Ocean. *Journal of Geophysical Research: Oceans*, *90*(C6), 11719–11725. Retrieved from https://doi.org/10.1029/JC090iC06p11719 doi: 10.1029/JC090iC06p11719

Richter, I., Behera, S. K., Masumoto, Y., Taguchi, B., Sasaki, H., & Yamagata, T. (2013). Multiple causes of interannual sea surface temperature variability in the equatorial Atlantic Ocean. *Nature Geoscience*, *6*(1), 43–47. Retrieved from http://www.nature.com/doifinder/10.1038/ngeo1660 doi: 10.1038/ngeo1660

Schlesinger, M. E., & Ramankutty, N. (1994, feb). An oscillation in the global climate system of period 65–70 years. *Nature*, *367*, 723. Retrieved from http://dx.doi.org/10.1038/367723a0http://10.0.4.14/367723a0

Smith, T. M., & Reynolds, R. W. (2003, may). Extended Reconstruction of Global Sea Surface Temperatures Based on COADS Data (1854–1997). *Journal of Climate*, *16*(10), 1495–1510. Retrieved from https://doi.org/10.1175/1520-0442-16.10.1495 doi: 10.1175/1520-0442-16.10.1495

Street, J. O., Carroll, R. J., & Ruppert, D. (1988, may). A Note on Computing Robust Regression Estimates via Iteratively Reweighted Least Squares. *The American Statistician*, *42*(2), 152–154. Retrieved from https://www.tandfonline.com/doi/abs/10.1080/00031305.1988.10475548

doi: 10.1080/00031305.1988.10475548

Takahashi, K., & Dewitte, B. (2016). Strong and moderate nonlinear El Niño regimes. *Climate Dynamics*, *46*(5), 1627–1645. Retrieved from https://doi.org/10.1007/s00382-015-2665-3 doi: 10.1007/s00382-015-2665-3

Takahashi, K., Montecinos, A., Goubanova, K., & Dewitte, B. (2011, may). ENSO regimes: Reinterpreting the canonical and Modoki El Niño. *Geophysical Research Letters*, *38*(10). Retrieved from http://dx.doi.org/10.1029/2011GL047364 doi: 10.1029/2011GL047364

Timmermann, A., An, S.-I., Kug, J.-S., Jin, F.-F., Cai, W., Capotondi, A., ... Zhang, X. (2018). El Niño–Southern Oscillation complexity. *Nature*, *559*(7715), 535–545. Retrieved from https://doi.org/10.1038/s41586-018-0252-6 doi: 10.1038/s41586-018-0252-6

Tokinaga, H., & Xie, S.-P. (2011). Weakening of the equatorial Atlantic cold tongue over the past six decades. *Nature Geoscience*, *4*(4), 222–226. Retrieved from http://dx.doi.org/10.1038/ngeo1078 doi: 10.1038/ngeo1078

Torrence, C., & Webster, P. J. (1998, dec). The annual cycle of persistence in the El Nño/Southern Oscillation. *Quarterly Journal of the Royal Meteorological Society*, *124*(550), 1985–2004. Retrieved from https://doi.org/10.1002/qj.49712455010 doi: 10.1002/qj.49712455010

Trenberth, K. E., Branstator, G. W., Karoly, D., Kumar, A., Lau, N.-C., & Ropelewski, C. (1998, jun). Progress during TOGA in understanding and modeling global teleconnections associated with tropical sea surface temperatures. *Journal of Geophysical Research: Oceans*, *103*(C7), 14291–14324. Retrieved from https://doi.org/10.1029/97JC01444 doi: 10.1029/97JC01444

Trenberth, K. E., & Hurrell, J. W. (1994). Decadal atmosphere-ocean variations in the Pacific. *Climate Dynamics*, *9*(6), 303–319. Retrieved from https://doi.org/10.1007/BF00204745 doi: 10.1007/BF00204745

Uppala, S. M., Kållberg, W. P., Simmons, J. A., Andrae, U., Costa, B., Fiorino, M., ... Woollen, J. (2006, dec). The ERA-40 re-analysis. *Quarterly Journal of the Royal Meteorological Society*, *131*(612), 2961–3012. Retrieved from https://doi.org/10.1256/qj.04.176 doi: 10.1256/qj.04.176

Wengel, C., Latif, M., Park, W., Harlaß, J., & Bayr, T. (2018). Seasonal ENSO phase locking in the Kiel Climate Model: The importance of the equatorial cold sea surface temperature bias. *Climate Dynamics*. Retrieved from https://doi.org/10.1007/s00382-017-3648-3 doi: 10.1007/s00382-017-3648-3

Xie, S.-P., Tanimoto, Y., Noguchi, H., & Matsuno, T. (1999, jun). How and why climate variability differs between the tropical Atlantic and Pacific. *Geophysical Research Letters*, *26*(11), 1609–1612. Retrieved from http://dx.doi.org/10.1029/1999GL900308 doi: 10.1029/1999GL900308

Yeh, S.-w., Kug, J.-s., Dewitte, B., Kwon, M.-h., Kirtman, B. P., & Jin, F.-f. (2009). El Niño in a changing climate. *Nature*, *461*(7263), 511–4. Retrieved from http://www.ncbi.nlm.nih.gov/pubmed/19779449 doi: 10.1038/nature08316

Zebiak, S. E., & Cane, M. A. (1987, oct). A Model El Niño–Southern Oscillation. *Monthly Weather Review*, *115*(10), 2262–2278. Retrieved from https://doi.org/10.1175/1520-0493(1987)115{\%}3C2262:AMENO{\%}3E2.0.COhttp://0.0.0.2 doi: 10.1175/1520-0493(1987)115⟨2262:AMENO⟩2.0.CO;2

Zheng, F., Fang, X.-H., Yu, J.-Y., & Zhu, J. (2014, nov). Asymmetry of the Bjerknes positive feedback between the two types of El Niño. *Geophysical Research Letters*, *41*(21), 7651–7657. Retrieved from http://dx.doi.org/10.1002/2014GL062125 doi: 10.1002/2014GL062125

Zhu, J., Kumar, A., & Huang, B. (2015, jun). The relationship between thermocline depth and SST anomalies in the eastern equatorial Pacific: Seasonality and decadal variations. *Geophysical Research Letters*, *42*(11), 4507–

4515. Retrieved from http://dx.doi.org/10.1002/2015GL064220 doi: 10.1002/2015GL064220

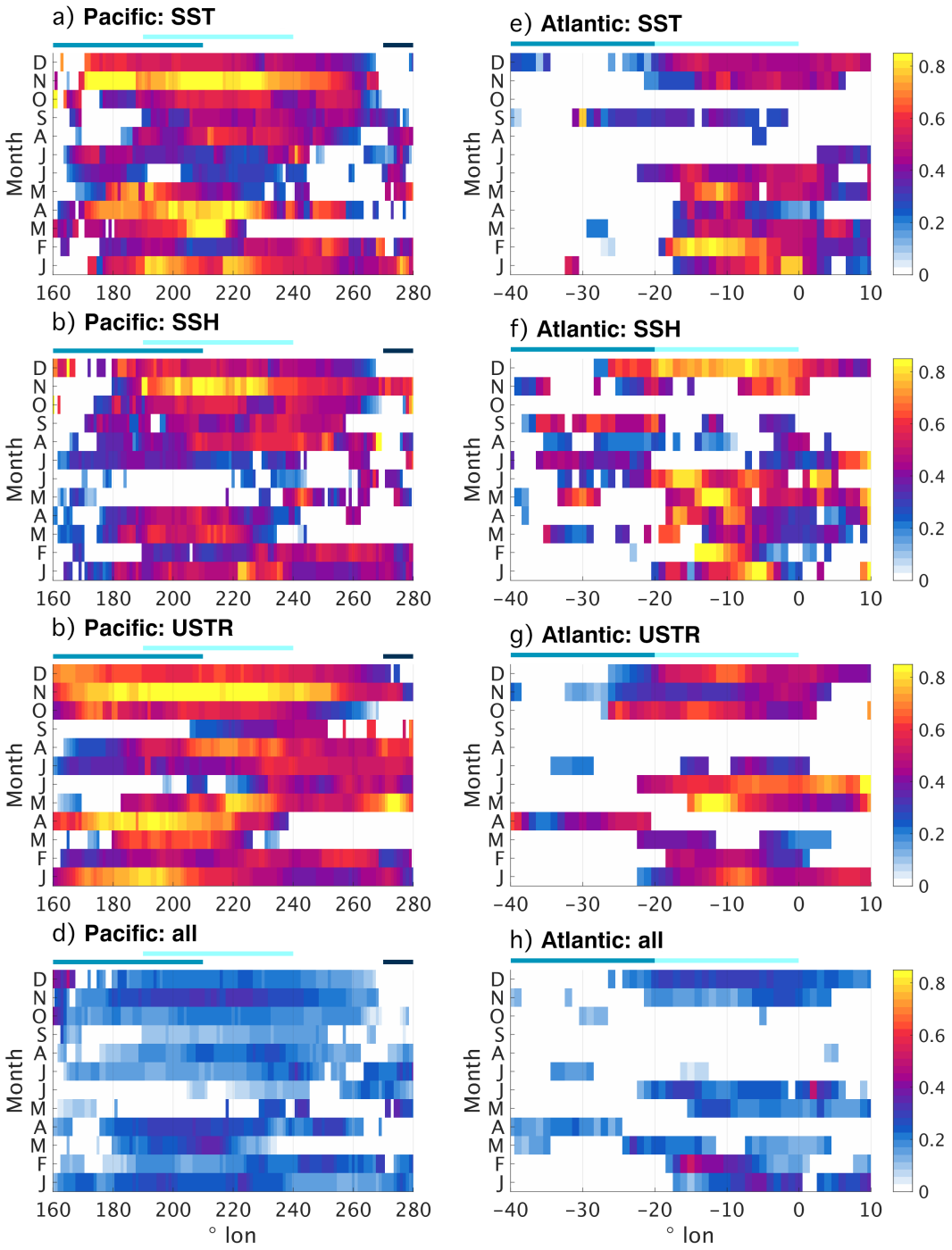

Figure A.3: *OBS-based comparison of different manifestations of the negative composite of the total Bjerknes feedback in the Pacific (left column, panels a-d) and the Atlantic (right column, e-h) for the period 1993-2012. All panels show total feedbacks along the equator (x-axis) and stratified into calendar months (y-axis). The first, second, third, and fourth rows show the negative composites of the total Bjerknes feedback using constant composites based on SST (a,e; these are the same as in the main text), SSH (b,f), constant composites based on USTR (c,g), and variable composites (d,h) (see text for details on the differences between the manifestations). Recall that the SST/SSH/USTR-based total feedback composites are a measure of the total Bjerknes feedback for when the SST/thermocline/zonal wind stress in the western ocean basin is warmer/deeper/more easterly (positive anomalies) or cooler/shallower/more westerly (negative anomalies) than on average. White indicates that at least one of the feedback elements contributing to the composite of the total feedback was negative. Coloured bars below the title indicate the zonal extent of the Nino4, Nino3.4, and Nino1.2 (WAtl and ATl3) regions in blue, light blue, and dark blue (blue and light blue) in the Pacific (Atlantic), respectively.*

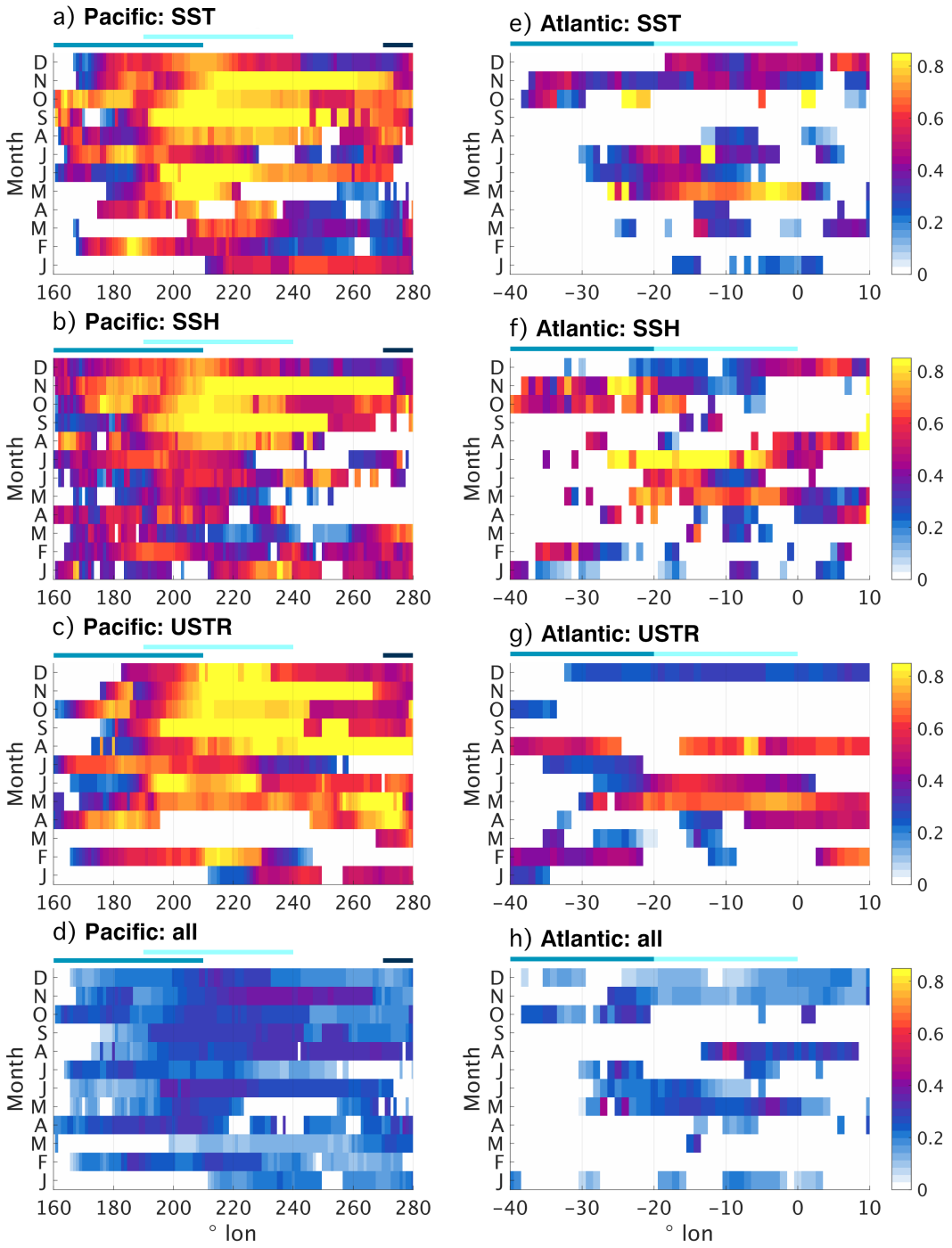

Figure A.4: *Same as Fig. SA.3, but for manifestations of the positive composites of the total Bjerknes feedback.*

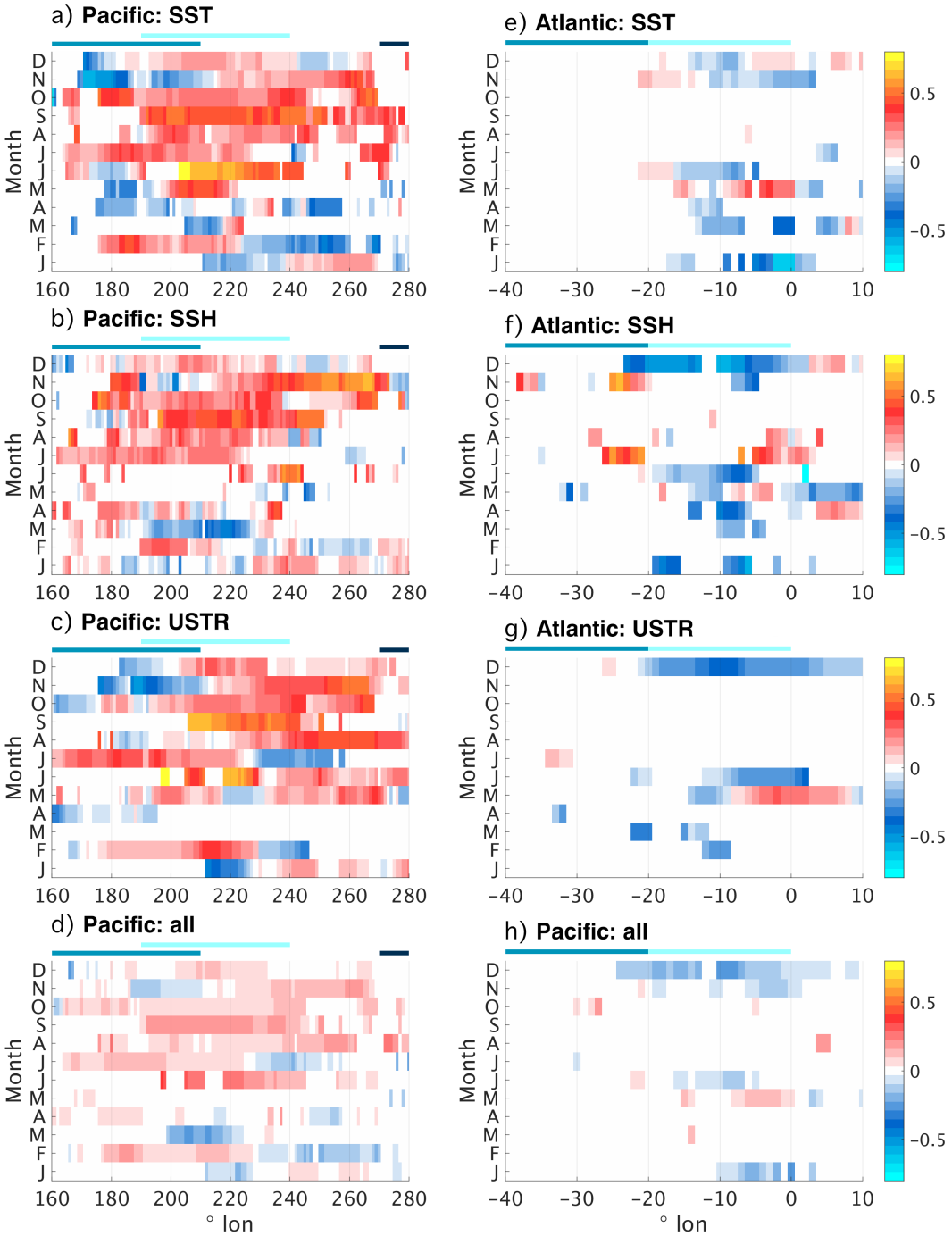

Figure A.5: *Same as Fig. SA.3, but for the difference between the positive and negative composites of different manifestations of the total Bjerknes feedback.*

Chapter 4

Can Climate Models simulate the observed strong Summer Surface Cooling in the equatorial Atlantic?

A STRONG WARM BIAS puts substantial obstacles in the way of model-based research in the equatorial Atlantic. This review paper discusses the physics of the seasonal cycle in the equatorial Atlantic and synthesises our current understanding of why the bias develops in state-of-the-art CGCMs.

Citation: **Dippe, T., M. Krebs, J. Harlaß, and J. F. Lübbecke (2018). "Can climate models simulate the observed strong summer surface cooling in the equatorial Atlantic?" In: *YOUMARES 8 – Oceans Across Boundaries: Learning from each other*. Ed. by S. Jungblut, V. Liebich, and M. Bode. Springer International Publishing, pp. 7-23**

The candidate's contributions to this manuscript are as follows. She

- Conceived the manuscript;
- Contributed to the development of the manuscript structure and the refinement of the "message";
- Produced Figures 2, 8, and 9;
- Authored the manuscript from first to final draft.

Can Climate Models Simulate the Observed Strong Summer Surface Cooling in the Equatorial Atlantic?

Tina Dippe, Martin Krebs, Jan Harlaß, and Joke F. Lübbecke

Abstract

Variability in the tropical Atlantic Ocean is dominated by the seasonal cycle. A defining feature is the migration of the inter-tropical convergence zone into the northern hemisphere and the formation of a so-called cold tongue in sea surface temperatures (SSTs) in late boreal spring. Between April and August, cooling leads to a drop in SSTs of approximately 5°. The pronounced seasonal cycle in the equatorial Atlantic affects surrounding continents, and even minor deviations from it can have striking consequences for local agricultures.

Here, we report how state-of-the-art coupled global climate models (CGCMs) still struggle to simulate the observed seasonal cycle in the equatorial Atlantic, focusing on the formation of the cold tongue. We review the basic processes that establish the observed seasonal cycle in the tropical Atlantic, highlight common biases and their potential origins, and discuss how they relate to the dynamics of the real world. We also briefly discuss the implications of the equatorial Atlantic warm bias for CGCM-based reliable, socio-economically relevant seasonal predictions in the region.

The Equatorial Atlantic: A Climate Hot Spot

The tropical oceans are a crucial element of the global climate system. Defined here as the ocean area between 15°N and 15°S, they occupy only about 13% of the earth's surface, but receive approximately 30% of the global net surface insolation.[1] Processes both in the ocean and the atmosphere redistribute surplus heat from low to higher latitudes. Without these mechanisms, the tropics would get steadily warmer, while the polar regions would radiate away more heat than they receive and hence continue to cool. The oceans help to establish the overall radiative equilibrium that is responsible for our relatively stable climate (Trenberth and Caron 2001).

Apart from the energy surplus, another defining feature of an equatorial ocean is that the effect of the earth's rotation vanishes at the equator, giving rise to a physical framework that is subtly different from its higher-latitude counterpart. The effect of the earth's rotation manifests in a pseudo-force that is called the Coriolis force. It deflects large-scale motion towards the right of the movement on the northern hemisphere and towards the left on the southern hemisphere. It provides rotation to large weather systems and explains why large-scale movement curves or even becomes circular. An exception is the equator, where the Coriolis force vanishes and movement can be straightforward. Additionally, the non-existent Coriolis force at the equator acts as a barrier for the transmission of information within the ocean, for example

[1] Based on data by Trenberth et al. (2009).

T. Dippe (✉) · M. Krebs · J. Harlaß
GEOMAR Helmholtz Centre for Ocean Research Kiel, Kiel, Germany
e-mail: tdippe@geomar.de; jharlass@geomar.de

J. F. Lübbecke
GEOMAR Helmholtz Centre for Ocean Research Kiel, Kiel, Germany

Faculty of Mathematics and Natural Sciences, Christian Albrechts University, Kiel, Germany
e-mail: jluebbecke@geomar.de

S. Jungblut et al. (eds.), *YOUMARES 8 – Oceans Across Boundaries: Learning from each other*,
https://doi.org/10.1007/978-3-319-93284-2_2

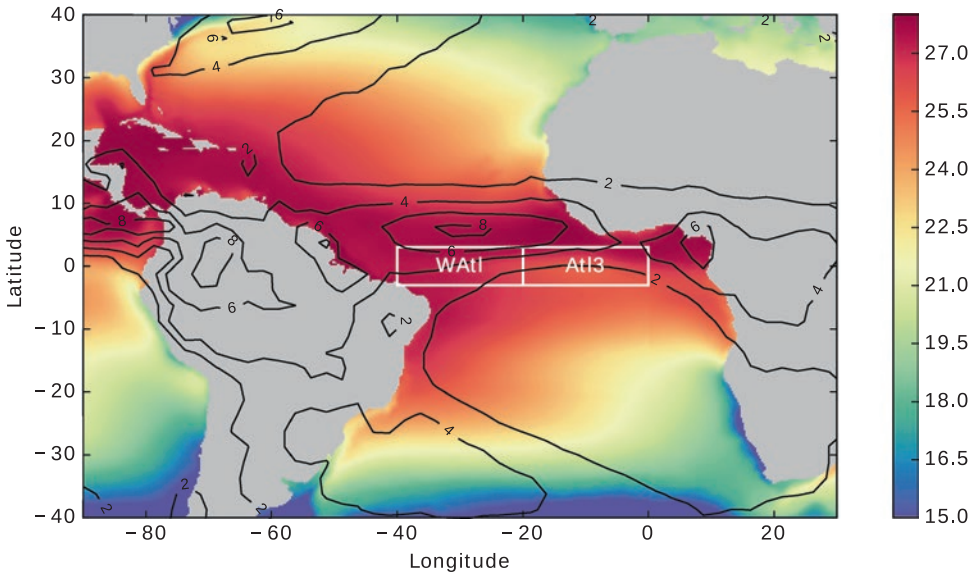

Fig. 1 The observed tropical Atlantic mean state sea surface temperature (SST) and precipitation: Annual mean sea surface temperatures are shown as shading, precipitation in contours. White boxes indicate the Atl3 and WAtl region in the eastern and western tropical Atlantic, respectively. The used datasets are the NOAA Optimum Interpolated SST dataset (OISST, Reynolds et al. 2007; Banzon et al. 2016), and the NOAA Climate Prediction Center (CPC) Merged Analysis of Precipitation dataset. (CMAP, Xie and Arkin 1997)

via equatorial Kelvin waves. Communicating information from the southern to the northern hemisphere and vice versa is hence a non-trivial enterprise in the ocean.

While the basic set-up of the marine tropical climate system is identical in all three tropical oceans, details differ between basins. The Pacific Ocean has the largest extent and is characterized by a relatively simple land-ocean geometry; it behaves much like a perfect theoretical ocean. The tropical Atlantic, in contrast, is much narrower and the surrounding continents interact with the ocean in complex ways. For example, the tropical Atlantic appears to be more susceptible to extra-equatorial influences (e.g., Foltz and McPhaden 2010; Richter et al. 2013; Lübbecke et al. 2014; Nnamchi et al. 2016), and variability is due to a number of interacting mechanisms on overlapping time scales (Sutton et al. 2000; Xie and Carton 2004). Therefore, the tropical Atlantic is less readily understood than the tropical Pacific, and still poses substantial challenges to the scientific community.

The mean state of the tropical Atlantic is characterized by a complex interplay of atmospheric and oceanic features. These are i) the trade wind systems of both the northern and southern hemispheres, ii) a system of alternating shallow zonal[2] currents in the ocean, and iii) a zonal gradient in upper-ocean heat content that is also reflected in a pronounced zonal gradient in sea surface temperatures (SSTs), with warm temperatures in the west and cooler surface waters in the east. Figure 1 illustrates the mean state of SST and precipitation.

The trade winds are part of the climate system's hemispheric response to the strong temperature gradient between the polar and the equatorial regions. Intense (solar) surface heating at the equator produces warm and humid, ascending air masses. During the ascend, part of the air moisture condensates and releases latent heat, which further accelerates the rising motion. The upward flow moves mass from the surface layer towards the top of the troposphere, effectively decreasing surface pressure and forming a low-pressure trough. At the surface, a compensation flow towards the low-pressure trough is established. Due to the rotation of the earth, however, the flow veers to the west and creates the surface trade winds. The northeasterly and southeasterly trade winds of the northern and southern hemispheres, respectively, converge in the inter-tropical convergence zone (ITCZ), a zonal band of intense precipitation and almost vanishing horizontal winds (Fig. 1). Because the ITCZ is located to the north of the equator in the Atlantic, the equatorial Atlantic is not dominated by the ITCZ itself, but by the trade wind system of the southern hemisphere that provides relatively steady easterly winds on the equator. (See below for why the ITCZ is, on average, not residing on the equator in the tropical Atlantic.)

A consequence of the easterly wind forcing at the ocean surface and the vanishing Coriolis force at the equator is that the wind pushes the warm surface waters westward. Water piles up to the east of Brazil in the Atlantic warm pool, providing water temperatures of approximately 28 °C at the surface. Conversely, the surface layer of warm water in the eastern tropical Atlantic is thinned out considerably – the eastern part of the basin stores much less heat in the upper ocean than the western part. A pronounced zonal gradient in upper-ocean heat content is established. Figure 8a illustrates this mean state.

The pressure below the ocean surface is not uniform across the basin either. At the equator, the bulk of warm water in the western ocean basin adds pressure to the water

[2] "Zonal" refers to an east-west orientation, i.e. one that is parallel to the equator. A north-south orientation is called "meridional".

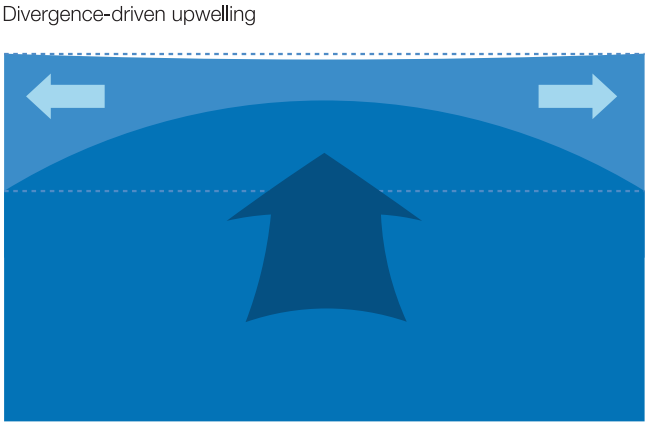

Fig. 2 Upwelling driven by horizontal divergence. Consider an ocean in a state of rest. In a simple model, a layer of warm water is sitting on top of a layer of colder water. Both the interfaces between the warm surface layer and the atmosphere, and between the colder subsurface water and surface layer are approximately even (horizontal dashed blue lines). When a divergence is created in the upper layer, mass is transported away from the divergence (light blue arrows in the surface layer). Because water is approximately incompressible, mass must be conserved. A vertical flow from the subsurface layer compensates the horizontal divergence (dark blue, upward arrow). In reality, this domes the interface between the surface and the subsurface layers. The sea surface adapts to the doming interface by decreasing in a similar fashion, albeit with a much smaller amplitude

column, while eastern ocean pressure is reduced. The resulting east-west pressure gradient is balanced by a strong eastward current right below the surface – the equatorial undercurrent (EUC) (Cromwell 1953; Cromwell et al. 1954). At the surface, on the other hand, the direct wind forcing and meridional pressure gradients produce a complex system of alternating zonal current bands (e.g., Schott et al. 2003; Brandt et al. 2006, 2008).

The three-dimensional flow of the upper equatorial oceans directly below the well-mixed surface layer is characterized by a slow but steady upward motion of, at best, a few meters per day (Rhein et al. 2010). This so-called "upwelling" is maintained by two processes. First, the Coriolis force deflects the off-equatorial components of the wind-induced westward displacement of surface water masses into opposite directions. On the northern hemisphere, westward flow veers north, while the Coriolis force directs it south on the southern hemisphere. Zonal wind-driven upper ocean mass transports diverge; they effectively transport mass away from the equator. However, because mass is conserved, sea level sags imperceptibly, and upwelling transports colder, subsurface water closer to the surface by creating a "dome" in the interface between the warm surface water and cooler subsurface water. The ratio between the surface and subsurface layer thicknesses changes in response to the surface divergence. Figure 2 illustrates how divergent flow in the surface layer creates upwelling and changes the geometry of the involved interfaces between both the atmosphere and the ocean, and the ocean surface and subsurface layers.

Second, a small meridional contribution to the equatorial wind field contributes to maintaining equatorial upwelling. These meridional contributions are illustrated in Fig. 7b by the equatorial wind vectors that do not point straight to the west but rather to the northwest, as they are part of the southern hemisphere trade wind regime crossing the equator into the northern hemisphere for most of the year. In the ocean, they induce meridional surface mass transports slightly off the equator (Philander and Pacanowski 1981). Again, the Coriolis force redirects these meridional motions into zonal mass transports of opposite signs, which contribute to the upper ocean horizontal divergence.

Over the course of the year, the set-up of this basic state varies. Due to the tilted rotational axis of the earth, the latitude of maximum insolation shifts into the northern hemisphere in boreal – i.e. northern hemispheric – summer, and into the southern hemisphere in boreal winter. The ITCZ, accompanied by the trade wind systems of both hemispheres, migrates in a similar fashion. However, the ITCZ does not oscillate around the equator but stays north of it for most of the year (Hastenrath 1991; Mitchell and Wallace 1992). Xie (2004) reviewed the "riddle" of the asymmetric ITCZ and concluded that it is, contrary to intuition, not so much the overall distribution of landmasses and oceans that anchors the Atlantic ITCZ to the northern hemisphere, but a combination of air-sea coupling and the shape of the West-African shoreline. More recently, Frierson et al. (2013) also demonstrated how the meridional temperature gradient between the warm northern hemisphere and the relatively colder southern hemisphere impacts the ITCZ behavior. All factors combine to pull the trade wind system of the southern hemisphere across the equator and establish the highest SSTs to the north of the equator.

Driven by the changing trade wind systems, the zonal surface current systems vary in strength and location. The intensity of the Equatorial Undercurrent, while firmly pinned to the equator, varies as well (Johns et al. 2014). Variations in the wind forcing lead to seasonally recurring intensifications of the zonal heat content gradient.

One of the most striking elements of the tropical Atlantic seasonal cycle is the formation of the Atlantic cold tongue in the eastern equatorial Atlantic during boreal summer. The cold tongue is characterized by an intense cooling of the upper ocean. Figure 3a shows that SSTs in the Atl3 region (3°S–3°N, 20°W–0°E) drop from 28 °C to about 23 °C between April and August, forming a distinct, tongue-shaped pattern of relatively cool surface water that stretches from the West African coast into the central equatorial Atlantic (Figs. 3b, c). The observed temperature difference between April and August in the upper 50 m of the Atl3 region alone corresponds to a change in thermal energy of

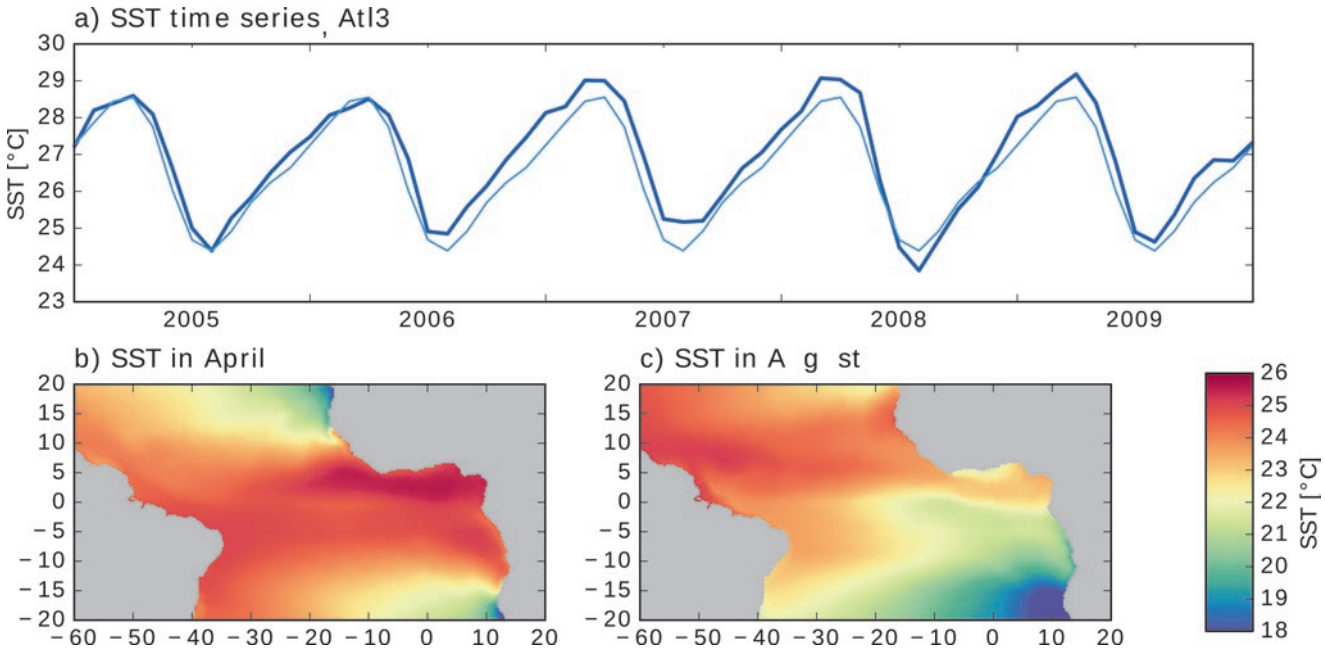

Fig. 3 Observed cold tongue based on the NOAA Optimum Interpolated SST dataset (OISST). (**a**) Exemplary time series of monthly mean Atl3 sea surface temperature (SST, dark blue) and the climatological seasonal cycle (light blue). For the seasonal cycle, monthly mean data has been averaged for each calendar month for the period 1981–2012. (**b**) and (**c**) Climatological SST fields for April and August, illustrating the climatological conditions when SSTs reach their maximum just before the onset of the cold tongue, and when the cold tongue is fully developed, respectively

1351.16 EJ.[3] That is 13 times the US-American energy consumption of 2014, or 2.6 times the total global energy consumption of 2011.

The formation of the cold tongue co-occurs with seasonal changes in the atmospheric circulation. An important and well-known aspect of this is the strong co-variability between the onset of the cold tongue and the onset of the West African monsoon (e.g., Okumura and Xie 2004; Brandt et al. 2011a; Caniaux et al. 2011), a key element of large-scale precipitation in western Africa and hence a crucial factor of agriculture. Understanding the complex processes that shape the coupled atmosphere-ocean-land climate system of the equatorial Atlantic is a task of high societal relevance.

In concert with accurate and long-term observations, climate models are an essential tool to investigate the equatorial Atlantic. Here we address the question of how well state-of-the-art climate models are able to reproduce the observed seasonal cycle of the equatorial Atlantic. The section "Climate models: A crash course" gives an overview on coupled climate models and introduces the concept of model biases. The section "Can climate models reproduce the observed seasonality of the equatorial atlantic climate system?" reports common biases in the tropical Atlantic and how they relate to the formation of the modeled cold tongue. An outlook in the last section addresses the usefulness of climate models for studies of cold tongue variability, a crucial source of tropical Atlantic climate variability that strongly affects the surrounding continents.

Climate Models: A Crash Course

Climate models numerically solve the Navier-Stokes equations for a set of specified assumptions. The Navier-Stokes equations are a system of non-linear partial differential equations that describe the behavior of fluids, from a drop of water that hits the surface of a puddle, to global circulation systems such as the trade wind systems. They are highly complex and can only be solved numerically when they are approximated to focus on a specific class of fluid processes. For climate models, these processes are mostly related to the large-scale global circulation, synoptic phenomena, and possibly mesoscale phenomena[4] such as ocean eddies. The approximated Navier-Stokes equations that are used in current climate models are called the primitive equations.

Climate models consist of a number of "building blocks". The two core building blocks are an atmosphere and an ocean general circulation model (GCM). Given appropriate surface and boundary forcing, both GCM types can be run

[3] Based on thermal data from the World Ocean Atlas (WOA2013v2, Locarnini et al. 2013).

[4] Size on the order of 10–50 km.

independently. Phillips (1956) demonstrated this by designing the first successful atmospheric GCM. To allow the oceanic and atmospheric blocks to interact with each other, a coupling module exchanges information at the air-sea interface. A coupler and the atmospheric and oceanic GCMs together form the simplest coupled GCM (CGCM). Such a basic CGCM lacks a number of relevant processes, relating for example to the land and sea ice components of the climate system or the impact of vegetation. To introduce these important aspects into the model, CGCMs are "upgraded" with additional building blocks to form earth system models. If a basic CGCM is a simple brick house of only one room, a full-fledged earth system model is a mansion with specialized rooms for different tasks. Important additional building blocks for an earth system model are modules that simulate the behavior of sea ice, ice sheets and snow cover on land, vegetation and other surface processes such as river runoff into the ocean, atmospheric chemistry, biogeochemistry in the ocean or even geological processes of varying complexity.

In order to solve the model equations numerically, CGCMs need to discretize the real world into finite spatial and temporal units. The basis for such a discretization is a three-dimensional grid of grid boxes that each contain a single value of a given variable. The CGCM applies the model equations to the grid boxes and integrates them forward in time. Essentially, each grid box is a mini-model that is, however, exchanging information with neighboring grid boxes.

An important characteristic of a model grid is its resolution, i.e. the size of its grid boxes.[5] It defines, among other things, which processes can be resolved. As an example, consider the development of cumulus clouds. While cumulus clouds have a horizontal scale of less than 10 km, state-of-the-art models use a resolution of about 100 km. On such a grid CGCMs cannot simulate cumulus clouds directly. Consequently, the climatic impacts of such clouds have to be parameterized, i.e. their effect must be captured by the model in a simpler way that is supported by observations. For convective[6] and mixing processes alone – important aspects of cumulus clouds -, a number of parameterization schemes exist that subtly alter the behavior of large-scale processes in the models.

In addition to horizontal processes, models must be able to capture vertical motions in the climate system. Cumulus clouds, for example, extent vertically throughout varying portions of the troposphere, and vertical movement within clouds is a key factor of precipitation. On a larger scale, ascending air masses within the ITCZ define an important aspect of the tropical climate system (cf. Section "The equatorial atlantic: A climate hot spot"). Models need to be able to reproduce these vertical movements. They require vertical layering, giving rise to the three-dimensional structure of a model grid. A common feature of all models is that their vertical levels are unevenly distributed. Because properties usually change drastically close to the air-sea interface, resolving these strong gradients requires a high vertical resolution. Conversely, the thickest levels are farthest away from the air-sea interface. In the ocean, the last model level usually ends at the sea floor; the atmosphere, however, is not bounded that clearly. Some models only resolve the troposphere, our "weather" sphere that reaches up to approximately 15 km, while a number of recent atmosphere models incorporate the stratosphere as well (up to 80 km).

Figure 4 illustrates schematically how the different "building blocks" of a CGCM work together and how the real world must be discretized into grid boxes to allow a numerical solution of the primitive equations.

CGCMs are initialized either from a state of rest – i.e. the ocean and atmosphere are without motion and only establish their general circulation patterns during the first stage of the simulation, the so-called "spin-up" – or from a more specific state that is generally derived from observations. In both cases, the model needs time to smooth out initial imbalances and establish an equilibrium. Additionally, climatically relevant forcing parameters must be prescribed to the model in the form of boundary conditions. A prominent example of such a boundary condition is the strength and variability of the solar forcing, our energy source on earth, or the atmospheric CO_2 concentration.

Climate models are used to address a host of research questions. They aid scientists in interpreting observations, infer mechanisms, or provide information on how the climate system might evolve in the future. All of these tasks, however, require that CGCMs are able to produce a realistic climate. Due to various limitations, this is not always the case. A common manifestation of the shortcomings of a climate model is the formation of biases.

A bias is a systematic difference between the modeled and the observed climate. This difference can occur in any statistical property of any model variable. While standard biases are routinely monitored during the development and application of climate models, non-obvious biases may be present in simulations that look fine otherwise. Consider, for example, SST in a given location. While routine bias controls may have found a realistic mean SST, closer inspection could reveal that SST anomalies tend to be too high. Because positive and negative anomalies cancel each other out on

[5] Note that, usually, not all grid boxes of a GCM have the same size, neither in terms of absolute surface area, nor in terms of longitudinal and latitudinal extent. A common practice in ocean models, for example, is to refine the latitudinal resolution towards the equator to better resolve the fine structures of the equatorial oceans. In a similar fashion, Sein et al. (2016) recently discussed grid layouts for ocean models that increase their spatial resolution in certain target areas.

[6] Convection: upward motion in the atmosphere.

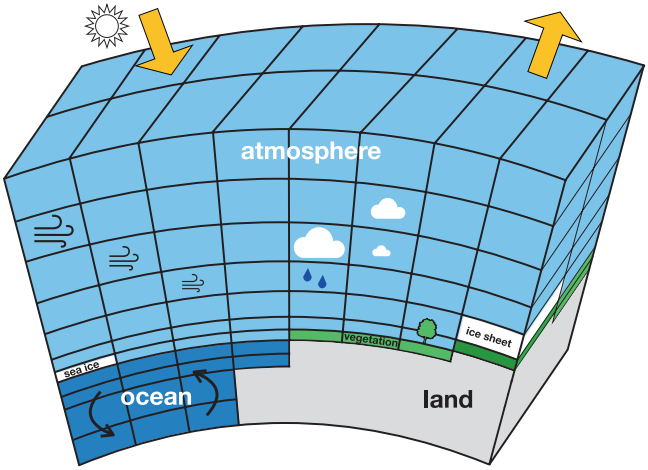

Fig. 4 Schematic of a Coupled General Circulation Model (CGCM). On the most basic level, the earth is a closed system that receives energy from the sun and radiates away thermal energy (yellow arrows at the "top of the atmosphere"). A CGCM tries to simulate the processes within this system. It consists of a number of modules that interact with each other. Important modules in state-of-the-art CGCMs are the ocean-and-sea-ice module, the atmospheric module, and additional modules that simulate, for example, land surface processes or vegetation. These "building blocks" of the CGCM exchange information with each other via an additional "coupling module". Coupling is a computationally expensive operation that can account for up to a third of the total required computational resources of a CGCM. A CGCM solves an approximation to the Navier-Stokes equations numerically. These are a set of non-linear partial differential equations that describe the motion of fluids. To solve them, the model must discretize the real world into finite spatial and temporal units. In the three-dimensional space domain, this discretization results in a layered grid. Each grid box contains a single value for each model variable. Processes acting on spatial scales that are smaller than the extent of the grid box must be parameterized. Prominent examples of these "sub-grid" processes are, for example, the formation of clouds and precipitation

average, this biased variance would not be obvious. In a similar manner, positive and negative SST anomalies might not be distributed realistically, with the model perhaps producing a few very strong positive anomalies and many weak negative anomalies that still form the expected average. In this case, the modeled SST distribution is skewed with respect to observations.

An additional limitation on the hunt for biases is that a bias can only be diagnosed in comparison to a reliable observational benchmark. Many parameters of the real climate system, however, are hard to observe or have only been observed for a short time. In general, large-scale patterns on the earth's surface and throughout the atmosphere can be observed relatively easily with satellite-borne remote sensing instruments. SST, for example, has been carefully monitored by a number of satellite missions since the 1980s. Processes below the ocean surface, however, can usually not be monitored from space. Instead, observational data have to be obtained by measurements from ships, moored instruments and autonomous vehicles such as gliders and floats. For the tropical oceans, the TAO/TRITON mooring array in the Pacific (McPhaden 1995), the PIRATA array in the Atlantic (Bourlès et al. 2008), and the RAMA array in the Indian Ocean (McPhaden et al. 2009) provide, among others, information on temperature, salinity, current velocities and air-sea fluxes. Additionally, an increasing number of hydrographic observations have become available over the last decade due to the Argo program (Roemmich et al. 2009). While all of these measurements provide invaluable information about the state of the tropical oceans, they are not spatially continuous and have only been operational for the last few decades. Obtaining information about the evolution of the climate system in the past remains a core challenge of climate research.

Although no climate model is exactly like the other, some biases are shared by a wide range of state-of-the-art CGCMs. Figure 5 shows the global pattern of the annual mean SST bias for the average of 33 CGCMs and an experiment with the Kiel Climate Model (KCM, Park et al. 2009). Positive values indicate that modeled SST is warmer than in observations and vice versa. We validated the performance of these CGCMs and the KCM in terms of SST against the satellite derived Optimum Interpolated SST dataset (OISST, Reynolds et al. 2007; Banzon et al. 2016). Figure 5 shows that while the KCM is a unique model that has individual flaws and strengths, the characteristics of its equatorial Atlantic SST bias are well comparable to other current CGCMs (examples of other models are shown, among others, in Wahl et al. 2011; Xu et al. 2014; Ding et al. 2015; Harlaß et al. 2017).

The KCM is a state-of-the-art CGCM that was integrated with radiative forcing for the period 1981–2012 in rather coarse resolution. The ocean-sea ice model NEMO (Madec 2008) was run with 31 vertical levels and a horizontal resolution of 2° that is refined to 0.5° in the equatorial region. The atmospheric model ECHAM5 (Roeckner et al. 2003) is run with 19 vertical levels and a global horizontal resolution of approximately 3.75°. Results from KCM simulations are selected here for consistency reasons. We stress again that while the KCM differs wildly from other CGCMs in some aspects, its simulation of the tropical Atlantic is representative for most current-generation CGCMs.

Can Climate Models Reproduce the Observed Seasonality of the Equatorial Atlantic Climate System?

The Equatorial Atlantic Warm Bias: Symptoms

The annual mean SST bias varies considerably between different regions of the ocean (Fig. 5). Striking features of the global SST bias pattern are the pronounced warm biases

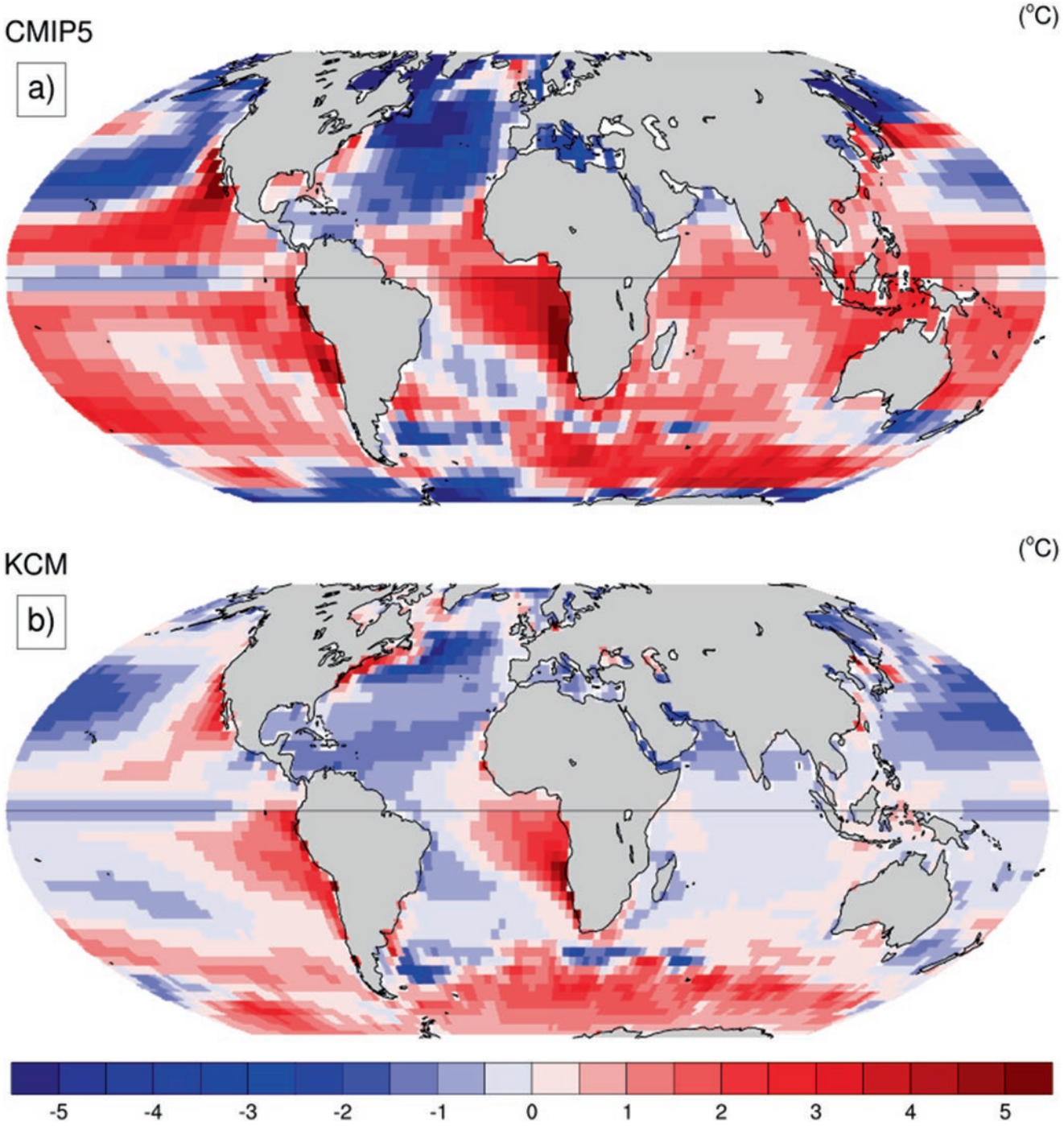

Fig. 5 Annual mean global sea surface temperature (SST) bias in (**a**) the ensemble mean of 33 Coupled General Circulation Models (CGCMs) contributing to the Coupled Model Intercomparison Project, Phase 5 (CMIP5, Taylor et al. 2012) and (**b**) one integration of the Kiel Climate Model (KCM). For CMIP5, the chosen experiments were "historical" experiments that were forced by the observed changes in atmospheric composition. The KCM was run with an atmospheric horizontal resolution of approximately 3.75° and with 19 vertical levels. The ocean model had a horizontal resolution of 2° that was refined to 0.5° towards the equator, and 31 vertical levels. The annual mean SST bias was diagnosed with respect to the NOAA Optimum Interpolated SST dataset (OISST) for the period 1982–2009. Using an ensemble mean of three ensembles instead of a single integration to diagnose the KCM SST bias changed the results only negligibly. This demonstrates how robust a feature the annual mean SST bias pattern is in the KCM

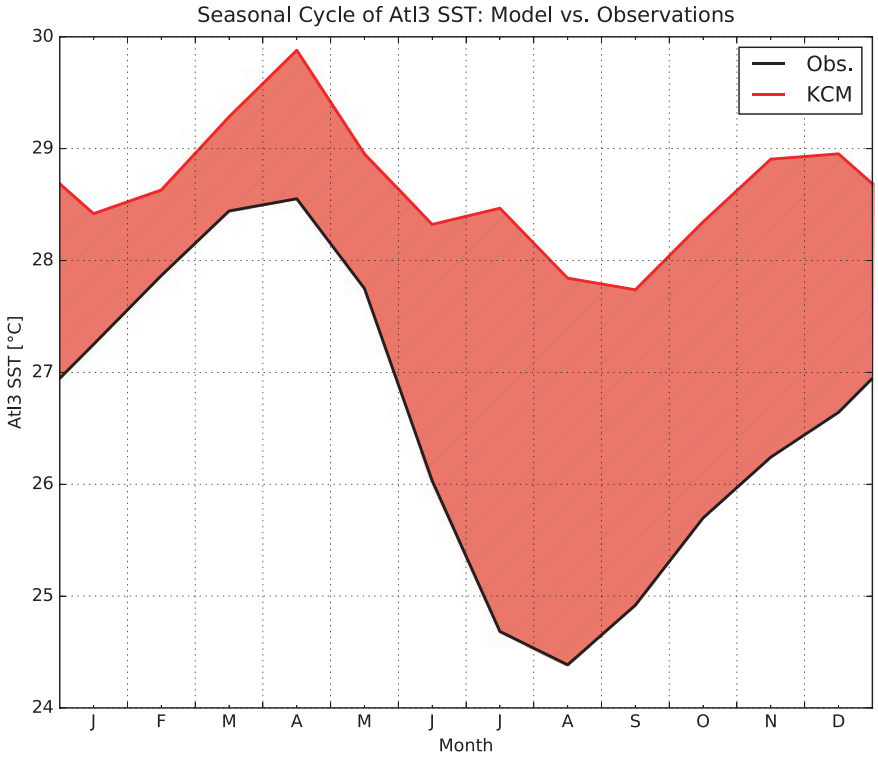

Fig. 6 Seasonal cycle of Atl3 sea surface temperature (SST) in observations (NOAA Optimum Interpolated SST dataset, black), and the Kiel Climate Model (KCM, red). Red shading illustrates the bias magnitude for each month

along the subtropical western shorelines of all continents. These biases appear, for example, along the western US-American as well as the Peruvian and Chilean coasts in the Pacific, or off Angola and Namibia in the Atlantic. They are anchored to the eastern boundary upwelling systems, where cold subsurface waters are brought close to the ocean surface. Here, SST biases can reach annual mean amplitudes of up to 7 °C in current climate models (Xu et al. 2014).

In this section, we focus on the pronounced warm bias that covers the equatorial Atlantic cold tongue region. The annual mean SST bias in the Atl3 region has a magnitude of approximately 2 °C.[7] In the upper 50 m of Atl3 in the KCM, this corresponds to a heat surplus of approximately 380 EJ, an amount of energy that could melt 47 times the ice volume of the Antarctic ice sheet.[8]

An important aspect of the equatorial Atlantic SST bias is that it varies over the course of the year. Figure 6 shows that the SST bias of the KCM is smallest in boreal winter, with a value of less than 1 °C in February. During the cold tongue formation, it rapidly increases to almost 4 °C until July. For the rest of the year, it slowly decreases again. This implies that the KCM struggles to simulate the observed strong cooling that is associated with the development of the cold tongue in boreal summer. Indeed, Fig. 6 shows that the KCM – similar to most state-of-the-art CGCMs (e.g., Richter and Xie 2008; Richter et al. 2014b) – does not produce a coherent cold tongue that is comparable in strength to observations. A key process of the equatorial Atlantic climate system is missing from the simulations.

Because the ocean and the atmosphere are strongly coupled in the tropics, the missing cold tongue is only one symptom of a fundamentally biased equatorial Atlantic in current climate models. Figure 7 illustrates the bias of the zonal wind component in the KCM. During spring, the KCM strongly underestimates the magnitude of zonal wind in the western tropical Atlantic (Fig. 7a). While the absolute value of zonal wind is higher in the KCM than in observations, especially during spring, the magnitude is much smaller. Instead of the generally easterly winds (negative values), associated with the trade winds, the KCM simulates very weak westerly winds (positive values). This "westerly wind bias" – so-called because the simulated zonal winds are much too westerly compared to the observed trade winds – is another typical bias pattern in state-of-the-art GCMs. It agrees with an ITCZ that is displaced too far to the south, a feature that is common to both coupled and atmosphere-only GCMs (e.g., Doi et al. 2012; Richter et al. 2012; Siongco et al. 2015).

An important question is: How do the different bias symptoms relate to each other dynamically, and how do these

[7] Note, however, that by no means *all* climate models develop such a strong equatorial Atlantic warm bias. Some models are capable of simulating a more realistic tropical Atlantic, but these models represent but a tiny minority of all current CGCMs.

[8] We used the thermal data from WOA2013v2 to compare our model results with. The Antarctic ice volume is based on the Bedmap2 dataset (Fretwell et al. 2013).

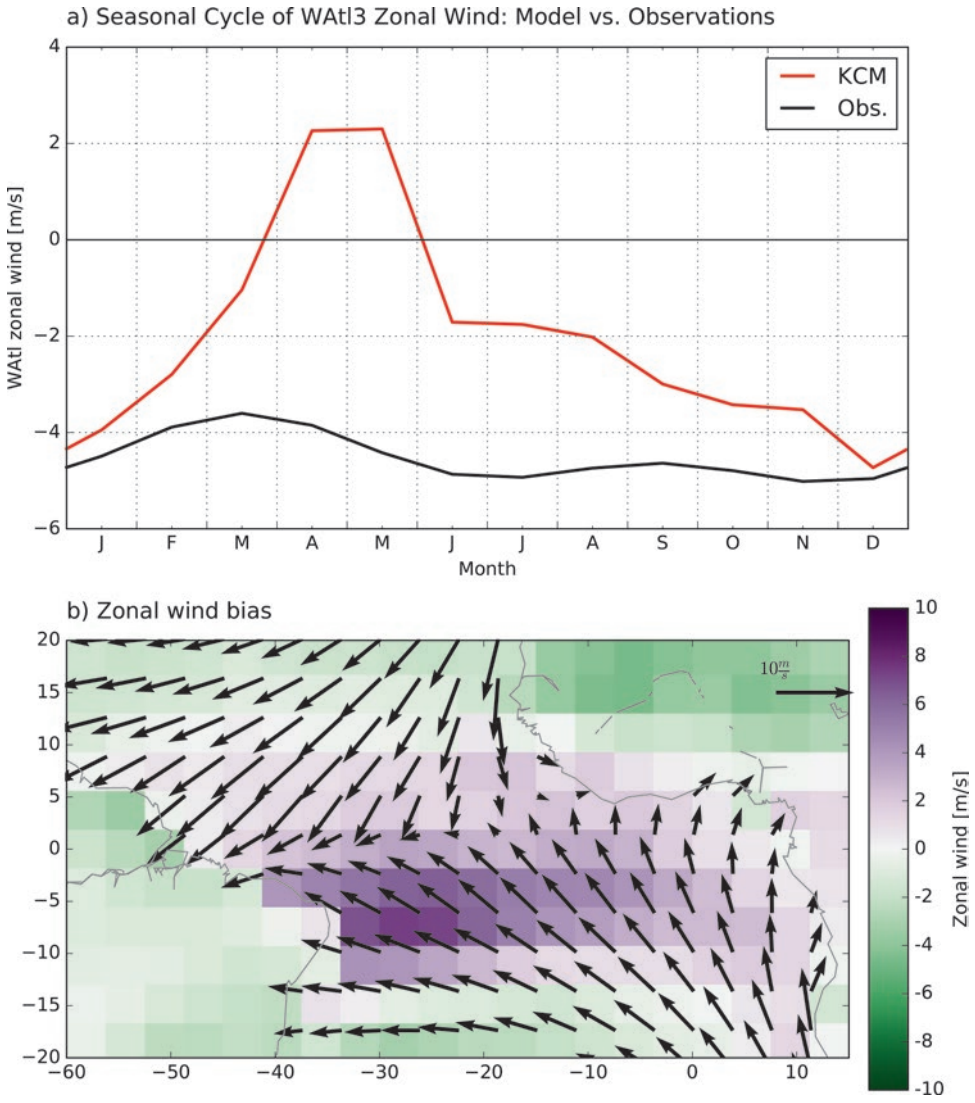

Fig. 7 Tropical Atlantic near-surface winds and zonal wind bias in spring. (**a**) Same as Fig. 6, but for the zonal component of 10 m wind in WAtl. (**b**) Climatological mean of observed 10 m wind (arrows) and the Kiel Climate Model (KCM) zonal wind bias in February–April (shading) in the equatorial Atlantic. The wind climatology is based on the Scatterometer Climatology of Ocean Winds (SCOW, Risien and Chelton (2008)). Arrows combine the zonal and meridional components of the climatological 10 m wind, while shading only refers to the zonal component of the wind

dynamics compare to the observed processes that shape the tropical Atlantic climate system? In the next subsection, we first review the basic processes that establish the observed seasonal cycle in the tropical Atlantic, and then compare the observations with what is happening in state-of-the-art climate models.

Which Processes Produce the Equatorial Atlantic Warm Bias?

A good first assumption about the seasonal cycle is that it is driven by the seasonal movement of the sun. Such a seasonal cycle should be symmetric. In the tropical Atlantic, however, it is clearly asymmetric. Figure 6 shows that the cooling period between April and August is much shorter – or, equivalently, more intense – than the subsequent period of gradual warming that lasts until the following April. Processes other than the seasonal forcing of solar insolation must contribute to the fast growth of the summer cold tongue.

Recent studies of the tropical Atlantic suggest that the rapid formation of the cold tongue involves a coupled, positive feedback (Keenlyside and Latif 2007; Burls et al. 2011; Richter et al. 2016). A feedback establishes a relationship between two or more variables. In a negative feedback small perturbations in one variable are compensated by changes in the other such that the system returns to its original, stable state. The opposite is true for a positive feedback. Here, a perturbation – even a small one – in one variable provokes changes in the other variables that reinforce the original perturbation. The system continues to diverge from its initial state. The perturbation grows until the feedback is disrupted.

The dominant positive feedback in the equatorial oceans is the Bjerknes feedback (Bjerknes 1969). It relates three key properties of an equatorial ocean basin to each other: SST in the eastern ocean basin; zonal wind variability in the western

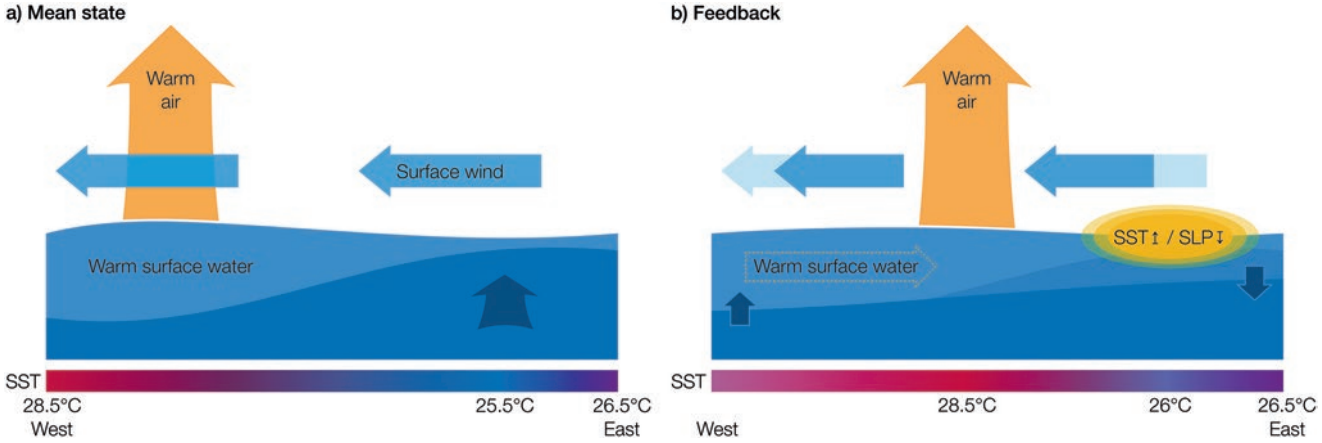

Fig. 8 The Bjerknes feedback. (**a**) Mean state. Along the equator, the surface wind field is dominated by the trade winds of the southern hemisphere. Both the zonal and meridional components of the trade winds contribute to surface divergences close to the equator, producing equatorial upwelling (thick blue arrow). Steady equatorial easterly wind forcing (blue arrows) pushes warm surface waters (light blue layer) towards the western ocean basin and builds up the warm pool. Warm and moist air rises above the warm pool (orange arrow). In contrast, the surface mixed layer is thin in the eastern basin, upwelling is more efficient there, and SSTs are, on average, cooler than in the warm pool (approximately 25.5 °C and 28.5 °C, respectively; the equatorial SST distribution is sketched in the bar below the figure). (**b**) The positive Bjerknes feedback alters the state of the tropical ocean. The trade winds weaken, and zonal surface winds in the western ocean basin decrease. The balance between the subsurface pressure gradient and wind stress forcing is disrupted, and part of the warm pool "sloshes back" into the central ocean basin, redistributing warm surface water more evenly across the ocean basin. The tilt in the interface between the surface and subsurface waters decreases, and upwelling is less efficient in providing cold subsurface water to the surface layer in the eastern ocean basin. The cold tongue region warms (orange ovals). Sea level pressure (SLP) over the warm anomalies decreases, and convection shifts towards the central ocean basin. The surface wind response to this shift in surface convection and the zonal SLP distribution further weakens the trade wind regimes and closes the feedback

ocean basin; and the zonal distribution of upper ocean heat content along the equator, with large heat reservoirs and thick surface layers in the western warm pool, and thin surface layers in the cold tongue region in the east.

Figures 8a and b illustrate, respectively, the mean state of an equatorial ocean and how the Bjerknes feedback alters it. Consider a weakening of the easterly trade winds in the western ocean basin (or equivalently a decrease in easterly zonal wind stress at the ocean surface). The balance between the wind stress and the piled-up warm water in the western ocean basin temporarily fades, and the piled-up warm pool "sloshes back" into the eastern ocean basin, redistributing the upper ocean heat content more evenly across the equatorial basin.[9] The zonal gradient in heat content is leveled out, and the additional heat in the eastern ocean basin helps to establish a positive SST anomaly. This process can last several months in the equatorial Pacific and approximately one month in the equatorial Atlantic. (These different time scales are mainly due to the different east-west extents of the basins and hence signal propagation speeds.)

In the tropics, the atmosphere is closely coupled to the ocean. It reacts strongly to underlying SST variability by developing an anomalous wind field that converges over a warmer-than-usual patch of water (Gill 1980). The local changes in the wind field co-occur with changes in the zonal pressure gradient along the equator. The altered zonal pressure gradient in turn induces further weakening of the easterly trade winds in the western ocean basin, closing the feedback loop. An equivalent process with opposite signs takes place when the trade winds intensify in the western ocean basin.

The Bjerknes feedback is restricted to the equatorial ocean basins. While the ingredients of the feedback – wind, upper ocean heat content and SST variability – are present in every region of the ocean and usually interact with each other in one way or the other, the fully coupled Bjerknes feedback requires that information is zonally transmitted across almost the entire zonal extent of the basin, both in the atmosphere and the ocean. This is only possible when the Coriolis force vanishes or is negligibly small, since it would otherwise deflect the involved physical motions into curved movements. A direct, zonal exchange between the eastern and western ocean basins would not be possible in the presence of the Coriolis force.

[9] In the framework of this explanation, an interesting observation is that the Bjerknes feedback can only operate as long as the reservoir of warm water in the western warm pool is not empty. Once this is the case, the feedback breaks down, the SST anomaly stops to grow and the warm pool fills up again. A negative feedback has replaced the positive feedback. For the tropical Pacific, this sequence of alternating feedbacks has been described by Jin (1997) in the framework of the *recharge oscillator*. The name relates to the idea that the equatorial ocean is "charged" with warm water in the warm pool region – or, equivalently, heat – that is then discharged to the atmosphere during a warm event.

In the tropical Atlantic, a number of seasonal processes in the coupled atmosphere-ocean system produce a climate state that allows the Bjerknes feedback to operate during early boreal summer. Although we explain the processes in a sequential manner below, note that clear causalities are hard to establish in a coupled system. Different aspects of the phenomenon – here: the northward movement of the ITCZ and the development of the Atlantic cold tongue – cannot be disentangled from each other. Neither does the ITCZ move north *because* of the cold tongue development, nor does the cold tongue develop *because* the ITCZ moves north. Rather, both phenomena co-occur as manifestations of the same coupled phenomenon.

One key ingredient of the equatorial Atlantic seasonal cycle is the northward migration of the marine ITCZ (Xie and Philander 1994). In boreal spring, the ITCZ is in its southernmost position. The trade wind regimes of both hemispheres converge close to the equator and produce weak equatorial surface winds. When the ITCZ moves north in late boreal spring, the southern hemisphere trade winds cross the equator. Starting in March–April, surface winds intensify (illustrated by an increase in magnitude in Fig. 7a) and contribute to enhanced equatorial upwelling.

The spring strengthening of western equatorial *zonal* surface winds enhances the zonal gradient in upper ocean heat content. Strong easterly winds push the surface waters more efficiently towards the western warm pool, thinning out the warm surface layer in the eastern ocean basin and transporting the cooling signal westward. As a result, cold subsurface water lodges closer to the ocean surface. This background state requires very little subsurface water to be mixed into the surface layer to produce a substantial cooling. The western equatorial zonal spring winds "precondition" the eastern equatorial Atlantic for the formation of the cold tongue (e.g., Merle 1980; Okumura and Xie 2006; Grodsky et al. 2008; Hormann and Brandt 2009; Marin et al. 2009).

In concert with the development of the first seasonal cooling signals in May and June, the West African monsoon sets in (e.g., Okumura and Xie 2004; Brandt et al. 2011b; Caniaux et al. 2011; Giannini et al. 2003). From an atmospheric perspective, the monsoon onset is characterized by accelerating southeasterly surface winds in the Gulf of Guinea in late boreal spring. The strengthening *meridional* component of these winds enhances upwelling slightly to the south of the equator, and downwelling slightly to the north. The intensified upwelling provides additional initial cooling to the eastern equatorial region by mixing colder subsurface water into the warm surface layer. From the ocean perspective, on the other hand, cooling SSTs in the eastern equatorial Atlantic intensify the southerly winds in the Gulf of Guinea, which in turn contributes to the northward migration of convection and rainfall associated with the West African monsoon (Okumura and Xie 2004).

Lastly, oceanic processes contribute to the formation of the cold tongue. A number of studies found that vertical mixing at the base of the surface layer – where temperature gradients are strongest – seasonally varies in strength (e.g., Hazeleger and Haarsma 2005; Jouanno et al. 2011; Hummels et al. 2013, 2014). A likely explanation for this is that the intensities of the westward surface current and the eastward equatorial undercurrent vary over the course of the year. When the relative velocities of the two currents are strong, the vertical velocity shear at their boundary increases,[10] and frictional processes mix colder subsurface water into the warm surface layer. Figure 9 illustrates both the spring state of the tropical Atlantic and the basic processes that produce the first cooling signals in early boreal summer.

The net effect of these interacting processes – the northward migration of the ITCZ and the associated strengthening of the southern hemisphere trade winds on the equator, the thinning of the of eastern equatorial surface layer, the enhanced upwelling along the equator and especially in the cold tongue region, and the increased mixing at the base of the surface mixed layer – is that the first cold anomalies develop in the eastern equatorial Atlantic in late April. The atmosphere in turn reacts to the cold anomalies, and the Bjerknes feedback sets in. Starting in May, it lends additional growth to the cold tongue (Burls et al. 2011). In August, the seasonally active Bjerknes feedback loop breaks down (Dippe et al. 2017) and a more moderate warming sets in. In the absence of the Bjerknes feedback the cold tongue can no longer be maintained and dissolves, due to mixing processes in the ocean and surface heat exchange with the atmosphere.

Many models struggle to simulate a seasonally active Bjerknes feedback that is comparable to observations in both strength and seasonality. Richter and Xie (2008) pointed out that model performance with respect to the Atlantic Bjerknes feedback is quite diverse between models that participated in the Coupled Model Intercomparison Project, Phase 3 (CMIP3, Meehl et al. 2007). Likewise, Deppenmeier et al. (2016) found systematic weaknesses in the CMIP5 models. For example, many models displace the Atlantic warm pool towards the central equatorial Atlantic (Chang et al. 2007; Richter and Xie 2008; Liu et al. 2013). This displacement is a consequence of the westerly wind bias in the western equatorial Atlantic (Wahl et al. 2011; Richter et al. 2012, 2014b). Figure 7 illustrates for the KCM that the spring winds are much weaker in the model than in observations. Consequently, the surface wind stress is not sufficient to pile up warm sur-

[10] "Velocity shear" is a different term for "velocity gradient". A flow is sheared when different layers of the flow have different velocities. Depending on the magnitude of the shear and the viscosity of the fluid, the shear produces local turbulence and mixing due to frictional processes within the fluid. If no turbulence occurs, the flow is called "laminar".

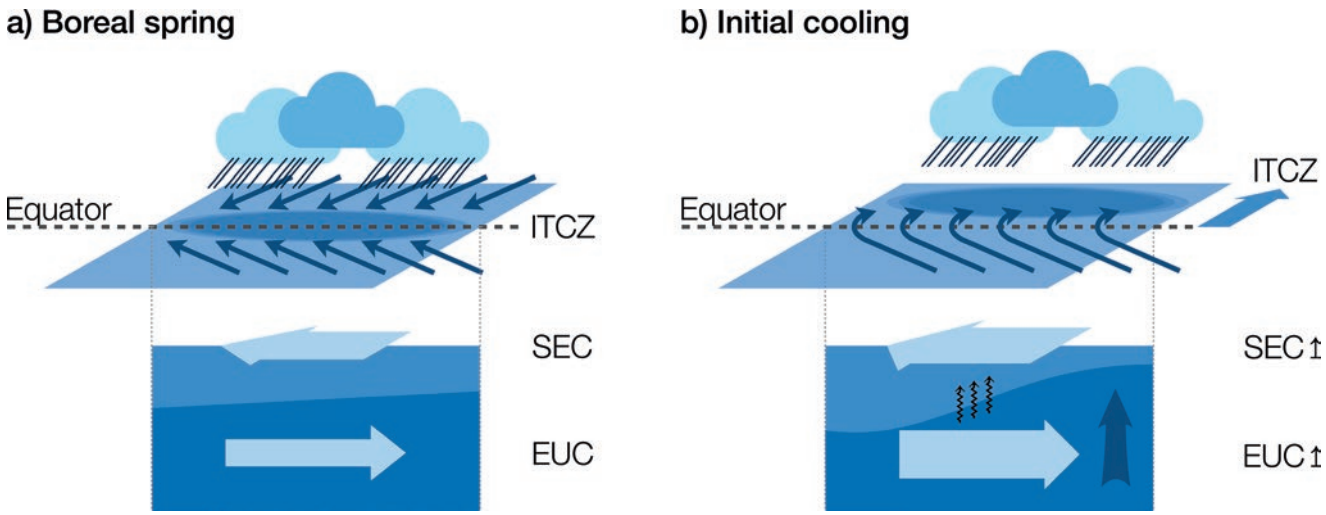

Fig. 9 Initial cold tongue cooling in the tropical Atlantic. (**a**) Spring conditions. The highest sea surface temperatures (SSTs) and the lowest sea level pressures (SLPs) are found approximately on the equator (dashed black line), forming the equatorial low pressure trough (dark-blue shading). The trade wind systems of both the northern and the southern hemispheres (dark blue arrows) converge in the trough and anchor the Inter-Tropical Convergence Zone (ITCZ, clouds and strong precipitation) to the equator. Zonal surface wind forcing is relaxed during spring, warm surface waters are distributed more evenly across the basin. At the ocean surface, the South Equatorial Current (SEC) transports water towards the west. Below the surface, close to the interface between the surface layer and the subsurface, the Equatorial Under-Current (EUC) transports water towards the east. (**b**) Initial cold tongue cooling: In early boreal summer, the ITCZ migrates away from the equator into the northern hemisphere. The trade winds of the southern hemisphere follow the low pressure trough and cross the equator. In the western ocean basin, zonal surface winds increase and push the warm surface water more efficiently towards the west. The warm pool deepens in the west, while the surface layer thins in the east. Additionally, both the meridional and zonal components of the wind field in the eastern ocean basin strengthen and contribute to a local surface divergence that is compensated by enhanced upwelling (thick, dark-blue arrow). Lastly, both the SEC and EUC increase in strength. Enhanced vertical velocity gradients in the vicinity of the interface between the surface and the subsurface water layers produce shear instabilities (black squiggly lines) that mix the cold subsurface water efficiently into the surface layer

face waters in the western ocean basin in a manner comparable to observations. Heat content is distributed more evenly across the equatorial ocean basin and supplies additional heat to the eastern surface layer. Even if the model produced wind variability that could serve as a valid initial perturbation to trigger the Bjerknes feedback,[11] the biased background state of the ocean could not support the feedback. The cold tongue fails to establish.

An interesting equivalent of this mechanism has been observed in the real ocean by Marin et al. (2009). The study compares the Atlantic cold tongue in two years with grossly different wind variability and finds that in the year with relatively weak spring winds in the western equatorial Atlantic – this compares well to the climatological, biased state in many CGCMs -, the zonal heat content gradient in the upper ocean does not develop. The winds fail to precondition the tropical Atlantic for the growth of the cold tongue.

Studies with current atmospheric GCMs have found the westerly wind bias in boreal spring to be an intrinsic feature of (uncoupled) atmospheric GCMs (Richter et al. 2012, 2014b; Harlaß et al. 2017). Coupling an already biased atmospheric GCM to an ocean GCM induces positive feedbacks that amplify the wind and SST biases in the equatorial Atlantic. Additionally, Grodsky et al. (2012) showed that an ocean GCM, too, is intrinsically biased in the tropical Atlantic, although the magnitude of this bias is much smaller than the warm bias in a coupled model.

The atmospheric westerly wind bias has been linked to a seesaw pattern in rainfall biases over South America and Africa (Chang et al. 2007; Richter et al. 2012, 2014b; Patricola et al. 2012). The proposed physical mechanism that links precipitation to the wind is the following: Tropical rainfall is tied to strong convection. Ascending moist and warm air masses create a local negative pressure anomaly at the surface that alters the zonal gradient in surface pressure along the equator. Surface winds, in turn, are dynamically related to surface pressure gradients.[12]

A current hypothesis of what prevents climate models from developing a cold tongue comparable to observations in

[11] This is by no means a given. As shown below and hinted at above, the equatorial Atlantic bias also manifests in the atmosphere and may well prevent the model from establishing the link between eastern ocean SST and western ocean wind variability that is necessary to close the Bjerknes feedback loop.

[12] Wind compensates pressure gradients. That is why large-scale storm systems are organized around low core pressures: The storm winds try to flow into the low pressure at the "heart" of the storm and eliminate the strong pressure gradient between the storm center and the storm environment. The Coriolis force provides rotation to storm systems by deflecting the pressure compensation flow.

boreal summer thus is: Opposing rainfall biases in South America and Africa produce a zonal surface pressure gradient along the equator that is weaker than in observations. The resulting winds in the equatorial western Atlantic are too weak in magnitude and cannot reproduce the observed distribution of upper ocean heat content. Consequently, the seasonally induced equatorial upwelling in early boreal summer is not sufficient to produce the observed cooling that finally triggers the Bjerknes feedback.

In agreement with these mechanisms, a number of studies have found that a physically sound way to reduce the equatorial Atlantic warm bias is to improve the atmospheric models. Tozuka et al. (2011) showed that tweaking the convection scheme can project strongly on the ability of the models to simulate the correct distribution of climatological SSTs in the equatorial Atlantic. Harlaß et al. (2015) conducted a number of experiments with the KCM that varied both the horizontal and vertical resolution of the atmospheric GCM, while keeping a constant coarse resolution for the ocean GCM. For sufficiently high atmospheric resolutions, the western equatorial wind bias strongly decreased and the equatorial Atlantic warm bias nearly vanished. The seasonal cycle as a whole greatly improved. In a follow-up study, Harlaß et al. (2017) found that sea level pressure and precipitation gradients along the equator are not sensitive to the atmospheric resolution. Nevertheless, the wind bias in their study decreased significantly. To explain this, they propose that the position of maximum precipitation and zonal momentum transport play an important role in giving rise to the zonal wind bias. Zonal momentum can be either transported by mixing it from the free troposphere into the boundary layer or by meridional advection into the western equatorial Atlantic (Zermeño-Diaz and Zhang 2013; Richter et al. 2014b, 2017). These findings agree with the study of Richter et al. (2014a), who found that zonal wind variability in the western equatorial Atlantic is strongly related to vertical momentum transports in the overlying atmosphere. Further studies by Voldoire et al. (2014), Wahl et al. (2011), and DeWitt (2005) confirm the importance of the atmospheric component of a CGCM to properly simulate the complex tropical Atlantic climate system.

Outlook: Implications for the Usability of CGCMs in the Equatorial Atlantic

Using the KCM, a CGCM that simulates the tropical Atlantic in a manner very similar to a wide range of state-of-the-art CGCMs, we have shown exemplary that coupled global climate models currently struggle to simulate a realistic equatorial Atlantic climate system. The dominant feature of this problem is that CGCMs struggle to simulate the defining feature of the seasonal cycle – the formation of the Atlantic cold tongue in early boreal summer. An important cause of this bias is a strong and seasonally varying westerly wind bias in equatorial zonal wind in atmospheric models that is present even in the absence of atmosphere-ocean coupling. While much progress has been made in understanding and reducing the equatorial Atlantic warm bias, many models still produce a profoundly unrealistic seasonal cycle in the equatorial Atlantic. How does this shortcoming affect the usefulness of coupled models in the equatorial Atlantic?

A key task of climate models is to forecast deviations from the expected climate state. For seasonal predictions, the expected climate state is the climatological seasonal cycle. Some of these deviations are generated randomly and are, by definition, unpredictable. Others are the product of – sometimes potentially predictable – climate variability.

In the tropical Atlantic, the dominant mode of year-to-year SST variability is the Atlantic Niño[13] (Zebiak 1993). The Atlantic Niño is essentially a modulation of the seasonal formation of the cold tongue (Burls et al. 2012). This modulation can manifest in a range of different cold tongue measures. For example, cold tongue growth might set in earlier (or later), the cold tongue might cool more strongly, or it might, in its mature phase, occupy a larger area in the tropical Atlantic than usual. Caniaux et al. (2011) argued that all of these measures reveal an aspect of cold tongue variability, but that they do not vary consistently with each other.

Still, the Atlantic Niño is generally described in terms of Atl3 summer SSTs. While the seasonal cycle of Atl3 SSTs spans a range of roughly 5 °C, interannual variations of Atl3 SST between May and July rarely exceed amplitudes of 1 °C (Fig. 10a). The seasonal cycle of the tropical Atlantic is by far the dominant signal in Atl3 SSTs (Fig. 10b). It is the background against which the interannual variability of the Atlantic Niño plays out.

Even though the Atlantic Niño constitutes only a relatively small deviation from the seasonal cycle, its effects on adjacent rainfall patterns can be substantial (e.g., Giannini et al. 2003; García-Serrano et al. 2008; Polo et al. 2008; Rodríguez-Fonseca et al. 2011). A key demand of African countries, where food security heavily relies on agriculture, is hence to be able to reliably predict the amplitude of the Atlantic Niño a few months, ideally even more than a season, ahead. Only such relatively long-ranged forecasts would allow African farmers to adapt their farming strategy

[13]The name “Atlantic Niño” refers to the Pacific El Niño, because the pattern of Atlantic Niño SST anomalies is similar to the Pacific El Niño. Apart from this, a number of differences exist between the two phenomena (discussed for example in Keenlyside and Latif (2007), Burls et al. (2011), Lübbecke and McPhaden (2012), Richter et al. (2013), and Lübbecke and McPhaden (2017)). Nnamchi et al. (2015, 2016) argued that the Atlantic Niño might not be dynamical in nature, but a product of atmospheric noise forcing. Alternative names for the Atlantic Niño are Atlantic Zonal Mode or Atlantic Cold Tongue Mode.

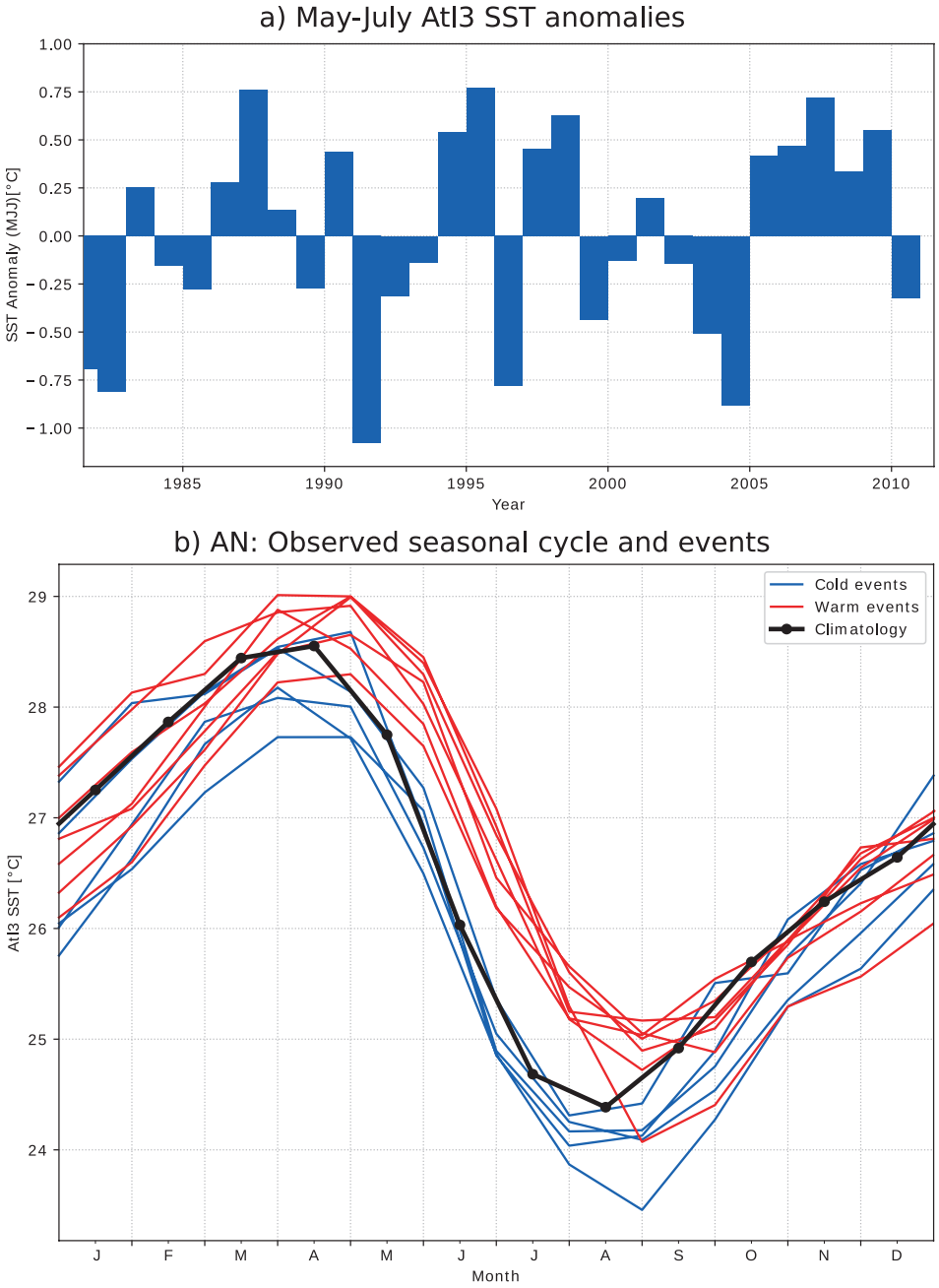

Fig. 10 The observed Atlantic Niño, based on the NOAA Optimum Interpolated SST dataset (OISST). (**a**) Time series of May–June-July (MJJ) Atl3 sea surface temperature (SST) anomalies. (Anomalies of a time series that, for each year, averaged MJJ monthly means together. Positive values indicate that the observed Atl3 region was warmer in MJJ of that year than on average.) (**b**) Observed seasonal cycle of Atl3 SST (black) and SST trajectories for individual years that produced warm (red) and cold (blue) Atlantic Niño events

for the upcoming season. Unfortunately, most models perform very poorly with respect to the Atlantic Niño and can provide hardly any predictive skill (Stockdale et al. 2006; Richter et al. 2017).

One reason for these shortcomings is that a prerequisite to simulate the variability of Atlantic cold tongue growth is a model that produces a realistic cold tongue. Indeed, Ding et al. (2015) showed that even a symptomatic – as opposed to a dynamically motivated and hence more process-oriented – reduction of the equatorial Atlantic SST bias in the KCM greatly improves the ability of the model to track the observed Atlantic Niño variability. This serves as an example of how the mean state interacts with climate variability. How the bias influences the predictive skill of the KCM for tropical Atlantic SST and whether the real climate system actually provides the potential to produce reliable forecasts of Atlantic Niño variability a few months in advance are the subjects of current research.

In general, the equatorial Atlantic warm bias has been an important issue since the earliest attempts of coupled global climate modeling (Davey et al. 2002) and continues to challenge the scientific community. It serves as an important reminder that model output should not always be taken at face value. Rather, models can struggle to represent observed physical processes, even though their physical basis in the form of the approximated Navier-Stokes equations is sound.

In the equatorial Atlantic, the entire coupled system is off-key in coupled global climate models due to the misrepresentation of crucial physical processes. However, alternative ways exist to study the tropical Atlantic with the help of models. Akin to early modeling studies of the El Niño-Southern Oscillation, statistical models can provide some insight into the equatorial Atlantic (e.g., Wang and Chang 2008; Chang et al. 2004). Simulations with ocean-only GCMs help to understand the oceanic response to atmospheric processes (e.g., Lübbecke et al. 2010). Additionally, regional climate models of the equatorial Atlantic have been employed successfully to study different aspects of the region (e.g., Seo et al. 2006; Burls et al. 2011, 2012). Lastly, computational power continues to increase and allows for higher spatial resolution. If the equatorial Atlantic contains predictive potential, future generations of improved CGCMs are likely to unlock it at some point.

The research into various biases, their origins, their dynamics, and, most importantly, possible ways to reduce them, remains a core challenge of the global climate modeling community.

Acknowledgements We would like to thank Richard Greatbatch, Peter Brandt, Mojib Latif, Rebecca Hummels, and Martin Claus for discussing the manuscript with us at an early stage and contributing valuable ideas.

While we finished work on the first submitted draft of the manuscript, our colleague and friend Martin Krebs passed away. We hope this study will serve as a reminder of Martin's outstanding scientific work. TD will fondly remember how she discussed first ideas for the manuscript with Martin and how they came up with a rather wayward way to illustrate how much energy was lost from the Atl3 region during the formation of the cold tongue. Turns out that 2.6 times the total global energy consumption of 2011 is enough to power roughly 70 billion generic 600 W fridges for 4 months.

Appendix

This article is related to the YOUMARES 8 conference session no. 3: "Physical Processes in the Tropical and Subtropical Oceans: Variability, Impacts, and Connections to Other Components of the Climate System". The original Call for Abstracts and the abstracts of the presentations within this session can be found in the appendix "Conference Sessions and Abstracts", chapter "1 Physical Processes in the Tropical and Subtropical Oceans: Variability, Impacts, and Connections to Other Components of the Climate System", of this book.

References

Banzon V, Smith TM, Chin TM et al (2016) A long-term record of blended satellite and in situ sea-surface temperature for climate monitoring, modeling and environmental studies. Earth Syst Sci Data 8(1):165–176. https://doi.org/10.5194/essd-8-165-2016

Bjerknes J (1969) Atmospheric teleconnections from the equatorial Pacific. Mon Weather Rev 97(3):163–172

Bourlès B, Lumpkin R, McPhaden MJ et al (2008) The Pirata program: history, accomplishments, and future directions. Bull Am Meteorol Soc 89(8):1111–1125. https://doi.org/10.1175/2008BAMS2462.1

Brandt P, Schott FA, Provost C et al (2006) Circulation in the central equatorial Atlantic: mean and intraseasonal to seasonal variability. Geophys Res Lett 33(7):L07609. https://doi.org/10.1029/2005GL025498

Brandt P, Hormann V, Bourlès B et al (2008) Oxygen tongues and zonal currents in the equatorial Atlantic. J Geophys Res Oceans 113(4):C04012. https://doi.org/10.1029/2007JC004435

Brandt P, Caniaux G, Bourlès B et al (2011a) Equatorial upper-ocean dynamics and their interaction with the West African monsoon. Atmos Sci Lett 12(1):24–30. https://doi.org/10.1002/asl.287

Brandt P, Funk A, Hormann V et al (2011b) Interannual atmospheric variability forced by the deep equatorial Atlantic ocean. Nature 473(7348):497–500. https://doi.org/10.1038/nature10013

Burls NJ, Reason CJC, Penven P et al (2011) Similarities between the tropical Atlantic seasonal cycle and ENSO: an energetics perspective. J Geophys Res Oceans 116(C11):C11010. https://doi.org/10.1029/2011JC007164

Burls NJ, Reason CJC, Penven P et al (2012) Energetics of the tropical Atlantic zonal mode. J Clim 25(21):7442–7466. https://doi.org/10.1175/JCLI-D-11-00602.1

Caniaux G, Giordani H, Redelsperger JL et al (2011) Coupling between the Atlantic cold tongue and the West African monsoon in boreal spring and summer. J Geophys Res Oceans 116(4):C04003. https://doi.org/10.1029/2010JC006570

Chang P, Saravanan R, Wang F et al (2004) Predictability of linear coupled systems. Part II: an application to a simple model of tropical Atlantic variability. J Clim 17(7):1487–1503. https://doi.org/10.1175/1520-0442(2004)017<1487:POLCSP>2.0.CO;2

Chang CY, Carton JA, Grodsky SA et al (2007) Seasonal climate of the tropical Atlantic sector in the NCAR community climate system model 3: error structure and probable causes of errors. J Clim 20(6):1053–1070. https://doi.org/10.1175/JCLI4047.1

Cromwell T (1953) Circulation in a meridional plane in the central equatorial Pacific. J Mar Res 23:196–213

Cromwell T, Montgomery RB, Stroup ED (1954) Equatorial undercurrent in Pacific ocean revealed by new methods. Science 119(3097):648–649. https://doi.org/10.1126/science.119.3097.648

Davey M, Huddleston M, Sperber K et al (2002) STOIC: a study of coupled model climatology and variability in tropical ocean regions. Clim Dyn 18(5):403–420. https://doi.org/10.1007/s00382-001-0188-6

Deppenmeier AL, Haarsma RJ, Hazeleger W (2016) The Bjerknes feedback in the tropical Atlantic in CMIP5 models. Clim Dyn 47(7–8):2691–2707. https://doi.org/10.1007/s00382-016-2992-z

DeWitt DG (2005) Diagnosis of the tropical Atlantic near-equatorial SST bias in a directly coupled atmosphere-ocean general circulation model. Geophys Res Lett 32(1):L01703. https://doi.org/10.1029/2004GL021707

Ding H, Greatbatch RJ, Latif M et al (2015) The impact of sea surface temperature bias on equatorial Atlantic interannual variability in partially coupled model experiments. Geophys Res Lett 42(13):5540–5546. https://doi.org/10.1002/2015GL064799

Dippe T, Greatbatch RJ, Ding H (2017) On the relationship between Atlantic Niño variability and ocean dynamics. Clim Dyn. https://doi.org/10.1007/s00382-017-3943-z

Doi T, Vecchi GA, Rosati AJ et al (2012) Biases in the Atlantic ITCZ in seasonal-interannual variations for a coarse- and a high-resolution coupled climate model. J Clim 25(16):5494–5511. https://doi.org/10.1175/JCLI-D-11-00360.1

Foltz GR, McPhaden MJ (2010) Interaction between the Atlantic meridional and Niño modes. Geophys Res Lett 37:L18604. https://doi.org/10.1029/2010GL044001

Fretwell P, Pritchard HD, Vaughan DG et al (2013) Bedmap2: improved ice bed, surface and thickness datasets for Antarctica. Cryosphere 7(1):375–393. https://doi.org/10.5194/tc-7-375-2013

Frierson DMW, Hwang YT, Fučkar NS et al (2013) Contribution of ocean overturning circulation to tropical rainfall peak in the northern hemisphere. Nat Geosci 6:940–944. https://doi.org/10.1038/ngeo1987

García-Serrano J, Losada T, Rodríguez-Fonseca B et al (2008) Tropical Atlantic variability modes (1979–2002). Part II: time-evolving atmospheric circulation related to SST-forced tropical convection. J Clim 21(24):6476–6497. https://doi.org/10.1175/2008JCLI2191.1

Giannini A, Saravanan R, Chang P (2003) Oceanic forcing of Sahel rainfall on interannual to interdecadal time scales. Science 302(5647):1027–1030. https://doi.org/10.1126/science.1089357

Gill AE (1980) Some simple solutions for heat-induced tropical circulation. Q J R Meteorol Soc 106(449):447–462. https://doi.org/10.1002/qj.49710644905

Grodsky SA, Carton JA, McClain CR (2008) Variability of upwelling and chlorophyll in the equatorial Atlantic. Geophys Res Lett 35(3):L03610. https://doi.org/10.1029/2007GL032466

Grodsky SA, Carton JA, Nigam S et al (2012) Tropical Atlantic biases in CCSM4. J Clim 25(11):3684–3701. https://doi.org/10.1175/JCLI-D-11-00315.1

Harlaß J, Latif M, Park W (2015) Improving climate model simulation of tropical Atlantic sea surface temperature: the importance of enhanced vertical atmosphere model resolution. Geophys Res Lett 42(7):2401–2408. https://doi.org/10.1002/2015GL063310

Harlaß J, Latif M, Park W (2017) Alleviating tropical Atlantic sector biases in the Kiel climate model by enhancing horizontal and vertical atmosphere model resolution: climatology and interannual variability. Clim Dyn 50:2605. https://doi.org/10.1007/s00382-017-3760-4

Hastenrath S (1991) Climate dynamics of the tropics. Springer, Dordrecht. https://doi.org/10.1007/978-94-011-3156-8

Hazeleger W, Haarsma RJ (2005) Sensitivity of tropical Atlantic climate to mixing in a coupled ocean-atmosphere model. Clim Dyn 25(4):387–399. https://doi.org/10.1007/s00382-005-0047-y

Hormann V, Brandt P (2009) Upper equatorial Atlantic variability during 2002 and 2005 associated with equatorial Kelvin waves. J Geophys Res Oceans 114:C03007. https://doi.org/10.1029/2008JC005101

Hummels R, Dengler M, Bourlès B (2013) Seasonal and regional variability of upper ocean diapycnal heat flux in the Atlantic cold tongue. Prog Oceanogr 111:52–74. https://doi.org/10.1016/j.pocean.2012.11.001

Hummels R, Dengler M, Brandt P et al (2014) Diapycnal heat flux and mixed layer heat budget within the Atlantic cold tongue. Clim Dyn 43(11):3179–3199. https://doi.org/10.1007/s00382-014-2339-6

Jin FF (1997) An equatorial ocean recharge paradigm for ENSO. Part I: conceptual model. J Atmos Sci 54(7):811–829

Johns WE, Brandt P, Bourlès B et al (2014) Zonal structure and seasonal variability of the Atlantic equatorial undercurrent. Clim Dyn 43(11):3047–3069. https://doi.org/10.1007/s00382-014-2136-2

Jouanno J, Marin F, Du Penhoat Y et al (2011) Seasonal heat balance in the upper 100 m of the equatorial Atlantic Ocean. J Geophys Res Oceans 116(9):C09003. https://doi.org/10.1029/2010JC006912

Keenlyside NS, Latif M (2007) Understanding equatorial Atlantic interannual variability. J Clim 20(1):131–142. https://doi.org/10.1175/JCLI3992.1

Liu H, Wang C, Lee SK et al (2013) Atlantic warm pool variability in the CMIP5 simulations. J Clim 26(15):5315–5336. https://doi.org/10.1175/JCLI-D-12-00556.1

Locarnini RA, Mishonov AV, Antonov JI et al (2013) World ocean atlas 2013. Vol. 1: Temperature. Levitus S (ed), Mishonov A (technical ed), NOAA Atlas NESDIS 73

Lübbecke JF, McPhaden MJ (2012) On the inconsistent relationship between Pacific and Atlantic Niños. J Clim 25(12):4294–4303. https://doi.org/10.1175/JCLI-D-11-00553.1

Lübbecke JF, McPhaden MJ (2017) Symmetry of the Atlantic Niño mode. Geophys Res Lett 44(2):965–973. https://doi.org/10.1002/2016GL071829

Lübbecke JF, Böning CW, Keenlyside NS et al (2010) On the connection between Benguela and equatorial Atlantic Niños and the role of the South Atlantic anticyclone. J Geophys Res Oceans 115(C9):C09015. https://doi.org/10.1029/2009JC005964

Lübbecke JF, Burls NJ, Reason CJC et al (2014) Variability in the South Atlantic anticyclone and the Atlantic Niño mode. J Clim 27(21):8135–8150. https://doi.org/10.1175/JCLI-D-14-00202.1

Madec G (2008) NEMO ocean general circulation model reference manuel. Tech. rep., Institut Pierre-Simon Laplace, Paris

Marin F, Caniaux G, Giordani H et al (2009) Why were sea surface temperatures so different in the eastern equatorial Atlantic in June 2005 and 2006? J Phys Oceanogr 39(6):1416–1431. https://doi.org/10.1175/2008JPO4030.1

McPhaden MJ (1995) The tropical atmosphere ocean array is completed. Bull Am Meteorol Soc 76:739–741

McPhaden MJ, Meyers G, Ando K et al (2009) RAMA: the research moored Array for African-Asian-Australian monsoon analysis and prediction. Bull Am Meteorol Soc 90(4):459–480. https://doi.org/10.1175/2008BAMS2608.1

Meehl GA, Covey C, Taylor KE et al (2007) THE WCRP CMIP3 multimodel dataset: a new era in climate change research. Bull Am Meteorol Soc 88(9):1383–1394. https://doi.org/10.1175/BAMS-88-9-1383

Merle J (1980) Seasonal heat budget in the equatorial Atlantic ocean. J Phys Oceanogr 10(3):464–469

Mitchell TP, Wallace JM (1992) The annual cycle in equatorial convection and sea surface temperature. J Clim 5(10):1140–1156

Nnamchi HC, Li J, Kucharski F et al (2015) Thermodynamic controls of the Atlantic Niño. Nat Commun 6:8895. https://doi.org/10.1038/ncomms9895

Nnamchi HC, Li J, Kucharski F et al (2016) An equatorial-extratropical dipole structure of the Atlantic Niño. J Clim 29(20):7295–7311. https://doi.org/10.1175/JCLI-D-15-0894.1

Okumura Y, Xie SP (2004) Interaction of the Atlantic equatorial cold tongue and the African monsoon. J Clim 17(18):3589–3602. https://doi.org/10.1175/1520-0442(2004)017<3589:IOTAEC>2.0.CO;2

Okumura Y, Xie SP (2006) Some overlooked features of tropical Atlantic climate leading to a new Nino-like phenomenon. J Clim 19(22):5859–5874

Park W, Keenlyside N, Latif M et al (2009) Tropical Pacific climate and its response to global warming in the Kiel climate model. J Clim 22(1):71–92. https://doi.org/10.1175/2008JCLI2261.1

Patricola CM, Li M, Xu Z et al (2012) An investigation of tropical Atlantic bias in a high-resolution coupled regional climate model. Clim Dyn 39(9):2443–2463. https://doi.org/10.1007/s00382-012-1320-5

Philander SGH, Pacanowski RC (1981) The oceanic response to cross-equatorial winds (with application to coastal upwelling in low latitudes). Tellus 33(2):201–210. https://doi.org/10.3402/tellusa.v33i2.10708

Phillips NA (1956) The general circulation of the atmosphere: a numerical experiment. Q J R Meteorol Soc 82(352):123–164. https://doi.org/10.1002/qj.49708235202

Polo I, Rodríguez-Fonseca B, Losada T et al (2008) Tropical Atlantic variability modes (1979–2002). Part I: time-evolving SST modes related to West African rainfall. J Clim 21(24):6457–6475. https://doi.org/10.1175/2008JCLI2607.1

Reynolds RW, Smith TM, Liu C et al (2007) Daily high-resolution-blended analyses for sea surface temperature. J Clim 20(22):5473–5496. https://doi.org/10.1175/2007JCLI1824.1

Rhein M, Dengler M, Sültenfuß J et al (2010) Upwelling and associated heat flux in the equatorial Atlantic inferred from helium isotope disequilibrium. J Geophys Res Oceans 115(C8):C08021. https://doi.org/10.1029/2009JC005772

Richter I, Xie SP (2008) On the origin of equatorial Atlantic biases in coupled general circulation models. Clim Dyn 31(5):587–598. https://doi.org/10.1007/s00382-008-0364-z

Richter I, Xie SP, Wittenberg AT et al (2012) Tropical Atlantic biases and their relation to surface wind stress and terrestrial precipitation. Clim Dyn 38(5–6):985–1001. https://doi.org/10.1007/s00382-011-1038-9

Richter I, Behera SK, Masumoto Y et al (2013) Multiple causes of interannual sea surface temperature variability in the equatorial Atlantic Ocean. Nat Geosci 6(1):43–47. https://doi.org/10.1038/ngeo1660

Richter I, Behera SK, Doi T et al (2014a) What controls equatorial Atlantic winds in boreal spring? Clim Dyn 43(11):3091–3104. https://doi.org/10.1007/s00382-014-2170-0

Richter I, Xie SP, Behera SK et al (2014b) Equatorial Atlantic variability and its relation to mean state biases in CMIP5. Clim Dyn 42(1–2):171–188. https://doi.org/10.1007/s00382-012-1624-5

Richter I, Xie SP, Morioka Y et al (2016) Phase locking of equatorial Atlantic variability through the seasonal migration of the ITCZ. Clim Dyn 48(11–12):3615–3629. https://doi.org/10.1007/s00382-016-3289-y

Richter I, Doi T, Behera SK et al (2017) On the link between mean state biases and prediction skill in the tropics: an atmospheric perspective. Clim Dyn 50:3355. https://doi.org/10.1007/s00382-017-3809-4

Risien CM, Chelton DB (2008) A global climatology of surface wind and wind stress fields from eight years of QuikSCAT scatterometer data. J Phys Oceanogr 38(11):2379–2413. https://doi.org/10.1175/2008JPO3881.1

Rodríguez-Fonseca B, Janicot S, Mohino E et al (2011) Interannual and decadal SST-forced responses of the West African monsoon. Atmos Sci Lett 12(1):67–74. https://doi.org/10.1002/asl.308

Roeckner E, Bäuml G, Bonaventura L et al (2003) The atmospheric general circulation model ECHAM5: part 1: model description. MPI Report 349. https://doi.org/10.1029/2010JD014036

Roemmich D, Johnson GC, Riser S et al (2009) The Argo program. Oceanography 22(2):34–43. https://doi.org/10.5670/oceanog.2009.36

Schott FA, Dengler M, Brandt P et al (2003) The zonal currents and transports at 35°W in the tropical Atlantic. Geophys Res Lett 30(7):1349. https://doi.org/10.1029/2002GL016849

Sein DV, Danilov S, Biastoch A et al (2016) Designing variable ocean model resolution based on the observed ocean variability. J Adv Model Earth Syst 8(2):904–916. https://doi.org/10.1002/2016MS000650

Seo H, Jochum M, Murtugudde R et al (2006) Effect of ocean mesoscale variability on the mean state of tropical Atlantic climate. Geophys Res Lett 33(9):L09606. https://doi.org/10.1029/2005GL025651

Siongco AC, Hohenegger C, Stevens B (2015) The Atlantic ITCZ bias in CMIP5 models. Clim Dyn 45(5):1169–1180. https://doi.org/10.1007/s00382-014-2366-3

Stockdale TN, Balmaseda MA, Vidard A (2006) Tropical Atlantic SST prediction with coupled ocean-atmosphere GCMs. J Clim 19(23):6047–6061. https://doi.org/10.1175/JCLI3947.1

Sutton RT, Jewson SP, Rowell DP (2000) The elements of climate variability in the tropical Atlantic region. J Clim 13(18):3261–3284

Taylor KE, Stouffer RJ, Meehl GA (2012) An overview of CMIP5 and the experiment design. Bull Am Meteorol Soc 93(4):485–498. https://doi.org/10.1175/BAMS-D-11-00094.1

Tozuka T, Doi T, Miyasaka T et al (2011) Key factors in simulating the equatorial Atlantic zonal sea surface temperature gradient in a coupled general circulation model. J Geophys Res Oceans 116(6):C06010. https://doi.org/10.1029/2010JC006717

Trenberth KE, Caron JM (2001) Estimates of meridional atmosphere and ocean heat transports. J Clim 14(16):3433–3443

Trenberth KE, Fasullo JT, Kiehl J (2009) Earth's global energy budget. Bull Am Meteorol Soc 90(3):311–323. https://doi.org/10.1175/2008BAMS2634.1

Voldoire A, Claudon M, Caniaux G et al (2014) Are atmospheric biases responsible for the tropical Atlantic SST biases in the CNRM-CM5 coupled model? Clim Dyn 43(11):2963–2984. https://doi.org/10.1007/s00382-013-2036-x

Wahl S, Latif M, Park W et al (2011) On the tropical Atlantic SST warm bias in the Kiel climate model. Clim Dyn 36(5–6):891–906. https://doi.org/10.1007/s00382-009-0690-9

Wang F, Chang P (2008) Coupled variability and predictability in a stochastic climate model of the tropical Atlantic. J Clim 21(23):6247–6259. https://doi.org/10.1175/2008JCLI2283.1

Xie SP (2004) The shape of continents, air-sea interaction, and the rising branch of the Hadley circulation. In: Diaz HF, Bradley RS (eds) The Hadley circulation: present, past and future. Springer, Dordrecht, pp 121–152

Xie P, Arkin PA (1997) Global precipitation: a 17-year monthly analysis based on gauge observations, satellite estimates, and numerical model outputs. Bull Am Meteorol Soc 78(11):2539–2558. https://doi.org/10.1175/1520-0477(1997)078<2539:GPAYMA>2.0.CO;2

Xie SP, Carton JA (2004) Tropical Atlantic variability: patterns, mechanisms, and impacts. In: Wang C, Xie SP, Carton JA (eds) Earth's climate: the ocean-atmosphere interaction. American Geophysical Union, Washington, DC, pp 121–142. https://doi.org/10.1029/147GM07

Xie SP, Philander SGH (1994) A coupled ocean-atmosphere model of relevance to the ITCZ in the eastern Pacific. Tellus A 46(4):340–350. https://doi.org/10.1034/j.1600-0870.1994.t01-1-00001.x

Xu Z, Chang P, Richter I et al (2014) Diagnosing southeast tropical Atlantic SST and ocean circulation biases in the CMIP5 ensemble. Clim Dyn 43(11):3123–3145. https://doi.org/10.1007/s00382-014-2247-9

Zebiak SE (1993) Air-sea interaction in the equatorial Atlantic region. J Clim 6(8):1567–1586

Zermeño-Diaz DM, Zhang C (2013) Possible root causes of surface westerly biases over the equatorial Atlantic in global climate models. J Clim 26(20):8154–8168. https://doi.org/10.1175/JCLI-D-12-00226.1

Chapter 5

Seasonal Predictions of equatorial Atlantic SST in a low-resolution CGCM with Surface Heat Flux Correction

The equatorial Atlantic warm bias inhibits realistic simulations and reliable predictions of the Atlantic Niño. In this chapter, a simple method is used to alleviate the equatorial Atlantic warm bias. The impact of the bias on the predictability of the Atlantic Niño is assessed.

Citation: **Dippe, T., R. J. Greatbatch, and H. Ding (2018). "Seasonal predictions of equatorial Atlantic SST in a low-resolution CGCM with surface heat flux correction". In preparation for *Atmospheric Science Letters***

The candidate's contributions to this manuscript are as follows. She

- Produced all seasonal hindcasts;
- Performed all the analyses;
- Produced all the figures;
- Authored the manuscript from first to current draft.

Seasonal Predictions of Equatorial Atlantic SST in a low-resolution CGCM with Surface Heat Flux Correction

Tina Dippe[1,1], Richard J. Greatbatch[1,2], and Hui Ding[3]

[1]GEOMAR Helmholtz Centre for Ocean Research Kiel, Germany

[2]Faculty of Mathematics and Natural Sciences, Christian Albrechts Universität, Kiel, Germany

[3]Cooperate Institute for Research in Environmental Sciences - University of Colorado and NOAA Earth Systems Research Laboratory, Boulder, USA

October 9, 2018

[1]tdippe@geomar.de

Abstract

Due to heavy mean state-biases most coupled global climate models are unable to simulate equatorial Atlantic variability. Here, we use the Kiel Climate Model (KCM) to assess the impact of bias reduction on the predictability of equatorial Atlantic sea surface temperature (SST). We compare a standard experiment (STD) with an experiment that employs surface heat flux correction to reduce the SST bias (FLX). Initial conditions for both experiments are generated in partially coupled mode, and seasonal hindcasts are run four times yearly. Bias reduction improves initial conditions for boreal summer. However, in boreal spring both sets of initial conditions fail to reproduce the observed variability. FLX produces better predictions than STD, yet, neither forecasting experiment consistently beats persistence. Lastly, the KCM forecast skill is seasonal: It is lowest in boreal spring and best in boreal winter.

1 Introduction

The Atlantic Niño is the dominant mode of interannual variability in tropical Atlantic sea surface temperature (SST) (*Zebiak*, 1993, *Xie and Carton*, 2004). It is closely related to both the mean state and the seasonal cycle in the tropical Atlantic. Akin to the tropical Pacific, the mean state is characterised by easterly winds on the equator, a warm pool on the western side of the ocean basin, and an east-west gradient in SSTs along the equator. The thermocline is deep in the western basin and shoals towards the east. Set against this backdrop, the development of the Atlantic cold tongue in the eastern ocean basin[1] dominates the seasonal cycle. Cold tongue growth and decay are not symmetrical: Cooling between April and August is enhanced relative to the more gradual warming between August and March. *Burls et al.* (2011) suggest that the reason for this is a seasonally active Bjerknes feedback (*Bjerknes*, 1969).

The Atlantic Niño is a modulation of the cold tongue development. It is phase-locked to the seasonal cycle and peaks in May-July. While the name "Atlantic Niño" suggests a phenomenon that is essentially an Atlantic version of the Pacific El Niño-Southern Oscillation (ENSO), a number of important distinctions exist (e.g. *Keenlyside and Latif* (2007)). In particular, total SST variability in the tropical Pacific depends to similar degrees on the seasonal cycle and interannual variability (e.g. *Burls et al.* (2011)) whereas in the tropical Atlantic, it is clearly dominated by the seasonal cycle. The amplitude of the Atlantic Niño is much smaller than its Pacific counterpart; and while the growth of both an Atlantic and Pacific Niño event is supported by the Bjerknes feedback, atmosphere-ocean coupling in the Atlantic appears to be weaker. *Burls et al.* (2012) argue that the Pacific Niño is supported by a Bjerknes feedback that acts on interannual time scales. In the Atlantic, on the other hand, the Bjerknes feedback is involved in establishing the seasonal cycle. The Atlantic Niño hence arises from an interannual modulation of the seasonally active feedback, and not from the feedback per se.

Irrespective of its dynamics, the Atlantic Niño is a mode of equatorial SST variability that produces a number of teleconnections *Mohino and Losada* (2015). Through its relationship with the ITCZ, it particularly affects rainfall variability over the surrounding continents, exerting a non-negligible socio-economic impact *Hirst and Hastenrath* (1983). This motivates efforts to forecast Atlantic Niño events on seasonal time scales.

Current-generation coupled global climate models (CGCMs), however, have trouble simulating the observed Atlantic Niño. The reason is that almost all state-of-the-

[1] A standard region associated with interannual tropical Atlantic SST variability is the Atlantic 3-region (ATL3). It encompasses the eastern ocean basin between [-3,3]°N and [-20,0]°E.

art CGCMs suffer from a severe bias in the equatorial-to-subtropical eastern South Atlantic (e.g. *Richter and Xie* (2008), *Grodsky et al.* (2012), *Wang et al.* (2014)), which is reflected in the SST field. Its annual mean pattern covers the Angolan-Namibian coast and stretches northwestwards into the ATL3 region. *Chang et al.* (2007) and *Richter et al.* (2012) have shown that the bias interferes with the modelled mean state and seasonal cycle. On the equator, the SST bias can reverse the sign of the SST gradient. This reversal is complemented by a shift in the warm pool, which moves away from the western ocean basin. The thermocline slope decreases, deepening the thermocline in the eastern ocean basin. Upwelling there is strongly reduced and the modelled coupled climate system is not able to support the seasonal development of the Atlantic cold tongue.

Here, we address the question: Does the presence of the SST bias affect the predictability of SST variability in the equatorial Atlantic? The study is based on earlier findings by *Ding et al.* (2015), who showed that a simple bias alleviation technique strongly reduces the SST bias of a CGCM and substantially improves the simulated SST variability in June-August. The rest of the paper is structured as follows: Section 2 introduces our model, experimental set-up, assimilation technique, and bias reduction method. Section 3 presents the effect of the bias reduction on the assimilation runs and assesses its impact on the predictive skill of SST in hindcast simulations. A discussion is provided in Section 4. In the supplementary material, we repeat our analysis for the tropical Pacific and compare it with the predictive skill in the tropical Atlantic. The skill we find in the tropical Pacific provides a verification of our initialization technique for seasonal hindcasts, indicating its potential for the tropical Atlantic.

2 Model and Methods

Validation of model results in this study is based on the ERA-Interim reanalysis dataset *Dee et al.* (2011) for the time period 1981-2012. While we are aware that a reanalysis is not identical with observations, for the scope of this study we assume ERA-Interim to be "true", i.e. to be identical with observations. When we discuss an "observed" feature of (SST) variability, we refer to this feature in the ERA-Interim dataset. The data was accessed at the home page of ERA-Interim at the European Centre of Medium-Range Weather Forecast (ECMWF)[2]. When we repeat our analysis with alternative validation datasets[3], we find that qualitative differences in the results are negligible. Hence, we limit our results to analyses based on ERA-Interim.

Model runs were performed with the Kiel Climate Model (KCM, *Park et al.* (2009)). The KCM is a coupled global climate model (CGCM) that consists of the ECMWF Hamburg atmospheric general circulation model version 5 (ECHAM5, *Roeckner et al.* (2003)) and the Nucleus of European Modeling of the Ocean (NEMO, *Madec et al.* (1998), *Madec* (2008)) ocean-sea ice general circulation model, using the Océan Parallelisé Version 9 (OPA9) as ocean model. The coupler is the Ocean Atmosphere Sea Ice Soil version 3 (OASIS3, *Valcke* (2013)). For our experiments, we used a low-resolution version of the KCM: ECHAM5 is run in T31 horizontal resolution with 19 vertical levels; OPA9 is run in the ORCA2-setup, which employs an average horizontal resolution of approximately 1.3° with refined resolution of up to 0.5° close to the equator, and 31 vertical levels.

We base our results on two experiments. The first experiment uses a standard version of the KCM (STD). The STD-SST climatology contains the SST bias in the tropical Atlantic (*Wahl et al.*, 2011), which is comparable to the corresponding bias in other low-resolution CGCMs (*Davey et al.*, 2002, *Richter and Xie*, 2008). The second set of experiments employs surface heat flux correction to reduce the SST bias (FLX, see below for details). For both experiments, we produced a partially coupled set of assimilation runs, which provided the initial conditions for our fully coupled hindcasts.

Partial coupling is an assimilation technique that seeks to minimize equatorial initialization shock when initializing fully coupled hindcasts (e.g. *Ding et al.* (2013)). *Bell et al.* (2004) showed that assimilation of thermal data on the equator can lead to spurious vertical ocean circulation that in turn triggers an initialization shock in the hindcasts. The reason is that the assimilation of thermal data disrupts the balance

[2]http://www.ecmwf.int/en/research/climate-reanalysis/era-interim

[3]Namely, the National Center for Environmental Prediction/National Center for Atmospheric Research (NCEP/NCAR) reanalysis 1 introduced by *Kalnay et al.* (1996), and the Hadley Centre Sea Ice and Sea Surface Temperature dataset described by *Rayner et al.* (2003).

between zonal wind stress and the ocean zonal pressure gradient. When assimilation stops at the beginning of the hindcast, the model adjusts abruptly to the imposed imbalance – it experiences a shock. Partial coupling avoids this specific kind of shock by forcing the ocean and sea ice components of the coupled model with observed wind stress anomalies that are added to the model's native wind stress climatology. This set-up retains thermal coupling between the atmosphere and ocean components and, specifically, preserves SST and the atmospheric wind field as fully prognostic variables. The balance between wind stress and the ocean pressure gradient is not disturbed. In our experiments, we use monthly mean wind stress anomalies from ERA-Interim and a long control experiment of the KCM to diagnose the model wind stress climatology. Note that the STD and FLX experiments require separate control runs since their wind stress climatologies are not identical. We run three and eight ensemble members for the STD and FLX initialization runs, respectively.

Surface heat flux correction is employed in the FLX-experiments to reduce the SST bias of the KCM. To diagnose the heat flux correction term, we use a long control run of the KCM during which we nudge the model towards the observed SST monthly mean seasonal cycle with a nudging time scale of 10 days. After 470 years, when the model climate has stabilized, we use the following 70 years of the integration to diagnose the monthly mean heat flux that is associated with the SST restoring term. This is the heat flux correction climatology that we add non-interactively to our SST equation when running the KCM in heat-flux corrected mode.

The assimilation runs for both the STD and FLX experiments are produced in partially coupled mode with the respective version of the KCM (i.e. standard for STD and heat flux corrected for FLX). From the assimilation runs, we start the fully coupled hindcasts (or "historical forecasts") that we use to assess the predictive skill of the KCM. Each hindcast consists of nine ensemble members and runs for six months. Hindcasts start on the first of February, May, August, and November, for each year from 1981 to 2012. A suite of different initial conditions for the individual hindcast ensemble members is obtained by mixing the atmospheric and oceanic states of the assimilation run ensemble members. Consider an initial condition that takes its oceanic and atmospheric components from the same ensemble member of the assimilation run. This initial condition is different from an initial condition that uses components from different ensemble members of the assimilation run. In this manner, we produce sets of nine different initial conditions for our hindcasts, both for the STD and FLX experiments.

Finally, an integral measure of both forecast skill and the assimilation run ensemble mean's ability to capture observed variability is the anomaly correlation coefficient

(ACC) between the model simulations and our validation dataset ERA-Interim. The reference frame for our monthly anomalies is what we term the "linear fit". To estimate the slope and intercept parameters of the linear fit, we fit each calendar month worth of data separately to a linear regression model of polynomial order 1 via least-squares fitting[4]. We then apply the slope and intercept to our monthly time steps and obtain our linear fit. Note that the linear fit captures the (linear) long-term variability of the data. It has an absolute value for each point in time, determined by the estimated slope and intercept parameters.

We calculate the linear fits separately for each dataset, using the following approaches: (i) For the continuous *assimilation runs and ERA-Interim*, we stratify the data into the calendar months and calculate the linear fit for each calendar month. The monthly anomaly is the difference between the linear fit and the actual data. The analysis period is 1981-2012. For the assimilation runs, we calculate the linear fits and hence the anomalies separately for each ensemble member. The ensemble mean monthly anomaly is the average of the monthly anomalies of all ensemble members. (ii) For the 6-months-long *hindcasts*, we stratify the data into ensembles and months. Consider all hindcasts that were started in February. For each ensemble member[5], we select a given lead month and concatenate the data into a pseudo-time series. For example, for lead month 1 of the February hindcasts, we combine the February data of the chosen ensemble member to produce a time series of February monthly means. For lead month 2, we produce March monthly mean time series, and so on. Based on this pseudo-time series, we compute the linear fit for the hindcast data. Note again that we do this for each of the nine ensemble members separately for the entire hindcasting period. Monthly anomalies and the ensemble mean anomaly are then calculated in the same manner as for the continuous datasets.

[4]For example, we calculate the linear fit for calendar month February by fitting the monthly mean February data for our analysis period 1981-2012. While the calendar month February refers to the pool of all February data available to our analysis, a single individual month is attached to a specifiy year. Hence, it is possible to fit the data of a calendar month, but not the data of a single month, since it consists of only one data point.

[5]Across all hindcasts of a given experiments, all ensemble members with the same label are based on the same combination of initial conditions from the assimilation runs.

3 Results

3.1 Assimilation Runs: Initial Conditions for the Hindcasts

Bias alleviation drastically reduces the equatorial SST bias. Figure 1 shows the seasonal cycle of ATL3 SST for the observations and the two assimilation runs. The observed seasonal cycle shows strong initial cooling in April-May. Cooling decreases in June and stops in August, when the cold tongue starts to dissolve. The STD experiment is heavily biased with respect to the observations throughout the entire year. While the bias is moderate in boreal winter, it rapidly intensifies from June onwards. Mean bias values are 2.00°C and 3.08°C in the annual mean and for June-September, respectively. Heat flux correction reduces the annual mean bias to 0.29°C. FLX-SST develops a cold tongue in boreal summer and is hardly distinguishable from observations in September-March. However, heat flux correction fails to completely eliminate the SST bias. This is especially evident in May-July, where ATL3-SSTs in FLX are on average 1.19°C warmer than in observations. The problem is that the model fails to produce the initial cooling in April-May that marks the onset of the observed cold tongue. Consequently, from April until August, FLX effectively lags behind the observed seasonal cycle by one month. Then, FLX too has fully established the cold tongue and starts to dissolve it until March. The bias is 0.76 on average from June-September and practically vanishes in boreal winter. Note that our SST bias reduction in boreal summer in ATL3 is comparable to the reduction that *Harlaß et al.* (2015) achieve by increasing the horizontal and vertical resolution of the KCM to T159 and 62 vertical levels, respectively.

As an extension of the work of *Ding et al.* (2015) who reported a substantial improvement of simulated variability in the FLX assimilation run for the period June-August, we next investigate the monthly variability of the two (partially coupled) assimilation runs. Figure 2 shows the anomaly correlation coefficient (ACC) between ERA-Interim and STD, FLX in ATL3-SST. STD fails to produce the observed SST variability throughout most of the year. A notable exception is boreal winter: STD is least biased then (Fig. 1) and the forcing with observed wind stress anomalies can act in concert with the model to produce roughly the observed variability. Compared to STD, FLX improves ACCs in boreal summer. ACC values are larger than 0.6 for June-February. This is encouraging, since it indicates that the FLX assimilation run is able to capture the boreal summer SST variability that is associated with the Atlantic Niño.

A caveat is that FLX, too, is not able to reproduce the observed SST variability in April and May. We think that this feature is related to FLX's failure to produce

the correct initial cooling during March-April. The discussion section explores this feature in more detail.

3.2 Skill of the seasonal Hindcasting Experiments

We present the skill of three distinct forecasts:

(i) The *anomaly persistence forecast* is our reference. It is based on ERA-Interim SST: For each forecast, we select the reanalysis SST for lead month 0, i.e. the month before the corresponding KCM forecast has been started. In this way, our persistence forecasts are directly comparable with our KCM forecasts, because their initial conditions are do not use data that has only been collected after the forecast start. We then calculate the anomaly of ERA-Interim SST relative to the linear fit and persist the anomaly throughout the forecast period. Recall that we calculate the linear fit in ERA-Interim separately for each month. The skill of the persistence forecasts is estimated via the ACC with ERA-Interim itself. The ACC for lead month 0 is 1 by definition. In Fig. 3, persistence forecasts are shown as a black line.

(ii) *Dynamical forecasts* are the hindcasts produced by the two fully-coupled experiments. Dynamical forecasts are shown in Fig. 3 as light blue and light red lines for the FLX and STD KCM hindcasts, respectively.

(iii) Since SST is free to evolve in the assimilation runs, initial conditions for the dynamical forecasts differ from observed SST; for lead month 1, the dynamical skill is usually lower than the skill of the persistence forecast (Fig. 3). To correct for this, we show the skill of *corrected forecasts*. These forecasts are based on the dynamical forecasts, but add the difference between the assimilation run and ERA-Interim SST at lead month 0 to each step of the dynamical forecast (for example, if we were to correct the assimilation runs in the same manner, the corrected assimilation runs would be identical with ERA-Interim at lead month 0). In this way, our offline correction technique effectively combines the persistence and dynamical hindcasts and the information we use for the correction is all known at the time of forecast start. In Fig. 3, the corrected forecasts are shown as blue and red lines for the FLX and STD KCM hindcasts, respectively.

Figure 3a-d shows the predictive skill of the five forecasts for each of the restart months (February, May, August, and November). Predictive skill for forecasts started in February is not satisfactory (Fig. 3a): All forecasts lose skill quickly, and neither the dynamical nor the corrected forecasts beat persistence. While corrected FLX forecasts perform marginally better than corrected STD forecasts, no clear improvement due to bias alleviation emerges from the dynamical forecasts. Note that, in accordance with Figure 2, the ACC for lead month 1 (i.e. February) is not too bad:

Dynamical STD and FLX achieve ACC values of about 0.44 and 0.53, values that are not considerably worse for hindcasts started in August or November (see below). However, skill drops quickly in February, implying that the February initial conditions contain little predictive potential. February forecasts are troublesome despite reasonable initial conditions.

May forecasts perform differently in a several aspects (Figure 3b). The skill of the corrected FLX forecasts is comparable to persistence and even slightly better throughout most of the forecast period. Also, FLX experiments perform better than STD experiments, and skill drops more slowly than in February. As indicated by Figure 2, skill for lead month 1 is very low for the (uncorrected) dynamical hindcasts, negative even for the STD experiment. This is due to the failure of the partially coupled KCM – in both its standard and bias-corrected set-up – to capture the observed SST variability. Both hindcasts, however, recover skill after a few months: FLX hindcasts achieve ACCs that are significantly different from 0 at the 95% level based on a one-sides Student t test in July and August, STD in October. This, importantly, implies that the initial conditions contain information that evolve into a predictable signal, despite being unrealistic at the time of initialization. Note that this information must not and probably does not reside in the SST field. Rather, we expect that subsurface processes such as thermocline displacement are responsible for the rise in forecast skill over the course of the hindcast.

Another interesting feature is that the skills of corrected STD forecasts and (uncorrected) dynamical FLX forecasts are comparable. Note that while the STD dynamical hindcasts are biased, we correct the bias in the month leading up to the forecast. Even without addressing the bias in the remainder of the forecast, we achieve better skill than in the uncorrected FLX hindcasts. This highlights how sensitive the skill of a forecast is to the quality of initial conditions. Corrected FLX forecasts perform considerably better than their dynamical counterparts for a similar reason. The considerable skill difference between the two corrected forecasts is possibly related to the background state in the two model versions: The FLX forecasts employ bias reduction and provide a climate system that is potentially able to capture observed processes; the STD forecasts do not. Overall, the corrected FLX May forecast achieves the best and most long-lived skill of our entire hindcasting experiment. Unfortunately, the dynamical skill of lead month 1 (May) is rather poor due to inaccurate initial conditions. We suspect that improving the skill of our initial conditions in April and May by reducing the remaining bias would substantially improve the early dynamical May forecasts.

Dynamical forecasts start to perform better when started in August (Figure 3c).

Skill decreases more slowly in the latter half of the forecast. Notably, corrected FLX forecasts also beat persistence, implying that dynamical forecasting adds to the forecast quality in August. Note also that dynamical FLX forecasts have an ACC of 0.6 for lead month 0 as opposed to -0.28 for dynamical STD, pointing to the sometimes drastic effect of bias alleviation. Again, while the initial conditions for the dynamical STD forecasts are unrealistic due to the presence of the SST bias, even the STD experiment contains information that appears to raise the ACC throughout the forecast, although the ACC values are never significant. This behaviour is encouraging, since it implies that the dynamical processes in both model versions are potentially able to capture aspects of observed SST variability.

Lastly, (uncorrected) dynamical forecasts are best in November (Figure 3d). While our correction still improves the dynamical forecasts, the effect is not as drastic as for the February or May forecasts. The skill of the dynamical forecasts is significantly different from 0 until lead month 4. Notably, dynamical STD skill even beats dynamical FLX skill from lead month 2 onwards.

4 Discussion

Bias alleviation generally improves forecast skill for tropical Atlantic SST. Additionally, we identify a pronounced seasonality of the forecast skill. Hindcasts are generally bad in late boreal winter and do not produce useful skill despite being started from acceptable (SST) initial conditions. May forecasts are similar but imply a dynamically different regime: While unrealistic initial conditions for SST constrain dynamical forecasts to start off with low skill, the forecasts recover skill throughout the forecast, pointing to the existence of a predictable signal in the May initial conditions. On the other hand, the corrected FLX forecasts started in May achieve the best skill of all forecasts. This, importantly, emphasizes how sensitive forecast skill is to realistic initial conditions. The skill of (uncorrected) dynamical forecasts is generally best in late boreal summer and early boreal winter, while no large variations occur for the skill of the corrected hindcasts.

Comparing the (uncorrected) *dynamical* forecast skills with the seasonality of tropical Pacific forecast skill (supplementary Figure S**??**) reveals rough similarities: In late boeal winter, forecasts lose skill quickly despite good initial conditions (Figs. S**??**a, S**??**). (Note, however, that the skill of the KCM beats persistence throughout the forecast.) In the case of ENSO, this rapid loss of skill is due to the well-documented spring predictability barrier in initial conditions (e.g. *Chen et al.* (1997), *Latif et al.* (1998), *Samelson and Tziperman* (2001), *Duan and Wei* (2013)). Possibly, a similar barrier exists in the tropical Atlantic. After the predictability barrier, ENSO forecasts get better and reach the highest levels of forecast quality in boreal winter (Fig. S**??**b-d), albeit the skill difference between the KCM and persistence forecasts decreases substantially. This coincides with the peak phase of ENSO variability. In the tropical Atlantic, dynamical forecasts are best in boreal winter, too, but the peak phase of the Atlantic Niño is in boreal summer – close to the presumed predictability barrier.

A caveat of our study is that our bias-corrected model fails to capture the observed SST variability in April and May (Fig 2). This is most likely related to the late onset of cold tongue development in our bias-corrected assimilation run (Fig 1). Hence, our model cannot capture the variability of the onset and initial strength of the cold tongue.

The reason for the delayed onset of the cold tongue is most likely related to a strong westerly bias in zonal wind stress in the western equatorial Atlantic during April and May (Fig. S**??**). *Marin et al.* (2009) show that western equatorial wind stress during boreal spring preconditions the tropical Atlantic for Atlantic Niño events in boreal summer. Only if the absolute magnitude of zonal wind stress is sufficiently high in the western ocean basin, the thermocline shoals in the Gulf of Guinea in late

boreal spring and cold tongue development sets in early. We suspect that the same mechanism is at work in both our STD and FLX assimilation runs: Here, the mean zonal wind stress in the western tropical Atlantic, too, is systematically weaker than in observations during April and May (Fig. S**??**). While partial coupling ensures that the wind stress variability is comparable to observations, the magnitude of the zonal wind stress is strongly biased. (In FLX, zonal wind stress is effectively vanishing in April and May, while it is westerly in STD with a magnitude of about 0.02 Pa). Our assimilation runs are not able to correctly precondition the tropical Atlantic climate – cold tongue development is delayed relative to observations.

Overall, our study emphasizes that a good portion of forecast quality hinges on realistic initial conditions. It is therefore of paramount importance for Atlantic Niño forecasts to keep extending our understanding of the mechanisms that produce the tropical Atlantic bias in CGCMS, and to simultaneously improve our bias reduction techniques – be they empirical as in our case or dealing directly with the origin of the bias by improving the model physics. Here, one possible route is to improve the model resolution – especially the vertical resolution – as implied by *Harlaß et al.* (2015)

References

Bell, M. J., M. J. Martin, and N. K. Nichols (2004), Assimilation of data into an ocean model with systematic errors near the equator, *Quarterly Journal of the Royal Meteorological Society*, *130*(598), 873–893, doi:10.1256/qj.02.109.

Bjerknes, J. (1969), Atmospheric Teleconnections From The Equatorial Pacific, *Monthly Weather Review*, *97*(3), 163–172, doi:10.1175/1520-0493(1969)097¡0163:ATFTEP¿2.3.CO;2.

Burls, N. J., C. J. C. Reason, P. Penven, and S. G. Philander (2011), Similarities between the tropical Atlantic seasonal cycle and ENSO: An energetics perspective, *Journal of Geophysical Research: Oceans*, *116*(C11), C11,010, doi:10.1029/2011JC007164.

Burls, N. J., C. J. C. Reason, P. Penven, and S. G. Philander (2012), Energetics of the Tropical Atlantic Zonal Mode, *Journal of Climate*, *25*(21), 7442–7466, doi:10.1175/JCLI-D-11-00602.1.

Chang, C. Y., J. A. Carton, S. A. Grodsky, and S. Nigam (2007), Seasonal climate of the tropical Atlantic sector in the NCAR community climate system model 3: Error structure and probable causes of errors, *Journal of Climate*, *20*(6), 1053–1070, doi:10.1175/JCLI4047.1.

Chen, D., S. S. E. Zebiak, M. A. Cane, and A. J. Busalacchi (1997), Initialization and Predictability of a Coupled ENSO Forecast Model*, *Monthly Weather Review*, *125*(5), 773–788, doi:10.1175/1520-0493(1997)125¡0773:IAPOAC¿2.0.CO;2.

Davey, M., M. Huddleston, K. Sperber, P. Braconnot, F. Bryan, D. Chen, R. Colman, C. Cooper, U. Cubasch, P. Delecluse, D. DeWitt, L. Fairhead, G. Flato, C. Gordon, T. Hogan, M. Ji, M. Kimoto, A. Kitoh, T. Knutson, M. Latif, H. Le Treut, T. Li, S. Manabe, C. Mechoso, G. Meehl, S. Power, E. Roeckner, L. Terray, A. Vintzileos, R. Voss, B. Wang, W. Washington, I. Yoshikawa, J. Yu, S. Yukimoto, and S. Zebiak (2002), STOIC: A study of coupled model climatology and variability in tropical ocean regions, *Climate Dynamics*, *18*(5), 403–420, doi:10.1007/s00382-001-0188-6.

Dee, D. P., S. M. Uppala, A. J. Simmons, P. Berrisford, P. Poli, S. Kobayashi, U. Andrae, M. A. Balmaseda, G. Balsamo, P. Bauer, P. Bechtold, A. C. M. Beljaars, L. van de Berg, J. Bidlot, N. Bormann, C. Delsol, R. Dragani, M. Fuentes, A. J. Geer, L. Haimberger, S. B. Healy, H. Hersbach, E. V. H{\'o}lm, L. Isaksen, P. K{\aa}llberg, M. K{\"o}hler, M. Matricardi, A. P. Mcnally, B. M. Monge-Sanz, J. J. Morcrette, B. K. Park, C. Peubey, P. de Rosnay, C. Tavolato, J.-N.

Th{\'e}paut, and F. Vitart (2011), The ERA-Interim reanalysis: Configuration and performance of the data assimilation system, *Quarterly Journal of the Royal Meteorological Society*, *137*(656), 553–597, doi:10.1002/qj.828.

Ding, H., R. J. Greatbatch, W. Park, M. Latif, V. a. Semenov, and X. Sun (2013), The variability of the East Asian summer monsoon and its relationship to ENSO in a partially coupled climate model, *Climate Dynamics*, *42*(1-2), 367–379, doi:10.1007/s00382-012-1642-3.

Ding, H., R. J. Greatbatch, M. Latif, and W. Park (2015), The impact of sea surface temperature bias on equatorial Atlantic interannual variability in partially coupled model experiments, *Geophysical Research Letters*, *42*(13), 5540–5546, doi:10.1002/2015GL064799.

Duan, W., and C. Wei (2013), The 'spring predictability barrier' for ENSO predictions and its possible mechanism: results from a fully coupled model, *International Journal of Climatology*, *33*(5), 1280–1292, doi:10.1002/joc.3513.

Grodsky, S. A., J. A. Carton, S. Nigam, and Y. M. Okumura (2012), Tropical Atlantic Biases in CCSM4, *Journal of Climate*, *25*(11), 3684–3701, doi:10.1175/JCLI-D-11-00315.1.

Harlaß, J., M. Latif, and W. Park (2015), Improving climate model simulation of tropical Atlantic sea surface temperature: The importance of enhanced vertical atmosphere model resolution, *Geophysical Research Letters*, *42*(7), 2401–2408, doi:10.1002/2015GL063310.

Hirst, A. C., and S. Hastenrath (1983), Atmosphere-ocean mechanisms of climate anomalies in the Angola-tropical Atlantic sector, *Journal of Physical Oceanography1*, *13*(7), 1146–1157, doi:10.1175/1520-0485(1983)013¡1146:AOMOCA¿2.0.CO;2.

Kalnay, E., M. Kanamitsu, R. Kistler, W. Collins, D. Deaven, L. Gandin, M. Iredell, S. Saha, G. White, J. Woollen, Y. Zhu, A. Leetmaa, R. Reynolds, M. Chelliah, W. Ebisuzaki, W. Higgins, J. Janowiak, K. C. Mo, C. Ropelewski, J. Wang, R. Jenne, and D. Joseph (1996), The NCEP/NCAR 40-year reanalysis project, *Bulletin of the American Meteorological Society*, *77*(3), 437–471, doi:10.1175/1520-0477(1996)077¡0437:TNYRP¿2.0.CO;2.

Keenlyside, N. S., and M. Latif (2007), Understanding Equatorial Atlantic Interannual Variability, *Journal of Climate*, *20*(1), 131–142, doi:10.1175/JCLI3992.1.

Latif, M., D. Anderson, and T. Barnett (1998), A review of the predictability and prediction of ENSO, *Journal of Geophysical Research: Oceans*, *103*, 14,375–14,393.

Madec, G. (2008), NEMO ocean general circulation model reference manuel, *Tech. rep.*, Institut Pierre-Simon Laplace, Paris.

Madec, G., P. Delecluse, M. Imbard, and C. Levy (1998), OPA 8.1 general circulation model reference manual, *Tech. rep.*, Institut Pierre-Simon Laplace, Paris.

Marin, F., G. Caniaux, H. Giordani, B. Bourlès, Y. Gouriou, and K. Erica (2009), Why Were Sea Surface Temperatures so Different in the Eastern Equatorial Atlantic in June 2005 and 2006?, *Journal of Physical Oceanography*, *39*(6), 1416–1431, doi:10.1175/2008JPO4030.1.

Mohino, E., and T. Losada (2015), Impacts of the Atlantic Equatorial Mode in a warmer climate, *Climate Dynamics*, *45*(7-8), 2255–2271, doi:10.1007/s00382-015-2471-y.

Park, W., N. Keenlyside, M. Latif, A. Ströh, R. Redler, E. Roeckner, and G. Madec (2009), Tropical Pacific Climate and Its Response to Global Warming in the Kiel Climate Model, *Journal of Climate*, *22*(1), 71–92, doi:10.1175/2008JCLI2261.1.

Rayner, N. A., D. Parker, E. Horton, C. Folland, L. Alexander, D. Rowell, E. Kent, and A. Kaplan (2003), Global analyses of sea surface temperature, sea ice, and night marine air temperature since the late nineteenth century, *Journal of Geophysical Research*, *108*(D14), 4407, doi:10.1029/2002JD002670.

Richter, I., and S.-P. Xie (2008), On the origin of equatorial Atlantic biases in coupled general circulation models, *Climate Dynamics*, *31*(5), 587–598, doi:10.1007/s00382-008-0364-z.

Richter, I., S. P. Xie, A. T. Wittenberg, and Y. Masumoto (2012), Tropical Atlantic biases and their relation to surface wind stress and terrestrial precipitation, *Climate Dynamics*, *38*(5-6), 985–1001, doi:10.1007/s00382-011-1038-9.

Roeckner, E., G. Bäuml, L. Bonaventura, R. Brokopf, M. Esch, M. Giorgetta, S. Hagemann, I. Kirchner, L. Kornblueh, A. Rhodin, U. Schlese, U. Schulzweida, and A. Tompkins (2003), The atmospheric general circulation model ECHAM5: Part 1: Model description, *MPI Report*, (349), 1–140, doi:10.1029/2010JD014036.

Samelson, R., and E. Tziperman (2001), Instability of the chaotic ENSO: The growth-phase predictability barrier, *Journal of the Atmospheric Sciences*, *58*, 3613–3625.

Valcke, S. (2013), The OASIS3 coupler: a European climate modelling community software, *Geoscientific Model Development Discussions*, *5*(3), 2139–2178, doi: 10.5194/gmdd-5-2139-2012.

Wahl, S., M. Latif, W. Park, and N. Keenlyside (2011), On the Tropical Atlantic SST warm bias in the Kiel Climate Model, *Climate Dynamics*, *36*(5-6), 891–906, doi:10.1007/s00382-009-0690-9.

Wang, C., L. Zhang, S. Lee, L. Wu, and C. R. Mechoso (2014), A global perspective on CMIP5 climate model biases, *Nature Climate Change*, *4*(February), 201–205, doi:10.1038/NCLIMATE2118.

Xie, S.-P., and J. A. Carton (2004), Tropical Atlantic Variability: Patterns, Mechanisms, and Impacts, in *Earth's Climate*, pp. 121–142, American Geophysical Union, doi:10.1029/147GM07.

Zebiak, S. E. (1993), Air–Sea Interaction in the Equatorial Atlantic Region, *Journal of Climate*, *6*(8), 1567–1586, doi:10.1175/1520-0442(1993)006¡1567:AIITEA¿2.0.CO;2.

5 List of figures

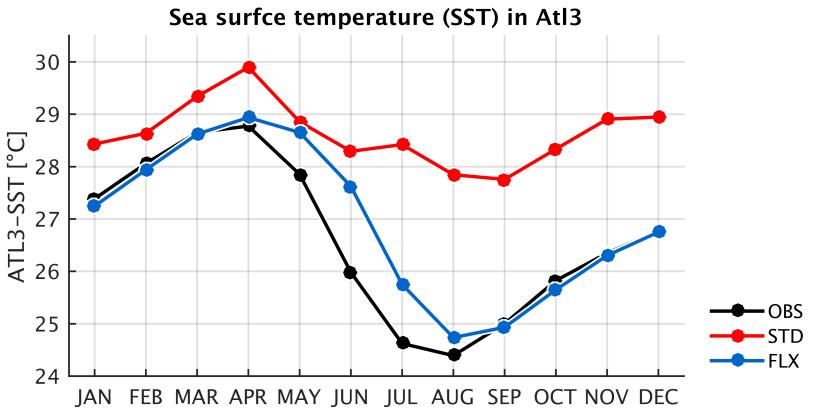

Figure 1: *Monthly mean SST in (black) ERA-Interim and (blue) the FLX and (red) initialization runs.*

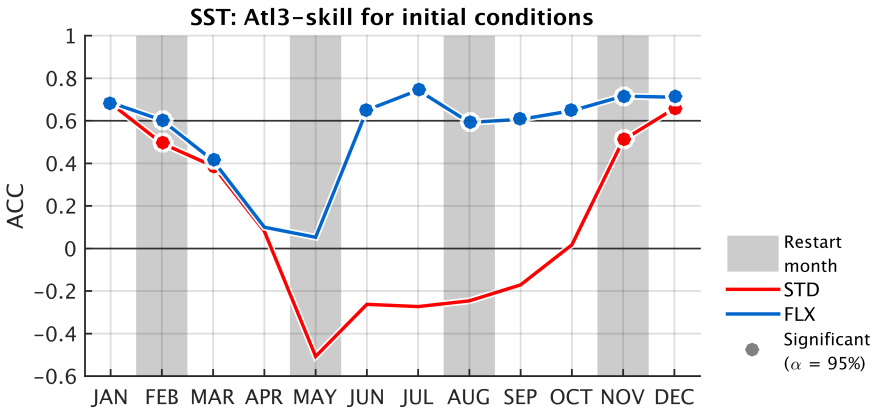

Figure 2: *Monthly anomaly correlation coefficient between ERA-Interim and the KCM initialization runs for the (blue) FLX and (red) STD experiments. ACC-values that are significantly different from 0 at the 95%-level are shown as circles. Grey background bars show months during which seasonal hindcasts have been started from the initialization runs.*

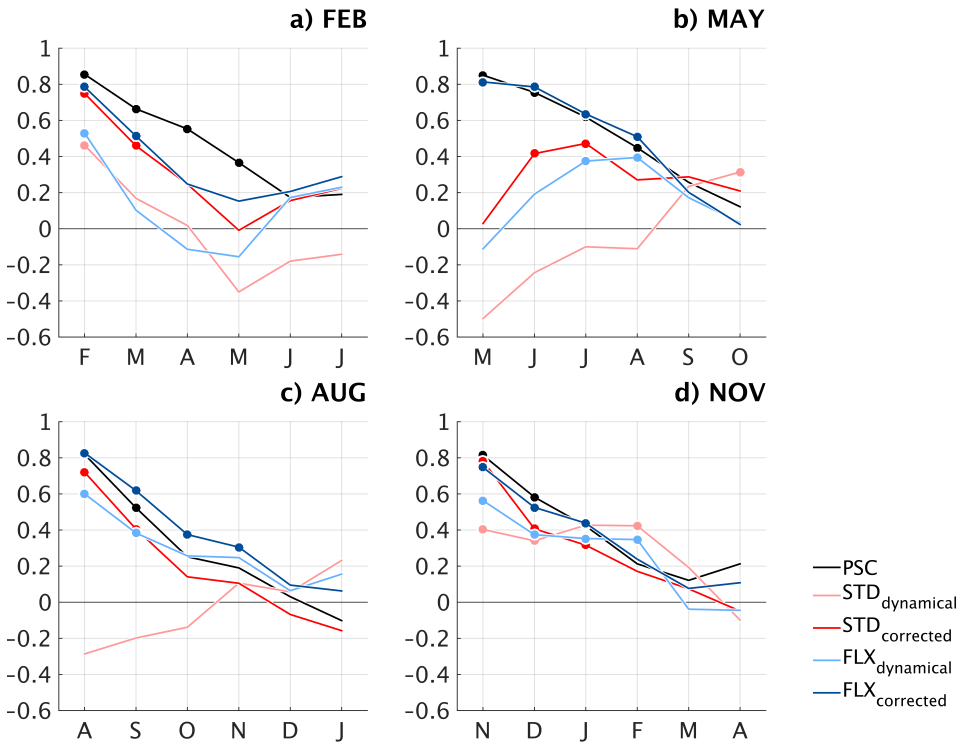

Figure 3: *Hindcast skill (ACC) for SST in ATL3 in (a) February, (b) May, (c) August, (d) November. Circles show ACCs that are significantly different from 0 at the 95%-level. Line colours show the different experiments (see text for details): (black) reference persistence forecast, (light red) dynamical STD, (light blue) dynamical FLX, (red) corrected STD, (blue) corrected FLX. Forecast skill is deemed "useful" when it exceeds an ACC value of 0.6 (grey line, Latif et al. (1998)).*

Seasonal Predictions of Equatorial Atlantic SST in a low-resolution CGCM with Surface Heat Flux Correction

— Supplementary Material —

Tina Dippe[1,1], Richard J. Greatbatch[1,2], and Hui Ding[3]

[1]GEOMAR Helmholtz Centre for Ocean Research Kiel, Germany

[2]Faculty of Mathematics and Natural Sciences, Christian Albrechts Universität, Kiel, Germany

[3]Cooperate Institute for Research in Environmental Sciences - University of Colorado and NOAA Earth Systems Research Laboratory, Boulder, USA

October 9, 2018

[1]tdippe@geomar.de

1 Bias Correction and Skill of initial conditions in the tropical Pacific

As for the tropical Atlantic, heat flux correction improves the mean state and the simulated variability in the KCM's tropical Pacific (Figs. S1 and S2). The NINO3.4-region[1] in the KCM suffers from a cold bias (Fig. S1) with a magnitude of 0.93 (1.21) and 1.17 (0.98)°C in FLX (STD) for the annual mean and September-December, respectively. Heat flux correction does not reduce the SST bias in Nino3.4 in boreal fall. It seems that in boreal fall in the tropical Pacific, whatever is causing the cold SST bias is too strong to be ameliorated by our simple surface flux correction. The result is that FLX is hardly distinguishable from STD in boreal fall. In boreal spring and summer on the other hand (March-July), when the cold bias in the eastern cold tongue region is strongest (1.53°C), FLX reduces the bias to 0.80°.

Initial conditions are generally good in the tropical Pacific (Fig. S2). ACCs between the assimilation runs and ERA-Interim are 0.92 (0.87) on average and minimum during July (July) with a value of 0.87 (0.69) in the FLX (STD) assimilation run. Note that heat flux correction improves the ability of the KCM to simulate interannual variability in boreal summer, particularly in July and August. This is interesting, because the SST bias during these months is comparable in both assimilation runs.

The predictive skill of the hindcasts for SST in the NINO3.4-region is shown in Fig. S3. Skill differences between dynamical and corrected hindcasts in the second half of the forecast are small and not coherent. This indicates that combining persistence with dynamical forecasts does not add substantial skill to the dynamical forecasts. Consistent differences between STD and FLX hindcasts do not exist. Lastly, predictive skill in the tropical Pacific shows a marked seasonality: The hindcasts lose skill relatively quickly for forecasts that are initialized in February and May, although they do generally better than persistence. After six months, these forecasts have generally lost their skill. In contrast, hindcasts that are started during August and November retain high skill until the end of the hindcasting period. November forecast perform best.

Note that the simple assimilation technique of partial coupling in the KCM produces initial conditions that sustain rather successful hindcasts for the tropical Pacific. The skill of our NINO3.4 hindcasts is comparable to the skill of other seasonal forecasting systems (e.g. *Baehr et al.*, 2014).

[1] [-5 5]°N, [-170 -120]°E

References

Baehr, J., K. Fröhlich, M. Botzet, D. I. V. Domeisen, L. Kornblueh, D. Notz, R. Piontek, H. Pohlmann, S. Tietsche, and W. A. Müller (2014), The prediction of surface temperature in the new seasonal prediction system based on the MPI-ESM coupled climate model, *Climate Dynamics*, pp. 1–13, doi:10.1007/s00382-014-2399-7.

2 List of supplementary Figures

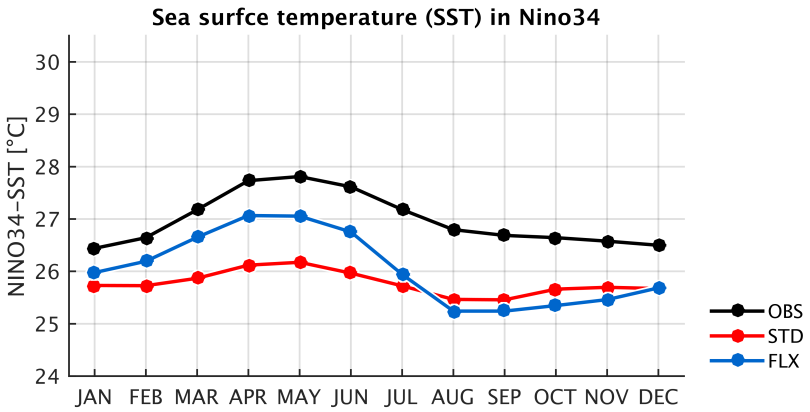

Figure S1: *Monthly mean SST bias in (black) ERA-Interim and (blue) the FLX and (red) initialization runs, area-averaged over the NINO3.4 Region: [-5,5]° N, [-170,-120]° E*

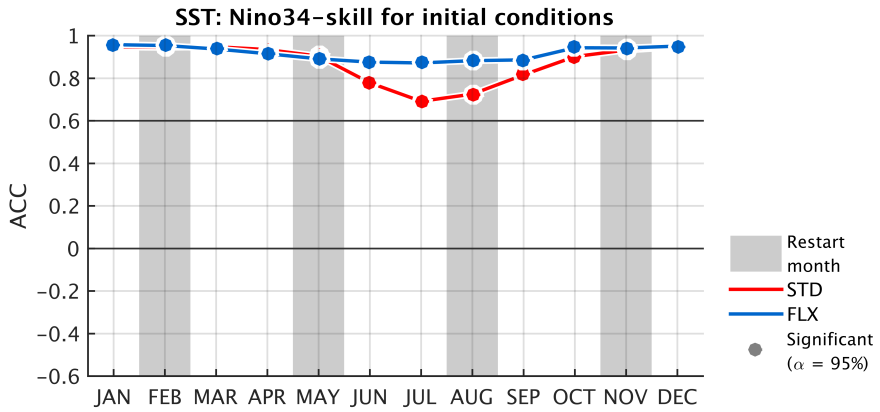

Figure S2: *Monthly anomaly correlation coefficient between ERA-Interim and the KCM initialization runs for the (blue) FLX and (red) STD experiments in the NINO3.4-region. ACC-values that are significantly different from 0 at the 95%-level are shown as circles. Grey background bars show months during which a seasonal hindcasts have been started from the initialization runs.*

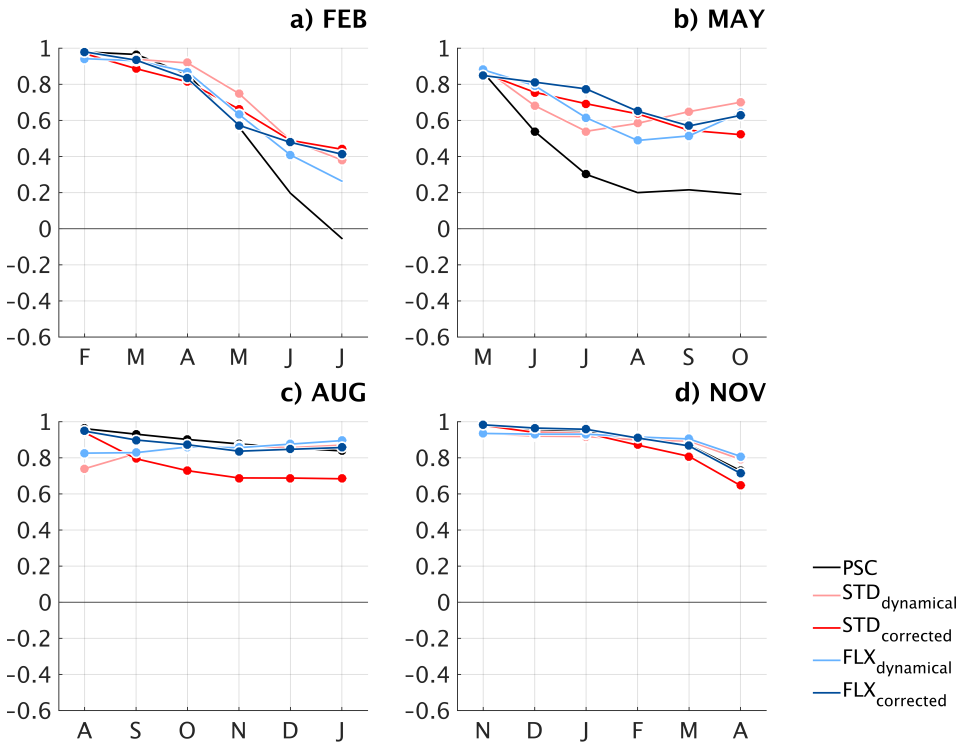

Figure S3: *Skill (ACC) for SST in NINO3.4 for hindcasts started at the beginning of (a) February, (b) May, (c) August, (d) November. Circles show ACCs that are significantly different from 0 at the 95%-level. Line colours show the different experiments (see text for details): (black) reference persistence forecast, (light red) dynamical STD, (light blue) dynamical FLX, (red) corrected STD, (blue) corrected FLX. Forecast skill is deemed "useful" when it exceeds an ACC value of 0.6 (grey line).*

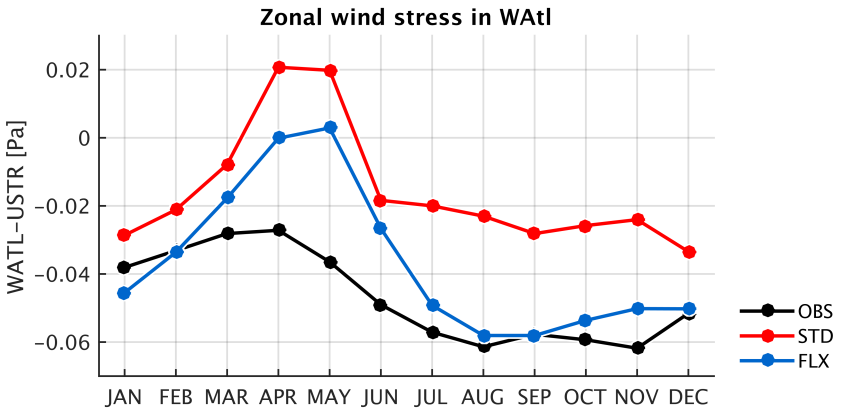

Figure S4: *Same as Figure S1 but for zonal wind stress in the WAtl region ([-3,3]° N, [-40,-20]° E).*

Chapter 6

Summary, Discussion, Outlook

6.1 Summary

The aim of this thesis was to better understand the mechanisms that drive Atlantic Niño variability, and to quantify the impact of the equatorial warm bias on the predictability of the Atlantic Niño. To this end, direct observational records were combined with atmospheric and oceanic reanalysis datasets and CGCM simulations, and a range of statistical analysis methods was employed to estimate the dynamical component of SST variability within the framework of the Bjerknes feedback.

Below, the questions posed in Section 1.5 are met with summary answers.

► Chapter 2: **How dynamical is the Atlantic Niño?**

Chapter 2 decomposes equatorial Atlantic SST variability into a dynamical part that is related to the Bjerknes feedback, and a residual part associated with stochastic processes. The method is based on multiple linear regression, which models SST with two predictor variables – sea surface height (SSH, a proxy for thermocline depth in central and eastern equatorial ocean basins) and equatorial zonal surface wind in the western basin –, taking into account appropriate lags that were diagnosed via a cross-correlation analysis.

In a dataset that combines direct satellite observations with atmospheric reanalyses, SST variability in the equatorial Atlantic shows clear dynamical components. The ratio of dynamical-to-stochastic SST variance varies strongly over the course of the year. During boreal summer, when the Atlantic Niño peaks, dynamical SST variability is 4-7 times larger than stochastic SST variability, indicating that the Bjerknes feedback is involved in establishing SST variability during this season, and, by extension, with the Atlantic Niño. The dynamical part of SST variability forms a secondary peak in boreal winter, associated with the winter Niño. In boreal spring and August, non-Bjerknes mechanisms dominate SST variability in the equatorial Atlantic.

Repeating the analysis for two simulations of the KCM – one developing a strong equatorial warm bias, the other employing a simple scheme to alleviate SST biases – shows that neither of the coarse-resolution experiments is able to reproduce the observed distribution of dynamical and stochastic SST variances. In the biased experiment, which fails to establish the Atlantic cold tongue in boreal summer, dynamical contributions to SST variability are out-valued by stochastic SST variability for most of boreal summer, creating a model simulation in which a realistic Atlantic Niño does not exist. The bias-corrected run, on the other hand, captures some features of the observations. While the cold tongue still forms a month late, the bias-corrected KCM does capture enhanced dynamical contributions to SST variability once the model established the cold tongue.

- Chapter 3: **How symmetric are the Atlantic and Pacific Bjerknes feedbacks? Are they stationary on decadal time scales?**

  Chapter 3 decomposes the Bjerknes feedback into three separate feedback elements. The feedback elements measure the strength of subsurface-surface coupling (SST-SSH feedback element), the relationship between SST and zonal wind stress variability in the western equatorial ocean basin (SST-USTR), and the sensitivity of SSH to USTR (USTR-SSH), emulating the closed Bjerknes feedback loop. A robust regression technique provides strength estimates for the three feedback elements. Each element is further partitioned into composites that relate its strength to either positive or negative anomalies of the variable that "drives" it (i.e. SSH, SST, and USTR for the SSH-SST, SST-USTR, and USTR-SSH feedback elements). Additionally, a simple measure of the overall strength of the closed Bjerknes feedback loop is introduced. In this case, the strength of the total feedback composites relates to either warm or cold SSTs.

  In the Pacific, results agree well with previous studies on ENSO complexity. Positive composites are generally stronger than negative composites for all feedback elements, resulting in a total Bjerknes feedback that is stronger when it acts on warm SSTs. The seasonality of the feedback elements is in agreement with previous ENSO research.

  In the Atlantic, asymmetries exist, but they are not as consistent between feedback elements as in the Pacific. The SSH-SST feedback element dominates the Atlantic Bjerknes feedback and is comparable in strength to its Pacific counterpart. In contrast, the two feedback elements that are related to western-basin zonal wind variability – SST-USTR and USTR-SSH – are much weaker than in the Pacific and constrain the Atlantic Bjerknes feedback to boreal summer and winter. Seasonalities of the feedback elements agree well with previous research on the Atlantic Niño.

  Expanding the results for the initial period 1993-2012, an ocean reanalysis is used to assess the stationarity of the findings by repeating the analysis for overlapping, consecutive 25-year periods from 1958-2009. Substantial variations occur in both basins for all feedback elements and affect their symmetry, particularly in the Atlantic. This indicates that the configuration of the Atlantic Bjerknes feedback is not likely to be stable on decadal time scales.

- Chapter 4: **What drives the development of the equatorial Atlantic warm bias?**

  This review paper synthesises our current understanding of the mechanisms that produce and maintain the equatorial Atlantic warm bias. A dipole pattern of deficient continental precipitation over South America and Africa weakens the surface pressure gradient along the equator and induces a westerly wind bias in the western equatorial ocean basin that is strongest in boreal spring. This wind bias is an intrinsic feature of current-generation atmospheric models and has been linked to the horizontal and vertical resolution of the model. Coupling the incipient westerly wind bias to an ocean model redistributes the ocean heat content along the equator by displacing the Atlantic warm pool into the central ocean basin. Model winds that are weakened by the westerly wind bias are not sufficient to initiate the spring thermocline shoaling in the central ocean basin. The Atlantic cold tongue, the key feature of the seasonal cycle in the equatorial Atlantic, cannot develop. Feedbacks between the atmosphere and the ocean are greatly distorted in the biased system, or do not emerge at all. Several studies have proposed model improvements based on these findings, demonstrating that the amplitude of the coupled bias in the equatorial Atlantic can be decreased substantially.

- Chapter 5: **Does the equatorial Atlantic warm bias affect the ability of a model to predict the Atlantic Niño?**

  To answer this question, two sets of seasonal hindcasting experiments were performed. The first set uses a standard version of the KCM that develops the equatorial Atlantic warm bias. The second set is produced by a heat-flux corrected version of the KCM. Heat flux correction keeps the seasonal cycle of SST in the model close to observations, effectively alleviating SST biases. (Note that this is a symptomatic approach to bias reduction that does not directly correct the physical shortcomings of the biased model.) To capture a possible seasonality of the KCM's predictive skill, 6-months-long hindcasts were initialised in February, May, August, and November.

  The heat-flux corrected model generally predicts SST variability better than the biased model. In particular, hindcasts that are initialised in May hugely benefit from bias reduction. In both the biased and the heat-flux corrected model runs, the predictability of SST is strongly seasonal. Hindcasts started in February loose their skill the quickest, while hindcasts started in May can maintain it for up to four months.

6.2 Discussion

Studies of the Atlantic Niño struggle with robustness. Results in climate science are robust if they are not overly sensitive to the chosen analysis method or dataset. In observational studies, robustness is closely linked to the statistical significance of a result, demanding a sufficiently large sample size on which to base the analysis. Modelling studies usually produce long integrations that provide large sample sizes. In this case, robustness is assessed by repeating a given analysis with output from a number of models, or by verifying in another way that small perturbations to the analysis method do not drastically change the results.

The observational record of the tropical Atlantic is short. Satellite-borne observational campaigns were first launched at the end of the 1970s, and a comprehensive direct observational network of buoys has only been implemented after 2001 (PIRATA, Bourlès et al., 2008). While some SST estimates reach back more than a hundred years based on reconstruction techniques, comprehensive datasets bundling up information about atmospheric conditions, air-sea interaction, and subsurface ocean variability are restricted to a few decades at best. A central concept of this thesis is the Bjerknes feedback (Bjerknes, 1966; Bjerknes, 1969). The Bjerknes feedback framework requires that SST, (a proxy for) thermocline depth, and surface wind variability are analysed simultaneously. Here, thermocline depth is approximated by sea surface height (SSH), which is provided by the satellite-based AVISO[1] dataset running from 1993 to the present. This work's analysis period is hence restricted to little more than 20 years. The resulting sample sizes are small, and, for the analysis of interannual variability based on monthly mean data, render statistical robustness weak.

Model studies on the other hand struggle with the equatorial Atlantic warm bias (Chapter 4). While the equatorial Pacific, too, develops substantial biases in model simulations (e.g. Bellenger et al., 2014), CGCMs are generally able to capture crucial ENSO characteristics and can hence produce reliable forecasts on seasonal time scales. This is not the case in the Atlantic. However, many studies have examined the dynamical cause of the equatorial Atlantic warm bias and proposed model improvements based on their findings (e.g. DeWitt, 2005; Harlaß, Latif, and Park, 2015, 2017; Richter et al., 2014a; Tozuka et al., 2011; Voldoire et al., 2014; Wahl et al., 2011). Initial simulations suggested that improved models are able to produce a much more realistic Atlantic Niño (e.g. Ding et al., 2015). Still, even the most drastic improvements discussed in Harlaß, Latif, and Park (2017) – a study that increases both the vertical and horizontal resolution of the atmospheric model and thereby strongly decreases the westerly wind bias in the western equatorial Atlantic – is not sufficient to produce entirely realistic SST variability in the central Atlantic. Specifically, seasonal SST variability is strongest a month late in the model simulations, suggesting a possible mismatch between SST, wind, and thermocline variability that could impede the Atlantic Niño.

[1] `https://www.aviso.altimetry.fr/en/home.html`

Last, numerous studies have highlighted the complex nature of the Atlantic Niño (e.g. Ruiz-Barradas, Carton, and Nigam, 2000; Sutton, Jewson, and Rowell, 2000; Zebiak, 1993). While this thesis focused on the dynamical framework of the Bjerknes feedback, other processes – such as interactions between the tropics and extra-tropics or equatorial wave processes that are omitted in the Bjerknes feedback – contribute to equatorial SST variability as well (e.g. Burmeister, Brandt, and Lübbecke, 2016; Foltz and McPhaden, 2010a,b; Richter and Xie, 2008). A detailed and comprehensive assessment of feedback processes other than the Bjerknes feedback could possibly further our understanding of the complex interactions that shape the variability of equatorial Atlantic climate.

6.3 Outlook

Chapters 2 and 5 demonstrated that a simple alleviation of the SST bias enhances the KCM's ability to simulate and predict the Atlantic Niño. However, Richter et al. (2017) discuss a link between atmospheric mean state biases and the predictability of atmospheric variability in the equatorial Atlantic, and cannot establish a categorical relationship. Future research should aim at assessing the degree to which it is the equatorial warm bias that keeps models from correctly capturing the Atlantic Niño.

A related aspect that has not been extensively discussed yet is the potential predictability of SST variability in the tropical Atlantic. Potential predictability is the optimum predictive skill inherent to an aspect of the physical climate system. Model-based studies estimate potential predictability within a pure "modelling world". They often use large ensembles to assess how well individual predictions agree on the evolution of the climate system (e.g. Latif et al., 2006; Rowell, 1998; Sutton, Jewson, and Rowell, 2000; F. Wang and P. Chang, 2008), or approach the problem in a "perfect model" franework. In this case, a model is run once to produce a "reality" that is subsequently "predicted" by a set of hindcasts, using a slightly perturbed version of the same model. However, studies of this type implicitly assume that models and the real world agree on the basic physics determining the climate system. This is not the case in heavily biased regions such as the tropical Atlantic. To avoid the limitations of model-based estimates of potential predictability, Feng, DelSole, and Houser (2012) introduced a method to derive the potential predictability of SST variability from observations alone. In the tropical Atlantic, they find that the predictable variance of SST during July-August is rather high and can reach values of $70 - 90\%$, suggesting that tropical Atlantic SST indeed can potentially be predicted rater well. How this potential will be unlocked, and on which time scales it will be relevant – seasons, as in the Pacific, or rather weeks, due to the small zonal extent of the basin? – remains to be seen.

In general, the effect of basin geometry on the properties of an equatorial Niño has not been assessed thoroughly yet. Feedbacks seem to depend on the zonal extent of the basin, but no sensitivity study has been performed. A series of idealized model experiments could be used to pin-point the exact orographic features that modulate Niño characteristics. Similar studies have been conducted for different aspects of the climate system. Brayshaw, Hoskins, and Blackburn (2009, 2011), for example, use a hierarchy of idealized models to assess the impact of orography and underlying strong SST gradients on the properties of the extra-tropical storm track. Given that equatorial Niños are an integral part of the climate system, a coordinated study on the impacts of boundary conditions, including bathymetry orography, could be interesting.

Once models are able to simulate a realistic Atlantic Niño, a number of unresolved questions can be examined. For example, the character of decadal modulations of the Atlantic Niño can be assessed more thoroughly, future changes of the phenomenon under greenhouse gas forcing will be easier to diagnose, and processes that have recently been

shown to affect ENSO can be studied in the Atlantic as well, such as the concept of state-dependent noise. Last, seasonal prediction systems could be able to provide reliable forecasts of SST conditions in the equatorial Atlantic, helping to improve agricultural planning and food security in equatorial Africa.

List of Figures

1.1 Time series of an Atlantic Niño index, 1981-2012, based on the HadISST dataset 10
1.2 Composite evolution of Atlantic Niño events, 1981-2012, based on HadISST 11
1.3 Seasonal cycle and evolution of individual events for the Atlantic and Pacific Niños, based on HadISST, 1981-2012 17
1.4 The equatorial Atlantic warm bias 20

Bibliography

Banzon, V., T. M. Smith, T. M. Chin, C. Liu, and W. Hankins (2016). "A long-term record of blended satellite and in situ sea-surface temperature for climate monitoring, modeling and environmental studies". In: *Earth System Science Data* 8.1, pp. 165–176. DOI: 10.5194/essd-8-165-2016.

Bellenger, H., E. Guilyardi, J. Leloup, M. Lengaigne, and J. Vialard (2014). "ENSO representation in climate models: from CMIP3 to CMIP5". In: *Climate Dynamics* 42.7, pp. 1999–2018. DOI: 10.1007/s00382-013-1783-z.

Bjerknes, J. (1966). "A possible response of the atmospheric Hadley circulation to equatorial anomalies of ocean temperature". In: *Tellus* 18.4, pp. 820–829. DOI: 10.3402/tellusa.v18i4.9712.

Bjerknes, J. (1969). "Atmospheric Teleconnections From The Equatorial Pacific". In: *Monthly Weather Review* 97.3, pp. 163–172. DOI: 10.1175/1520-0493(1969)097<0163:ATFTEP>2.3.CO;2.

Bourlès, B., R. Lumpkin, M. J. McPhaden, F. Hernandez, P. Nobre, E. Campos, L. Yu, S. Planton, A. Busalacchi, A. D. Moura, J. Servain, and J. Trotte (2008). "The Pirata Program: History, Accomplishments, and Future Directions". In: *Bulletin of the American Meteorological Society* 89.8, pp. 1111–1125. DOI: 10.1175/2008BAMS2462.1.

Brandt, P., A. Funk, V. Hormann, M. Dengler, R. J. Greatbatch, and J. M. Toole (2011). "Interannual atmospheric variability forced by the deep equatorial Atlantic Ocean". In: *Nature* 473.7348, pp. 497–500.

Brandt, P., F. A. Schott, C. Provost, A. Kartavtseff, V. Hormann, B. Bourlès, and J. Fischer (2006). "Circulation in the central equatorial Atlantic: Mean and intraseasonal to seasonal variability". In: *Geophysical Research Letters* 33.7. DOI: 10.1029/2005GL025498.

Brayshaw, D. J., B. Hoskins, and M. Blackburn (2009). "The Basic Ingredients of the North Atlantic Storm Track. Part I: Land–Sea Contrast and Orography". In: *Journal of the Atmospheric Sciences* 66.9, pp. 2539–2558. DOI: 10.1175/2009JAS3078.1.

— (2011). "The Basic Ingredients of the North Atlantic Storm Track. Part II: Sea Surface Temperatures". In: *Journal of the Atmospheric Sciences* 68.8, pp. 1784–1805. DOI: 10.1175/2011JAS3674.1.

Burls, N. J., C. J. C. Reason, P. Penven, and S. G. Philander (2011). "Similarities between the tropical Atlantic seasonal cycle and ENSO: An energetics perspective". In: *Journal of Geophysical Research: Oceans* 116.C11, p. C11010. DOI: 10.1029/2011JC007164.

— (2012). "Energetics of the Tropical Atlantic Zonal Mode". In: *Journal of Climate* 25.21, pp. 7442–7466. DOI: 10.1175/JCLI-D-11-00602.1.

Burmeister, K., P. Brandt, and J. F. Lübbecke (2016). "Revisiting the cause of the eastern equatorial Atlantic cold event in 2009". In: *Journal of Geophysical Research: Oceans* 121.7, pp. 4777–4789. DOI: 10.1002/2016JC011719.

Caniaux, G., H. Giordani, J. L. Redelsperger, F. Guichard, E. Key, and M. Wade (2011). "Coupling between the Atlantic cold tongue and the West African monsoon in boreal spring and summer". In: *Journal of Geophysical Research: Oceans* 116.4. DOI: 10.1029/2010JC006570.

Carton, J. A., X. Cao, B. S. Giese, and A. M. Da Silva (1996). "Decadal and Interannual SST Variability in the Tropical Atlantic Ocean". In: *Journal of Physical Oceanography* 26.7, pp. 1165–1175. DOI: 10.1175/1520-0485(1996)026<1165:DAISVI>2.0.CO;2.

Carton, J. A. and B. Huang (1994). "Warm Events in the Tropical Atlantic". In: *Journal of Physical Oceanography* 24.5, pp. 888–903. DOI: 10.1175/1520-0485(1994)024<0888:WEITTA>2.0.CO;2.

Chang, C. Y., J. A. Carton, S. A. Grodsky, and S. Nigam (2007). "Seasonal climate of the tropical Atlantic sector in the NCAR community climate system model 3: Error structure and probable causes of errors". In: *Journal of Climate* 20.6, pp. 1053–1070. DOI: 10.1175/JCLI4047.1.

Claus, M., R. J. Greatbatch, and P. Brandt (2014). "Influence of the Barotropic Mean Flow on the Width and the Structure of the Atlantic Equatorial Deep Jets". In: *Journal of Physical Oceanography* 44.9, pp. 2485–2497. DOI: 10.1175/JPO-D-14-0056.1.

Cromwell, T. (1953). "Circulation in a meridional plane in the central equatorial Pacific". In: *Journal of Marine Research* 23, pp. 196–213.

Cromwell, T., R. B. Montgomery, and E. D. Stroup (1954). "Equatorial Undercurrent in Pacific Ocean Revealed by New Methods". In: *Science* 119, pp. 648–649.

Deppenmeier, A.-L., R. J. Haarsma, and W. Hazeleger (2016). "The Bjerknes feedback in the tropical Atlantic in CMIP5 models". In: *Climate Dynamics*, pp. 1–17. DOI: 10.1007/s00382-016-2992-z.

DeWitt, D. G. (2005). "Diagnosis of the tropical Atlantic near-equatorial SST bias in a directly coupled atmosphere-ocean general circulation model". In: *Geophysical Research Letters* 32.1. DOI: 10.1029/2004GL021707.

Ding, H., R. J. Greatbatch, M. Latif, and W. Park (2015). "The impact of sea surface temperature bias on equatorial Atlantic interannual variability in partially coupled model experiments". In: *Geophysical Research Letters* 42.13, pp. 5540–5546. DOI: 10.1002/2015GL064799.

Ding, H., N. S. Keenlyside, and M. Latif (2012). "Impact of the Equatorial Atlantic on the El Niño Southern Oscillation". English. In: *Climate Dynamics* 38.9-10, pp. 1965–1972. DOI: 10.1007/s00382-011-1097-y.

Dippe, T., R. J. Greatbatch, and H. Ding (2018). "On the relationship between Atlantic Niño variability and ocean dynamics". In: *Climate Dynamics* 51.1, pp. 597–612. DOI: 10.1007/s00382-017-3943-z.

Dippe, T., M. Krebs, J. Harlaß, and J. F. Lübbecke (2018). "Can Climate Models Simulate the Observed Strong Summer Surface Cooling in the Equatorial Atlantic?" In: *YOUMARES 8 – Oceans Across Boundaries: Learning from each other*. Ed. by S. Jungblut, V. Liebich, and M. Bode. Springer International Publishing, pp. 7–23.

Doi, T., G. A. Vecchi, A. J. Rosati, and T. L. Delworth (2012). "Biases in the Atlantic ITCZ in Seasonal–Interannual Variations for a Coarse- and a High-Resolution Coupled Climate Model". In: *Journal of Climate* 25.16, pp. 5494–5511. DOI: 10.1175/JCLI-D-11-00360.1.

Feng, X., T. DelSole, and P. Houser (2012). "A Method for Estimating Potential Seasonal Predictability: Analysis of Covariance". In: *Journal of Climate* 25.15, pp. 5292–5308. DOI: 10.1175/JCLI-D-11-00342.1.

Folland, C. K., A. W. Colman, D. P. Rowell, and M. K. Davey (2001). "Predictability of Northeast Brazil Rainfall and Real-Time Forecast Skill, 1987–98". In: *Journal of Climate* 14.9, pp. 1937–1958. DOI: 10.1175/1520-0442(2001)014<1937:PONBRA>2.0.CO;2.

Foltz, G. R. and M. J. McPhaden (2010a). "Abrupt equatorial wave-induced cooling of the Atlantic cold tongue in 2009". In: *Geophysical Research Letters* 37.24. DOI: 10.1029/2010GL045522.

— (2010b). "Interaction between the Atlantic meridional and Niño modes". In: *Geophysical Research Letters* 37.May, pp. 1–5. DOI: 10.1029/2010GL044001.

Fontaine, B. and S. Janicot (1996). "Sea surface temperature fields associated with West African rainfall anomaly types". In: *Journal of Climate*. DOI: 10.1175/1520-0442(1996)009<2935:SSTFAW>2.0.CO;2.

Fu, X. and B. Wang (2001). "A Coupled Modeling Study of the Seasonal Cycle of the Pacific Cold Tongue. Part I: Simulation and Sensitivity Experiments". In: *Journal of Climate* 14.5, pp. 765–779. DOI: 10.1175/1520-0442(2001)014<0765:ACMSOT>2.0.CO;2.

Grodsky, S. A., J. A. Carton, S. Nigam, and Y. M. Okumura (2012). "Tropical Atlantic Biases in CCSM4". In: *Journal of Climate* 25.11, pp. 3684–3701. DOI: 10.1175/JCLI-D-11-00315.1.

Harlaß, J., M. Latif, and W. Park (2015). "Improving climate model simulation of tropical Atlantic sea surface temperature: The importance of enhanced vertical atmosphere model resolution". In: *Geophysical Research Letters* 42.7, pp. 2401–2408. DOI: 10.1002/2015GL063310.

Harlaß, J., M. Latif, and W. Park (2017). "Alleviating Tropical Atlantic Sector Biases in the Kiel Climate Model by Enhancing Horizontal and Vertical Atmosphere Model Resolution: Climatology and Interannual Variability". In: *Climate Dynamics*.

Harzallah, A., J. O. Rocha de Aragão, and R. Sadourny (1996). "Interannual rainfall variability in north-east Brazil: Observation and model simulation". In: *International Journal of Climatology* 16.8, pp. 861–878. DOI: 10.1002/(SICI)1097-0088(199608)16:8<861::AID-JOC59>3.0.CO;2-D.

Hazeleger, W. and R. J. Haarsma (2005). "Sensitivity of tropical Atlantic climate to mixing in a coupled ocean-atmosphere model". In: *Climate Dynamics* 25.4, pp. 387–399. DOI: 10.1007/s00382-005-0047-y.

Horel, J. D. (1982). "On the Annual Cycle of the Tropical Pacific Atmosphere and Ocean". In: *Monthly Weather Review* 110.12, pp. 1863–1878. DOI: 10.1175/1520-0493(1982)110<1863:OTACOT>2.0.CO;2.

Hu, Z.-Z. and B. Huang (2007). "The Predictive Skill and the Most Predictable Pattern in the Tropical Atlantic: The Effect of ENSO". In: *Monthly Weather Review* 135.5, pp. 1786–1806. DOI: 10.1175/MWR3393.1.

Huang, B., P. W. Thorne, V. F. Banzon, T. Boyer, G. Chepurin, J. H. Lawrimore, M. J. Menne, T. M. Smith, R. S. Vose, and H.-M. Zhang (2017). "Extended Reconstructed Sea Surface Temperature, Version 5 (ERSSTv5): Upgrades, Validations, and Intercomparisons". In: *Journal of Climate* 30.20, pp. 8179–8205. DOI: 10.1175/JCLI-D-16-0836.1.

Hummels, R., M. Dengler, and B. Bourlès (2013). "Seasonal and regional variability of upper ocean diapycnal heat flux in the Atlantic cold tongue". In: *Progress in Oceanography* 111, pp. 52–74. DOI: 10.1016/j.pocean.2012.11.001.

Hummels, R., M. Dengler, P. Brandt, and M. Schlundt (2014). "Diapycnal heat flux and mixed layer heat budget within the Atlantic Cold Tongue". In: *Climate Dynamics* 43.11, pp. 3179–3199. DOI: 10.1007/s00382-014-2339-6.

Jansen, M. F., D. Dommenget, and N. S. Keenlyside (2009). "Tropical Atmosphere–Ocean Interactions in a Conceptual Framework". In: *Journal of Climate* 22.3, pp. 550–567. DOI: 10.1175/2008JCLI2243.1.

Jouanno, J., F. Marin, Y. Du Penhoat, J. Sheinbaum, and J. M. Molines (2011). "Seasonal heat balance in the upper 100 m of the equatorial Atlantic Ocean". In: *Journal of Geophysical Research: Oceans* 116.9. DOI: 10.1029/2010JC006912.

Keenlyside, N. S. and M. Latif (2007). "Understanding Equatorial Atlantic Interannual Variability". In: *Journal of Climate* 20.1, pp. 131–142. DOI: 10.1175/JCLI3992.1.

Kucharski, F., A. Bracco, J. H. Yoo, and F. Molteni (2008). "Atlantic forced component of the Indian monsoon interannual variability". In: *Geophysical Research Letters* 35.4. DOI: 10.1029/2007GL033037.

Kushnir, Y., W. A. Robinson, P. Chang, and A. W. Robertson (2006). "The Physical Basis for Predicting Atlantic Sector Seasonal-to-Interannual Climate Variability*". In: *Journal of Climate* 19.23, pp. 5949–5970. DOI: 10.1175/JCLI3943.1.

Latif, M., M. Collins, H. Pohlmann, and N. S. Keenlyside (2006). "A Review of Predictability Studies of Atlantic Sector Climate on Decadal Time Scales". In: *Journal of Climate* 19.23, pp. 5971–5987. DOI: 10.1175/JCLI3945.1.

Liu, H., C. Wang, S.-K. Lee, and D. Enfield (2013). "Atlantic Warm Pool Variability in the CMIP5 Simulations". In: *Journal of Climate* 26.15, pp. 5315–5336. DOI: 10.1175/JCLI-D-12-00556.1.

Losada, T. and B. Rodríguez-Fonseca (2016). "Tropical atmospheric response to decadal changes in the Atlantic Equatorial Mode". In: *Climate Dynamics* 47.3-4, pp. 1211–1224. DOI: 10.1007/s00382-015-2897-2.

Lübbecke, J. F., C. W. Böning, N. S. Keenlyside, and S.-P. Xie (2010). "On the connection between Benguela and equatorial Atlantic Niños and the role of the South Atlantic Anticyclone". In: *Journal of Geophysical Research: Oceans* 115.C9. DOI: 10.1029/2009JC005964.

Lübbecke, J. F., N. J. Burls, C. J. C. Reason, and M. J. McPhaden (2014). "Variability in the South Atlantic Anticyclone and the Atlantic Niño Mode". In: *Journal of Climate* 27.21, pp. 8135–8150. DOI: 10.1175/JCLI-D-14-00202.1.

Lübbecke, J. F. and M. J. McPhaden (2012). "On the inconsistent relationship between Pacific and Atlantic Niños". In: *Journal of Climate* 25.12, pp. 4294–4303. DOI: 10.1175/JCLI-D-11-00553.1.

— (2013). "A comparative stability analysis of Atlantic and Pacific Niño modes". In: *Journal of Climate* 26.16, pp. 5965–5980. DOI: 10.1175/JCLI-D-12-00758.1.

Lübbecke, J. F., B. Rodríguez-Fonseca, I. Richter, M. Martín-Rey, T. Losada, I. Polo, and N. S. Keenlyside (2018). "Equatorial Atlantic variability—Modes, mechanisms, and global teleconnections". In: *Wiley Interdisciplinary Reviews: Climate Change* 9.4, e527. DOI: 10.1002/wcc.527.

Martín-Rey, M., I. Polo, B. Rodríguez-Fonseca, T. Losada, and A. Lazar (2017). "Is There Evidence of Changes in Tropical Atlantic Variability Modes under AMO Phases in the Observational Record?" In: *Journal of Climate* 31.2, pp. 515–536. DOI: 10.1175/JCLI-D-16-0459.1.

McCreary, J. P. and P. Lu (1994). "Interaction between the Subtropical and Equatorial Ocean Circulations: The Subtropical Cell". In: *Journal of Physical Oceanography* 24.2, pp. 466–497. DOI: 10.1175/1520-0485(1994)024<0466:IBTSAE>2.0.CO;2.

Meehl, G. A., C. Covey, K. E. Taylor, T. Delworth, R. J. Stouffer, M. Latif, B. McAvaney, and J. F. B. Mitchell (2007). "The WCRP CMIP3 Multimodel Dataset: A New Era in Climate Change Research". In: *Bulletin of the American Meteorological Society* 88.9, pp. 1383–1394. DOI: 10.1175/BAMS-88-9-1383.

Merle, J. (1980). "Seasonal Heat Budget in the Equatorial Atlantic Ocean". In: *Journal of Physical Oceanography* 10.3, pp. 464–469. DOI: 10.1175/1520-0485(1980)010<0464:SHBITE>2.0.CO;2.

Mitchell, T. P. and J. M. Wallace (1992). "The Annual Cycle in Equatorial Convection and Sea Surface Temperature". In: *Journal of Climate* 5.10, pp. 1140–1156. DOI: 10.1175/1520-0442(1992)005<1140:TACIEC>2.0.CO;2.

Mulholland, D. P., K. Haines, S. N. Sparrow, and D. Wallom (2017). "Climate model forecast biases assessed with a perturbed physics ensemble". In: *Climate Dynamics* 49.5, pp. 1729–1746. DOI: 10.1007/s00382-016-3407-x.

Namias, J. (1972). "Influence of northern hemisphere general circulation on drought in northeast Brazil1". In: *Tellus* 24.4, pp. 336–343. DOI: 10.1111/j.2153-3490.1972.tb01561.x.

Nnamchi, H. C., J. Li, F. Kucharski, I.-S. Kang, N. S. Keenlyside, P. Chang, and R. Farneti (2015). "Thermodynamic controls of the Atlantic Niño". In: *Nature Communications* 6. DOI: 10.1038/ncomms9895.

— (2016). "An Equatorial–Extratropical Dipole Structure of the Atlantic Niño". In: *Journal of Climate* 29.20, pp. 7295–7311. DOI: 10.1175/JCLI-D-15-0894.1.

Nobre, P. and J. Shukla (1996). "Variations of Sea Surface Temperature, Wind Stress, and Rainfall over the Tropical Atlantic and South America". In: *Journal of Climate* 9.10, pp. 2464–2479. DOI: 10.1175/1520-0442(1996)009<2464:VOSSTW>2.0.CO;2.

Okumura, Y. M. and S.-P. Xie (2004). "Interaction of the Atlantic Equatorial Cold Tongue and the African Monsoon". In: *Journal of Climate* 17.18, pp. 3589–3602. DOI: 10.1175/1520-0442(2004)017<3589:IOTAEC>2.0.CO;2.

— (2006). "Some overlooked features of tropical Atlantic climate leading to a new Nino-like phenomenon". In: *Journal of Climate* 19.22, pp. 5859–5874.

Park, W., N. S. Keenlyside, M. Latif, A. Ströh, R. Redler, E. Roeckner, and G. Madec (2009). "Tropical Pacific Climate and Its Response to Global Warming in the Kiel Climate Model". In: *Journal of Climate* 22.1, pp. 71–92. DOI: 10.1175/2008JCLI2261.1.

Patricola, C. M., M. Li, Z. Xu, P. Chang, R. Saravanan, and J.-S. Hsieh (2012). "An investigation of tropical Atlantic bias in a high-resolution coupled regional climate model". In: *Climate Dynamics* 39.9, pp. 2443–2463. DOI: 10.1007/s00382-012-1320-5.

Rayner, N. A., D. Parker, E. Horton, C. Folland, L. Alexander, D. Rowell, E. Kent, and A. Kaplan (2003). "Global analyses of sea surface temperature, sea ice, and night marine air temperature since the late nineteenth century". In: *Journal of Geophysical Research* 108.D14, p. 4407. DOI: 10.1029/2002JD002670.

Reynolds, R. W., T. M. Smith, C. Liu, D. B. Chelton, K. S. Casey, and M. G. Schlax (2007). "Daily high-resolution-blended analyses for sea surface temperature". In: *Journal of Climate* 20.22, pp. 5473–5496. DOI: 10.1175/2007JCLI1824.1.

Richter, I., S. K. Behera, T. Doi, B. Taguchi, Y. Masumoto, and S.-P. Xie (2014a). "What controls equatorial Atlantic winds in boreal spring?" In: *Climate Dynamics* 43.11, pp. 3091–3104. DOI: 10.1007/s00382-014-2170-0.

Richter, I., S. K. Behera, Y. Masumoto, B. Taguchi, H. Sasaki, and T. Yamagata (2013). "Multiple causes of interannual sea surface temperature variability in the equatorial Atlantic Ocean". In: *Nature Geoscience* 6.1, pp. 43–47. DOI: 10.1038/ngeo1660.

Richter, I., T. Doi, S. K. Behera, and N. S. Keenlyside (2017). "On the link between mean state biases and prediction skill in the tropics: an atmospheric perspective". In: *Climate Dynamics*. DOI: 10.1007/s00382-017-3809-4.

Richter, I. and S.-P. Xie (2008). "On the origin of equatorial Atlantic biases in coupled general circulation models". English. In: *Climate Dynamics* 31.5, pp. 587–598. DOI: 10.1007/s00382-008-0364-z.

Richter, I., S.-P. Xie, S. K. Behera, T. Doi, and Y. Masumoto (2014b). "Equatorial Atlantic variability and its relation to mean state biases in CMIP5". In: *Climate Dynamics* 42.1-2, pp. 171–188. DOI: 10.1007/s00382-012-1624-5.

Richter, I., S.-P. Xie, A. T. Wittenberg, and Y. Masumoto (2012). "Tropical Atlantic biases and their relation to surface wind stress and terrestrial precipitation". In: *Climate Dynamics* 38.5-6, pp. 985–1001. DOI: 10.1007/s00382-011-1038-9.

Rowell, D. P. (1998). "Assessing Potential Seasonal Predictability with an Ensemble of Multidecadal GCM Simulations". In: *Journal of Climate* 11.2, pp. 109–120. DOI: 10.1175/1520-0442(1998)011<0109:APSPWA>2.0.CO;2.

Ruiz-Barradas, A., J. A. Carton, and S. Nigam (2000). "Structure of Interannual-to-Decadal Climate Variability in the Tropical Atlantic Sector". In: *Journal of Climate* 13.18, pp. 3285–3297. DOI: 10.1175/1520-0442(2000)013<3285:SOITDC>2.0.CO;2.

Schott, F. A., M. Dengler, P. Brandt, K. Affler, J. Fischer, B. Bourlès, Y. Gouriou, R. L. Molinari, and M. Rhein (2003). "The zonal currents and transports at 35°W in the tropical Atlantic". In: *Geophysical Research Letters* 30.7, p. 1349. DOI: 10.1029/2002GL016849.

Siongco, A. C., C. Hohenegger, and B. Stevens (2015). "The Atlantic ITCZ bias in CMIP5 models". In: *Climate Dynamics* 45.5, pp. 1169–1180. DOI: 10.1007/s00382-014-2366-3.

Smith, T. M. and R. W. Reynolds (2003). "Extended Reconstruction of Global Sea Surface Temperatures Based on COADS Data (1854–1997)". In: *Journal of Climate* 16.10, pp. 1495–1510. DOI: 10.1175/1520-0442-16.10.1495.

Stockdale, T. N., M. A. Balmaseda, and A. Vidard (2006). "Tropical Atlantic SST Prediction with Coupled Ocean–Atmosphere GCMs". In: *Journal of Climate* 19.23, pp. 6047–6061. DOI: 10.1175/JCLI3947.1.

Stramma, L. and F. A. Schott (1999). "The mean flow field of the tropical Atlantic Ocean". In: *Deep Sea Research Part II: Topical Studies in Oceanography* 46.1, pp. 279–303. DOI: https://doi.org/10.1016/S0967-0645(98)00109-X.

Sutton, R. T., S. P. Jewson, and D. P. Rowell (2000). "The Elements of Climate Variability in the Tropical Atlantic Region". In: *Journal of Climate* 13.18, pp. 3261–3284. DOI: 10.1175/1520-0442(2000)013<3261:TEOCVI>2.0.CO;2.

Taylor, K. E., R. J. Stouffer, and G. A. Meehl (2012). "An Overview of CMIP5 and the Experiment Design". In: *Bulletin of the American Meteorological Society* 93.4, pp. 485–498. DOI: 10.1175/BAMS-D-11-00094.1.

Tozuka, T., T. Doi, T. Miyasaka, N. S. Keenlyside, and T. Yamagata (2011). "Key factors in simulating the equatorial Atlantic zonal sea surface temperature gradient in a coupled general circulation model". In: *Journal of Geophysical Research: Oceans* 116.6. DOI: 10.1029/2010JC006717.

Voldoire, A., M. Claudon, G. Caniaux, H. Giordani, and R. Roehrig (2014). "Are atmospheric biases responsible for the tropical Atlantic SST biases in the CNRM-CM5 coupled model?" In: *Climate Dynamics* 43.11, pp. 2963–2984. DOI: 10.1007/s00382-013-2036-x.

Wahl, S., M. Latif, W. Park, and N. S. Keenlyside (2011). "On the Tropical Atlantic SST warm bias in the Kiel Climate Model". In: *Climate Dynamics* 36.5-6, pp. 891–906. DOI: 10.1007/s00382-009-0690-9.

Wang, C. (2006). "An overlooked feature of tropical climate: Inter-Pacific-Atlantic variability". In: *Geophysical Research Letters* 33.12. DOI: 10.1029/2006GL026324.

Wang, F. and P. Chang (2008). "Coupled Variability and Predictability in a Stochastic Climate Model of the Tropical Atlantic". In: *Journal of Climate* 21.23, pp. 6247–6259. DOI: 10.1175/2008JCLI2283.1.

Wyrtki, K. (1965). "The annual and semiannual Variation of Sea Surface Temperature in the North Pacific Ocean". In: *Limnology and Oceanography* 10.3, pp. 307–313. DOI: 10.4319/lo.1965.10.3.0307.

Xie, S.-P. and J. A. Carton (2004). "Tropical Atlantic Variability: Patterns, Mechanisms, and Impacts". In: *Earth's Climate*. American Geophysical Union, pp. 121–142. DOI: 10.1029/147GM07.

Xie, S.-P. and S. G. H. Philander (1994). "A coupled ocean-atmosphere model of relevance to the ITCZ in the eastern Pacific". In: *Tellus A* 46.4. DOI: 10.1034/j.1600-0870.1994.t01-1-00001.x.

Xie, S.-P., Y. Tanimoto, H. Noguchi, and T. Matsuno (1999). "How and why climate variability differs between the tropical Atlantic and Pacific". In: *Geophysical Research Letters* 26.11, pp. 1609–1612. DOI: 10.1029/1999GL900308.

Zebiak, S. E. (1993). "Air–Sea Interaction in the Equatorial Atlantic Region". In: *Journal of Climate* 6.8, pp. 1567–1586. DOI: 10.1175/1520-0442(1993)006<1567:AIITEA>2.0.CO;2.

Zermeño-Diaz, D. M. and C. Zhang (2013). "Possible Root Causes of Surface Westerly Biases over the Equatorial Atlantic in Global Climate Models". In: *Journal of Climate* 26.20, pp. 8154–8168. DOI: 10.1175/JCLI-D-12-00226.1.

Zhu, J., B. Huang, and Z. Wu (2012). "The Role of Ocean Dynamics in the Interaction between the Atlantic Meridional and Equatorial Modes". In: *Journal of Climate* 25.10, pp. 3583–3598. DOI: 10.1175/JCLI-D-11-00364.1.

Own Publications

- **Dippe, T.**, X. Zhai, R. J. Greatbatch, and W. Rath (2015). "Interannual variability of wind power input to near-inertial motions in the North Atlantic". In: *Ocean Dynamics* 65.6, pp. 859–875. DOI: 10.1007/s10236-015-0834-x. This paper is part of the *Topical Collection on Atmosphere and Ocean Dynamics: A Scientific Workshop to Celebrate Professor Dr. Richard Greatbatch's 60th Birthday, Liverpool, UK, 10-11 April 2014*

- **Dippe, T.**, R. J. Greatbatch, and H. Ding (2018). "On the relationship between Atlantic Niño variability and ocean dynamics". In: *Climate Dynamics* 51.1, pp. 597-612. DOI: 10.1007/s00382-017-3943-z

- **Dippe, T.**, M. Krebs, J. Harlaß, and J. F. Lübbecke (2018). "Can climate models simulate the observed strong summer surface cooling in the equatorial Atlantic?" In: *YOUMARES 8 – Oceans Across Boundaries: Learning from each other*. Ed. by S. Jungblut, V. Liebich, and M. Bode. Springer International Publishing, pp. 7-23. DOI: 10.1007/978-3-319-93284-2_2

- Scaife. A. A., L. Ferranti, O. Alves, P. Athanasiadis, J. Baehr, M. Dequé, **T. Dippe**, N. Dunstone, D. Fereday, R. G. Gudgel, R. J. Greatbatch, L. Hermanson, Y. Imada, S. Jain, A. Kumar, C. MacLachlan, W. Merryfield, W. A. Müller, H.-L. Ren, D. Smith, Y. Takaya, G. Vecchi, and X. Yang (2018). "Tropical rainfall predictions from multiple seasonal forecast systems". In: *International Journal of Climatology*. DOI: 10.1002/joc.5855

- **Dippe, T.**, J. F. Lübbecke, and R. J. Greatbatch (2018). "A comparison of the Atlantic and Pacific Bjerknes feedbacks: Seasonality, Symmetry, and Stationarity". Submitted to *Journal of Geophysical Research: Oceans*

- **Dippe, T.**, R. J. Greatbatch, and H. Ding (2018). "Seasonal predictions of equatorial Atlantic SST in a low-resolution CGCM with surface heat flux correction". In preparation for *Atmospheric Science Letters*

Acknowledgements

This thesis would not have been possible without my supervisor Richard Greatbatch. Thank you, Richard, for supporting my ideas, being a reliable, competent, and frighteningly immediate source of comments and thorough critique, and sending me around the world to attend conferences and exchange ideas with outstanding scientists. Thank you as well for introducing me to some fascinating reads and the odd hailed brew, and not least for caring not only about the scientific output of your PhD candidates, but also about their private struggles.

Thanks for invaluable scientific input and discussions on short notice are due to my second supervisor Joke Lübbecke. Additionally, Hui Ding had a lot of patience with me in the early stages of my PhD and starred in the role of my technology wizard when it came to running models. My third supervisor Peter Brandt provided fantastic input and thorough critique. Mojib Latif was my second supervisor for the first half of my PhD and contributed valuable ideas and discussions. Additional help with running the MPI-ESM was provided with great patience by Kameswarrao Modali and Jürgen Kröger from the MPI Hamburg.

I'm also indebted to Kiel's Integrated School of Ocean Sciences, especially Nina Bergmann and Avan Antia, for helping me get through the odd difficult situation. I also want to thank GEOMAR's administrative staff for having my back when it came to forms – especially our secretaries Sabine Niewels and Nikole Lorenz, and Ines Staben from the business travel department.

Speaking of moral support, I'm grateful I shared my PhD time with a bunch of great fellow candidates: Katha, Annika, Siren, Fine, Sabine, Christina, and Swantje, to name just a few.

Of course, my entire education, including this last bit, would not have been possible without the unwavering support of my family and friends. Thank you for being there and helping me through the occasional doubts – Mutti and Papa, my great-parents, aunts, uncles, and cousins, and friends like Helga, Jenny, Adrian, Gabriel, Nasrin, Albrecht and Paula, and all the rest of them.

And finally, of course, thank you so much, Paul, for sharing your life with me. You're my safe haven when life throws unexpected obstacles at me. I can't imagine being without you.

Selbstständigkeitserklärung

Hiermit erkläre ich an Eides statt, dass ich die vorliegende Arbeit selbstständig und ohne fremde Hilfe angefertigt habe – abgesehen von der Beratung durch meinen Doktorvater Prof. Dr. Richard J. Greatbatch –, dass ich keine anderen als die angegebenen Quellen benutzt und wörtlich oder inhaltlich übernommene Passagen ausdrücklich als solche kenntlich gemacht habe. Diese Dissertation hat in gleicher oder ähnlicher Form noch keiner Prüfungsbehörde vorgelegen. Sie ist unter Einhaltung guter wissenschaftlicher Praxis entstanden, entsprechend der Regelungen der Deutschen Forschungsgemeinschaft. Bisher wurde mir kein akademischer Grad entzogen.

Tina Dippe,
Kiel, im Dezember 2018